UNIVERSITY OF CALIFORNIA,
IRVINE

PIAS1 modulates the transcriptional landscape and DNA damage repair in Huntington's disease

DISSERTATION

submitted in partial satisfaction of the requirements
for the degree of

DOCTOR OF PHILOSOPHY

in Biological Sciences

by

Eva Louise Lombardi Morozko

Dissertation Committee:
Professor Leslie M. Thompson, Chair
Professor Marcelo Wood
Professor Peter Kaiser
Professor Kyoko Yokomori
Professor Mathew Blurton-Jones

2019

DEDICATION

For

My mother whom may not be here physically but will always be in my heart. The fire and fight she exhibited during such unimaginable circumstances taught me to never give up, to love and support those around me, and to seek the truth. She will forever motivate me to keep moving forward, no matter what obstacles may be placed before me, for the road goes ever on and on.

To my father for his unconditional support and belief in me and for the sacrifices he made for our family.

To my wife who reminds me that love knows no boundaries and no distance. Her constant love and belief in me made this journey possible.

To my cats, who always know.

TABLE OF CONTENTS

LIST OF FIGURES

LIST OF TABLES

LIST OF ABBREVIATIONS

AD	Alzheimer's disease
AGE	Agarose Gel Electrophoresis
ALS	Amyotrophic lateral sclerosis
AO	Age of onset
BER	Base excision repair
DDR	DNA Damage Repair
DEG	Differentially Expressed Gene
DSB	Double strand breaks
FA	Fanconi Anemia
FL HTT	Full Length HTT protein
gDNA	genomic DNA
GO	Gene Ontology
GWAS	Genome-wide association studies
HD	Huntington's disease
Het	Heterozygous mouse
HMW	High Molecular Weight
HR	Homologous Recombination
HTT	Huntingtin protein or gene
ICL	Interstrand crosslink
IPA	Ingenuity Pathway Analysis
iPSC	Induced Pluripotent Stem Cell
KD	Knock-down
KI	Knock-In
LD	Ligase dead
mHTT	mutant huntingtin
mHTTex1p	mutant huntingtin protein encoded by exon 1 only
MMR	Mismatch repair
N17	17 N-terminal amino acids of HTT before CAG repeat region
NER	Nucleotide excision repair
NHEJ	Non-homologous end-joining
NT	Non-transgenic
PCA	Principal Component Analysis
PD	Parkinson's disease
PolyQ	Polyglutamine tract
PTM	Post translational modification
R-loop	DNA:RNA hybrid structure
ROS	Reactive Oxygen Species
SASP	Senescence associated secretory phenotype
SIM	SUMO Interaction Motif
SSB	Single Strand Breaks
STUbLs	SUMO-targeted ubiquitin ligases
TCR	Transcription coupled repair
UPS	Ubiquitin Proteasome System
WT	Wild type

ACKNOWLEDGMENTS

I would like to acknowledge and thank the members of my committee, Dr. Marcelo Wood, Dr. Peter Kaiser, and Dr. Kyoko Yokomori for all of their support and feedback towards my project. Their critiques and input were invaluable towards the evolution and success of this project. A special thanks to Dr. Mathew Blurton-Jones for his support.

Thank you to Dr. Leslie Thompson who has been a supportive and encouraging mentor throughout my graduate studies. Thank you for tolerating my "devil's advocate" scientific debates/discussions and helping me transform into the motivated and thoughtful scientist I am today. Your training, mentoring, and support were integral towards my own personal and scientific growth.

To my collaborators and their labs, for which this project would not have been possible - their support and scientific input were priceless. To Dr. Beverly Davidson and her lab, especially Alejandro Mas Monteys for his work generating clones, miRNA, and viral vectors to knock-down PIAS1. To Dr. Partha Sarkar and his lab for their mechanistic contributions regarding DNA damage repair, especially Subrata Pradhan for his technical assistance. To Dr. William Yang and Peter Langfelder for their help analyzing transcriptional data. To Dr. Vanessa Wheeler, for her expertise on somatic repeat expansion.

Thank you to Dr. Jack Reidling for his constant support and mentorship and for our shared intellectual approach. I am forever grateful for the support, criticisms, guidance, and feedback you provided me throughout my journey.

I am entirely grateful to the Thompson Laboratory for their help and support towards this work. Specifically, I would like to thank Alice Lau for her extensive technical knowledge and laughs in the lab, Lexi Kopan and Illiana Orellana for their technical help and support, and Giana Fote for being an amazing friend and companion and providing sound, intellectual insights into my project. I also want to thank Dr. Charliene Smith-Geater for being an amazing teammate for team Unicorn aka PIAS1 project. I am so grateful that we got to work together to explore these exciting new mechanisms; thank you for sharing your story with me.

These years would not have been possible without amazing friends and family. I want to thank my parents and my sister for maybe not understanding my work beyond "something gross with mice" but supporting me none-the-less. Thank you to my incoming graduate class for their camaraderie over the years – knowing we are all on this together made it possible. Specifically, I'd like to thank Maria Montchal and Susan Gil for being the dopest ladies and putting up with my crap. And Isabella Sanchez; it was amazing sharing my Thompson-lab graduate journey with you. I also want to thank my UCI Archery team and crew; for supporting me and making me laugh no matter what the situation and for teaching me that the most important arrow is in the bow.

Finally, this would not have been possible if not for the amazing support from my wife, Meaghan. We had no idea where we would end up when this all started but we only grew stronger over this journey and her support was my foundation for success. I'm so happy we get to share our life journey together. I'm looking forward to the adventures to come.

This work was supported in parts by NSF GRFP 2016137353, the ARCs foundation, and NINDS RO1NS090390. I thank the IOS Press and the Journal of Huntington's disease for permission to include copyrighted figures and text as part of Chapter 1 of my dissertation.

CURRICULUM VITAE

Eva Louise Lombardi Morozko

EDUCATION

2014 – 2019	University of California, Irvine, CA Doctor of Philosophy: Biological Sciences, Neurobiology and Behavior
2014 – 2017	University of California, Irvine, CA Master of Science: Biological Sciences
2008 – 2012	Seton Hall University, South Orange, NJ Bachelor of Science: Biochemistry, Minor: Classical Studies Magna Cum Laude

HONORS AND AWARDS

2018	UCI, CNLM Renee Harwick Advanced Graduate Student Award
2018	UCI MIND, ReMIND Outstanding Predoctoral Scholar Award
2017 – 2019	ARCS Foundation, Inc. Scholar, UC, Irvine Graduate Division
2017	Fine Science Tools Graduate Travel Award in Neurobiology, School of Biological Sciences
2017	Amgen Scholars Alumni Travel Award
2017, 18, 19	Graduate Student Travel Award, Office of the Associate Dean, School Of Biological Sciences
2016 – 2019	NSF Graduate Research Fellowship Program Awardee
2015	NSF Graduate Research Fellowship Program Honorable Mention
2012	New Jersey Institute of Chemists Biochemistry Award
2012	Best Senior Academy Poster Award, New Jersey Academy of Science
2011	Amgen Scholar
2010 – 2012	Clare Booth Luce Scholar
2008 – 2012	Seton Hall University Dean's List, all semesters
2010 – 2012	Seton Hall University Department of Chemistry and Biochemistry Honors Program
2010	ΑΦΔ (Alpha Phi Delta) Merit Scholarship Recipient
2008 – 2010	National M.S. Society Scholarship Recipient
2008	New Jersey Interscholastic Athletic Association Scholar Athlete

GRADUATE FUNDING

2017 – 2019	ARCS Foundation Fellowship
2016 – 2019	NSF Graduate Research Fellowship (NSF 2016137353)
2015 – 2019	NIH NINDS (RO1-NS090390)

RESEARCH EXPERIENCE

2015 – 2019 Graduate Student, Ph.D. Candidate, Lab of Dr. Leslie Thompson
University of California, Irvine, Dept. of Neurobiology and Behavior
Project: PIAS1 functional mechanisms in Huntington's disease

- Utilized HeLa, HEK293T, and ST14A mammalian cell lines for transfection with Lipofectamine 2000 to investigate protein functional domains, protein-protein interactions, post-translational modifications, and protein aggregation
- Investigated the role of PIAS1 SUMO E3 ligase in Huntington's disease (HD) pathology, protein homoestasis, and genomic homoestasis in HD zQ175 mice
- Analyzed shifts in protein homeostasis associated with HD by immunohistochemistry and western blots on the HD R6/2 and zQ175 mouse models
- Performed and analyzed Rotarod, Pole test, Elevated Plus maze, and Irwin test as behavioral analyses of the HD R6/2 and zQ175 mouse models and performed perfusions and tissue harvest on sacrificed animals

2015 Rotating Graduate Student, Lab of Dr. Dritan Agalliu
University of California, Irvine, Dept. of Developmental Biology
Project: Investigating Apcdd1 Associated Angiogenesis and Barrier Properties

- Utilized immunohistochemistry to investigate neuronal cell populations in the retinas of mice lacking the Wnt inhibitor Apcdd1
- Investigated the effect of Apcdd1 loss on the blood brain barrier by using transendothelial electrical resistance (TEER) assays on endothelial cell cultures in vivo

2014 Rotating Graduate Student, Lab of Dr. John Weiss
University of California, Irvine, Dept. of Anatomy and Neurobiology
Project: Zn^{+} excitotoxicity in ALS

- Cultured primary cortical neurons from neonatal and postnatal mice to investigate the role of zinc in neurotoxicity
- Performed spinal cord dissections for use in tissue culture to investigate immune responses associated with amyotrophic lateral sclerosis

2012 – 2014 Post-baccalaureate researcher, Lab of Dr. Thomas B. Friedman
National Institutes of Health, National Institute on Deafness and Other Communication Disorders, Laboratory of Molecular Genetics
Projects: 1) Taperin function and protein-protein interactions, 2) Characterization of an Ildr1 Knockout Mouse as a Model for DFNB42

- Performed Auditory Brainstem Response (ABR) and Distortion Product Otoacoustic Emission (DPOAE) testing to investigate hearing phenotypes of multiple mouse strains
- Managed mouse colonies by maintaining inventories, breeding, and genotyping mice
- Determined localization of proteins using immunofluorescent staining on microdissected sensory epithelia of mouse cochlea and confocal microscopy
- Characterized protein binding motif by designing, cloning, and sequencing (Sanger sequencing) full length and fragments of proteins to generate cDNA libraries for use in cell-based protein-protein interaction assay
- Cultured Cos-7 mammalian cells for transfection via electroporation and explant cultured organotypic inner ear sensory epithelial for transfection with Helios gene gun

2011 – 2012 Undergraduate Academic Researcher, Labs of Dr. David Sabatino and Dr. Allan Blake
Seton Hall University, Depts. of Chem. and Biochem. and Bio. Sci.
Project: Synthesis and Characterization of GRP78-siRNAs for Potential Anti-Cancer Applications

- Synthesized lipid-conjugated branch-point amidites using solution phase synthesis
- Utilized solid phase synthesis to generate siRNA sequences as chemotherapeutic agents using synthesized branch-point amidites
- Cultured mammalian HEPG-2 liver cancer cells for biological evaluation using western blots to determine protein expression

2011 Amgen Scholars Summer Program, Lab of Dr. Catherine F. Clarke
University of California, Los Angeles, Dept. of Chem. and Biochem.
Project: Characterization of the Coenzyme Q Biosynthetic Complex

- Investigated the Coenzyme Q biosynthetic pathway in *S. cerevisiae* and identified specific proteins in a mitochondria located complex using Co-Immunoprecipitation assays
- Cloned and produced a novel yeast strain for use in Co-Immunoprecipitation assays

2010 – 2011 Undergraduate Academic Researcher, Lab of Dr. James E. Hanson
Seton Hall University, Dept. of Chemistry and Biochemistry
Project: Synthesis of meso-Tetrapyridylporphyrin Derivatives for DNA Quadraplex Binding

- Synthesized meso-Tetrapyridylporphyrin and quaternizing nitrogens on pyridine rings to increase binding affinity for quadruplex DNA for use as cancer therapeutics
- Purified and analyzed synthesized products using thin-layer and column chromatography, UV-Visible spectroscopy and Nuclear Magnetic Resonance

2009 Undergraduate Academic Researcher, Lab of Dr. George Turner
Seton Hall University, Dept. of Chemistry and Biochemistry
Project: Mutation Effects on bR Expression in *H. salinarium*

- Researched genetic mutations of the Bacteriorhodopsin protein gene in Halobacterium salinarium to understand how they affected protein expression

PUBLICATIONS

Morozko E.L.*, Smith-Geater C.*, Pradhan S., Mas Monteys A., Lim R., Langfelder P, Kachemov M., Wu J., Ochaba J., Miramontes R., , Lau A., Orellana I., Kopan L., Yeung S., Reidling J.C., Yang X.W., Steffan J.S., Davidson B.L.#, Sarkar P.S.#, Thompson L.M.#, 'Neuronal Pias1 reduction improves Transcription Coupled Repair and PNKP activity in vivo and in HD iPSC-neurons.' *Manuscript in preparation*. *Co-First authors, #Co-Corresponding Authors.

Morozko E.L., Ochaba J., Hernandez S., Lau A., Sanchez I., Orellana I., Kopan L., Overman J., Yeung S., Steffan J.S., Reidling J., and Thompson L.M. 'Longitudinal Biochemical Assay Analysis of Mutant Huntingtin Exon 1 Protein in R6/2 Mice.' *J. Huntingtins Dis.*, November 2018, 7(4):321-335.

Ochaba J., **Morozko E.L.,** Thompson L.M. 'Fractionation for Resolution of Soluble and Insoluble Huntingtin Species'. *JoVE*, February. 2018.

Grima J., Daigle J.G., Arbez N., Cunningham K.C., Zhang K., Ochaba J., Geater C., **Morozko E.**, Stocksdale J., Glatzer J.C., Pham J.T., Ahmed I., Peng Q., Wadhwa H., Pletnikova O., Troncoso J.C., Duan W., Snyder S.H., Ranum L.P.W., Thompson L.M., Lloyd T.E., Ross C.A., Rothstein J.D. 'Mutant Huntingtin Disrupts the Nuclear Pore Complex'. *Neuron*, April 2017, 94(1):93-107.

Bird J.E., Barzik M., Drummond M.C., Sutton D.C., Goodman S.M., **Morozko E.L.**, Cole S.M., Boukhvalova A.K., Skidmore J., Syam D., Wilson E.A., Fitzgerald T., Rehman A.U., Martin D.M., Boger E.T., Belyantseva I.A., Friedman T.B. 'Harnessing molecular motors for nanoscale pulldown in live cells'. *Molecular Biology of the Cell*. February 2017, 28(3):463-475.

Morozko E.L.*, Nishio A*, Ingham, N.J., Chandra R, Fitzgerald T, Martelletti E, Borck G, Wilson E, Riordan G.P., Wangemann P, Forge A, Steel K.P., Liddle R.A., Friedman T.B., Belyantseva I.A. 'ILDR1 null mice, a model of human deafness DFNB42, show structural aberrations of tricellular tight junctions and degeneration of auditory hair cells'. *Human Molecular Genetics*, February 2015, 24(3):609-24. *Co-first authors.

Maina A, Blackman B.A., Parronchi C.J., **Morozko E**, Bender M.E., Blake A.D., Sabatino D. 'Solid-phase synthesis, characterization and RNAi activity of branch and hyperbranch siRNAs'. *Bioorganic & Medicinal Chemistry Letters*, October 2013, 23(19):5270-4.

RESEARCH PRESENTATIONS

Modulating Huntington's disease through DNA damage repair

April, 2019	Selected Lightning Talk and Poster Presentation for the Ubiquitin, Autophagy and Disease Meeting. Cold Spring Harbor Laboratory, Cold Spring Harbor, NY
March, 2019	Oral presentation for the ARCS Scholars 19th Scholar Awards Dinner. Irvine, CA
February, 2019	Poster Presentation for the Research and Education in Memory Impairments and Neurological Disorders 10th Annual Emerging Scientists Symposium. University of California, Irvine, CA
January, 2019	Neuroblitz Seminar presentation, University of California, Irvine, Department of Neurobiology and Behavior, Irvine, CA

Contribution of SUMOylation towards Huntington's disease pathogenesis

August, 2018	Poster Presentation for the Hereditary Disease Foundation HD2018 annual Conference: "The Milton Wexler Celebration of Life," Cambridge, MA

Protein Balance in Neurodegenerative Disease

April, 2018	Oral "TED-Style" presentation, UC, Irvine Associated Graduate Students Annual Graduate Research Symposium. University of California, Irvine, CA– Winner, People's Choice Award

Contribution of SUMOylation towards Huntington's disease pathogenesis

March, 2018	Selected Abstract Oral Presentation and Poster Presentation for the Research and Education in Memory Impairments and Neurological Disorders 9th Annual Emerging Scientists Symposium. University of California, Irvine, CA – Winner, Outstanding Predoctoral Scholar Award

PIAS1 Functional Mechanisms in Huntington's disease

April, 2017 Poster Presentation for the Ubiquitin Family Meeting. Cold Spring Harbor Laboratory, Cold Spring Harbor, NY

May, 2017 Poster Presentation for the UCI, NSF-GRFP "Training for Tomorrow" symposium. University of California, Irvine, CA

June, 2017 Poster Presentation for the Gordon Research Seminar & Gordon Research Conference, CAG Triplet Repeat Disorder. Mount Snow, West Dover, VT

Longitudinal Assessments of R6/2 Mice Aid in Evaluation of Preclinical Disease Interventions

February, 2017 Poster Presentation for the Research and Education in Memory Impairments and Neurological Disorders 8th Annual Emerging Scientists Symposium. University of California, Irvine, CA

PIAS1 functional mechanisms in Huntington's disease

February, 2017 Neuroblitz Seminar presentation, University of California, Irvine, Department of Neurobiology and Behavior, Irvine, CA

Comprehensive Biochemical Analysis of Protein Homeostasis in R6/2 Mice

August, 2016 Poster Presentation for the Hereditary Disease Foundation HD2016 annual Conference: "The Milton Wexler Celebration of Life," Cambridge, MA

A Comprehensive Biochemical Analysis of HD Pathogenesis in the R6/2 Mouse Model

April, 2016 Neuroblitz Seminar presentation, University of California, Irvine, Department of Neurobiology and Behavior, Irvine, CA

Investigating Apcdd1 Associated Angiogenesis and Barrier Properties

April, 2015 Neuroblitz Seminar presentation, University of California, Irvine, Department of Neurobiology and Behavior, Irvine, CA

Characterization of an Ildr1 Knockout Mouse as a Model for DFNB42

June, 2014 Trainee Talk Oral Seminar, National Institutes of Health, National Institute on Deafness and Other Communication Disorders, Irvine, CA

An Ildr1 Knockout Mouse is a Model of Human Deafness DFNB42

February, 2014 Poster presentation for the Association for Research in Otolaryngology's 37th Annual Midwinter Meeting, San Diego, CA

May, 2014 Poster presentation for National Institutes of Health Postbac Poster Day, Bethesda, MD

Synthesis and Characterization of GRP78-siRNAs for Potential Anti-Cancer Applications

April, 2012 — Poster presentation for the 16th Annual Petersheim Academic Expositions at Seton Hall University, South Orange, NJ

April, 2012 — Poster presentation for the 57th Annual New Jersey Academy of Science Meeting at Seton Hall University, South Orange, NJ– Winner, Best Senior Academy Poster Presentation

Characterization of the Coenzyme Q Biosynthetic Complex in *Saccharomyces cerevisiae*

August, 2011 — Amgen Scholars Program Research Presentation, University of California, Los Angeles. Los Angeles, CA

Synthesis of meso-Tetrapyridylporphyrin Derivatives for DNA Quadraplex Binding

April, 2010, 11 — Poster presentation for the 14th and 15th Annual Petersheim Academic Expositions at Seton Hall University. South Orange, NJ

Mutation Effects on bR Expression in *H. salinarium*

April, 2009 — Poster and Oral presentation for the 13th Annual Petersheim Academic Exposition at Seton Hall University. South Orange, NJ

TEACHING EXPERIENCE

2016 – 2017 — Teaching Assistant, Neurobiology Laboratory N113L Supervised by Professor Andrea Nicholas
University of California, Irvine, Dept. of Neurobiology and Behavior

2016 — Teaching Assistant, Intro to Neurobiology N110
University of California, Irvine, Dept. of Neurobiology and Behavior

2015 – 2018 — Guest Instructor, Neurodegeneration N150
Instructed by Dr. Leslie Thompson
University of California, Irvine, Dept. of Neurobiology and Behavior

2010 – 2012 — Teaching Fellow, Organic Chemistry, Nursing Biochemistry
Supervised by Dr. Stephen P. Kelty
Seton Hall University, Dept. of Chemistry and Biochemistry

PROFESSIONAL DEVELOPMENT AND LEADERSHIP

2018 – 2019	Professional Development Committee Co-Chair University of California, Irvine Center for the Neurobiology of Learning and Memory Ambassadors Program
2017 – 2018	Graduate Student Representative NBB/MIND Assistant Professor Search Committee
2016 – 2018	Series Coordinator, NeuroBlitz Graduate Student Seminar University of California, Irvine, Dept. of Neurobiology and Behavior
2015 – 2019	Member, GPS-BIOMED professional development program University of California, Irvine
2015 – 2017	Graduate Representative, Interdepartmental Neuroscience Program, University of California, Irvine
2016	Participant, Activate to Captivate Public Speaking workshop University of California, Irvine
2015	Participant, Becoming an Effective Mentor workshop School of Biological Sciences, University of California, Irvine
2008 – 2012	Secretary and Member, Biology Society Seton Hall University

ABSTRACT OF THE DISSERTATION

PIAS1 modulates the transcriptional landscape and DNA damage repair in Huntington's disease

By

Eva Louise Lombardi Morozko

Doctor of Philosophy in Biological Sciences

University of California, Irvine, 2019

Professor Leslie M. Thompson, Chair

Disruption of protein homeostasis, leading to accumulation of insoluble high molecular weight protein complexes containing the Huntingtin (HTT) protein and SUMOylated proteins, and transcriptional dysregulation are key features in Huntington's disease (HD). Genetic modifiers contributing to HD age of onset have recently been identified and have critical roles in DNA damage repair (DDR) pathways. The mechanisms involved in DDR rely strongly on signaling cascades and post-translational modifications such as SUMO to maintain genomic integrity. Further, the Huntingtin (HTT) protein itself scaffolds DDR proteins. We previously showed that striatal reduction of the E3 SUMO ligase PIAS1 was neuroprotective and modulated disease associated pathologies including accumulation of mutant HTT in a mouse model of HD. However, the exact mechanistic contributions of PIAS1 towards HD pathogenesis have not yet been fully elucidated. To further evaluate PIAS1 function in the context of HD, knock-down was investigated in human patient medium spiny neurons differentiated from induced pluripotent stems cells and two disease

mouse models. My findings suggest that PIAS1 functions as a key regulator of post-translational modification and protein homeostasis in HD neurons and mediates the functional activity of the transcription-coupled DNA damage repair complex in the striatum. Reduction of PIAS1 facilitated DNA repair, normalized aberrant transcriptional profiles related to synaptic function, and may stabilize the CAG-repeat within HTT. The results of this research provide the first mechanistic link between SUMOylation and DNA damage repair in the central nervous system. Specifically, they provide insight into how DNA damage repair pathways and post-translational modifications might contribute towards HD, and overall for targeting pathway mediators to restore homeostatic balance, with broad implications for HD and other neurodegenerative diseases.

INTRODUCTION

Huntington's disease genetics and pathology

Huntington's disease (HD) is an autosomal-dominant, neurodegenerative disorder, caused by a trinucleotide CAG repeat expansion within exon 1 of the *huntingtin* (*HTT*) gene (Group, 1993). Typical age of adult-onset for HD is between 35 and 50 years of age with an inverse relationship existing between the length of the CAG repeat and age of onset (Langbehn et al., 2004). A repeat length of 40 CAGs is associated with nearly complete penetrance of the disease with unaffected individuals having between 6 and 34 repeats. Incomplete penetrance exists with individuals carrying between 36 and 39 repeats and there is an increased risk of offspring inheriting the disease due to somatic repeat expansion in unaffected individuals with 27-35 repeats, particularly if the mutant allele is inherited from the father (Norremolle et al., 1995; Semaka et al., 2006). A juvenile variant of the disease with more than 60 repeats typically develops symptoms before the age of 20 with greater severity and a more rapid progression of neuropathology (Nance and Myers, 2001). However, the correlation between repeat length and age of onset (AO) is not fully predictive for adult onset HD and only accounts for 40-50% of the variance in AO, suggesting the influence of disease modifiers including genetic or environmental factors (Wexler et al., 2004). Indeed, recent Genome-wide association studies (GWAS) identified several genetic contributors to the observed variance in age of onset (GeM-HD, 2015, 2019).

Movement abnormalities, cognitive deficits, and personality changes are the hallmark symptoms of HD (Goh et al., 2018). In addition to these clinically observed symptoms,

Huntington's is associated with numerous pathogenic outcomes. The CAG-repeat expansion codes for a polyglutamine (PolyQ) tract within the mutant HTT protein (mHTT). The presence of this expansion results in aberrant misfolding, proteolysis, and accumulation of mHTT associated with disease pathogenesis (Koyuncu et al., 2017; Sathasivam et al., 2013). This disruption of protein homeostasis, including protein quality control networks, is also a hallmark of other neurodegenerative disorders such as Alzheimer's disease (AD), Parkinson's disease (PD) and Amyotrophic lateral sclerosis (ALS) (Hipp et al., 2014; Kurtishi et al., 2019; Ross and Poirier, 2004). Neuropathology presents as notable degeneration of GABAergic medium spiny neurons (MSNs) in the striatum (caudate and putamen), cortical atrophy, and loss of striatal projection neurons (Ross and Tabrizi, 2011; Rub et al., 2016; Zuccato et al., 2010). After clinical onset there is a mean survival rate of about 20 years for individuals with HD with patients ultimately passing away due to falls or swallowing difficulties leading to aspiration pneumonia (Bates et al., 2002; Zuccato et al., 2010). To date, no disease modifying treatment exists for HD.

Homozygous loss of *Htt* in mice shows embryonic lethality prior to the formation of the nervous system (Nasir et al., 1995) and conditional loss of WT *Htt* during development results in neurodegenerative phenotypes in adult mice (Dragatsis et al., 2000). Mutant HTT itself is functional and can rescue null mice (Leavitt et al., 2001), however normal function appears to be impaired upon CAG repeat expansion. While not sufficient to drive disease in the absence of mHTT, loss of normal HTT function appears to contribute to disease (Liu and Zeitlin, 2017).

The HTT protein is involved in multiple normal cellular processes from its function as a critical scaffold protein and loss of these functions may contribute to disease. For instance, a key characteristic of HD is BDNF (Brain Derived Neurotrophic Factor) deficiency with loss of trophic support potentially contributing to neuronal dysfunction and neurodegeneration (Ferrer et al., 2000; Zuccato and Cattaneo, 2009). One of the first functions for HTT was defined as a mediator of BDNF trafficking along microtubules. Loss of this function could in part contribute to the observed regional vulnerability of MSNs due to loss of trophic support from the cortex to the striatum (Gauthier et al., 2004). Further, HTT binds numerous transcription factors, which initially suggested that HTT functions in gene transcription (Cha, 2007; Steffan et al., 2000) and HTT has recently been defined as a scaffold for selective autophagy by interacting with key autophagic proteins that are important for the formation of autophagosomes (Ochaba et al., 2014; Rui et al., 2015). Finally, recent studies have shown the HTT protein scaffolds DNA repair processes (Gao et al., 2019; Maiuri et al., 2017). Therefore, scaffolding functions of HTT are required for multiple cellular processes including selective autophagy and DNA damage repair and these functions are compromised in disease. Together, reduced normal HTT function in conjunction with a toxic gain of function for mHTT together appear to result in the observed molecular hallmarks associated with HD.

Due to the genetic nature of HD, multiple cell and mouse models were developed in an effort to understand the molecular progression that contributes to disease pathogenesis. The design of these animals varies; from transgenic fragments to knock-in at the endogenous murine locus and each provides a platform for studying different aspects of

the disease (Brooks and Dunnett, 2015). Summarized are the models that I used in for my dissertation work.

The R6/2 model was the first HD model generated by a transgenic overexpression of the first 1.9 kb of human *HTT* with a PolyQ tract of ~115-150 followed by the human proline-rich region on a hybrid CBAxC57BL/6 background (Mangiarini et al., 1996). Originally, it was developed to study repeat instability *in vivo*, however was found to exhibit robust and progressive neurological deficits similar to features of HD. Phenotypes include early onset of involuntary movements such as dyskinesia, impaired performance on motor tasks such as pole test and Rotarod, seizures, and progressive biochemical pathology (Carter et al., 1999). While motor deficits appear as early as 5 weeks of age, cognitive deficits are also observed in R6/2 mice as early as 3.5 weeks of age and include decreased spatial navigation capacity and deficits in visual recognition and discrimination tasks (Lione et al., 1999). There is a progressive formation of mHTT intranuclear inclusions throughout the brain in these animals along with substantial loss in overall brain volume (Davies et al., 1997; Mangiarini et al., 1996). R6/2 mice have reduced levels of BDNF at both the transcript and protein levels, recapitulating an important phenotype in human patients (Zuccato et al., 2010). A notable loss of neurotransmitter receptors in R6/2 mice on striatal projection neurons may in part account for observed neuronal dysfunction and neurodegeneration (Cha et al., 1998). This is accompanied by electrophysiological alterations in MSNs in the striatum causing excitotoxicity, affecting synaptic properties, and resulting in decreased amplitude of action potentials (Klapstein et al., 2001). Progressive genomic instability is notable in these animals with increased oxidative damage to genomic

DNA (Bogdanov et al., 2001) and strand breaks observed (Enokido et al., 2010; Illuzzi et al., 2009).

Due to the rapid progression and shortened lifespan (10-15 weeks), presence of juvenile onset repeat, and presence of a toxic fragment that is typically generated during the course of disease, the R6/2 transgenic line is roughly representative of juvenile HD or later stage HD. Taking advantage of its robust phenotype, it has been used for countless initial preclinical studies to evaluate interventions *in vivo* (Gil and Rego, 2009). However, R6/2 mice and associated lines (e.g R6/1 that has transgene in a different integration site) may be less suitable for investigating molecular mechanisms that are implicated early on in the disease, prior to onset of motor or even cognitive phenotypes. HD mouse models carrying full-length HTT with the expanded repeat mutation have relatively delayed onset of motor phenotypes and additional cognitive neurological deficits have been detected (Brooks and Dunnett, 2015; Menalled and Brunner, 2014). Full-length models tend to live longer and cognitive tests, such as those testing learning and memory, can be conducted with less performance confounds due to motor deficits. The zQ175 mouse model of HD is a knock-in (KI) mouse model at the endogenous locus of murine *Htt* on a C57Bl/6 background derived from a spontaneous expansion of a well-established Q140 knock-in line (Menalled et al., 2012). Notably, this mouse has a chimeric full-length HTT with the human CAG-repeat expansion and adjacent proline-rich region of human HTT within endogenous mouse *Htt*.

zQ175 mice show onset of motor and cognitive deficits in both homozygous and heterozygous mice with heterozygous animals exhibiting later onset. Heterozygous mice

therefore mimic the autosomal dominant inheritance trait of HD. Behavioral deficits include decreased body weight, hypoactivity, and motor deficits as assessed by Rotarod behavioral task with phenotypes manifesting around 20 weeks of age in heterozygotes. Transcriptional dysregulation including decreased expression of striatal gene markers such as *Darpp-32* is detected as early as 12 weeks of age (Heikkinen et al., 2012; Menalled et al., 2012). More recently, zQ175 mice were included in an in-depth allelic series analysis of transcriptional and proteomic profiling where transcriptional signatures were characterized into disease-associated modules (Langfelder et al., 2016). Transcriptional modules associated with disease included those which enriched for MSN identity genes, cellular signaling, and DNA damage repair (DDR) pathways thereby establishing a baseline for observed molecular changes in this mouse model of HD. In addition to DDR pathways being upregulated transcriptionally (Langfelder et al., 2016), zQ175 animals have increased levels of strand breaks and a corresponding decrease in genomic stability (Gao et al., 2019; Gasset-Rosa et al., 2017).

MSNs in the striatum of zQ175 mice are hyperexcitable with smaller action potentials with deficits in neurotransmitter release by 6-9 months of age in heterozygotes (Heikkinen et al., 2012) accompanied by a decrease in striatal and cortical volumes by MRI as early as 4 months of age. Later studies have shown a considerable amount of striatal and cortical atrophy in homozygous mice as early as 3 months of age, preceding behavioral deficits (Peng et al., 2016). Decreased post-synaptic density is observed in zQ715 mice with corresponding alterations in striatal metabolites such as decreases in glutamate and GABA and an increase in glutamine (Peng et al., 2016). Further, these animals have altered

neurotransmission and synaptic vesicle release. Taken together, zQ175 mice exhibit molecular dysregulation that recapitulates aspects of HD pathogenesis (Chen et al., 2018; Heikkinen et al., 2012). Overall, mouse models of HD provide a powerful genetic tool to help elucidate the pathogenic complexities of the disease. Utilizing these two specific models allows us to investigate the contribution of the expanded PolyQ within a toxic fragment (i.e. R6/2 transgene fragment) and full-length mHTT protein (i.e. KI mouse models). Investigating the functional contributions of different molecular pathways in a complex *in vivo* system such as the mouse brain, aids in elucidating mechanisms driving disease pathogenesis in a translational context.

Cross-model investigation of therapeutic interventions will greatly aid in preclinical drug design. In addition to utilizing multiple mouse models of HD, the ability to induce pluripotency in human patient fibroblasts has become a powerful tool for studying human diseases. Termed induced pluripotent stem cells (iPSCs), these cells are reprogrammed into a pluripotent state allowing them to be differentiated into numerous cell types using a variety of transcription factors, small molecules, and small RNAs that can then be used to study specific human cell types in culture (Singh et al., 2015). These iPSCs can be derived from human subjects with specific diseases and differentiated into relevant cell types to study related pathologies. For HD, patient-derived iPSCs can be differentiated into MSNs, other neurons or glia, allowing for experimental manipulation of an otherwise inaccessible cell type (Geater et al., 2018). Therefore, for my dissertation I sought to utilize numerous genetic models of HD, ranging from human, patient neurons to animal models, to elucidate the molecular mechanisms of disease pathogenesis.

Protein and genomic homeostasis in Huntington's disease

Investigations into the biological mechanisms underlying HD and identification of potential therapeutic targets have shed light on the ways mHTT is processed throughout the disease. Mutant HTT undergoes conformational flux and processing which leads to increased protein fragmentation and formation of both soluble and insoluble aggregate species (Hoffner and Djian, 2014, 2015; Ross et al., 2017). Intranuclear inclusions of aggregated NH2-terminal fragments are one of the hallmarks of HD pathogenesis first described by DiFiglia et al. in 1997 in post-mortem brain tissue from HD patients and by the Bates group in R6/2 mice (Davies et al., 1997; DiFiglia et al., 1997). In later studies, the Bates group showed that incomplete splicing can also result in the endogenous expression of a pathogenic exon 1 fragment of mHTT that may contribute to disease progression in HD (Neueder et al., 2017). Mutant HTT forms aggregates in a progressive manner corresponding with stage of disease, likely serving as a surrogate marker of disease progression and aberrant protein homeostasis (Davies et al., 1997; DiFiglia et al., 1997). However, intranuclear inclusions and mHTT aggregates are an end-product of dyshomeostasis and mHTT undergoes several changes in conformation prior to entering an insoluble aggregate phase (Hoffner and Djian, 2014).

During the aggregation process, mHTT transitions from a soluble monomer stage through soluble oligomeric species and β-sheet fibrils to insoluble aggregates and inclusions, though in a non-linear path (Arndt et al., 2015; Hoffner and Djian, 2014). Soluble, monomeric mHTT containing the expanded PolyQ region first forms prefibrillar or protofibrilar soluble oligomers (Poirier et al., 2002). Proposed globular intermediates

bridge between soluble and insoluble fibrils but ultimately β-sheet amyloid-like fibers form (Scherzinger et al., 1997) followed by insoluble accumulated species, aggregates, or inclusions. However, the "toxic conformer" of mHTT is not yet defined and the temporal formation of each form has not been systematically evaluated in parallel. A number of assays are now available to follow mHTT protein species throughout disease progression such as soluble oligomeric species (Sontag et al., 2012), insoluble accumulated species (O'Rourke et al., 2013; Ochaba et al., 2016; Ochaba et al., 2018), and insoluble fibrillary species (Wanker et al., 1999). Further, due to the chemically distinct nature of difference conformers, establishing optimal cell lysis methods or biochemical assays to resolve mHTT species to compare to behavioral phenotypes, peripheral effects, and cellular networks would greatly assist researchers in preclinical studies.

Alterations in transcription and genome stability are also observed in HD. These may in part be due to a loss of HTT function, an aberrant function of mHTT, or driven by aberrant compensatory mechanisms to counterbalance the presence of mHTT protein. Transcriptional dysregulation has been well documented in HD and other PolyQ diseases (Hodges et al., 2006; Labadorf et al., 2015; Moumne et al., 2013; Xiang et al., 2018). Some of this observed dysregulation has been attributed to mHTT binding to transcription factors, directly binding DNA, or altering chromatin structure (Benn et al., 2008; Kumar et al., 2014), although the emerging literature suggests highly complex mechanisms involved. Overall, transcriptional dysregulation in HD has been associated with loss of neuronal identity gene expression which may contribute to neuronal malfunction (Achour et al., 2015; Hodges et al., 2006; Labadorf et al., 2015).

While aberrant transcriptional profiles are an indicator of altered genomic structure and regulation, in HD, genomic instability is also observed. In HD patients, genetic variants within DNA damage repair genes associate with disease progression and account for some of the observed variability for AO, suggesting maintenance of genomic stability is a critical component of disease pathogenesis (Bettencourt et al., 2016; GeM-HD, 2015; Moss et al., 2017). Additionally, somatic repeat expansion of the disease-causing CAG-repeat is a significant predictor of AO from analysis of HD patient post-mortem cortical samples (Swami et al., 2009). This expansion is attributed to the instability of the CAG-repeat and is seen primarily in the most overtly affected striatum (Telenius et al., 1994). Germline repeat instability, which causes repeat expansions between generations, are primarily due to instability during gametogenesis with the largest expansions arising in sperm (Telenius et al., 1994; Wheeler et al., 1999) suggesting that expansion is related to DNA replication. However, in neurons where DNA is not replicated but is highly transcribed, the observed somatic repeat expansion has been primarily attributed to aberrant or inappropriate repair of damaged DNA after misalignment or formation of other unusual DNA structures (Schmidt and Pearson, 2016). Alternatively, a loss of adequate repair has also been proposed to decrease genomic stability in the HD brain such that increased oxidative stress and DNA damage have been reported in both human postmortem brain samples and mouse models of HD (Bogdanov et al., 2001; Browne et al., 1997; Enokido et al., 2010; Giuliano et al., 2003; Illuzzi et al., 2009). This suggested that a decrease in genomic stability may also contribute to the observed transcriptional dysregulation in HD. Supporting this, evidence from the zQ175 mouse striatum has shown a deficit in adequate DDR corresponded to decreased genomic stability of key neuronal genes (Gao et al., 2019). Further, increased

levels of DNA damage correspond to hyperactivation of ATM signaling pathways which may further contribute to disease pathogenesis (Gao et al., 2019; Giuliano et al., 2003). Understanding the functional mechanisms that drive genomic instability throughout disease pathogenesis will therefore aid in development of targeted therapeutics to delay AO.

SUMO modification in HD and neurodegeneration

Mutant HTT-containing neuronal inclusions co-localize with ubiquitin suggesting that mHTT is targeted for degradation but is unable to be cleared by the ubiquitin proteasome system (UPS) or autophagy and implicates post-translational modifications (PTMs) in disease-affected mechanisms (Hipp et al., 2014; Ravikumar et al., 2004; Waelter et al., 2001). PTMs are additions onto translated proteins that can alter function, localization, interactions or homeostasis. There are a variety of different PTMs ranging from phosphorylation to conjugation of small peptides such as ubiquitin, with each impacting cellular networks. Ubiquitination on target lysine residues canonically marks a misfolded or unfolded protein for degradation by the proteasome as a recycling mechanism for cellular components (Hershko and Ciechanover, 1998; Kocaturk and Gozuacik, 2018). However, there are other functions that are dictated by the manner of ubiquitin conjugation on lysines of the target protein, such as histone ubiquitination modulating gene expression at the epigenetic level (Bonnet et al., 2014).

Another PTM, Small ubiquitin-like modifier (SUMO), also associates with protein inclusions in neurodegenerative disorders including HD, suggesting a pathologic role for SUMO

modification in neurodegenerative pathogenesis (Anderson et al., 2017; Ma et al., 2019). Further, many disease proteins themselves are SUMOylated, suggesting that the SUMO modification directly regulates protein aggregation perhaps by mediating solubility or protein-protein interactions ((Liebelt and Vertegaal, 2016), Table 1). Establishing the precise molecular mechanisms of SUMO contribution in the disease state will help inform how this PTM (and similar modifications) contribute towards maintaining protein homeostasis.

HTT is post-translationally modified at multiple residues and by diverse PTMs, with each influencing the function of normal HTT or the toxicity and clearance of mHTT (Sambataro and Pennuto, 2017). In the presence of expanded mHTT, normal modification pathways may be perturbed. There are three lysines in the 17 amino acid N-terminus of HTT preceding the PolyQ tract (referred to as N17 from hereon); K6, K9, and K15. These lysines were shown to be both ubiquitin and SUMO modified, indicating a possible competitive homeostatic balance that is further modulated by phosphorylation (O'Rourke et al., 2013; Steffan et al., 2004; Thompson et al., 2009). These studies focused on the pathogenic, N-terminal fragment of mHTT and the group has since shown that HTT may be SUMOylated further downstream with a number of potential SUMO consensus sites (O'Rourke et al., 2013). Since SUMOylation and ubiquitination are associated with HD and accumulation of mHTT, understanding the contribution of SUMO towards HD pathogenesis provided a unique opportunity to understand protein homeostasis in HD as well as identify potential targets for future disease-modifying interventions.

Like ubiquitin, SUMO is conjugated to lysine residues, typically within a ψKXE SUMO consensus motif where ψ is a hydrophobic amino acid (Liebelt and Vertegaal, 2016). Competition between SUMO and ubiquitin may mediate substrate stability and function through a tightly regulated balance between conjugation and deconjugation. Further, SUMO conjugation onto target lysines can act in concert with ubiquitin as SUMO-targeted ubiquitin ligases (STUbLs) recognize SUMOylated substrates as targets for ubiquitination and clearance (Liebelt and Vertegaal, 2016). SUMO, however, has independent roles from ubiquitin as well. Addition of SUMO on a target protein alone can activate or repress function, mediate interactions with different binding partners, or change subcellular localization. SUMO modulates transcriptional activity of several transcription factors and at the epigenetic level, modifies histones directly (Liebelt and Vertegaal, 2016). Epigenetic SUMOylation is associated with transcriptional repression of biogenesis encoding genes and serves as a global transcriptional repressor by mediating chromatin modifiers in response to DNA damage (Hendriks et al., 2015; Neyret-Kahn et al., 2013). Further, maintenance of genome stability through a key role in DDR pathways has been well established for SUMO (Schwertman et al., 2016; Su et al., 2019). To utilize the diverse functionality of SUMO, SUMO target specificity and subsequent functionality is orchestrated by a cascade of processing enzymes that activate and covalently link SUMO to substrates.

The biochemical mechanism for SUMO conjugation is similar to that of ubiquitin (Figure 1). SUMO isoforms have high sequence similarities but distinct functions. SUMO 2 and 3 are 95% identical in sequence, making it difficult to distinguish between these isoforms using traditional biochemical approaches. Therefore, they are often referred to together as

SUMO2/3. SUMO modification is highly dynamic and reversible. To initiate the conjugation cascade, SUMO proteins first undergo a maturation process by SUMO-specific proteases (SENPs, (Kunz et al., 2018)). SENPs, which are also responsible for SUMO deconjugation, first expose a C-terminal diglycine motif allowing for further downstream access for enzymatic activity. This initial step allows for discrimination between different SUMO isoforms, with different SENPs recognizing different SUMOs based on surface charge complementarity, thereby allowing transcriptional and subcellular regulation of SUMO-specific conjugation (Dorval and Fraser, 2007; Reverter and Lima, 2004). SUMO then undergoes an activation reaction with specific SUMO activating enzymes (E1 enzymes SAE1 and SAE2). This step is an ATP-dependent series of chemical reactions in which the C-terminus of SUMO is cleaved and a high-energy thioester bond formed between the E1 enzyme and the processed SUMO facilitated by a conformational change in E1 (Cappadocia and Lima, 2017).

After activation, SUMO is transferred onto the SUMO conjugating enzyme (E2) through a transthioesterification reaction with the E1-SUMO structure. There is only one known SUMO E2 ligase: Ubc9. Ubc9 is capable of conjugating SUMO to substrate proteins by interacting with the SUMOylation consensus motif but with no specificity (Liebelt and Vertegaal, 2016). However, there are several families of SUMO E3 ligases in mammals which increase substrate specificity, increase the rate of SUMOylation, and are necessary for SUMO conjugation *in vivo*. SUMO is transferred from E2 to E3 ligases through another transthioesterification reaction. With the E3 thioester-SUMO product, SUMO can be efficiently transferred onto a lysine residue of the target protein (Cappadocia and Lima,

2017). Alternatively, E3 ligases can promote optimal conformation of E2-SUMO with the substrate allowing for nucleophilic attack of the thioester bond. SUMO E3 ligases canonically possess a RING domain which is required for the ligase activity (Yunus and Lima, 2009). SUMOylation is a transient, reversible modification and SUMO can be rapidly removed by SENPs and recycled to start the conjugation process over again (Kunz et al., 2018).

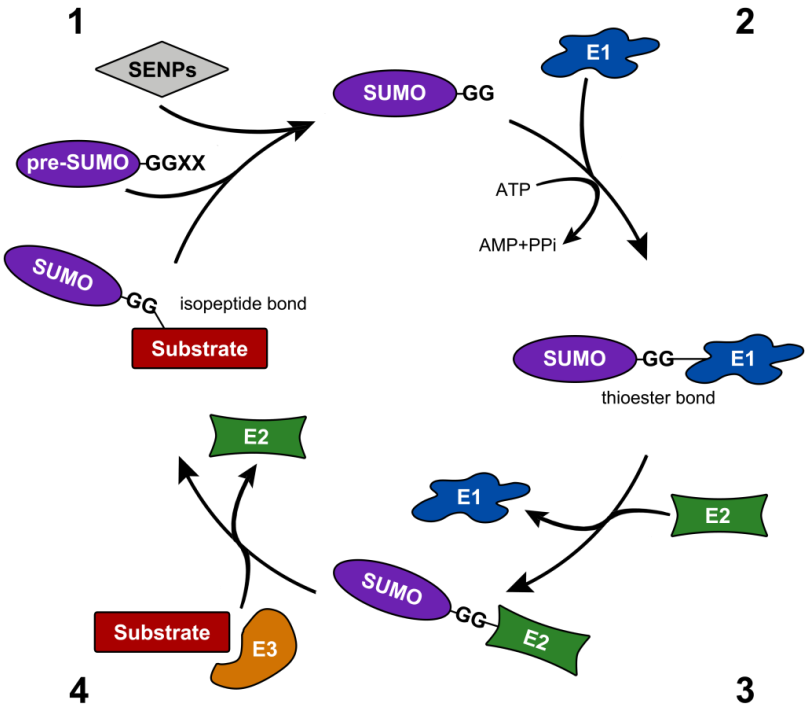

Figure 1: The SUMO conjugation pathway. 1) SUMO processing by SUMO-specific proteases (SENPs) recycles conjugated or prepares free SUMO moieties for conjugation by exposing the diglycine motif. 2) Activation of SUMO by E1 activating enzymes is ATP dependent and generates a thioester bond. 3) SUMO transfer onto E2 conjugating enzyme followed by 4) transfer to E3 ligase through transthioesterification reactions to conjugate SUMO moiety onto target substrate.

The broad repertoire for SUMO as a regulatory PTM comes from the existence of multiple E3 ligases and from the different ways substrates can be SUMOylated. Isoforms SUMO2 and

3 are known to form polySUMO chains and SUMO2 and SUMO3 may have prominent roles in the cytoplasm and in nuclear bodies respectively (Su and Li, 2002). The sequence and structure of SUMO1 prevents further conjugation of additional SUMO proteins. SUMO1 therefore is often conjugated to target proteins as a monomer or as a cap for polySUMO chains of other SUMO isoforms (such as SUMO2 or 3, (Gareau and Lima, 2010)). However, SUMO isoforms can be modified directly by ubiquitin, further increasing the functional capabilities of this PTM (Sun et al., 2007).

SUMOylation can mediate protein-protein interactions and complex formation by non-covalent binding through SUMO Interaction Motifs (SIMs, (Song et al., 2004)). SIMs are composed of a conserved sequence of four amino acids containing three hydrophobic residues (VVXV or VXVV where V=V/I) that are flanked by phosphorylatable acidic residues (Song et al., 2004; Stehmeier and Muller, 2009). Binding of SUMO is facilitated by a β-strand tertiary structure adopted by the SIM which then complements the hydrophobic β-sheet groove within SUMO in either parallel or antiparallel orientations (Cappadocia and Lima, 2017). Proteins containing a series of tandem SIMs have high affinity for polySUMO chains such as the STUbL RNF4 which ubiquitinates SUMOylated proteins for degradation by the UPS, converging SUMO and ubiquitin proteostatic pathways (Sun et al., 2007).

SUMOylation of disease-associated proteins often corresponds to a shift in solubility and aggregation propensity (Table 1). However, whether this is a direct functional role for SUMO on these target substrates or a consequence of disease-associated pathogenesis requires additional study. One possibility is that SUMO conjugation mediates protein

solubility thereby affecting levels of toxic, soluble conformations of mutant or misfolded proteins. For example, mHTT can be modified by SUMO2 which is associated with its increased accumulation and aggregation potential (O'Rourke et al., 2013). Another suggested mechanism is through sequestration of cellular components through non-covalent SIM-mediated binding to SUMOylated proteins within protein aggregates (Dorval and Fraser, 2007). A third possibility is that SUMOylation can affect subcellular localization (Borden, 2002). This might drive aggregate formation such that SUMO is a significant component of intranuclear inclusions (Ma et al., 2019). Indeed, phosphorylated N17 HTT regulates both nuclear localization and poly-SUMOylation potential of HTT (Thompson et al., 2009). Nuclear retention or subcellular mislocalization can greatly affect the transcriptional landscape in affected neurons providing an explanation of the transcriptional dysregulation often associated with neurodegenerative diseases (Dorval and Fraser, 2007). Targeting SUMO and SUMOylation machinery will help elucidate the role of SUMO in neurodegenerative diseases, including HD.

SUMO E3 ligase PIAS1 may represent a therapeutic target for Huntington's disease

To begin understanding the molecular contributions of SUMO and SUMOylated mHTT in HD and to develop a therapeutic target distinct from SUMO itself given its broad functionality, the conjugation mechanism for SUMO was investigated and of the PIAS E3 ligases, PIAS1 was identified as the form which predominantly enhanced SUMOylation by both SUMO1 and SUMO 2/3 of HTT (O'Rourke et al., 2013). PIAS1 was originally identified and named for its ability to inhibit activated STAT1 (Protein inhibitor of activated STAT1 (Liu et al., 1998)). STAT proteins are transcription factors that, when activated by

cytokines, translocate to the nucleus to activate genes associated with immune response pathways. However, PIAS1 and other PIAS isoforms (PIAS2/x, PIAS3, PIAS4/y) have several functions including serving as SUMO E3 ligases (Rytinki et al., 2009). Specifically, PIAS proteins are RING-domain containing ligases and PIAS1 interacts directly with Ubc9 through this domain to mediate the rate and substrate specificity for SUMO conjugation by either increasing Ubc9 substrate binding or orienting Ubc9 in a beneficial position for optimal transfer of SUMO (Mascle et al., 2013). As an E3 ligase, PIAS1 regulates inflammatory processes (Liu and Shuai, 2008), recruits proteins to DNA damage break sites (Galanty et al., 2009), and targets proteins for degradation by the UPS (Galanty et al., 2012).

For mHTT specifically, overexpression of PIAS1 increased accumulation of an insoluble high molecular weight (HMW) aggregate species in cell culture (O'Rourke et al., 2013). Inversely, knock-down (KD) of PIAS1 in cell culture using an siRNA against PIAS1 drastically reduced accumulated, insoluble mHTT (O'Rourke et al., 2013) indicating that PIAS1 may be a viable therapeutic target for disease intervention in HD by modulating protein accumulation. Whether PIAS1 modulation had a direct effect on SUMO modification of HTT versus through impacting the SUMO network or PIAS1 function is not yet known.

In vivo KD of Pias1 in the striatum of the R6/2 mouse model of HD showed behavioral rescue of grip strength, pole test, Rotarod, and clasping deficits, suggesting that modulation of Pias1 is behaviorally beneficial in HD animals (Ochaba et al., 2016). Overexpression of Pias1 in the striatum of a separate cohort of R6/2 mice exacerbated HD-associated behavioral deficits highlighting the molecular balance affected in the disease

state. Biochemically, KD of Pias1 in R6/2 mice significantly reduced accumulation of insoluble HMW mHTT and aggregate species of mHTT which were accompanied by reductions in both global SUMO and ubiquitin insoluble conjugates with KD. Pias1 modulation also affected levels of synaptophysin in the striatum of treated mice; reduced Pias1 restored synaptophysin levels to non-disease state, suggesting that Pias1 may be influencing synaptic proteins as well. Further, reduction of Pias1 in R6/2 mice normalized dysregulated inflammatory markers and reduced microglial activation suggesting that the function of Pias1 in innate immunity may be altered in HD (Ochaba et al., 2016). This was accompanied by restoring nuclear localization of NfκB, negatively regulated by Pias1, potentially freeing NfκB to function as a transcription factor for proinflammatory pathways, and providing a possible mechanism of action for Pias1 in HD for restoring disease-associated dyshomeostasis. However, the exact mechanisms of Pias1 in HD remained unresolved.

PIAS1 contains several functional domains (Figure 2.1). SUMO E3 ligase activity, as discussed, is mediated through the RING domain. This domain is also crucial for protein-protein interactions and specific ligase functionality includes the interaction with Ubc9 mediated through several cysteines within the RING domain (Kahyo et al., 2001). Mutation of these cysteines produces a ligase-dead, functionally null PIAS1 protein (Lee et al., 2003; Yurchenko et al., 2006). If direct SUMOylation of mHTT by PIAS1 mediates aggregation propensity, it would therefore be hypothesized that a ligase-dead PIAS1 would not promote HMW mHTT accumulation when overexpressed. In addition to the RING domain mediating ligase activity, PIAS1 interaction with Ubc9 is mediated in part through the SIM

domain following the RING domain, in a ternary complex with a SUMO moiety (Mascle et al., 2013). The SIM within PIAS1 may therefore aid in proper loading and stabilization of the Ubc9-SUMO structure for optimal transfer of the SUMO moiety onto a substrate protein (Cappadocia and Lima, 2017). It is therefore possible that the PIAS1 SIM is important for mediating adequate SUMOylation of PIAS1 substrates such as HTT, thereby mediating accumulation of mHTT protein.

While overall SUMOylation may contribute to protein stability and turnover, it is possible that SUMOylation also may regulate proteostatic balance of transcriptional regulators. SUMOylation of transcription factors often serves as a negative regulator of transcription (Rosonina et al., 2017). In the nervous system specifically, numerous transcription factors that drive neuronal identity and survival genes are regulated by SUMO (Table 2). Therefore, SUMOylation may be an integral component of disease associated transcriptional dysregulation. PIAS1 specifically has been identified as the E3 for many of these factors (Estruch et al., 2016; Gregoire and Yang, 2005; Riquelme et al., 2006; Tai et al., 2016) indicating that it could play a crucial role in mediating neuronal development, survival, and identity.

In addition to directly modulating transcription of neuronal genes, SUMOylation also contributes to the structure and function of neurons at the synapse (Henley et al., 2018; Schorova and Martin, 2016). Specifically, purified synaptosomes are enriched for SUMO-modified proteins (Feligioni et al., 2009) suggesting that SUMO may modify components of the synapse directly. Indeed, dozens of synaptic proteins have been identified as putative

SUMO substrates although through unknown E3 ligases (Table 3). For some of these substrates, SUMOylation modulates synaptic excitability suggesting that SUMO plays a neuroprotective role to prevent excitotoxic events in response to neuronal injury (Peters et al., 2017). Therefore, dysregulated SUMOylation at the synapse may contribute to neuronal dysfunction observed in neurodegenerative disease. At the pre-synaptic terminal, PIAS1 serves as an E3 ligase for glutamate receptors though with unknown functional consequences (Dutting et al., 2011; Tang et al., 2005). It is therefore possible that a direct role for PIAS1 exists at the synapse, mediating localization or protein-protein interactions to contribute to neuronal function.

Another well characterized function for SUMO and related PTMs is in mediating DNA damage repair (DDR) pathways (Schwertman et al., 2016; Su et al., 2019). While the majority of these functions have been defined in dividing cells with major implications for cancer therapeutics (Han et al., 2018), little is known about their role in maintaining neuronal genomic homeostasis. SUMOylation of DDR factors in dividing cells has numerous functions ranging from nuclear localization and factor recruitment to degradation, and often involves PIAS1 or other PIAS family members for SUMOylation (Table 4). While many of these functions contribute to Homologous Recombination (HR), which requires the presence of the sister chromatid during replication, several contribute to repair processes that may be utilized in non-dividing cells. Neurons accrue DNA damage over time and lack access to repair mechanisms that require DNA replication (Abner and McKinnon, 2004; McKinnon, 2009). Further, inclusion bodies have been reported to contain DDR proteins associated with SUMO (Ma et al., 2019). Therefore, it is critical to begin to elucidate the

possible roles for SUMOylation in neuronal DDR mechanisms, particularly given the overwhelming current evidence linking DNA damage repair mechanisms to disease pathogenesis in HD (Flower et al., 2019; GeM-HD, 2015; Massey and Jones, 2018; Moss et al., 2017). Given that DDR factors modulate AO of HD, the HTT protein serves as a scaffold for repair factors, and that PIAS1 also participates in repair mechanisms, it is possible that SUMOylation by PIAS1 is modulating repair pathways in the brain.

DNA damage and SUMOylation; implications in HD and the Nervous System

DNA damage repair (DDR) pathways help guarantee the fidelity of our genetic code. Mutations in repair factors involved in these pathways have been linked to numerous diseases; particularly cancer but including anemias, developmental neuropathologies, and neurodegenerative disorders ((McKinnon, 2017), Table 5). Further, DDR contributes to pathogenesis of neurodegenerative diseases, including HD, even in absence of mutations of repair factors (Maiuri et al., 2019). In replicating cells, viable and robust repair mechanisms are crucial for passing genetic information onto sister cells and therefore have been extensively studied in the context of immortalized or cancerous cell lines. However, non-replicating cells such as neurons face a different type of genetic hurdle: maintaining genetic stability without the chance of DNA being replenished. Post-mitotic cells are at risk for generating and accumulating DNA damage overtime which needs to be repaired without a template chromosomal copy that is available during mitosis. Neurons in particular are especially vulnerable to damage as they are highly active and produce more DNA damaging reactive oxygen species (ROS) compared to other cell types (Barzilai, 2007). The high transcription rate of neurons also makes them more prone to damage and mutagenesis

(Jinks-Robertson and Bhagwat, 2014) leading to the hypothesis that sustained DNA damage may be linked to aging and neurodegenerative disorders (Chow and Herrup, 2015). Direct evidence about how DNA repair mechanisms function in neurons and the brain specifically is hard to come by due to the inaccessibility of these cell types for experimental manipulation. However, numerous studies using genetic animal models have characterized key components involved in maintaining genomic integrity in the brain (Madabhushi et al., 2014) and have shed light on the repair mechanisms utilized by post-mitotic neurons.

DDR pathways encompass a large array of intricate cellular response networks that have evolved to respond to numerous types of DNA damage. Endogenous damage can include double stranded breaks (DSB), single-stranded breaks (SSB), DNA:RNA hybrid structures (R-loops), mismatches, slipped hairpin loops, or base modifications such as oxidation (Figure 2A). Upon DNA damage accrual, a series of steps initiates to recognize and repair the lesion in several distinct pathways. The initial damage site is first recognized by "sensor" proteins which signal to "transducers" to propagate the response signal to downstream "effectors". The canonical transducers for DDR are ATM (ataxia-telangiectasia mutated) and ATR (ataxia-telangiectasia and RAD3-related), with ATR primarily acting in replication-related repair (Marechal and Zou, 2013). Through signaling cascades, downstream "effectors" are recruited to process and repair the DNA (Barzilai, 2007). This cascade relies heavily on protein-protein interactions and PTMs to activate, recruit, and evict repair factors in a delicate balance. Disruption of this balance often leads to diseases including cancer and a variety of neuropathies ((McKinnon, 2017), Table 5).

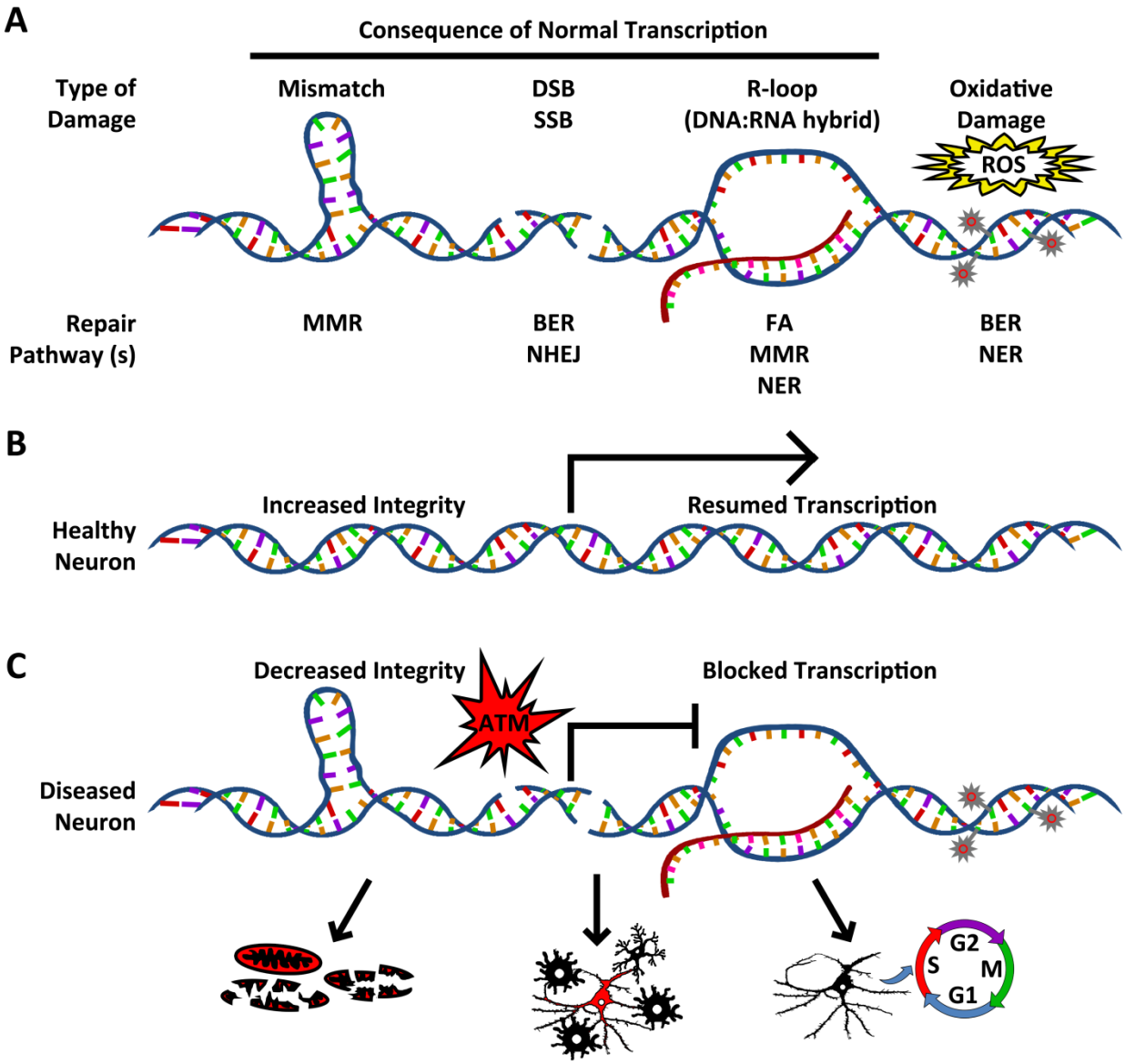

Figure 2: Accrual of damage and consequences in neurons. A) Several types of DNA damage can be caused by active transcription in neurons as well as from high production of ROS. Damage can prevent transcription leading to neuronal malfunction. Several pathways have been shown to repair these types of lesions, many of which have been linked to neurodegenerative diseases. B) In a healthy neuron, DNA is repaired, increasing genomic stability allowing transcription to resume. C) In a diseased neuron, repair is either impaired or aberrantly contributes to decreased genomic integrity. This leads to further blockage of transcription and hyperactivation of signaling pathways such as ATM. Potential consequences of unrepaired DNA include mitochondrial malfunction and apoptosis, persistence in a senescent like state which might trigger neuroinflammation, or attempted re-entry into the cell cycle which could result in abortive cell death.

Base and Nucleotide excision repair: Damage to individual bases due to oxidative metabolism relies primarily on the base excision repair pathway (BER). The overproduction of ROS in neurons leaves DNA at risk for oxidative damage which can serve as a major road block for cellular processes if left unresolved (Crouch and Brosh, 2017). The BER pathway functions to correct such damage through use of DNA glycosylases (each serving as a sensor for a specific lesion type) to remove the modified base and repair the remaining single strand DNA (Jacobs and Schar, 2012). After recognizing the specific damaged nucleotide, glycosylases remove it, leaving a break behind. This break is subsequently processed by the endonuclease APE1 to prepare it for ligation. PNKP is another end processing enzyme that classically participates in BER to resolve oxidative damage by phosphorylating the 5' and dephosphorylating the 3' nucleic acid at the break site to prep for re-ligation (Jilani et al., 1999). This damage site is subsequently filled in and ligated by DNA polymerases and ligases, scaffolded by XRCC1 (Krokan and Bjoras, 2013; Svilar et al., 2011).

Longer stretches of nucleotides or larger structural, transcription-impeding DNA lesions can be excised and repaired by the similar nucleotide excision repair (NER) pathway. NER often functions in conjunction with transcription (Marteijn et al., 2014) as the main form of transcription-coupled repair (TCR) which removes bulky adducts or lesions on the template DNA strand that impede RNA polymerase progression (Spivak and Ganesan, 2014). After the damage is recognized, the NER effectors excise a stretch of 22-35 nucleotides surrounding the damage site leaving single strand DNA behind which is then filled by components of the BER pathway such as PCNA, XRCC1, or a number of DNA

polymerases. XRCC1 is a SUMO substrate and SUMOylation of XRCC1 is necessary to recruit DNA polymerase β for efficient repair (Hu et al., 2018). The yeast homolog of PIAS1, Siz1, is known to SUMOylate PCNA requiring its PINIT domain to do so (Yunus and Lima, 2009) indicating that SUMO is a key mediator of BER and NER pathways.

Base excision repair has been implicated in HD pathogenesis in several ways. Accumulation of ROS in fibroblasts of HD patients leads to an increase in damaged DNA in an expanded repeat dependent manner (Giuliano et al., 2003). Metabolic dysfunction and oxidative stress is observed in HD post-mortem brain, with increased oxidative damage recorded in caudate compared to age-matched control samples, suggesting a BER dysregulation under HD-associated genotoxic stress (Browne et al., 1997). Notably, repair of oxidized nucleotides through the BER pathway is linked to somatic expansion of the HD-associated CAG repeat in mice (Kovtun et al., 2007; Mollersen et al., 2012). Additionally, HTT itself functions as a scaffold for the ATM-mediated BER pathway in retinal epithelial cells and human HD patient derived immortalized fibroblasts, mediated through phosphorylation of HTT N17 as a functional consequence of sensing ROS (DiGiovanni et al., 2016). HTT localization at the site of damaged chromatin under oxidative stress requires ATM activity and HTT co-localizes with the BER endonuclease APE1. In addition to co-localizing with APE1, HTT interacts with other components of the BER pathway: XRCC1, FEN1, and phosphorylated ATM (Maiuri et al., 2017). Overall, recruitment of mHTT to damage sites but with a decreased repair response suggested a dominant negative gain of function for mHTT in DNA damage by failure to mediate adequate repair.

Transcription Coupled Repair: As mentioned, NER is utilized frequently to repair transcription-induced DNA strand breaks (Spivak and Ganesan, 2014). However, transcription-coupled repair (TCR) more broadly repairs several types of DNA lesions that can arise from active transcription and often samples from numerous distinct repair processes to do so. Actively transcribing genes are more exposed to endogenous damage causing agents due to the unwound state of DNA bound to polymerases and DNA breaks can form as a normal consequence of transcription (Jinks-Robertson and Bhagwat, 2014). Specifically, topoisomerases serve to maintain the topology of DNA during transcription by inducing breaks to remove torsional stress from the DNA and prevent hyper winding. Different types of topoisomerases result in single strand (SSB) and double strand (DSB) breaks which then need to be repaired to maintain genome integrity, with aberrant activity contributing to cellular malfunction (McKinnon, 2016; Pommier et al., 2016; Vos et al., 2011). In addition to being necessary to relieve torsional stress on DNA, strand breakage mediated by topoisomerases induces expression of immediate early genes. In the brain, these genes are necessary for synaptic strengthening in response to activity (Madabhushi et al., 2015). Therefore, in addition to chemical insults on DNA, in actively transcribing and terminally differentiated cells such as neurons, DNA breaks are acquired as a consequence of normal transcription (Madabhushi et al., 2015; McKinnon, 2017) and TCR serves as a response mechanism to combat accrual of these lesions and maintain genomic integrity.

Stalled RNA polymerase serves as the initial sensor for downstream TCR pathways. In an ATP-dependent manner, TCR effectors are recruited by interacting with the stalled polymerase (Laine and Egly, 2006). The first effectors to be recruited are the Cockayne

syndrome proteins (CSA and CSB) which serve to alter the topology of the DNA near the damage site and recruit additional factors (Beerens et al., 2005). SUMO may be involved in mediating this initial process as a potential intermediate degradation signal for CSB (Lecona et al., 2016; Sin et al., 2016). Downstream repair factors from other pathways such as NER and BER are then recruited to remove the lesion and repair the damaged DNA (Pani and Nudler, 2017). To resolve SSBs that arise from active transcription, BER is primarily utilized (Abbotts and Wilson, 2017). CSB can promote BER protein scaffold XRCC1 (Menoni et al., 2018), which utilized end processing enzyme PNKP to facilitate repair (Chakraborty et al., 2015).

Mutations in CSA and CSB result in the premature aging disease Cockayne syndrome, with CSB mutations leading to syndrome-associated neuropathies (Table 5). While traditional TCR utilizes NER proteins, CSA and CSB proteins can work to repair strand breaks (both DSB and SSB) that arise from active transcription (Pascucci et al., 2018; Wei et al., 2015). Therefore, TCR may more broadly be applied to any type of damage that arises as a consequence of transcription and may sample repair factors from additional pathways to maintain genome integrity, especially in the aging brain.

Double Strand Break repair: Two canonical and powerful pathways serve to repair DSBs: Homologous recombination (HR) and Non-homologous end-joining (NHEJ). HR depends on the presence of a sister chromatid, serving as a template for the site of DNA damage (Prakash et al., 2015). Therefore, HR operates only in the S and G2 phases of the cell cycle making this repair system inaccessible in senescent and post-mitotic cells. Unlike HR, NHEJ

does not require a template for the repair process. Instead, NHEJ brings each end of the damaged site together and reseals the DNA by direct ligation, making this system more error prone (Chiruvella et al., 2013). HR is utilized in proliferating or differentiating neurons and defects in this pathway have been linked to neurodevelopmental disorders (Abner and McKinnon, 2004). While there is a need of a template for HR, fully differentiated neurons rely heavily on NHEJ over HR to combat DSBs.

Signaling cascades to repair DNA strand breaks are activated by initial epigenetic changes at the site of damage. Breaks are first recognized by the sensor MRN complex which activates ATM as a transducer (Marechal and Zou, 2013; Petrini and Stracker, 2003). Activated ATM subsequently phosphorylates serine 139 on the histone H2AX (Rogakou et al., 1998). Referred to as γH2AX, this epigenetic alteration marks damage sites as nuclear foci, ultimately recruiting downstream repair factors. The phosphorylation of H2AX is propagated along chromatin adjacent to the break site due to interaction of the protein MDC1 (Lou et al., 2006). SUMOylation of MDC1 is necessary for recruitment of further downstream repair factors and subsequent ubiquitination and clearance of MDC1 from repair sites (Luo et al., 2012). MDC1 is also phosphorylated by ATM which allows for additional epigenetic modifications near the DNA break site. These changes are key for recruiting 53BP1 or BRCA1 which act as competing crossing guards for NHEJ over HR respectively (Bunting et al., 2010). Recruitment of 53BP1 has been shown to be SUMO-dependent and 53BP1 itself is SUMOylated (Galanty et al., 2009), suggesting that a depletion in SUMO or SUMOylation of 53BP1 may mediate activation of HR repair.

In mammalian cells, NHEJ is initiated by the recruitment of the Ku complex to sites of DSB marked by γH2AX (Mischo et al., 2005). The Ku complex consists of a heterodimer of Ku70 and Ku80 which protects broken DNA ends and recruits additional effectors. End-processing factors including DNA-dependent protein kinase (DNA-PKc), which serves as an additional transducer, and the nuclease Artemis are recruited to trim 5' and 3' overhangs at the damage site, prepping the ends for ligation (Ma et al., 2002). PNKP has also been shown to participate in end processing of NHEJ facilitated repair including those arising from active transcription (Chakraborty et al., 2016; Chappell et al., 2002). After adequate end-trimming, DNA binding proteins including XRCC4 bring the broken ends within mending proximity. XRCC4 has been shown to be SUMOylated by PIAS1 and PIAS2 with SUMOylation being critical for its nuclear localization (Yurchenko et al., 2006). XRCC4 forms a tight complex with DNA ligase IV to facilitate strand ligation (Chiruvella et al., 2013).

Deficits in DSB repair are suggested in HD, based in part on the observed increased of strand breaks in patient striatum as defined by elevated levels of γH2AX (Enokido et al., 2010). This may be due to the interaction between Ku70 and HTT in a mutation dependent manner, which leads to sequestration of Ku70 in mHTT intranuclear inclusions and increased presence of DSBs (Enokido et al., 2010). Overexpression of Ku70 in R6/2 mice rescued behavioral deficits and reduced the number of DSB detected *in vivo*. Therefore, inability to repair DSB may contribute to HD pathogenesis.

Fanconi Anemia: Another potential consequence of transcription is the formation of DNA:RNA hybrids, or R-loops. These are structures that form when the recently transcribed RNA transcript anneals to the DNA template leaving the unannealed strand vulnerable to additional damage and lead to genome instability if left unresolved (Aguilera and Gomez-Gonzalez, 2017; Freudenreich, 2018; Jinks-Robertson and Bhagwat, 2014). Both the Fanconi Anemia (FA) and TCR pathways can repair these structures (Garcia-Rubio et al., 2015; Sollier et al., 2014). While the FA pathway was canonically defined to resolve interstrand crosslinks (ICL) which can form from agents endogenously produced by cellular processes such as aldehydes, recent work has characterized its contribution to resolving R-loops, indicating this pathway contributes to preventing transcription-coupled genome instability (Okamoto et al., 2019; Schwab et al., 2015).

The initiating component of the ICL-repair FA pathway is lesion sensing by a FANCM-containing complex followed by ATR-mediated signaling transduction. This initiating factor recruits a large core complex with ubiquitin ligase capability (Ceccaldi et al., 2016) which is necessary for the monoubiquitination activation of effectors FANCD2 and FANCI to drive the FA repair process (Miles et al., 2015). Activated FANCD2 is required for nucleolytic incisions near the damage site and recruiting endonucleases necessary for unhooking lesions (Klein Douwel et al., 2014; Knipscheer et al., 2009). Another key function of monoubiquitinated FANCD2 is the interaction with FAN1, an additional nuclease which is critical for locating the lesion, unwinding, and orienting the DNA to promote incisions (Zhao et al., 2014). Monoubiquitinated FANCD2 and FANCI are SUMOylated by PIAS1/4 and subsequently recognized by the STUbL RNF4 and polyubiquitinated resulting in

eviction from repair sites (Gibbs-Seymour et al., 2015). After lesions are removed, polymerases are recruited to the site to facilitate error prone repair by bypassing the lesion and leaving behind possible point mutations, but generating an intact DNA duplex that subsequently utilized proteins in the HR repair pathway to mend DNA (Long et al., 2011; Prakash et al., 2015). Repair factors from the TCR and mismatch repair (MMR, below) pathways are utilized by the FA pathway to repair transcription-associated lesions (Datta and Brosh, 2019; Ravikumar et al., 2004; Williams et al., 2011).

The FA pathway was implicated in HD pathogenesis with the identification of the nuclease FAN1 as a genetic modifier of HD onset. Two significant single nucleotide polymorphisms at the *FAN1* locus on chromosome 15 were uncovered using GWAS: one corresponded to 6.1 years early onset of clinical HD while the other delayed onset by 1.4 years (Bettencourt et al., 2016; GeM-HD, 2015). The identification of inversely affecting variants within the same genetic modifier suggests that a robust and functional DNA repair mechanism may help carry the burden of DNA damage and delay clinical onset of disease. Indeed, FAN1 stabilizes trinucleotide repeat expansions, including that within *HTT* (Goold et al., 2019; Zhao and Usdin, 2018). Therefore, a robust and accurate repair system serves a protective role in post-mitotic cells by maintaining genomic stability. In disease, these pathways may be out of balance and suggests that facilitating appropriate repair may be therapeutically beneficial.

Mismatch Repair: Mismatch repair (MMR) is utilized to address structural abnormalities that arise from misaligned or slipped DNA after replication or transcription. These

structures are similar to R-loops which MMR also serves to resolve (Freudenreich, 2018). While mismatches can occur during replication, MMR is preferentially used to safeguard stability of actively transcribing genes and can utilize TCR components to do so (Huang and Li, 2018). Though in the case of repeat-expansions, may inadvertently contribute to genome instability (Schmidt and Pearson, 2016).

MMR is initiated with recognition of the mismatch by sensors MutSα or MutSβ, heterodimers composed of Msh proteins (Kunkel and Erie, 2005) which then facilitates interaction with downstream transducers and effectors including PCNA and Mlh proteins. MutLα (Mlh and Pms-containing protein) activates MutH to nick the nascent DNA strand at the mismatch (Acharya et al., 2003; Au et al., 1992). Exonuclease Exo1 is recruited as an effector to excise the mismatch and allow for DNA polymerases to fill the gap using the parental DNA strand as a template (Liberti et al., 2013; Longley et al., 1997; Tishkoff et al., 1998). DNA ligases then completes repair by ligating the newly synthesized DNA at the nick site (Kunkel and Erie, 2005).

In HD, MMR facilitates somatic-repeat expansion within the *HTT* gene (Schmidt and Pearson, 2016). Since expansion of the CAG-repeat in HD-patient cortex serves as a predictor of disease onset (Swami et al., 2009) and greater expansion is observed in brain regions most overly affected by disease (Telenius et al., 1994) the mechanism of somatic repeat expansion has been extensively investigated. Nucleotide repeats are unstable: they are prone to slip upon annealing (Pearson et al., 2002), leading to a misalignment that is aberrantly targeted by MMR which further contributes to instability. Longer repeat regions

lead to larger slip-formed structures and therefore may be more mutagenic (Pearson et al., 2002) with the probability of slippage increasing in a repeat-length associated manner (Pearson et al., 1997). MMR protein Msh2 preferentially binds disease-relevant CAG-repeat lengths providing a possible selective function for DDR in promoting trinucleotide expansion through inappropriate repair in non-replicating cells (Pearson et al., 1997; Shelbourne et al., 2007).

In addition to genetic variants within *FAN1* associating with altered AO identified by GWAS, a modifier locus within the MMR gene *MLH1* also associated with a 0.7-0.9 year exacerbation in HD AO (GeM-HD, 2015; Lee et al., 2017). While the functional consequences of variants within the *MLH1* locus are yet to be defined, earlier GWAS studies in HD mouse models had identified *Mlh1* as a genetic variant associated with *HTT CAG* repeat instability (Pinto et al., 2013). Identification of genetic variants at the human *MLH1* locus therefore strengthened the negative association of MMR and disease pathogenesis driven by somatic repeat expansion as genetic ablation of *Mlh1* in mice stabilizes the *HTT CAG* (Pinto et al., 2013). In a separate GWAS study, the variants within the MMR gene *MSH3* were associated with HD progression in human patients (Moss et al., 2017). An associated *MSH3* variant corresponded with decreased *MSH3* expression, a reduced rate of somatic expansion, delayed onset, and slower disease progression (Flower et al., 2019; Moss et al., 2017). Several genetic studies in mouse models of HD define how MMR genes might mediate somatic repeat expansion.

In HD knock-in mice with ~111 repeats, genetic ablation of MMR gene *Msh3* (part of the MutSβ sensor) prevented striatal somatic repeat expansion of the *Htt* CAG (Dragileva et al., 2009). Deletion of MMR gene *Msh2* (part of the MutSα sensor) in the same model similarly prevented expansion and delayed appearance of intranuclear inclusions (Wheeler et al., 2003). Removing *Msh2* in MSNs specifically yielded similar results, providing evidence that aberrant MMR in neurons may be driving the observed outcomes (Kovalenko et al., 2012). In addition to slipping, repeat expansions that are GC rich are prone to forming R-loops leading to decreased stability. This is observed in HD-associated CAG repeats and MMR aberrantly repairs these structures (Freudenreich, 2018).Together these studies highlight how some repair pathways may be hijacked in the presence of expanded repeats, leading to inappropriate repair and further expansion. This suggests that mediating these repair pathways to restore appropriate repair in neurons would be therapeutically beneficial.

It is notable that while many studies implicate DNA repair in mediating genomic instability or disease pathogenesis in the brain, less is known about the exact mechanistic contributions of repair factors towards the repair process. For example, PIAS isoforms have several unique or overlapping roles in DNA damage signaling cascades but due to expression profiles, PIAS-specific functionality may be mediated by distinct isoforms in different cellular contexts. For instance, PIAS1 is the most abundantly expressed family member in the brain and notably in the caudate (Human Protein Atlas) indicating that DNA damage pathways in specific brain regions may rely heavily on one PIAS isoform over the other. Further, since there have been few studies investigating the contribution of PIAS1 towards these pathways in non-dividing cells, it is possible that the exact functional

components may be tissue specific or recycled between canonically distinct repair mechanisms. Therefore, it is important to understand what repair mechanism may be being utilized by post-mitotic neurons. Determining how PIAS1 may be contributing to maintaining genomic stability in the brain will begin to elucidate these mechanisms.

Consequences of unrepaired DNA towards neuronal viability

In normal, healthy neurons, repair pathways maintain genomic integrity to allow for transcription and function (Figure 2B). Loss of adequate repair or facilitation of inappropriate repair can lead to neuronal malfunction and potentially degeneration. However, the exact mechanisms contributing towards these potential outcomes remain unclear but several possibilities have been proposed (Figure 2C). Neurons with elevated damage also have activated caspase-3 suggesting that accrual of DNA damage in neurons can lead to an activation of cell-death pathways (Chechlacz et al., 2001). This is likely caused by upstream ATM and p53 signaling leading to mitochondrial dysfunction and activation of apoptosis (Chong et al., 2000; Gilman et al., 2003; Herzog et al., 1998; Martin and Liu, 2002). Therefore, diseased neurons accruing damaged DNA may elicit aberrant ATM signaling leading to pro-apoptotic signaling. Supporting this theory, in both HD patient neurons and zQ175 mouse cortex and striatum with decreased repair, a hyperactivation of ATM and p53-related pathways with accrual of damaged DNA was recently observed (Gao et al., 2019). Caspase activation has long been considered a contributor or marker of neurodegenerative associated cell death in HD (Wang et al., 2015). Activation of caspases due to induction of DDR pathways therefore suggests a potential direct consequence of damaged DNA in neurons (Figure 2C).

Activation of the ATM pathway upon accumulation of DNA damage may also activate the cell-cycle in an effort for neurons to manage the detrimental load (Folch et al., 2012). DNA damage is closely linked to cell-cycle control. Increased expression of cell-cycle specific proteins is documented in multiple neurodegenerative diseases including HD (Chow and Herrup, 2015; Fernandez-Fernandez et al., 2011; Pelegri et al., 2008), potentially facilitating "re-entry" into the cell-cycle followed by delayed cellular death. Expression of these cell-cycle proteins can be induced by DNA damage in the brain (Fielder et al., 2017) and may be linked to the observed increased aneuploidy in aging and diseased brains indicating active DNA replication in post-mitotic cells (Chow and Herrup, 2015; Fielder et al., 2017; Katchanov et al., 2001). Cells attempting to replicate highly damaged DNA are then at risk for replication stress, with genomic instabilities being incompatible with normal cellular homeostasis resulting in abortive cell death (Yurov et al., 2011). Aberrant cell-cycle re-entry triggered by DNA damage in post-mitotic cells would therefore be unsustainable and lead to degeneration (Figure 2C).

Alternatively, neurons may be able to prevent cell-cycle re-entry through expression of cell-cycle inhibitors even under persistent low-level DNA damage. Therefore, instead of abortive cell death, neurons may enter a senescent-like state which allows for prolonged survival but may unintentionally promote neuronal malfunction (Fielder et al., 2017). Cellular senescence can be induced by persistent DNA damage mediated by ATM, p53 and expression of cell-cycle inhibitor p21 by inhibiting p53-mediated apoptosis (Mallette and Ferbeyre, 2007; Passos et al., 2010; van Deursen, 2014). Persisting in a senescence-like state can lead to downstream mitochondrial and neuronal malfunction by compromising

cellular metabolism and synaptic function (Fielder et al., 2017). Additionally, senescing neurons trigger the production of pro-inflammatory markers. A hallmark of senescence is the presence of the senescence associated secretory phenotype (SASP) which includes production of inflammatory cytokines, such as IL-6, which is mediated by NFkB signaling (Fielder et al., 2017; Rodier et al., 2009). This can lead to neuronal malfunction as elevated IL-6 results in an imbalance of excitatory and inhibitory synaptic transmission (Wei et al., 2012). Meanwhile, SASP can signal to neighboring cells and has been suggested to be linked to the observed neuroinflammatory profiles of AD and PD (Chinta et al., 2015). It is therefore possible that persistent DDR signaling may be intimately linked to neuroinflammatory-mediated cell death in the brain by activating microglia (Fielder et al., 2017). Overall, while entering a senescent state may be initially pro-survival for neurons accruing DNA damage, the downstream negative consequences of senescence can contribute to neuronal malfunction and ultimately contribute to the observed neuropathologies in degenerative diseases (Figure 2C).

SUMMARY

Huntington's disease is caused by a CAG-repeat mutant expansion within the *HTT* gene, leading to a plethora of downstream pathologies and molecular dyshomeostasis. Accumulation of mHTT conformers associates with disease progression and may in part contribute to the observed atrophy in HD patient brains. However, due to the biochemical heterogeneity of different conformers such as soluble oligomers and insoluble fibrils, preclinical assessments often exhibit variable results. Characterizing the temporal formation of each form using a variety of established lysis buffers has not been

systematically evaluated in parallel. Establishing a baseline for different mHTT conformers would be a valuable resource for researchers interpreting preclinical studies including those modulating PIAS1.

The post translational modification SUMO is implicated in HD and PIAS1, serving as a SUMO E3 ligase for the HTT protein, may serve as a potential therapeutic target through its ability to mediate HD-associated phenotypes including accumulation of insoluble mHTT. However, the exact function of PIAS1-associated SUMOylation in the context of HD is unknown. SUMO may serve to mediate solubility and aggregation propensity of disease-associated proteins.

Additionally, SUMO and PIAS1 may be contributing to DDR mechanisms in the brain. Deficits or inaccuracies in repair pathways contribute to HD pathogenesis and AO, suggesting that imbalances in maintaining genomic stability contribute to neurodegenerative disease. In replicating cells, SUMO and PIAS proteins contribute towards maintaining genomic homeostasis by mediating DNA damage response pathways. Post-mitotic neurons can readily accrue damage, likely as a consequence of active transcription and the increased metabolic activity of neurons resulting in ROS production (Figure 2). With numerous pathways serving to repair damaged DNA, many have been shown to be implicated in HD, driving disease pathogenesis either by contributing to somatic repeat expansion or overall genomic instability in the brain. Decreased genomic stability can lead to neurodegeneration or neuronal malfunction in several potential ways. Hyperactivation of DDR signaling pathways may also lead to further imbalances and

contribute to detrimental downstream consequences. Defining a function for PIAS1 in neuronal DDR will aid in understanding what repair pathways are contributing to disease pathogenesis, and how.

Data provided in my dissertation describes a novel modulatory role for PIAS1 in regulating DNA damage repair pathways. This may represent a separate function from contributions to accumulation of mHTT, with baseline molecular landscapes driven by either disease progression or inflammatory insults dictating the potential outcome of PIAS1 modulation in the brain. This also supports a pleotropic role for PIAS1 which should be strongly considered for timing and context of clinical intervention. However, my thesis provides evidence that PIAS1 is a key component of transcription-coupled DNA damage repair by serving as an E3 ligase for the end processing enzyme PNKP. Though the mechanistic contribution of PNKP SUMOylation remains to be elucidated, reducing PIAS1 in HD patient neurons and HD mouse striata restores PNKP enzymatic activity, normalizes aberrant transcription, and may potentially stabilize the CAG-repeat within *HTT.* This suggests that PIAS1-associated repair pathways may be aberrantly activated and out of balance in HD with KD serving to restore accurate repair and transcription. Since both protein accumulation and perturbed DNA damage repair are implicated in other neurodegenerative diseases, data presented here may be applicable to overall degenerative mechanisms in the brain.

INTRODUCTION

TABLES

Table 1: SUMO modification in neurodegenerative disease

Neurological disorder	SUMO substrate	Functional Consequence	Reference(s)
Huntington's disease	HTT	Increased protein stability	(O'Rourke et al., 2013; Steffan et al., 2004)
Parkinson's disease	α-synuclein	Inhibits aggregation and toxicity	(Abeywardana and Pratt, 2015; Krumova et al., 2011; Shahpasandzadeh et al., 2014)
	DJ-1	Promotes insolubility	(Shinbo et al., 2006)
Alzheimer's disease	Amyloid-β	Decreases production	(Takahashi et al., 2008; Yun et al., 2013)
	Tau	Inhibits degradation	(Luo et al., 2014)
Ischemia	Drp1	Prevents caspase-mediated cell death	(Guo et al., 2013)
DRPLA	Atrophin-1	Enhanced aggregation	(Terashima et al., 2002)
SBMA	Androgen Receptor	Unknown	(Mukherjee et al., 2009)
SCA -1	Ataxin-1	Enhanced aggregation	(Ryu et al., 2010)
	Ataxin-3	Increased stability, Decreased aggregation	(Zhou et al., 2013)
	Ataxin-7	Increased protein stability, degradation	(Janer et al., 2010)
ALS	SOD1	Increased protein stability and aggregation	(Fei et al., 2006; Niikura et al., 2014)
	EAAT2	Promotes accumulation	(Foran et al., 2011)

Table 2: SUMO modification of neuronal transcription factors

Substrate	E3	SUMO isoform	Pathway	Function of SUMOylation	Reference(s)
MEF-2A	PIASx	SUMO1	postsynaptic differentiation	Represses transcription	(Shalizi et al., 2007; Shalizi et al., 2006)
MEF-2A	PIAS1	SUMO1, 2	postsynaptic differentiation	Represses transcription	(Gregoire and Yang, 2005; Riquelme et al., 2006),
MEF-2C	PIASxB	SUMO1, 2	Excitatory synapse repression	Represses transcription	(Gregoire and Yang, 2005; Kang et al., 2006)
MEF-2D	Unknown	SUMO1, 2	Neuronal differentiation	Represses transcription	(Gregoire and Yang, 2005)
c-Fos	PIASxB	All	Transcription (proliferation, response to stress)	Represses transcription	(Bossis et al., 2005)
c-Jun	Unknown	SUMO1	Transcription	reduces transactivation activity	(Muller et al., 2000)
p53	Unknown	SUMO1	Transcription	impairs apoptotic function	(Muller et al., 2000)
MeCP2	Unknown	SUMO1	Transcription for Synaptic development	represses transcription	(Cheng et al., 2014)
MeCP2	PIAS1	SUMO1	Transcription for Synaptic development	K412 enhances Bdnf expression	(Tai et al., 2016)
CREB	PIAS1	SUMO1	Transcription, memory formation	K290 enhances Bdnf expression	(Chen et al., 2014)
FOXP2	Unknown	SUMO1, 3	Brain development of speech and language areas	Represses transcription	(Meredith et al., 2016)
FOXP2	PIAS1	All	Brain development of speech and language areas	No mechanism determined	(Estruch et al., 2016)
FOXP2	PIAS3	SUMO1, 2	Brain development of speech and language areas	Promotes neuronal maturation	(Usui et al., 2017)

Table 3, part 1: Synaptic SUMOylation substrates

Substrate	E3	SUMO isoform	Pathway	Function of SUMOylation	Reference(s)
GluR6/GluK2	PIAS3	SUMO1	Post-synaptic inhibitory	Stimulates endocytosis of the kainate receptor	(Chamberlain et al., 2012; Martin et al., 2007)
CASK	Unknown	SUMO1	synaptic transmembrane protein anchoring, spine morphology	Inhibits spine formation	(Chao et al., 2008)
EAAT2	Unknown	SUMO1	synaptic glutamate clearance	Intracellular localization (decrease in function)	(Foran et al., 2014; Gibb et al., 2007)
K2P1	Unknown	SUMO1	potassium channel modulation	Silences leak channel	(Rajan et al., 2005)
Kv1.5	KChAP? Unknown	All	Voltage-gated potassium channel	prevents hyperpolarization	(Benson et al., 2007)
Kv2.1	Unknown	SUMO1	Voltage-gated potassium channel	Inactivates channel	(Dai et al., 2009)
Kv2.1	Unknown	SUMO1	Voltage-gated potassium channel	Increased sensitivity of channel	(Plant et al., 2011)
Kv1.1	Unknown	SUMO1 SUMO2	Voltage-gated potassium channel	Increased excitability of channel	(Qi et al., 2014)
Kv7.2	Unknown	SUMO2	Voltage-gated sodium channel	Increased excitability of channel	(Qi et al., 2014)
NaV1.2	Unknown	SUMO1	Voltage-gated potassium channel	Increases sodium currents	(Plant et al., 2016)
mGluR8b	PIAS1	SUMO1	Presynaptic transmission	unknown	(Dutting et al., 2011)
mGluR8a	PIAS1	SUMO1	Presynaptic transmission	unknown	(Tang et al., 2005)
mGluR7	Unknown	SUMO1 SUMO2	Presynaptic excitatory transmission	unknown, potentially receptor recycling	(Choi et al., 2016; Wilkinson and Henley, 2011; Wilkinson et al., 2008)

Table 3, part 2: Synaptic SUMOylation substrates continued

Substrate	E3	SUMO isoform	Pathway	Function of SUMOylation	Reference(s)
TβRI	Unknown	SUMO1	transcription signaling	enhances receptor function	(Kang et al., 2008)
MEF-2A	PIASx	SUMO1	postsynaptic differentiation	Represses transcription	(Shalizi et al., 2007; Shalizi et al., 2006)
PTB1B	PIAS1	SUMO1	structural plasticity through regulation of phosphorylation	inhibits activity	(Dadke et al., 2007)
La	Unknown	SUMO1 SUMO2	axonal mRNA transport	retrograde transport	(van Niekerk et al., 2007)
NaV1.2	Unknown	SUMO1	membrane depolarization	increases voltage-gated sodium current	(Plant et al., 2016)
Syn1	Unknown	SUMO1	Synaptic vesicle release	Increases association with synaptic vesicles	(Tang et al., 2015)
Stx1	Unknown	SUMO1	Synaptic vesicle release	Increases interaction with SNARE proteins	(Craig et al., 2015)
Syt1	Unknown	SUMO1	Neurotransmitter release	Potentially, decrease in synaptic activity	(Matsuzaki et al., 2015)
RIM1α	Unknown	SUMO1	Presynaptic vesicle docking	Vesicle exocytosis	(Girach et al., 2013)
Arc	Unknown	SUMO1	Synaptic plasticity	Unknown	(Craig et al., 2012)
Gephrin	PIAS3, 2a	SUMO1 SUMO2	Postsynaptic scaffold	Increase scaffolding	(Ghosh et al., 2016)

Table 4: DNA damage SUMOylation substrates

Substrate	E3	Pathway	Function of SUMOylation	Reference(s)
Polη	PIAS1	Trans-lesion	Required for replication at forks	(Despras et al., 2016)
Ku70	PIAS1, PIASXB	NHEJ	Stabilizes	(Yurchenko et al., 2008)
XRCC4	PIAS1	NHEJ	Recruitment to damage sites	(Yurchenko et al., 2006)
XRCC1	TOPORS	BER	Recruits Polb for efficient repair	(Hu et al., 2018)
HERC2	PIAS4	DSB	Stabilization with RNF8	(Danielsen et al., 2012)
MDC1	PIAS4	DSB	Removal and Degradation from break sites	(Luo et al., 2012)
53BP1	PIAS1/4	NHEJ	Maybe Localization/unknown	(Galanty et al., 2009)
RNF168	PIAS4	DSB	Recruitment to damage sites	(Danielsen et al., 2012)
BRCA1	PIAS1	DSB	Enhances Ligase activity	(Morris et al., 2009)
WRN	p14	BER, HR, NHEJ	Nuclear localization	(Woods et al., 2004)
VCP	Unknown	DSB	Localization of VCP to cellular compartments	(Wang et al., 2016)
MRE11	Ad5 E4-ORF3	DSB	Unknown	(Sohn and Hearing, 2012)
NBS1	Ad5 E4-ORF3	DSB	Unknown	(Sohn and Hearing, 2012)
CtIP	CBX4	HR	Promotes HR over NHEJ	(Soria-Bretones et al., 2017)
EXO1	PIAS4	HR	Reduces stability	(Bologna et al., 2015)
RPA70	Unknown	HR	Repair foci formation/recruitment	(Dou et al., 2010)
RAD52	Unknown	HR	Nuclear Transport	(Saito et al., 2010)
CSB	Unknown	TCR	Unknown, maybe STUbL signal	(Sin et al., 2016)
XPC	Unknown	NER	Stabilizes protein, Interaction necessary for efficient repair and clearance	(Akita et al., 2015; Wang et al., 2005)
Ataxin3	Unknown	TCR	Autophagy-mediated degradation	(Hwang and Lee, 2017; Zhou et al., 2013)
FANCD2	PIAS1/4	ICL	STUbL signal for eviction	(Gibbs-Seymour et al., 2015)
FANCI	PIAS1/4	ICL	STUbL signal for eviction	(Gibbs-Seymour et al., 2015)

Table 5: DDR genes associated with neuropathologies

Gene	Gene function	repair pathway(s)	Associated disease(s)	Neuropathology	Reference(s)
CSB	DNA topology/repair complex scaffolding	NER/TCR	Cockayne Syndrome	micrencephaly, neurodegeneration	(van der Horst et al., 1997; Weidenheim et al., 2009)
APTX	End Processing, diadenosine polyphosphate hydrolase	SSB	Ataxia with Occulomotor Apraxia-1	ataxia, neurodegeneration	(El-Khamisy et al., 2009; Moreira et al., 2001)
ATM	Serine/threonine protein kinase, DNA damage sensor	DSB	Ataxia-telangiectasia	ataxia, neurodegeneration	(Choy and Watters, 2018; Herzog et al., 1998)
ATR	Serine/threonine protein kinase, DNA damage sensor	DSB	Seckel syndrome	microcephaly, mental retardation	(Brown and Baltimore, 2003; O'Driscoll et al., 2003)
MRE11	Exonuclease	DSB	Ataxia-telangiectasia-like disorder	ataxia, neurodegeneration	(Sedghi et al., 2018; Xiao and Weaver, 1997)
LIG4	Ligase	DSB	LIG4 syndrome	microcephaly	(Altmann and Gennery, 2016; Frank et al., 2000)
TDP1	End Processing/DNA Phosphodiesterase	SSB	Spinocerebellar ataxia with axonal neuropathy	ataxia, neurodegeneration	(Katyal et al., 2007; Takashima et al., 2002)
PNKP	End Processing/DNA 5'-Kinase/3'-Phosphatase	BER/TCR	AOA, MCSZ	Ataxia, Microcephaly	(Bras et al., 2015; Shen et al., 2010)
NBN	DNA damage sensor, Response to DSB	DSB	Nijmegen breakage syndrome	microcephaly	(Chrzanowska et al., 2012; Frappart et al., 2005)

CHAPTER 1

Longitudinal Biochemical Assay Analysis of Mutant Huntingtin Exon 1 Protein in R6/2 Mice

SUMMARY OF CHAPTER 1

Our previous work has involved assessment of mutant huntingtin (mHTT) aggregated intermediates as a readout for altered protein homeostasis in HD. For instance, we evaluated the effect of Pias1 knock-down (KD) in R6/2 mice on the formation of an insoluble, accumulated species of mHTT protein, which accumulated in human brain and was reduced by Pias1 KD. However, the relevance of modulating this species is unknown as the mHTT protein undergoes numerous changes in conformation over time. Further, while biochemical analysis of mutant huntingtin (mHTT) aggregation species in HD mice is a common measure to track disease, a longitudinal and systematic study of how tissue processing affects detection of conformers had not yet been reported. Understanding the homeostatic flux of mHTT over time and under different processing conditions would aid in interpretation of pre-clinical assessments of disease interventions such as Pias1 KD. Therefore, I systematically evaluated tissue lysis methods and biochemical assays in parallel with behavioral readouts in R6/2 mice to establish a baseline for HTT exon1 protein accumulation. This portion of my dissertation explores the formation of the insoluble, high-molecular weight (HMW) accumulated mHTT exon 1 protein species that was modulated by Pias1 in R6/2 mice. Understanding the accumulation dynamics of this species and overall flux of mHTT exon 1 protein conformational changes provided insight into the possible functional consequences of reducing HMW mHTT with Pias1 KD. Further, I established a toolbox for assessing mHTT conformers for pre-clinical assessments that I

could utilize throughout my dissertation and for other investigators in the field. Established biochemical methods were utilized to process tissue from R6/2 mice of specific ages following behavior tasks to track conformers associated with behavioral deficits. Aggregation states and accumulation of mHTT exon 1 protein were evaluated using multiple break and assay methods to determine potential conformational flux in detection of mHTT species, and tissue specificity of conformers. Detection of mHTT exon 1 protein species varied based on biochemical processing and analysis providing a baseline for subsequent studies in R6/2 mice. Insoluble, HMW species of mHTT exon 1 protein increased and tracked with onset of behavioral impairments in R6/2 mice using multiple assay methods. Overall, conformational flux from soluble monomer to insoluble, HMW species of mHTT exon 1 protein was generally consistent for multiple assay methods throughout R6/2 disease progression. However, these results have important implications for assessing pre-clinical interventions in protein-aggregation associated neurodegenerative fields as data reveals inconsistencies between detecting mHTT exon 1 conformers depending on biochemical processing methods. Use of multiple methods or maintaining consistent methods throughout studies is critical.

Portions of Chapter reprinted with permission from IOS Press from publication:

Morozko E.L., Ochaba J., Hernandez S., Lau A., Sanchez I., Orellana I., Kopan L., Overman J., Yeung S., Steffan J.S., Reidling J., and Thompson L.M. 'Longitudinal Biochemical Assay Analysis of Mutant Huntingtin Exon 1 Protein in R6/2 Mice.' J. Huntingtins Dis., November 2018, 7(4):321-335. The publication is available at IOS Press through http://dx.doi.org/10.3233/JHD-180329

INTRODUCTION

The CAG-coding polyglutamine repeat (polyQ) expansion within the *Huntingtin* (*HTT*) gene results in aberrant misfolding, incomplete splicing, proteolysis, and accumulation of the mutant huntingtin protein (mHTT), which may contribute to Huntington's disease (HD) pathogenesis (Koyuncu et al., 2017; Sathasivam et al., 2013). Investigations into the biological mechanisms underlying HD and identification of pathways that impact disease have implicated progressive mHTT accumulation as an indicator of pathogenesis. Accrued evidence from multiple studies supports the following. Mutant HTT undergoes conformational flux, modification, and processing resulting in increased protein fragmentation and accumulation of insoluble aggregate species as the disease progresses (Hoffner and Djian, 2014, 2015; Ross et al., 2017). Intranuclear inclusions of aggregated, amino-terminal fragments and ubiquitin are one of the hallmarks of HD pathogenesis (Davies et al., 1997; DiFiglia et al., 1997) with the degree of aggregation corresponding with the stage of disease, likely as a surrogate marker of disease progression and aberrant protein homeostasis. Juvenile onset cases of HD, which are caused by longer repeat lengths above ~60 polyQs, have an even higher aggregate load (DiFiglia et al., 1997). Aggregates accumulate in medium spiny neurons (MSNs) of the striatum and cortex, which are significantly impacted by disease, but are notably absent from the cerebellum (DiFiglia et al., 1997). However, mHTT undergoes changes in conformation prior to entering the visible inclusion phase (Hoffner and Djian, 2014).

Many HD-associated studies have focused on mHTT exon 1 protein (mHTTex1p) due to its robust effects on mHTT accumulation and aggregation, and on behavioral and biochemical

deficits associated with HD in mice and flies (Mangiarini et al., 1996; Steffan et al., 2001). For *in vivo* studies, the first HD mouse model generated was an amino-terminal human exon 1 transgenic mouse (Mangiarini et al., 1996). Recently, the Bates and Housman groups showed that incomplete splicing can produce an endogenous, pathogenic mHTTex1p in full-length knock-in mouse models and human patient fibroblasts, equivalent to the transgene expressed in R6/2 mice (Mangiarini et al., 1996), that may contribute to disease progression in HD (Neueder et al., 2017; Sathasivam et al., 2013). The process of aggregation is representative of the progressive nature of the disease, beginning from soluble monomers, assembly into soluble species such as oligomers and β-sheet fibrils and ultimately forming insoluble aggregates and inclusions (Arndt et al., 2015; Hoffner and Djian, 2014). Soluble oligomers can go on to form spherical prefibrillar or protofibrilar soluble oligomers (Poirier et al., 2002) before maturing into amyloid-like aggregates (Scherzinger et al., 1997) and fibrils (Wanker et al., 1999). However, aggregation of mHTT and other amyloidgenic disease-associated proteins appears to progress in a non-linear path (Arndt et al., 2015; Eisele et al., 2015).

While the precise contribution of aberrant accumulation and aggregation of protein to disease pathogenesis is complex, altered proteostasis may serve as a useful surrogate in evaluating preclinical efficacy of genetic and pharmacologic interventions on pathologies. Therefore, systematic detection of mHTT protein and the overlap with disease phenotypes is important for evaluating *in vivo* perturbations and their impact on disease onset and progression. Conformational species of mHTT have been tracked over time previously in HdhQ150 mice using uniform processing (Marcellin et al., 2012). However, due to

biochemical heterogeneity of mHTT conformers, we suggest that sample processing may impact detection of different mHTT species. As a first step in systematically evaluating conformational transitions throughout disease progression, we performed a longitudinal analysis of tissues from transgenic R6/2 mice expressing human mHTTex1p using a battery of biochemical cell lysis methods (Table 1.1) and several specific assays developed over the years to detect and resolve mHTT protein species to investigate how they impact detection of mHTTex1p. Conformational transitions we measured include soluble oligomeric species (Legleiter et al., 2010; Sontag et al., 2012; Weiss et al., 2008), insoluble accumulated species (Kim et al., 2011; O'Rourke et al., 2013; Ochaba et al., 2016; Ochaba et al., 2018), and insoluble fibrillary species (Wanker et al., 1999). We tracked these species in parallel with behavioral phenotypes to provide a baseline to guide studies, and also show that the ability to detect specific species and their abundance is influenced by the tissue processing techniques employed.

RESULTS

R6/2 mice exhibit classical behavioral deficits

A longitudinal assessment of mHTTex1p species and tissue processing methods was performed in R6/2 transgenic mice based on their rapid progression of HD modeled phenotypes, the formation of detergent-insoluble aggregated species of mHTT and the extensive use of this model for preclinical studies (Li et al., 2005). These mice express the first exon of human HTT (CAG repeat of ~125) encoding mHTTex1p and show reproducible and rapidly progressing motor and metabolic symptoms at 6 weeks of age and eventually develop tremors, lack of coordination, excessive weight loss, and early

death (~12 weeks). Animals were assessed in behavior tasks and tissue collected for biochemical assays at time points of 5, 7, 9 and 11 weeks of age. Behavioral deficits were consistent with reported data (Hickey et al., 2005; Mangiarini et al., 1996), allowing direct comparison to molecular readouts. R6/2 mice had a significantly decreased latency to fall in the Rotarod task compared to non-transgenic controls (NT) at 7, 9, and 11 weeks of age (Figure 1.1A; $p<0.0001$). This latency to fall was progressive over time in R6/2 mice ($F_{2,49}=5.62$, $p<0.01$). Motor deficits were further characterized by a significantly increased time to descend on the pole test task between NT and R6/2 mice at 8 ($p<0.001$) and 10 ($p<0.01$) weeks of age, which represented maximal dysfunction that did not progress further in the later time points (Figure 1.1B; $F_{2,51}=2.86$, $p>0.05$). At 6, 8, and 10 weeks of age, R6/2 mice show significantly impaired forelimb strength as measured by the grip strength test compared to NT mice (Figure 1.1C; $p<0.0001$), progressively worsening over time in R6/2 mice ($F_{2,51}=10.99$, $p<0.0001$). Additionally, clasping phenotype increased over the course of the disease indicating progressive dyskinesia and beginning at week 7, R6/2 mice show plateaued weight gain as compared to their NT littermates (Figure 1.1D, E; Genotype: $F_{1, 272} =70.69$, $p<0.0001$).

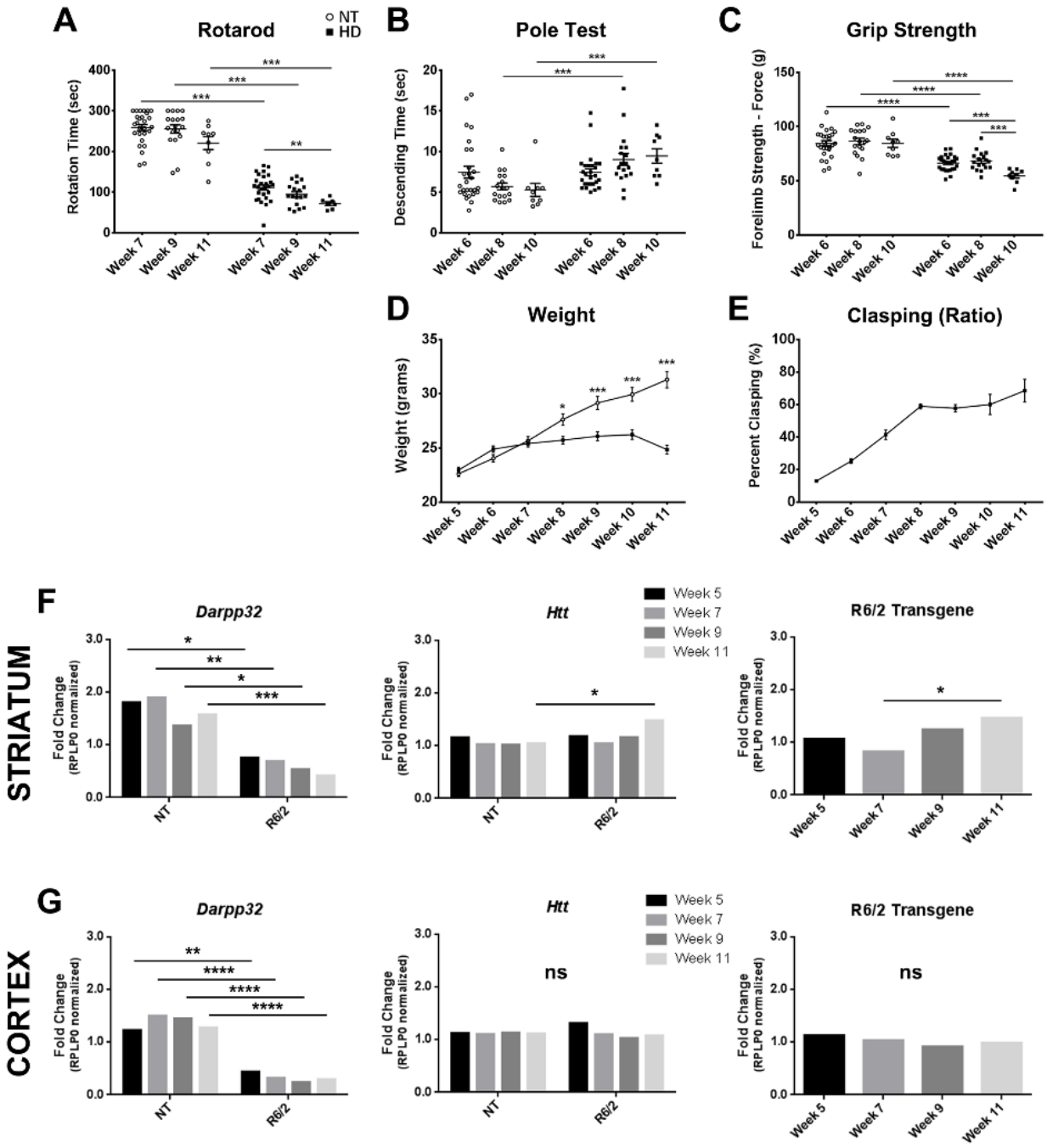
A
Rotarod
NT
HD
Rotation Time (sec)
Week 7
Week 9
Week 11
B
Pole Test
Descending Time (sec)
Week 6
Week 8
Week 10
C
Grip Strength
Forelimb Strength - Force (g)
D
Weight
Weight (grams)
Week 5
Week 6
Week 7
Week 8
Week 9
Week 10
Week 11
E
Clasping (Ratio)
Percent Clasping (%)
F
STRIATUM
Darpp32
Htt
R6/2 Transgene
Fold Change (RPLP0 normalized)
NT
R6/2
G
CORTEX
ns

Figure 1.1: Progressive motor and transcriptional changes as quality control for R6/2 mice. A) R6/2 mice have significantly decreased latency to fall compared to non-transgenic controls (NT) that progressed over time. B) R6/2 mice display progressive and significantly increased time to descend on the pole test task through disease progression. C) R6/2 mice show significantly impaired forelimb strength as measured by the grip strength test compared to NT and progressively worsened over time. D) R6/2 mice show plateaued weight gain beginning at week 7 (Genotype: $F_{1, 272}$ =70.69, p<0.0001). E) Clasping deficits increase over the course of the disease. F) Striatal RNA shows significant fold change in *Darpp-32* (Genotype: $F_{1,16}$=58.54, p<0.0001) and full length murine *Htt* (Genotype: $F_{1,16}$=5.22, p<0.05) relative to NT week 5. An increase in the R6/2 Transgene ($F_{3,8}$=4.41, p<0.05) fold change relative to R6/2 week 5 is observed. G) Cortical RNA shows significant changes in *Darpp-32* (Genotype: $F_{1,16}$=160.1, p<0.0001) but not *Htt* (Age: $F_{1,16}$=2.69, p>0.05, Genotype: $F_{1,16}$=0.02, p>0.05) relative to NT week 5 or R6/2 transgene relative to week 5 R6/2 animals ($F_{3,8}$=0.62, p>0.05). Behavior: n= 36 (week 5); 27 (week 7); 18 (week 9); 9 (week 11). *P<0.05, **P<0.01, ***P<0.001, values represent means ± SEM. Statistical significance of genotypic differences was determined by unpaired, 2-tailed t-test for all behavioral analysis. 2-way ANOVA followed by Bonferroni post-hoc test for weight comparison. qPCR: n=3 for each gene and timepoint. Statistical analysis was completed using 2-way ANOVAs for comparing to NT animals followed by Sidak's multiple comparison's test and 1-way ANOVAs comparing R6/2 mice at different ages followed by Tukey's multiple comparison test.

For quality control and to assess a molecular readout of disease progression supporting the validity of protein fluctuations in our longitudinal cohort of R6/2 animals, qPCR analysis was conducted on *Ppp1r1b (Darpp-32),* known to be dysregulated in R6/2 mice (Bibb et al., 2000; Luthi-Carter et al., 2000), endogenous murine *huntingtin* (*Htt*), and the R6/2 transgene. *Darpp-32* was significantly decreased at all ages in R6/2 mice compared to NT littermates in both the striatum (Genotype: $F_{1,16}$=58.54, p<0.0001) and the cortex (Genotype: $F_{1,16}$=160.1, p<0.0001, Figure 1.1F,G, Figure 1.2A,B) as reported (Bibb et al., 2000; Luthi-Carter et al., 2000). In the striatum, endogenous *Htt* increased in R6/2 mice at week 11 compared to week 11 NT littermates showing a significant genotype effect ($F_{1,16}$=5.22, p<0.05). A significant increase in R6/2 transgene by week 11 compared to week 7 was detected in R6/2 mice ($F_{3,8}$=4.41, p<0.05, Figure 1.1F, Figure 1.2A). In the cortex there was no detectable difference in *Htt* in R6/2 compared to NT littermates at

each age tested (Age: $F_{3,16}$=2.69, p>0.05, Genotype: $F_{1,16}$=0.02, p>0.05, Figure 1.1G, Figure 1.2B). While there was a significant increase in R6/2 transgene between weeks 7 and 11 of age in the striatum, there was no significant change in R6/2 transgene in the cortex ($F_{3,8}$=0.62, p>0.05). No genotype-related transcriptional changes were detected for *Rplp0*, which was used as a normalization factor. Further, reverse-transcriptase-negative controls showed no significant signal in any sample (data not shown).

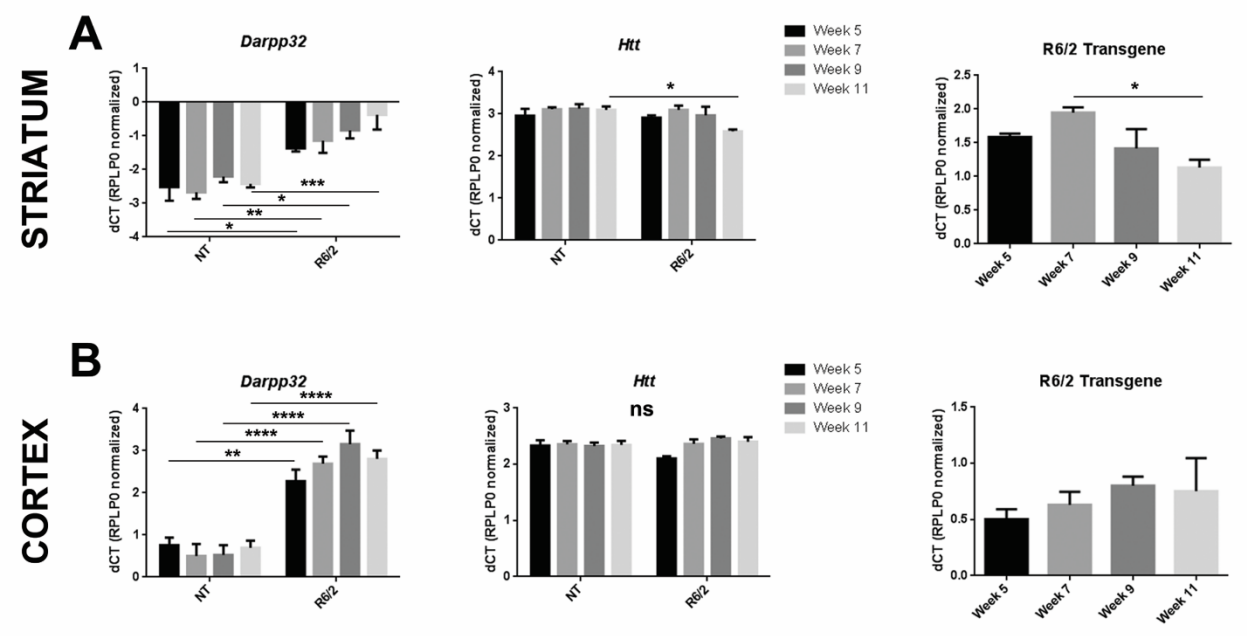

Figure 1.2: Delta CT (dCT) values used to analyze transcriptional alterations detected by qPCR in R6/2 mice. Delta CT (dCT) values used to analyze transcriptional alterations detected by qPCR in R6/2 mice. A) Striatal gene dCT values relative to NT week 5 shows a significant progressive increase in full length murine *Htt* (Genotype: $F_{1,16}$=5.22, p<0.05) and decrease in *Darpp-32* (Genotype: $F_{1,16}$=58.54, p<0.0001). Striatal gene dCT values relative to R6/2 week 5 shows a progressive increase of R6/2 Transgene expression ($F_{3,8}$=4.41, p<0.05). B) Cortical gene dCT values relative to NT week 5 shows significant changes in *Darpp-32* (Genotype: $F_{1,16}$=160.1, p<0.0001) but not *Htt* (Age: $F_{1,16}$=2.69, p>0.05, Genotype: $F_{1,16}$=0.02, p>0.05) or R6/2 transgene relative to week 5 R6/2 animals ($F_{3,8}$=0.62, p>0.05). *P<0.05, **P<0.01, ***P<0.001, ****P<0.0001, values represent mean fold change. n=3 for each gene and timepoint. Statistical analysis was completed using 2-way ANOVAs for comparing to NT animals followed by Sidak's multiple comparison's test and 1-way ANOVAs comparing R6/2 mice at different ages followed by Tukey's multiple comparison test.

Mutant HTT undergoes conformational flux over time in R6/2 mice

A standard outcome measure used to measure mHTT flux is the detection of intranuclear inclusion bodies by immunohistochemistry using aggregation specific antibodies (e.g. EM48, (Gutekunst et al., 1999)), therefore, we evaluated inclusions in the R6/2 mouse striatum and cortex over time. R6/2 mice showed a progressive increase in mHTT inclusion body formation in both the striatum ($F_{3,8}$=13.28, $p<0.01$) and the cortex ($F_{3,8}$=25.42, $p<0.001$) compared from 5 weeks of age to later time points (Figure 1.3). This is consistent with a conformational flux towards insoluble, aggregate species of mHTT beginning at the time of overt disease onset. Although striatum shows the most overt degeneration at late stages, cortical regions have significantly more inclusion bodies by 9 and 11 weeks of age compared to the striatum (Region: $F_{1, 16}$=34.69, $p<0.0001$, Age: $F_{3, 16}$=37.89, $p<0.0001$), consistent with what has previously been reported (Figure 1.3) (Davies et al., 1997).

We have previously described a Soluble/Insoluble Fractionation protocol and Western blot analysis to distinguish soluble monomeric and accumulated insoluble mHTT species in late stage R6/2 mice (Ochaba et al., 2016; Ochaba et al., 2018). This technique was used for this longitudinal analysis of R6/2 mouse tissue and compared to other tissue lysis methods of striatum, cortex, hippocampus, cerebellum, and peripheral tissues (liver and skeletal muscle) using a HTT antibody that selectively detects human mHTTex1p.

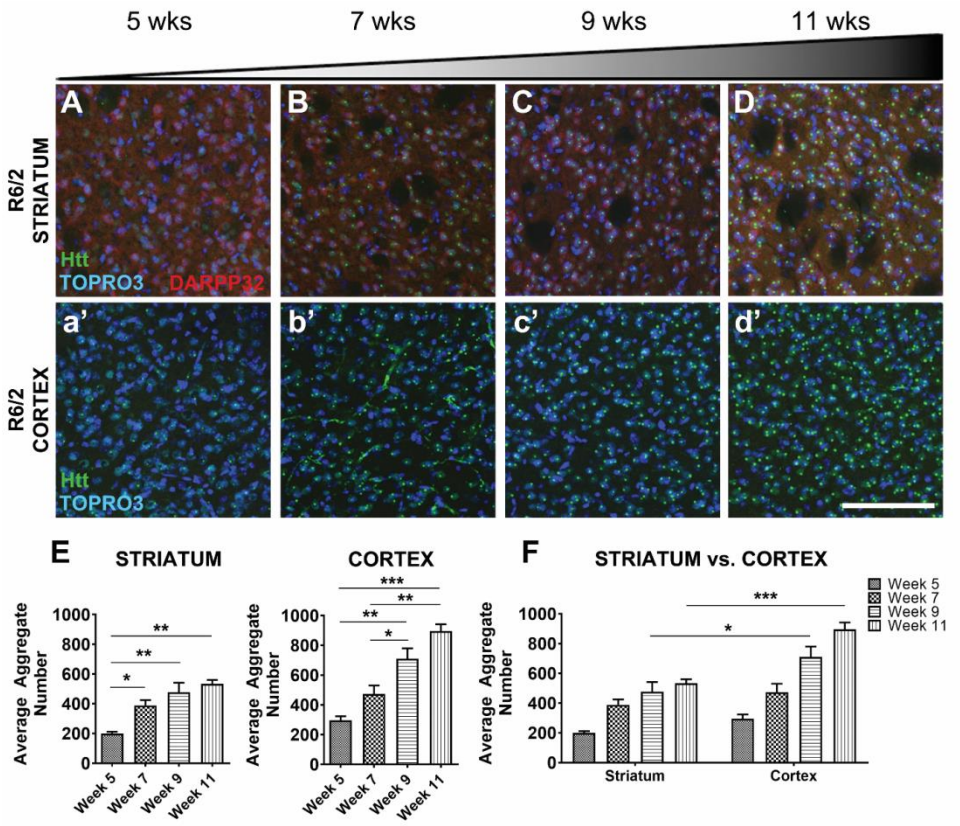

Figure 1.3: Progressive mHTT inclusion body formation in cortex and striatum of R6/2 mice. A-D) 5-11 week R6/2 mice show progressive inclusion body formation in striatum. a'-d') Corresponding cortical area at 5-11 weeks indicates this site shows early and progressive inclusion formation (Striatum: $F_{3,8}$=13.28, p<0.01, Cortex: $F_{3,8}$=25.42, p<0.001) with more inclusions in the cortex than striatum (Region: $F_{1,16}$=34.69, p<0.0001, Age: $F_{3,16}$=37.89, p<0.0001). mHTT inclusion bodies stained with EM48 (green). Striatal tissue marked with DARPP-32 (red) and nuclei of all cells stained with TOPRO3 (blue). All images taken from coronal slices at 10x magnification, striatal and cortical images were taken from the same slice, quantified by IMARIS software, and analyzed by 1-way ANOVA followed by Tukey's multiple comparison test or 2-way ANOVA followed by Sidak's multiple comparison test. Representative images shown. Scale bar 100 μm. *P<0.05, **P<0.01, ***P<0.001, values represent means ± SEM. n=3 for all time points.

Striatum: Following fractionation, the soluble protein fragment of human HTT encoded by the transgene in R6/2 mice, mHTTex1p, was detectable as a monomeric protein species in the Soluble Fraction, with highest levels at the first time point tested at 5 weeks of age in the striatum (Figure 1.4A). Over the disease course the detectable amount of soluble mHTTex1p monomer decreased significantly ($F_{3,8}$=15.51, p<0.01) and appeared to be

accompanied by a corresponding increase in the insoluble, HMW species of mHTTex1p, potentially reflecting the dynamic shift in mHTTex1p conformation from soluble monomer into an insoluble, accumulated species. However, significance was only supported by 1-way ANOVA and was not detected following post-hoc analysis ($F_{3,8}$=4.274, $p<0.05$, Figure 1.4A). The observed fluctuation in size of the detectable monomer is not likely due to a somatic expansion in the striatum as the number of repeats present in the transgene was similar in the striatum compared to tail genomic DNA (Table 1.2, CAG repeat sizes in tails and striatum). Accompanying the apparent increase in insoluble HMW mHTTex1p resolved by PAGE and western blotting was an observed increase in insoluble fibrils of mHTTex1p from the Insoluble Fraction as detected by a filter retardation assay (Figure 1.4A). To examine methods used to process samples then assess levels of mHTTex1p, a series of commonly used tissue lysis buffers specific for given assays were tested to compare outcomes (Table 1.1). An inverse fluctuation from monomeric mHTTex1p towards progressive detection of HMW mHTTex1p retained in the top of the gel were detected in striatal samples lysed in either T-PER (Monomer: $F_{3,8}$=5.85, $p<0.05$, HMW: $F_{3,8}$=12.12, $p<0.01$) or RIPA (Monomer: $F_{3,8}$=25.44, $p<0.001$, HMW: $F_{3,8}$=4.06, $p>0.05$) buffers as with the Soluble/Insoluble Fractionation (Figure 1.4B, C) and summarized in Table 1.3. TRIzol reagent was also tested since it has the advantage of collection of both RNA and protein from processed tissue. However, TRIzol reagent showed extensive variability in detection of both soluble monomer and HMW species of mHTTex1p compared to other methods, precluding its use as an assay for shifts in solubility (Figure 1.5A).

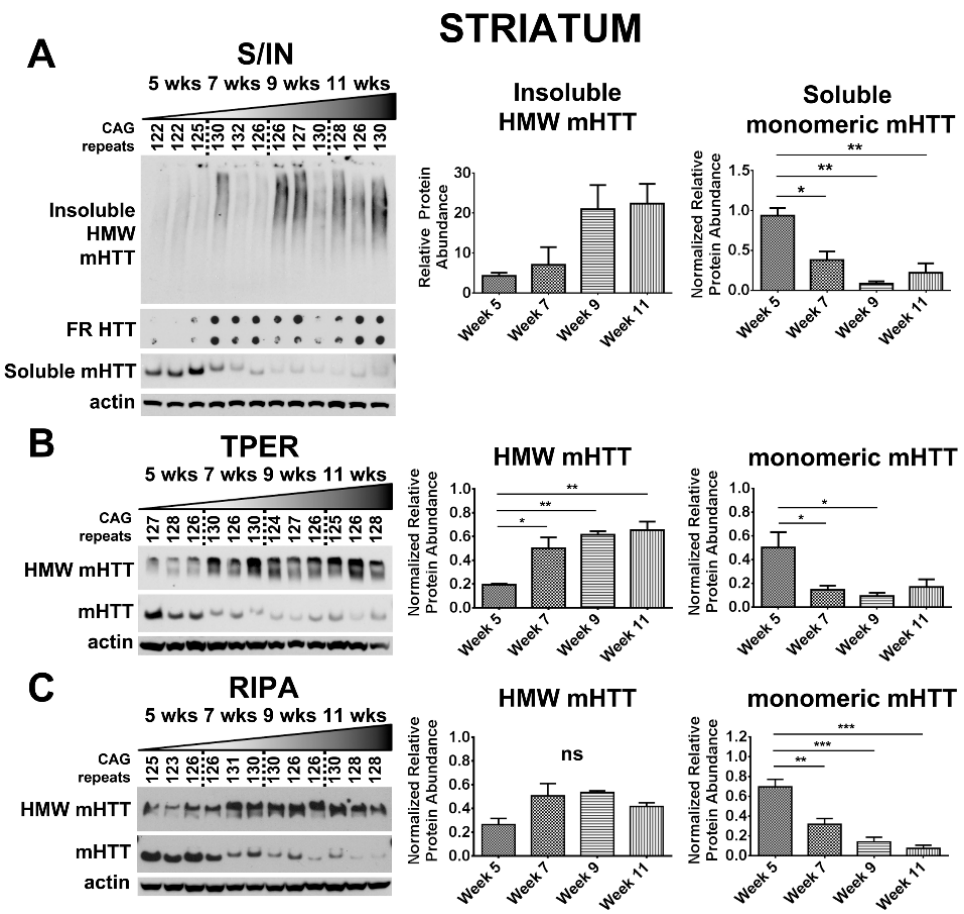

Figure 1.4: Detection of mHTTex1p in striatum of R6/2 mice. A) Striatal time-course samples were fractionated into Soluble and Insoluble proteins. Insoluble fraction reveals an increase in a HMW species of mHTTex1p throughout disease progression ($F_{3,8}$=4.274, p<0.05). Soluble fraction shows an inverse, significantly decreased monomeric form of mHTTex1p throughout disease progression ($F_{3,8}$=15.51, p<0.01). Insoluble aggregates detected by filter retardation assay may show a slight increase throughout disease progression‡. Striatal tissue samples broken in B) T-PER (Monomer: $F_{3,8}$=5.85, p<0.05, HMW: $F_{3,8}$=12.12, p<0.01) and C) RIPA (Monomer: $F_{3,8}$=25.44, p<0.001, HMW: $F_{3,8}$=4.06, p>0.05) reagents show a significant reduction of monomeric mHTex1pT throughout disease progression. Fluctuations in soluble, monomeric mHTTex1p correspond to varying CAG repeats in R6/2 mice. Western blots quantified by mean pixel value. Soluble fraction normalized to actin and analyzed by 1-way ANOVA followed by Tukey's multiple comparison test. *P<0.05, **P<0.01, values represent means ± SEM. n=3 for all time points. HTT antibody MAB5492 used to detect mHTTex1p. Panel (A) has been modified with permission (Grima et al., 2017). ‡Reprinted from Grima et al., 2017 (Grima et al., 2017) with permission from Elsevier.

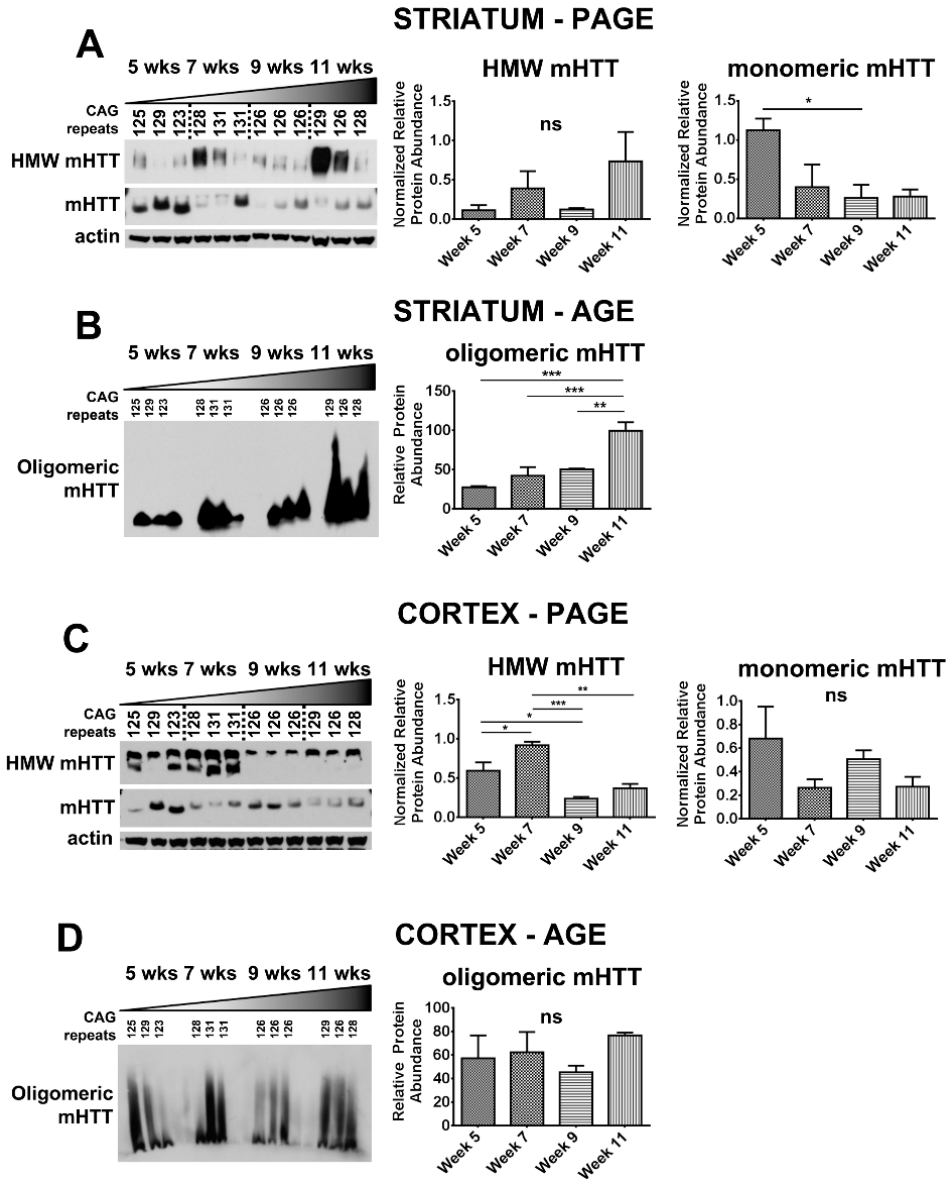

Figure 1.5: Detection of mHTTex1p is highly variable using TRIzol reagent. A) Striatal and C) Cortical protein samples recovered from TRIzol preparations show highly variable detection of both soluble monomeric and soluble HMW mHTTex1p as analyzed by PAGE and western blot. AGE analysis of B) Striatal and samples show a significant change in oligomer levels ($F_{3,8}$=16.02, p<0.001) while D) Cortical samples do not ($F_{3,8}$=0.95, p>0.05). Western blots quantified by mean pixel value and normalized to actin. AGE blots were quantified by mean pixel value. Data analyzed by 1-way ANOVA followed by Tukey's multiple comparison test. *P<0.05, **P<0.01, values represent means ± SEM. n=3 for all time points. HTT antibody MAB5492 used to detect mHTTex1p.

Cortex: Cortical tissue samples were processed using the same methods in parallel and samples showed a similar dynamic shift from soluble, monomeric mHTTex1p to HWM mHTTex1p as observed in the striatum (Table 1.3, Figure 1.6). Insoluble, HWM mHTTex1p significantly increased ($F_{3,8}$=9.88, p<0.01), while soluble, monomeric mHTTex1p significantly decreased ($F_{3,8}$=8.78, p<0.01, Figure 1.6A). This shift was also accompanied by an observed increase in insoluble fibrils from the Insoluble Fraction similar to striatal samples (Figure 1.6A). T-PER-processed samples showed significant reduction in monomeric mHTTex1p and increase in HMW mHTTex1p (Monomer: $F_{3,8}$=10.91, p<0.01, HMW: $F_{3,8}$=8.42, p<0.01, Figure 1.6B), similarly seen in RIPA-processed samples (Monomer: $F_{3,8}$=7.21, p<0.05, HMW: $F_{3,8}$=10.85, p<0.01, Figure 1.6C). Extensive variability in TRIzol-processed samples was again observed (Figure 1.5C).

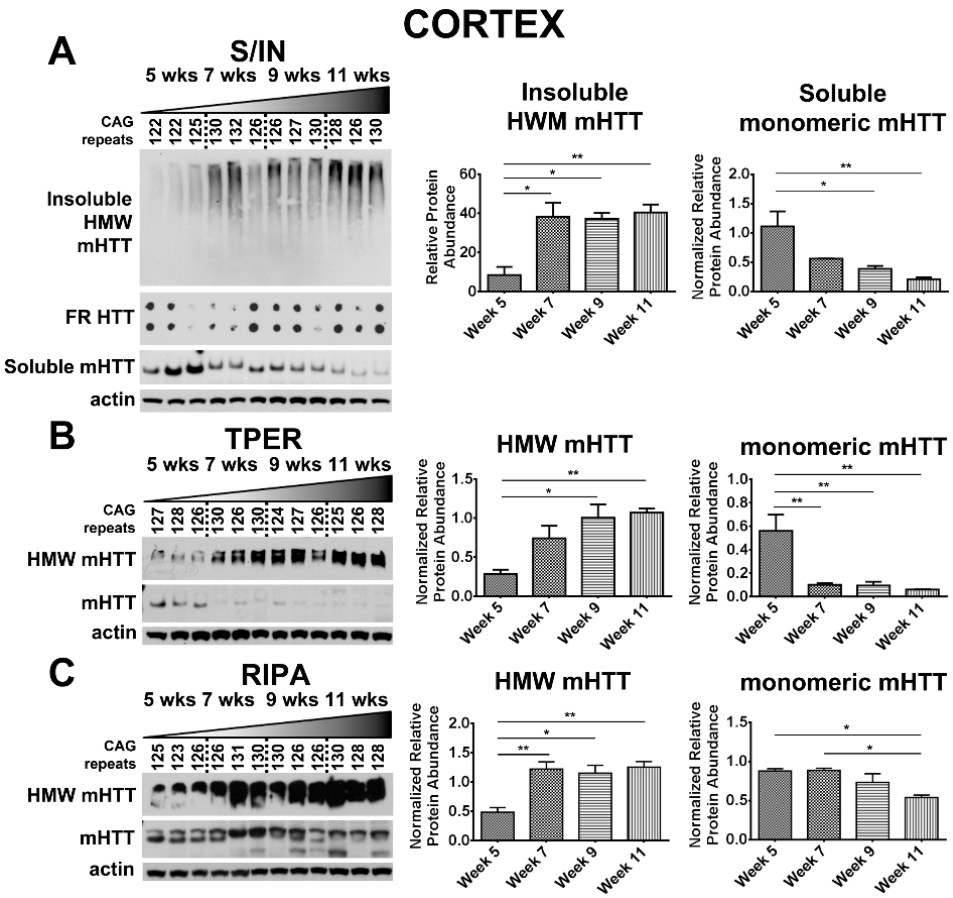

Figure 1.6: Detection of mHTTex1p in cortex of R6/2 mice. A) Cortical time-course samples were fractionated into Soluble and Insoluble proteins. Insoluble fraction reveals a significant increase in a HMW species of mHTT throughout disease progression ($F_{3,8}$=9.88, p<0.01). Soluble fraction shows an inverse, significantly decreased monomeric form of mHTTex1p throughout disease progression ($F_{3,8}$=8.78, p<0.01). Insoluble aggregates detected by filter retardation assay show no apparent change. Cortical tissue samples broken in B) T-PER (Monomer: $F_{3,8}$=10.91, p<0.01, HMW: $F_{3,8}$=8.42, p<0.01) and C) RIPA (Monomer: $F_{3,8}$=7.21, p<0.05, HMW: $F_{3,8}$=10.85, p<0.01) reagents show a significant reduction of monomeric mHTTex1p throughout disease progression accompanied by a significant increase in HMW mHTTex1p detected in the soluble fraction. Fluctuations in soluble, monomeric mHTTex1p correspond to varying CAG repeats in R6/2 mice. Western blots quantified by mean pixel value. Soluble fraction normalized to actin and analyzed by 1-way ANOVA followed by Tukey's multiple comparison test. *P<0.05, **P<0.01, values represent means ± SEM. n=3 for all time points. HTT antibody MAB5492 used to detect mHTTex1p.

Hippocampus and Cerebellum: The dynamic shift between soluble monomer and insoluble HMW mHTTex1p was observed in the hippocampus following Soluble/Insoluble Fractionation, showing significant conformational flux (Monomer: $F_{3,8}$=142.2, p<0.0001, HMW: $F_{3,8}$=21.05, p<0.001; Table 1.3, Figure 1.7A). R6/2 mice have been previously reported to have deficits in spatial learning (Lione et al., 1999), a hippocampal-dependent process, as well as decreased hippocampal volume (Rattray et al., 2013) and spine density (Bulley et al., 2012), suggesting that this insoluble, HMW mHTTex1p protein could correlate with observed deficits in these animals. This shift, however, was not detected in tissue samples processed in T-PER reagent, showing no decrease in monomeric mHTTex1p (Monomer: $F_{3,8}$=0.13, p>0.05) but an increase in the unresolved, HMW accumulated mHTTex1p species ($F_{3,8}$=5.41, p<0.05, Figure 1.7B). Insoluble, HMW mHTTex1p in the cerebellum significantly increased ($F_{3,8}$=29.11, p<0.0001), but the Soluble Fraction did not show significant soluble monomer flux throughout disease progression ($F_{3,8}$= 2.51, p>0.05), indicating that mHTTex1p may be sequestered into a different form or aggregate species in the cerebellum and may provide insight into tissue specificity and vulnerability in HD

(Table 1.3, Figure 1.7C). Cerebellar tissue samples broken in T-PER reagent, however, showed a significant increase in accumulated mHTTex1p ($F_{3,8}$=6.32, $p<0.05$) and a corresponding decrease in soluble monomer ($F_{3,8}$=4.25, $p<0.05$, Figure 1.7D). These results suggest that while accumulated HMW mHTTex1p tracks with disease pathogenesis and may serve as a robust measure of disease progression, additional methods to detect additional species of mHTT or levels of full-length endogenous HTT may be necessary to investigate tissue specific vulnerabilities or normal HTT levels (Franich et al., 2018).

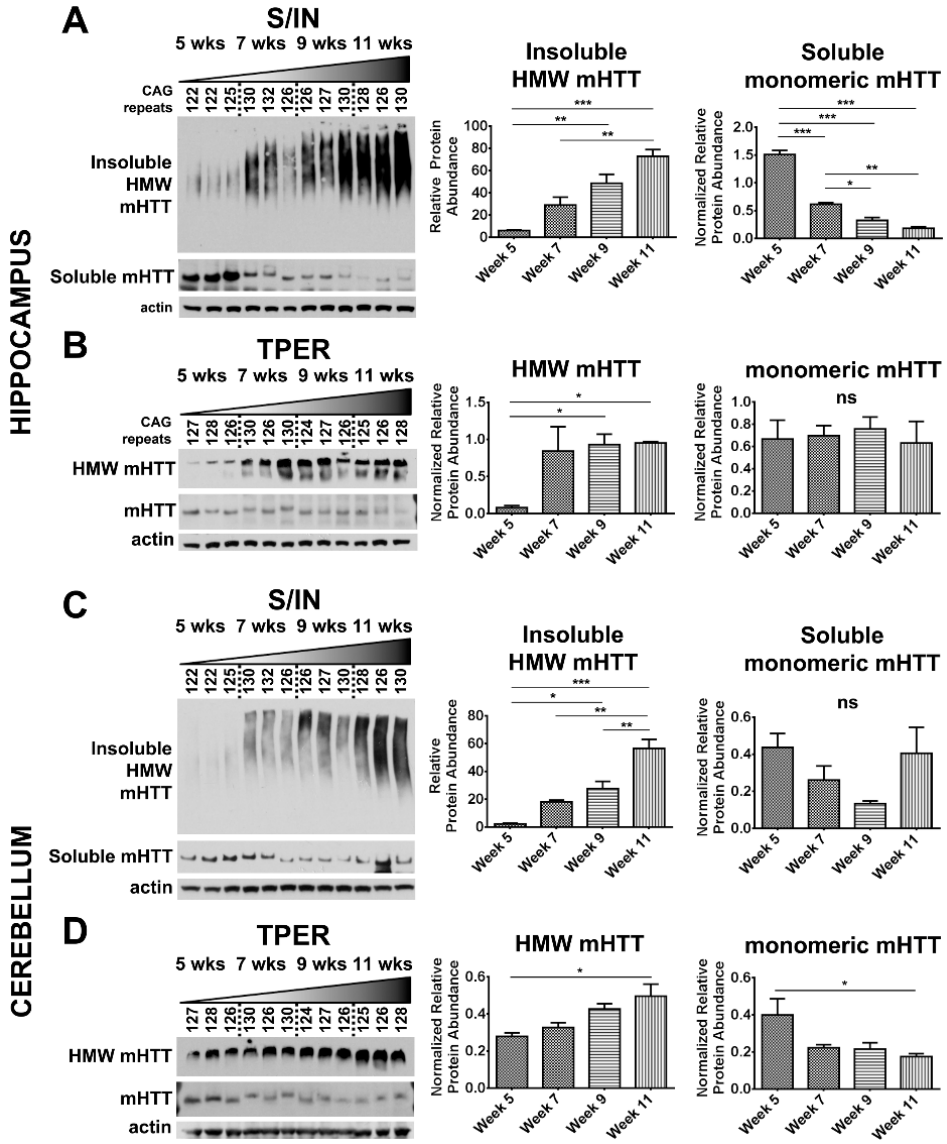

Figure 1.7: Detection of mHTTex1p in hippocampus and cerebellum of R6/2 mice varies depending on break method. Insoluble fraction in A) hippocampus reveals a significant increase in a HMW species of mHTTex1p throughout disease progression ($F_{3,8}$=21.05, p<0.001). Soluble fraction shows an inverse, significantly decreased monomeric form of mHTTex1p throughout disease progression ($F_{3,8}$=142.2, p<0.0001). B) T-PER processed hippocampal tissue samples did not show decrease in soluble monomeric mHTTex1p ($F_{3,8}$=0.13, p>0.05) or HMW accumulated mHTTex1p ($F_{3,8}$=5.41, p<0.05). Insoluble fraction in C) cerebellum reveals a significant increase in HMW species of mHTTex1p throughout disease progression ($F_{3,8}$=29.11, p<0.0001). Soluble fraction did not detect a significant decreased monomeric form of mHTTex1p ($F_{3,8}$= 2.51, p>0.05). However, soluble monomeric mHTTex1p decrease was detected in D) T-PER processed cerebellar tissue samples (HMW: $F_{3,8}$=6.32, p<0.05, Monomer: $F_{3,8}$=4.25, p<0.05). Fluctuations in soluble, monomeric mHTTex1p correspond to varying CAG repeats in R6/2 mice. Western blots quantified by mean pixel value. Soluble fraction normalized to actin and analyzed by 1-way ANOVA followed by Tukey's multiple comparison test. *P<0.05, **P<0.01, values represent means ± SEM. n=3 for all time points. HTT antibody MAB5492 used to detect mHTTex1p.

Liver and Skeletal Muscle: We also evaluated liver and skeletal muscle samples for accumulation of HMW mHTTex1p in comparison to the brain tissue results. Liver samples show significant accumulation of insoluble, HMW mHTTex1p ($F_{3,8}$=83.34, p<0.0001). The soluble monomer, however, was not detectable using Soluble/Insoluble Fractionation (Figure 1.8A, data not shown). Significant accumulation of HMW mHTTex1p was detected in samples broken in T-PER reagent ($F_{3,8}$=12.79, p<0.01) and interestingly, soluble monomeric mHTTex1p was also detectable in liver samples broken in T-PER reagent but no change in protein abundance during disease progression was detected with this break method ($F_{3,8}$=2.95, p>0.05, Figure 1.8B). Like liver, significant accumulation of insoluble, HMW mHTTex1p was detectable in skeletal muscle only using Soluble/Insoluble Fractionation ($F_{3,8}$=7.53, p<0.05). No soluble monomer of mHTTex1p was detectable in skeletal muscle broken with either Soluble/Insoluble Fractionation or T-PER reagent. HMW mHTTex1p was not detected in T-PER (Figure 1.8C, data not shown).

Oligomeric mHTT detection varies based on tissue processing

Agarose Gel Electrophoresis (AGE) has been used to resolve soluble, oligomeric species of mHTT in RIPA buffer as described (Sontag et al., 2012; Weiss et al., 2008). Tissue samples from striatum and cortex that were lysed using methods as above (Table 1.1) were also analyzed using AGE to compare how biochemical processing affected detection of mHTT species resolved by AGE. Detection of oligomeric mHTTex1p species on AGE gels throughout the course of the disease in R6/2 mice varied greatly depending on break method as summarized in Table 1.3 (Figure 1.9). Striatal tissue samples from R6/2 mice broken in RIPA buffer showed an increase in oligomeric mHTTex1p through week 9 followed by a significant decrease by week 11 ($F_{3,8}$=27.21, $p<0.001$). However, R6/2 striatal samples showed increased oligomeric mHTTex1p through week 11 in both Insoluble ($F_{3,8}$=27.31, $p<0.001$) and Soluble ($F_{3,8}$=7.30, $p<0.05$) Fractions, and samples broken in T-PER ($F_{3,8}$=24.70, $p<0.001$, Figure 1.9A), and TRIzol ($F_{3,8}$=16.02, $p<0.001$, Figure 1.5B). Cortical tissue samples broken using identical methods more consistently showed a significant increase in oligomer formation (RIPA: $F_{3,8}$=19.56, $p<0.001$, Insoluble: $F_{3,8}$=29.95, $p<0.001$, T-PER: $F_{3,8}$=109.3, $p<0.0001$, Figure 1.9B) with the exception of the Soluble Fraction ($F_{3,8}$=2.291, $p>0.05$) and of TRIzol samples ($F_{3,8}$=0.95, $p>0.05$, Figure 1.5D) which showed no significant accumulation of mHTTex1p oligomers. Therefore, the variability in detectable oligomeric mHTTex1p among tissue processing methods is an important consideration when analyzing data in preclinical studies.

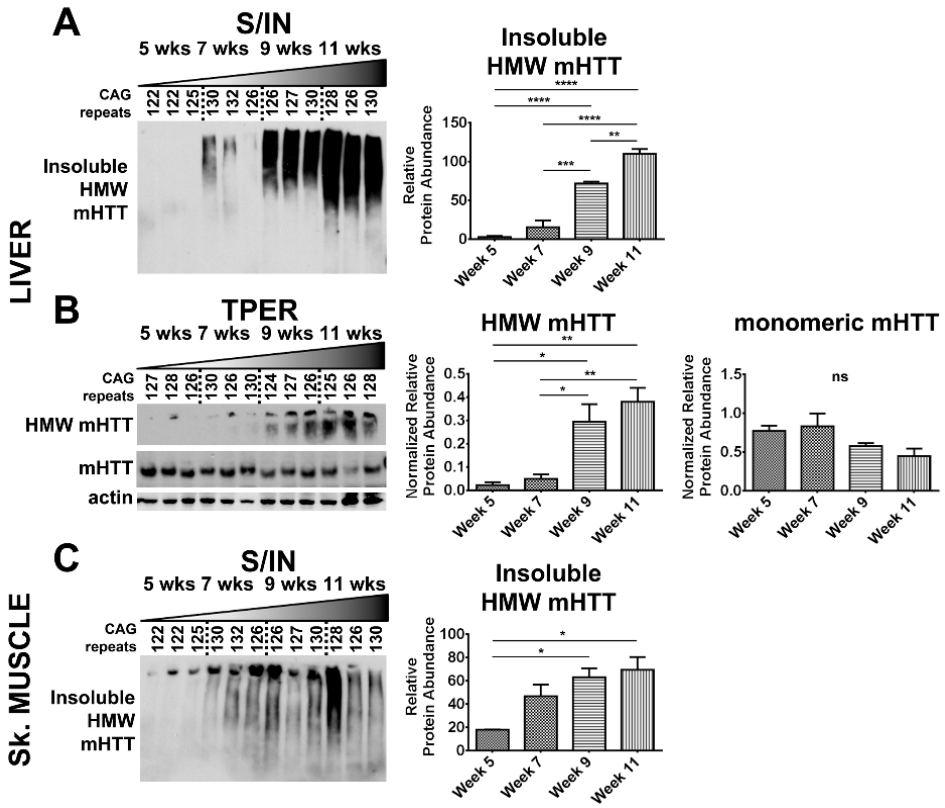

Figure 1.8: Detection of mHTTex1p in peripheral tissue varies depending on break method. A) Insoluble HMW mHTTex1p increases significantly throughout disease progression in Liver ($F_{3,8}$=83.34, p<0.0001) but Soluble, monomeric mHTTex1p is not detectable. B) Liver tissue broken in T-PER resolves soluble monomer revealing no change in detectable protein abundance ($F_{3,8}$=2.95, p>0.05) while HMW mHTTex1p showed a significant increase ($F_{3,8}$=12.79, p<0.01). C) Skeletal muscle also reveals a significant increase in insoluble HMW mHTTex1p ($F_{3,8}$=7.53, p<0.05). Soluble monomer is not detected in either Soluble/Insoluble fractionated samples. Western blots quantified by mean pixel value. Soluble fraction normalized to actin (liver) or GAPDH (Skeletal Muscle) and analyzed by 1-way ANOVA followed by Tukey's multiple comparison test. *P<0.05, **P<0.01, values represent means ± SEM. n=3 for all time points. HTT antibody MAB5492 used to detect mHTTex1p.

DISCUSSION

Proteostasis in HD is perturbed by the expression of mHTT, shifting homeostatic balance and associated downstream cascades. Molecular and biochemical readouts such as aberrant mHTT accumulation and transcriptional alterations can be correlated to behavioral phenotypes in an effort to track disease modification. Our longitudinal cohort of

R6/2 mice exhibited behavioral phenotypes as previously reported (Figure 1.1, (Bibb et al., 2000; Hickey et al., 2005; Luthi-Carter et al., 2000; Mangiarini et al., 1996)), allowing for a systematic comparison of changes in mHTTex1p conformations using selected cell lysis and biochemical assays in an HD model over time.

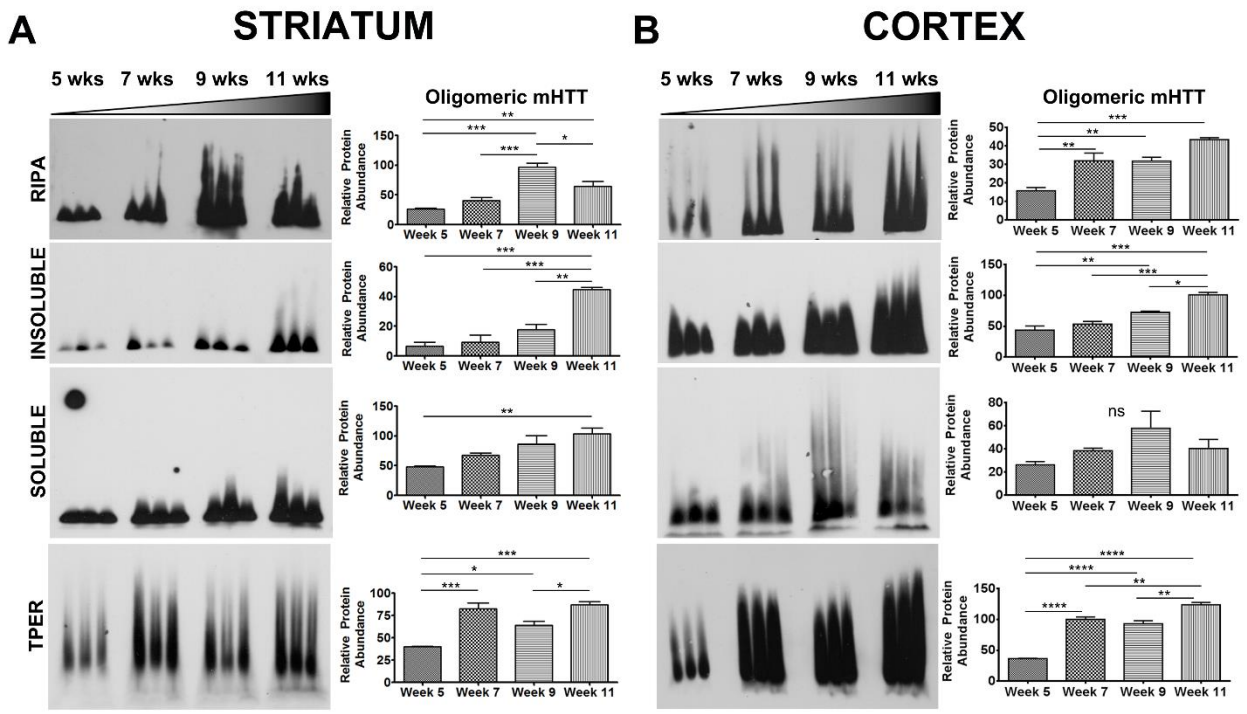

Figure 1.9: Detection of mHTTex1p on AGE gels varies based by break method. A) Striatal tissue samples broken in indicated buffers and analyzed by Agarose Gel Electrophoresis (AGE). R6/2 mice show an increase in oligomeric mHTTex1p through week 9 followed by a significant decrease by week 11 in RIPA broken samples ($F_{3,8}$=27.21, p<0.001). Increased, disease-endpoint mHTTex1p detected in Insoluble ($F_{3,8}$=27.31, p<0.001), Soluble ($F_{3,8}$=7.30, p<0.05), and T-PER ($F_{3,8}$=24.70, p<0.001) broken samples showed a significant increase by week 7, followed by a decrease in week 9 before increased again by week 11. B) Cortical samples broken in RIPA buffer ($F_{3,8}$=19.56, p<0.001), Insoluble ($F_{3,8}$=29.95, p<0.001) and Soluble fractionation ($F_{3,8}$=2.291, p>0.05), and T-PER buffer ($F_{3,8}$=109.3, p<0.0001) show either no change or significant increase in formation of oligomers by week 11. AGE blots were quantified by mean pixel value and analyzed by 1-way ANOVA followed by Tukey's multiple comparison test. *P<0.05, **P<0.01, ***P<0.001, ****P<0.0001 values represent means ± SEM. n=3 for all time points. HTT antibody MAB5492 used to detect mHTTex1p.

At the level of transcription, expression of *Darpp-32* (Bibb et al., 2000; Luthi-Carter et al., 2000) was decreased in R6/2 mice as expected, thus providing a reliable molecular quality control marker (Figure 1.1, Figure 1.2). While previously reported that transgene expression was within range of the endogenous murine gene in R6/2 mice (Mangiarini et al., 1996), there was a moderate increase in the levels of endogenous *Htt* transcript in R6/2 mice in this study by 11 weeks of age in the striatum compared to age-matched NT controls, perhaps indicating an upregulation to compensate for transgene genotoxic stress or for the declining wild-type endogenous HTT protein levels we observed in HD knock-in mice during aging (Franich et al., 2018). Intriguingly, this increase also extended to expression of the R6/2 transgene in striatum, potentially reflecting compensatory upregulation of *Htt* given that the transgene is expressed from the human *Htt* promoter (Mangiarini et al., 1996). The upregulation of the transgene and of endogenous *Htt* was not observed in cortex, potentially reflecting some aspect of tissue specificity. Thus, when making assessments of protein levels, differential transcription may be considered in addition to changes in protein clearance mechanisms, such that the observed increase in R6/2 transgene expression in the striatum could also contribute to the detected increase in accumulated species of mHTTex1p.

Given that mHTT conformations have different biochemical properties, it is important to evaluate how tissue processing and analytical technique impact detection of conformers, and we assessed this *in vivo* assaying mHTTex1p from transgenic R6/2 HD mice. We first sought to resolve soluble and insoluble species of mHTTex1p in different brain regions and peripheral tissues. Accumulation of insoluble, HMW mHTTex1p resolved from the

Insoluble Fraction was consistently detected in every tissue tested (Table 1.3, Figure 1.7, 1.8), and the appearance of the insoluble mHTTex1p accumulation tracked with onset of disease phenotypes. In striatum, cortex, and hippocampus, this increase was accompanied with a progressive decrease in the soluble mHTTex1p monomer associated with the transgene. The decrease in soluble mHTTex1p and corresponding increase in insoluble HMW species of mHTTex1p, tracking with disease progression, suggests that preventing this flux through therapeutic modulation may be therapeutically beneficial. Supporting this, our previous data showed that modulation of the insoluble, HMW species by reduction of the E3 SUMO ligase, Protein Inhibitor of Activated Stat 1 (PIAS1) in the striatum of R6/2

mice corresponded with beneficial behavioral and molecular alterations (Ochaba et al., 2016) and treatment with a compound that corresponds with worsened behavioral phenotypes, JQ1, increased levels of this insoluble, HMW specifies (unpublished results, Thompson). However, while this insoluble, HMW species tracked with disease progression and observed behavioral deficits, it did not provide insight into tissue specificity involved in disease pathogenesis. Therefore, this species may serve as a reliable readout for molecular progression of disease but not of tissue-specific vulnerabilities. An alternative methodology to further define levels of HTT species recently reported that levels of full-length mHTT protein do not decline robustly in cerebellum with aging, unlike in cortex and striatum, in two homozygous knock-in models, highlighting the importance of tracking multiple full-length and protein fragment species of both HTT and mHTT (Franich et al., 2018).

While accumulation of insoluble, HMW mHTTex1p was detectable in peripheral tissue (skeletal muscle and liver), Soluble/Insoluble Fractionation was unable to resolve the soluble, monomeric transgene protein product (Figure 1.8). This could indicate an accelerated or differential aggregation pathway or preferential clearance of the monomer in peripheral tissue. Being able to accurately detect mHTT conformers would aid in establishing tissue intrinsic differences.

Whole-cell lysis techniques, such as RIPA and T-PER reported here, were able to resolve soluble monomeric mHTTex1p albeit with variability compared to other techniques used (Table 1.3). Interestingly, a HMW mHTTex1p species from whole-cell tissue processing methods was retained at the top of the gel when analyzed by PAGE and Western blot. It is possible that this HMW species contains both soluble and insoluble proteins and multiple mHTTex1p conformers and therefore cannot be directly compared to the insoluble, HMW mHTTex1p detected in the Insoluble Fraction that resolves in low-percentage PAGE gels. However, the whole-cell lysis HMW species reliably increased in some brain regions broken in both RIPA and T-PER buffers and therefore may also serve as a readout for molecular progression of disease.

Soluble oligomeric mHTT was previously shown to be detectable at an early age in HdhQ150 mice. Levels of this soluble species, detected by size exclusion chromatography, diminished over time and corresponded with an increase in intranuclear inclusion formation (Marcellin et al., 2012). Though our findings present a similar trend, detection of an earlier oligomeric species of mHTTex1p is dependent on tissue processing (Table 1.3,

Figure 1.5B, D, Figure 1.9). Alternatively, due to the heterogeneity of oligomeric mHTT (Hoffner and Djian, 2014), certain biochemical processing methods may favor one soluble species over the other. Conformation-specific antibodies facilitate studies of various mHTT species and their association with pathogenesis (e.g. 3B5H10 (Miller et al., 2011), 1C2 (Trottier et al., 1995), MW8 (Ko et al., 2001), EM48 (Gutekunst et al., 1999)). Therefore, future in depth analysis using conformer specific antibodies may provide further insight (Legleiter et al., 2009).

Taken together, the data presented here is consistent with the dynamic shift of the soluble mHTT transgene protein product in R6/2 mice to an insoluble, HMW accumulated mHTTex1p species accompanied by a change in oligomeric mHTTex1p over the time course of the disease. Significantly, protein processing methods influence the detection and temporal effects. Protein processed in TRIzol reagent yielded the greatest amount of variation between assays for detecting different species of mHTTex1p (Figure 1.5), precluding its use in these studies. However, TRIzol may be useful in detection of non-aggregating proteins to enable parallel protein and RNA processing.

The shift to insoluble, HMW and aggregated mHTTex1p from soluble monomer is associated with increasing behavioral dysfunction compared to NT mice and represents a robust protein assay to track disease progression in R6/2 mice. Understanding the outcomes of standard protein homeostasis assays to assess mHTTex1p flux in R6/2 mice provides a baseline for cross comparisons of preclinical interventions. It will be beneficial to conduct similar assessments of mHTTex1p flux in brain expressing full-length mutant

HTT, given that mHTTex1p is expressed in knock-in HD mouse models and in patient brain (Neueder et al., 2017; Sathasivam et al., 2013), and may be relevant to the onset of HD pathogenesis. A recent report showed a decrease in soluble mHTTex1p monomer in the zQ175 HD knock-in mouse model over time (Neueder et al., 2017), suggesting that detecting this species as well as the insoluble, mHTTex1p species may be powerful cross-model molecular correlates. Indeed, in the assays here, decreasing monomeric mHTTex1p from fractionation of striatal tissue or breaking in RIPA appeared qualitatively to track most closely with the progression of phenotypes in the R6/2 mice. We have previously published a decrease in full-length HTT with age in striatum and cortex of two HD homozygous knock-in models and in wild-type controls, which may reflect a loss of full-length HTT protein function over time (Franich et al., 2018). Due to the dynamic shift between mHTTex1p conformations throughout the course of the disease we propose using multiple and consistent, optimized biochemical analyses, potentially in combination with high context histological approaches as described for knock-in zQ175 mice (Carty et al., 2015) to determine the impact of potential therapeutics on the protein flux of both mHTTex1p and full-length HTT protein.

EXPERIMENTAL PROCEDURES

Animals

R6/2 mice were obtained from Jackson Laboratories at 5 weeks of age and allowed to age to 7, 9, or 11 weeks. CAG repeat sizing of genomic DNA harvested from tails was performed by Laragen. Experiments were carried out in strict accordance with the Guide for the Care and Use of Laboratory Animals of the NIH and an approved animal research protocol by the

Institutional Animal Care and Use Committee (IACUC) at the University of California, Irvine. Animals were humanely euthanized by an injection of Euthasol at age 5, 7, 9 or 11 weeks followed by cardiac perfusion with PBS then decapitation. Brain and peripheral tissues used for biochemical assessment were flash-frozen on dry ice and stored at -80°C until further use. Brain tissue used for immunofluorescence was drop fixed in 4% paraformaldehyde for 48 hours then protected in 30% sucrose with 0.02% sodium azide.

Behavioral Paradigms: Motor deficits were assessed in pole test, rotarod, and grip strength assays as previously described (Ochaba et al., 2016). For pole test, mice were tested at 6, 8, and 10 weeks of age for their ability to descend a vertical pole (1 cm in diameter, 60 cm high) by recording and averaging time to descend over four trials for analysis. Rotarod was carried out using an accelerating apparatus (Dual Species Economex Rota-Rod; 0207-003M; Columbus Instruments) at 7, 9, and 11 weeks of age. Animals were trained on Rotarod for 5 minutes on day 1 and tested the following day by an accelerating assay recording and averaging time to fall for three, 5-minute trials test day.

Grip strength was assessed 6, 8, and 10 weeks of age to measure forelimb strength using a meshed force gauge which retained the peak force applied (IITC Life Science instrument, Woodland Hills, CA) and averaging the top 4 strongest pulls of 5 trials in grams of force applied to the meter. Dyskinesia was assessed by recording percent of animals clasping from weeks 5-11 as described previously (Mangiarini et al., 1996) and body weights were recorded at the same time daily from weeks 5-11.

Immunohistochemistry and Quantitation

Post-fixed brains were processed as 40 μm sections, used for immunohistochemistry and imaged by confocal microscopy. The following primary antibodies were used: anti-HTT mEM48 (Millipore MAB5374) and anti-DARPP-32 (Santa Cruz SC-11365). Following antibody incubation, nuclei of slices were stained with TO-PRO™-3 iodide nuclear stain (Thermo Fisher T3605) and mounted onto microscope slides using Fluoromount-G (SouthernBiotech 0100-01). A LeicaDM2500 confocal microscope was used to acquire images. Six representative sections were used per animal. Two comparable z-stack images per section were acquired at 40x and used for quantification. EM48-positive puncta were automatically counted using Imaris Bitplane 5.0 spots setting with a diameter threshold of 0.5 μm and consistent threshold between samples.

Tissue Lysis

Flash frozen brain and peripheral mouse tissue were lysed by douncing 30 times in a glass 2 mL vial. Soluble and Insoluble Fractionation was performed on tissue samples in lysis buffer containing 10 mM Tris (pH 7.4), 1% Triton X-100, 150 mM NaCl, 10% glycerol, and 0.2 mM PMSF, and supplemented with protease inhibitors and NEM as previously described (O'Rourke et al., 2013; Ochaba et al., 2016; Ochaba et al., 2018). Samples were lysed for 60 minutes on ice followed by a 20-minute centrifugation at 15,000 xg at 4°C. Supernatant served as Soluble Fraction and pellet was washed twice with lysis buffer before being re-suspended in lysis buffer supplemented to 4% SDS and served as the Insoluble Fraction. Insoluble samples were sonicated for 30 seconds at 40% amplitude and boiled for 30 minutes. Protein fractions were quantified using Lowry protein assay (Bio-

Rad). Whole cell tissue lysis was performed in T-PER or RIPA buffers supplemented with protease inhibitors protease inhibitors (Complete Mini, Roche Applied Science), 0.1 mM PMSF, 25 mM NEM, 1.5 mM aprotinin, and 23.4 mM leupeptin by douncing as above then sonicated for 10 seconds, 3 times at 40% amplitude on ice. T-PER samples were quantified using Bradford protein assay and RIPA samples were analyzed using Lowry protein assay. Protein fraction from tissue samples processed using TRIzol™ (Thermo Fisher A33251) reagent was prepared according to manufacturer's protocol to solubilize organic protein phase and analyzed by Bradford protein assay.

Western Blot analysis

Soluble Fractions, T-PER, and RIPA lysates were resolved by reducing and running 30µg of protein on 4-12% Bis-Tris Poly-Acrylamide gels (PAGE) at 150V and transferred onto 0.45µM nitrocellulose membrane. 30µg of reduced, insoluble protein from Insoluble Fractions were resolved on 3-8% Tris-Acetate Poly-Acrylamide gels run at 150V and transferred onto 0.45µM nitrocellulose membrane. Membranes were blocked in Starting block (Invitrogen) for 20 minutes at room temperature and probed in primary antibody overnight at 4°C. The following primary antibodies were used: anti-HTT (Millipore MAB5492) to detect HTTex1p, anti-actin (Sigma A5060), and anti-GAPDH (Novus Biologicals NB100-56875). Western blot data was quantified by determining the mean pixel intensity using Scion Image processing software. Soluble Fractions, T-PER, and RIPA lysates were normalized to house-keeping protein loading control (GAPDH or Actin) prior to statistical analysis. Insoluble protein was quantified as relative protein abundance as previous (Ochaba et al., 2016; Ochaba et al., 2018).

Agarose Gel Electrophoresis analysis

Oligomeric species of mHTTex1p were detected using Agarose Gel Electrophoresis (AGE) as previously described (Sontag et al., 2012) using a 1%, 375mM Tris-HCl, pH 8.8, 1% SDS agarose gel. 30µg of protein was suspended in a non-reducing loading buffer (4x, 300 mM Tris-HCl pH 6.8, 66% glycerol, 2.4%SDS with BPB) and loaded onto an agarose gel without boiling. Samples were run in a 192 mM glycine, 24.8 mM Tris base, 0.1% SDS running buffer and transferred using an Invitrogen Novex Semi-Dry blotter onto 0.45 µm PVDF membrane at 10V for 1 hour. Membranes were blocked in starting block (Invitrogen) for 1 hour at room temp and probed with primary antibody overnight at 4°C. mHTTex1p was detected using anti-HTT (Millipore MAB5492) antibody. AGE data was quantified by determining the mean pixel intensity using Scion Image processing software as a relative protein abundance.

Filter Retardation assay

Insoluble fibrils of mHTTex1p were detected using a filter retardation assay (Wanker et al., 1999) with modifications. 30µg of insoluble samples obtained from Soluble/Insoluble Fractionation were suspended in 200 µl of 0.1% SDS, boiled for 5 minutes, loaded on to a dot blot apparatus (BioRad), and blotted onto 0.2 µm Cellulose Acetate membrane. Membrane was blocked for 1 hour at room temperature in 5% milk in TBST. Fibrils were detected with anti-HTT antibody (Enzo PW0595).

RNA Isolation and Real-Time qPCR

Flash frozen brain regions harvested from R6/2 longitudinal animals were homogenized in TRIzol™ (Thermo Fisher A33251) and RNA was collected using manufacturer's procedures then purified using RNEasy Mini kit (QIAGEN). Residual DNA was removed by DNase treatment incorporated into RNEasy protocol as per manufacturer's suggestion. Following RNA isolation, reverse transcription was performed using SuperScript 3 First-strand synthesis system according to manufacturer's protocol (Invitrogen). Both oligo (dT) and random hexamer primers were used in a 1:1 ratio with a total of 1 μg RNA per sample. Final synthesized cDNA was diluted 1:10 in DEPC treated water and stored at -20°C until use. The following primers were used to amplify and detect cDNA from transcripts: full-length *Htt* (F: GCAGGG-AAAGAGCTTGAGACAC, R: CCTCATTCTCCTTGTGGCACTG), R6/2 transgene (F: CCGCTCAGGTTCTGCTTTTA, R: TGGAGGGACTTGAGGGACTC), *Darpp-32/Ppp1r1b* (F: TCTCAGAGCACTCCTCACCAGA, R: CACTCAAGTTGCTAATGGTCTGC), *Rplp0* (F: GCTTCGTGTTCACCAAGGAGGA, R: GTCCTAGACCAGTGTTCTGAGC).

Statistical analysis

All data represented as mean ± SEM with a p value of $p<0.05$ considered statistically significant. Analyses were completed in GraphPad Prism software. Student's two-tailed t-tests, assuming equal variance were performed for behavioral comparisons at designated time points between non-transgenic (NT) and R6/2 mice. Behavioral comparisons between R6/2 animals over time were completed by performing a 1-way ANOVA. Densitrometry and aggregate count from EM48 positive immunolabeling studies were analyzed by performing a 1-way ANOVA to assess changes overtime or 2-way ANOVA to compare

between brain regions. Pixel intensity values were obtained from western blots and subjected to 1-way ANOVA to assess changes in protein quantify overtime in R6/2 mice. Statistical analysis was completed on the delta CT (dCT) values obtained from qPCR reactions normalized to *Rplp0*. When comparing relative to NT week 5, a 2-way ANOVA was used to assess changes in genotype and time. When comparing between R6/2 mice only, a 1-way ANOVA was used to assess changes over time in transcription. All 1-way ANOVAs were followed by Tukey's multiple comparisons test. All 2-way ANOVAs were followed by Sidak's multiple comparisons test.

CHAPTER 1

TABLES

Table 1.1: **Break methods optimized for detection of specific mHTT species.**

Break Method	Optimized detection/rationale	Optimized Assay	Reference
Soluble/Insoluble fractionation	Soluble monomeric mHTT Insoluble HMW, accumulated mHTT	SDS-PAGE Filter retardation	(Kim et al., 2011; O'Rourke et al., 2013; Ochaba et al., 2016; Ochaba et al., 2018)
RIPA whole cell break	Soluble, Oligomeric mHTT	AGE	(Legleiter et al., 2010; Sontag et al., 2012; Weiss et al., 2008)
T-PER whole cell break	Aggregated protein species, commercially available and common reagent	SDS-PAGE	(Chabrier et al., 2014)
TRIZOL	Allows for analysis of RNA, DNA, and protein	SDS-PAGE	n/a

Table 1.2: mHTTex1p size fluctuation due to CAG repeat length.

Animal	Age (weeks)	$(CAG)_n$ Genomic DNA (Tail)	$(CAG)_n$ cDNA (Striatum)
1	5	125	125
2	5	129	129
3	5	123	123
4	7	128	128
5	7	131	131
6	7	131	130
7	9	126	126
8	9	126	126
9	9	126	126
10	11	129	129
11	11	126	127
12	11	128	127

Table 1.2: CAG repeats from genomic tail DNA comparable to counts obtained from striatal cDNA from the same animal showing lack of somatic expansion in these animals. cDNA generated from RNA harvested from striatum. CAG repeat sizing of cDNA was performed by Laragen.

Table 1.3: **Summary heat map of mHTTex1p detected using various break methods and assays at 5, 7, 9, and 11 weeks of age.**

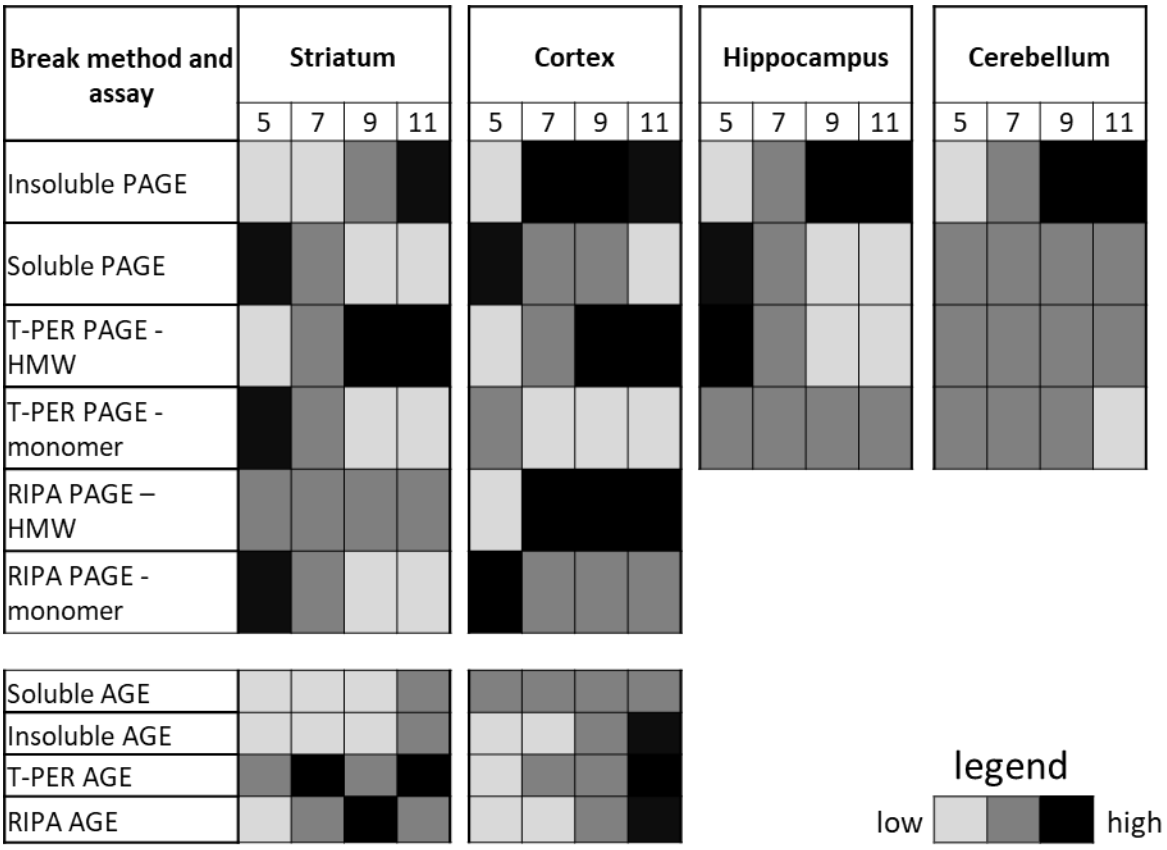

Table 1.3: Representative gradient for each assay based on ease of detection for general comparison. Cannot quantify between assay methods for relative protein abundance.

CHAPTER 2

PIAS1 SUMO-Interaction Motif May Modulate Accumulation of Mutant Huntingtin Protein

SUMMARY OF CHAPTER 2

Disruption of protein homeostasis, leading to accumulation of insoluble high molecular weight protein complexes containing the huntingtin protein and SUMOylated proteins, is a key feature of Huntington's disease (HD). We previously showed that exogenous expression of the E3 SUMO ligase PIAS1 enhanced SUMO modification and accumulation of the huntingtin protein (HTT) and that reduction of Pias1 *in vivo* reduced this accumulation. However, the functional contributions of PIAS1 domains towards accumulation of mutant HTT had not yet been studied. Structurally, PIAS1 contains a SUMO-interaction motif (SIM) and a RING-ligase domain and the contribution of these domains towards HTT SUMOylation and accumulation is unknown. Using informed mutagenesis combined with cell culture, preliminary experiments investigating the effects of the PIAS1 SUMO-interaction motif and RING domain on mutant HTT accumulation were carried out. The data suggests that the PIAS1 SIM domain may be mediating formation of an insoluble aggregation species of mutant HTT but results were confounded by issues related to transient transfection and promoter effects. Future studies utilizing CRISPR directed mutagenesis will greatly aid in elucidating the precise contribution of PIAS1 functional domains on HTT accumulation. Identification of specific mutant HTT-modulating proteins and the specific functional domains involved will inform future targeted drug design for disease intervention with broad relevance to protein dyshomeostasis in other neurodegenerative diseases.

INTRODUCTION

Neurodegenerative disorders such as Alzheimer's disease (AD), Parkinson's disease (PD) and Amyotrophic lateral sclerosis (ALS) exhibit hallmark disruption of protein homeostasis, including of protein quality control networks, similar to Huntington's disease (HD, (Hipp et al., 2014; Kurtishi et al., 2019; Ross and Poirier, 2004)). Disease is accompanied by accumulation of disease-related proteins and post-translational modifiers Ubiquitin and SUMO associate with protein inclusions (Anderson et al., 2017). In addition to an association of SUMO with protein aggregates in disease, many disease proteins themselves are SUMOylated, suggesting that the SUMO modification directly regulates protein aggregation perhaps by mediating solubility, degradation, or protein-protein interactions (Liebelt and Vertegaal, 2016). Therefore, understanding functional components contributing towards protein accumulation and the contribution of SUMOylation machinery, including the E3 ligases that regulate SUMO modification of target proteins, will prove valuable with broad relevance to other neurodegenerative diseases.

The HTT protein itself is SUMOylated with SUMOylation of mHTT potentially affecting subcellular localization and stability (Steffan et al., 2004). We identified PIAS1 as the E3 ligase (Figure 1) which enhanced SUMOylation (by SUMO1 and SUMO2/3) of HTT and modulated mHTT accumulation *in vitro* (O'Rourke et al., 2013). *In vivo* knock-down of Pias1 in the striatum of the rapidly progressing R6/2 mouse model of HD significantly altered the SUMO and ubiquitin landscape in these animals (Ochaba et al., 2016). Reduction of accumulated, insoluble High-molecular weight (HMW) mHTT and aggregate species was accompanied by reductions in both global SUMO and ubiquitin insoluble conjugates.

However, the exact contribution of PIAS1 domains towards mHTT accumulation remained unknown as mHTT undergoes changes in conformation and solubility prior to entering SUMO-positive inclusions ((Morozko et al., 2018), Chapter 1, unpublished data).

PIAS1 contains several functional domains (Figure 2.1). Of particular interest are the SUMO-interaction motif (SIM) and the RING-ligase domain within PIAS1. SUMO E3 ligase activity is mediated through the RING domain (Cappadocia and Lima, 2017). This domain is crucial for protein-protein interactions and selective ligase functionality includes the interaction with Ubc9 mediated through several cysteines within the RING domain (Kahyo et al., 2001). Mutation of these cysteines produces a Ligase-dead (LD), functionally null PIAS1 protein (Lee et al., 2003; Yurchenko et al., 2006). Further, this domain has been implicated in PIAS1 autoSUMOylation, which in turn impacts the overall function of PIAS1 (Alagu et al., 2018).

SUMOylation can mediate protein-protein interactions and formation of protein complexes by non-covalent binding through SIMs which are composed of a conserved sequence of four amino acids containing three hydrophobic residues (VVXV or VXVV where V=V/I) that are flanked by phosphorylatable acidic residues (Cappadocia and Lima, 2017). Phosphorylation of these residues by the serine/threonine kinase CK2 acts as a molecular switch for enhancing or preventing SUMO binding (Stehmeier and Muller, 2009). The SIM within PIAS1 may therefore aid in proper loading and stabilization of the Ubc9-SUMO structure for optimal transfer of the SUMO moiety onto a substrate protein mediated by phosphorylation (Cappadocia and Lima, 2017; Stehmeier and Muller, 2009).

Whether PIAS1 has a direct effect on SUMO modification of HTT and accumulation of insoluble substrates is unknown. Alternatively, modulating PIAS1 in the HD context may impact the global SUMO network or a different mechanistic pathway to modify disease indirectly. Investigating the functional impact of both the SIM and Ligase PIAS1 functional domains towards mediating mHTT solubility and accumulation may provide insight into the role of PIAS1 in the disease context. Therefore, these studies explore the underlying mechanism whereby PIAS1 may modulate protein-protein interactions and HTT protein accumulation.

RESULTS

PIAS1 phospho-SIM mutants express at the same levels

To evaluate how the PIAS1 SIM domain affects mHTT accumulation, we generated constructs containing mutations in the SIM domain of PIAS1. Constructs harboring mutations within the PIAS1 SIM or the phosphorylatable region directly downstream of the PIAS1 SIM (Figure 2.1) were generated. PIAS1 SIM was interrupted using alanine mutagenesis to replace VIDLT (AA459-463) of PIAS1 with alanines (ΔSIM). A phospho-resistant PIAS1 was created using alanine mutagenesis at serines 466-468 (S466-8A) as preventing phosphorylation of these residues perturbs SUMO binding to the SIM (Stehmeier and Muller, 2009). A complementary, phospho-mimetic PIAS1 mimicking phosphorylation of serines 466-468 was also generated by substituting them with aspartic acid residues (S466-8D), therefore facilitating SUMO binding to the PIAS1 SIM.

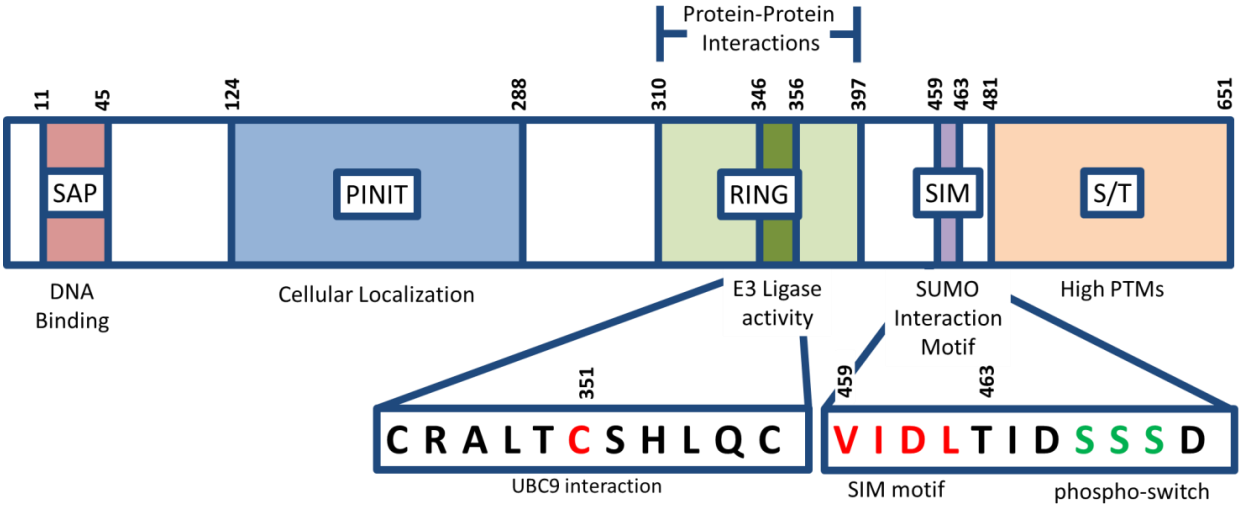

Figure 2.1 PIAS1 has numerous functional domains: PIAS1 contains numerous functional domains which aid in E3 ligase activity, protein-protein interactions, DNA binding, and post-translational modifications. Specifically, the RING domain and SIM of are particular interest due to their roles in modulating SUMOylation and associated machinery.

To evaluate whether PIAS1 SIM mutations alter PIAS1 protein levels, we first tested whether the mutations influenced expression of the construct. Using qPCR analysis, there were no differences in the levels of CMV-PIAS1 transcript expressed between WT and phospho-SIM-mutant constructs (1-Way ANOVA, post-hoc $p>0.05$, Figure 2.2B). However, the levels of *CMV-PIAS1ΔSIM* were consistently elevated compared to WT transcript (1-Way ANOVA, $F(3,8)=9.08$, $p<0.01$). CMV-PIAS1 constructs did not affect levels of endogenous *PIAS1* transcript (1-Way ANOVA, $F(4,10)=0.72$, $p>0.05$), providing a baseline to allow us to draw conclusions regarding mHTT accumulation in the presence of overexpressed PIAS1 phospho-SIM constructs. CMV-PIAS1 expression did not affect transcription of a transfection control, *CMV-myc-actin* (1-Way ANOVA, $F(4,10)=2.41$, $p>0.05$), but increased levels of exogenous CMV-myc-actin protein levels in samples containing overexpressed PIAS1 constructs compared to endogenous PIAS1 control (1-Way

ANOVA, F(4,10)=10.34, p<0.01, Figure 2.2A). Similar to transcript expression levels, PIAS1ΔSIM protein levels were significantly elevated compared to other PIAS1 mutants (1-Way ANOVA, F(4,10)=47.64, p<0.0001, Figure 2.2A). Due to the elevated levels of both PIAS1 transcript and protein associated with ΔSIM mutant that could confound interpretation, phospho-SIM-mutants were used for subsequent evaluation of this domain on mHTT accumulation.

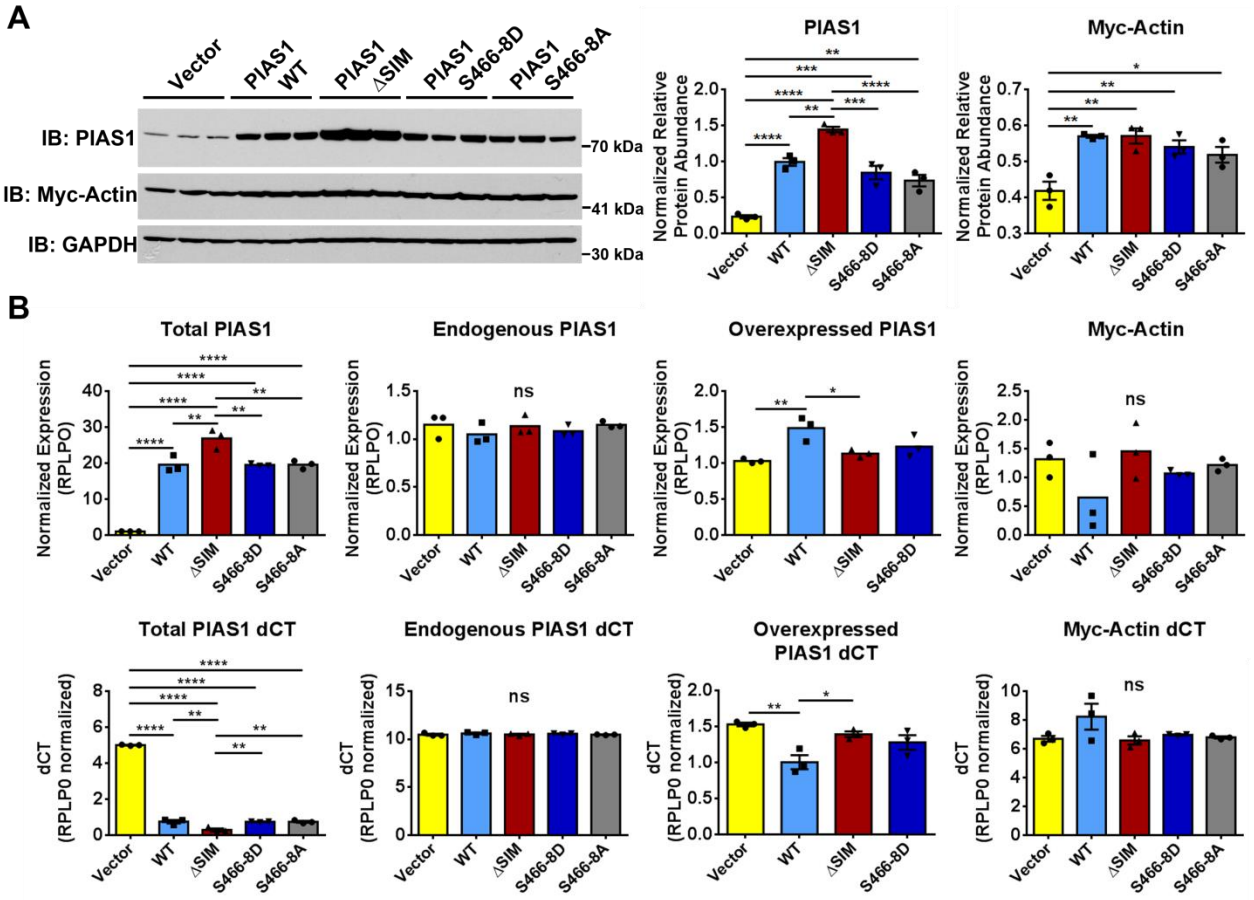

Figure 2.2: PIAS1 phospho-mutants express at the same level: A) Whole-cell Western Blot analysis of PIAS1 over-expression constructs. PIAS1ΔSIM construct expressed at higher levels than WT and S466-8D and S466-8A mutant constructs. B) qPCR analysis of CMV-driven over-expression (O.E.) constructs and endogenous *PIAS1* transcripts (Endog.) revealed a significant increase in *PIAS1ΔSIM* transcript suggesting a post-transcriptional modulation that is confounding protein-level associated readouts. Western Blots were quantified by mean pixel value. All samples were analyzed by 1-way ANOVA followed by Tukey's multiple comparison test. *P<0.05, **P<0.01, ***P<0.001, ns=not significant, values represent means ± SEM.

PIAS1 SIM modulates accumulation of mHTTex1p in human cells

To determine whether PIAS1 may modulate solubility of the mHTT exon-1 97QP protein fragment (mHTTex1p) in a human cell-line, I first examined mHTT accumulation in human HEK293T cells. This fragment rapidly forms an insoluble, HMW species that is modulated by PIAS1 (O'Rourke et al., 2013). Control and phospho-mutant PIAS1 constructs were transfected together with mHTTex1p expressing constructs in HEK293T cells to assess mHTTex1p accumulation using Soluble/Insoluble fractionation (Ochaba et al., 2018). Preventing phosphorylation of the PIAS1 SIM (S466-8A) increased accumulation of HMW, insoluble mHTTex1p (1-Way ANOVA, $F(3,7)=53.43$, $p<0.0001$, Figure 2.3A, B), suggesting that the phosphorylation status of the PIAS1 SIM is involved in modulating mHTTex1p accumulation and solubility (Figure 2.3). This increase corresponded with a significant decrease in both soluble, monomeric mHTTex1p (1-Way ANOVA, $F(3,8)=19.87$, $p<0.001$) and insoluble, fibrillar mHTTex1p (Figure 2. 3A, B). For overexpression of WT PIAS1, one sample had insufficient transfection efficiency (middle lane, Figure 2.3A of WT PIAS1) and was therefore not included in analyses. PIAS1 was increased in the soluble fraction of samples with phospho-resistant PIAS1 overexpression (Figure 2.A PIAS1 S466-8A lanes, 1-Way ANOVA, $F(3,8)=35.81$, post-hoc $p<0.05$), compared to other PIAS1 constructs, indicating a possible shift in subcellular localization of PIAS1 as the soluble fraction serves as a crude cytosolic fraction (Insoluble as crude nuclear, (Ochaba et al., 2016)). Samples with overexpressed PIAS1 phospho-mimetic (S466-8D) constructs did not show any shift in mHTTex1p solubility or PIAS1 fractionation compared to control WT PIAS1.

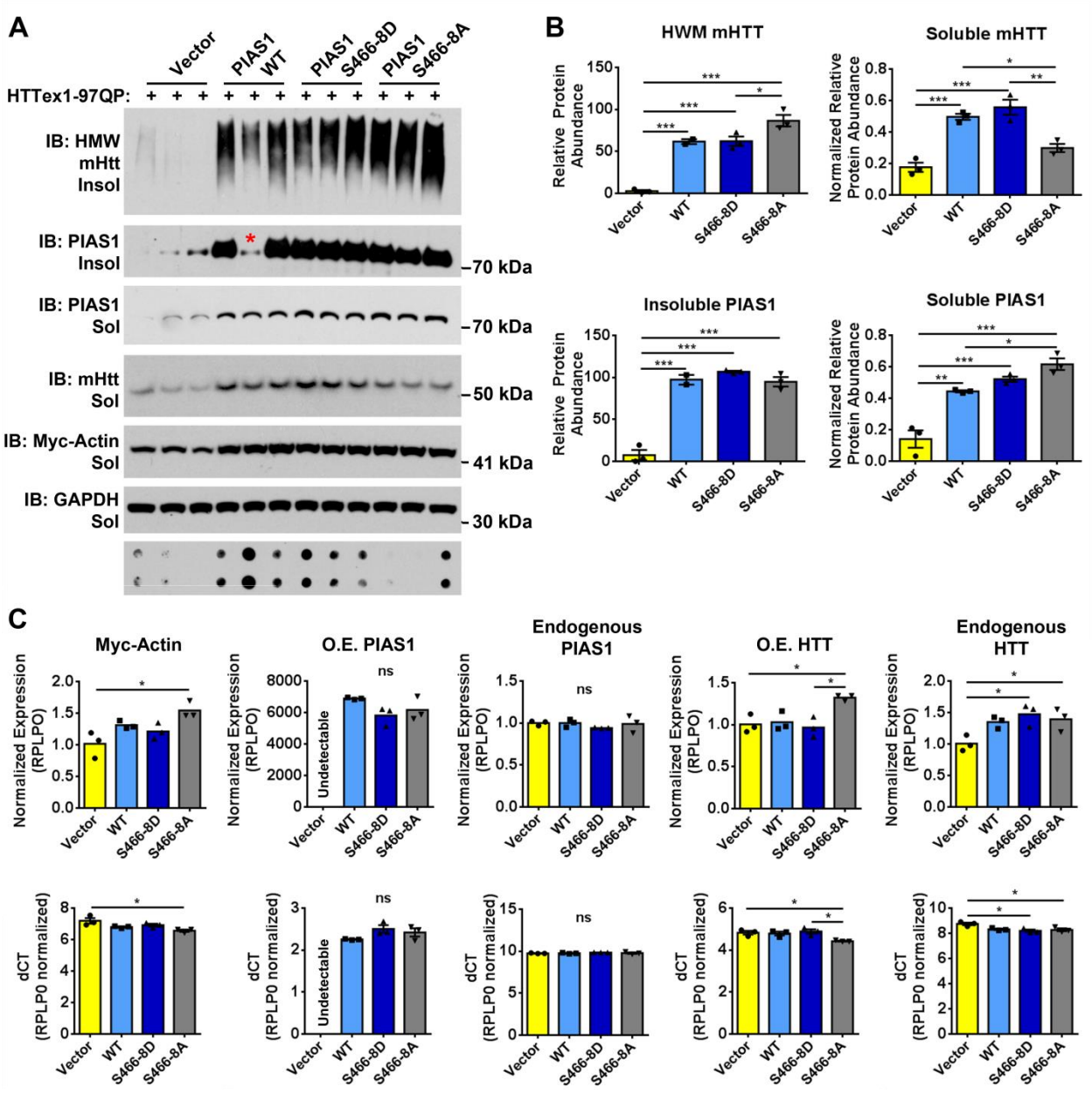

Figure 2.3: PIAS1 SIM may modulate mHTT solubility in Human cells: A) Insoluble and Soluble Western Blot analysis and B) subsequent relative protein abundance from HEK293T (Human embryonic kidney cell type) cells co-transfected with PIAS1 phospho-SIM mutants and mHTTex1p shows an increase in PIAS1 S466-8A in the Insoluble fraction, corresponding to a decrease increase in HMW mHTTex1p. C) qPCR analysis of CMV-driven over-expression (O.E.) constructs and endogenous *PIAS1* and *HTT* transcripts. Western Blots were quantified by mean pixel value. Red asterisk indicates sample with insufficient PIAS1 overexpression and was not included in analysis. All samples were analyzed by 1-way ANOVA followed by Tukey's multiple comparison test. *P<0.05, **P<0.01, ***P<0.001, ns=not significant, values represent means ± SEM.

To determine if protein accumulation in the presence of the phospho-resistant mutant was in part due to an impact on *HTT* expression, qPCR was carried out. We observed a significant increase in both endogenous (1-Way ANOVA, $F(3,8)=6.50$, $p<0.05$) and overexpressed (1-Way ANOVA, $F(3,8)=5.58$, $p<0.05$) *HTT* transcript levels with PIAS1 phospho-mutant expression (Figure 2.3C). The effect on exogenous *HTT* could in part be due to influence on CMV-promoter as *Myc-Actin* transcript levels were also increased in these samples (1-Way ANOVA, $F(3,8)=5.76$, $p<0.05$). However, this effect on *Myc-Actin* transcription was not observed with overexpression of PIAS1 constructs alone (Figure 2.2) and could indicate a compound effect with the presence of mHTTexp1 on expression of CMV-driven overexpression constructs, though this possibility is not clear in this present dataset. The results therefore may suggest that the inability to phosphorylate the SIM domain causes an increase in endogenous expression and thus accumulation of HMW mHTT species.

PIAS1 SIM modulates accumulation of mHTTex1p in striatal-derived cells

I next investigated whether the PIAS1 SIM was modulating mHTTex1p accumulation in an immortalized striatal cell line to investigate accumulation dynamics in cells derived from a neuronal linage. The experiment was therefore repeated in immortalized rat, striatal ST14A cells (Ehrlich et al., 2001). In ST14A cells, overexpression of wild-type PIAS1 had an inverse effect on mHTTex1p accumulation compared to HEK293T cells (Figure 2.4A); overexpression of WT PIAS1 resulted in a significant decrease in HMW accumulated, insoluble mHTTex1p (1-Way ANOVA, $F(3,8)=23.83$, post-hoc $p<0.01$, Figure 2.4A, B). PIAS1 phospho-resistant overexpression slightly prevented this reduction in HMW insoluble

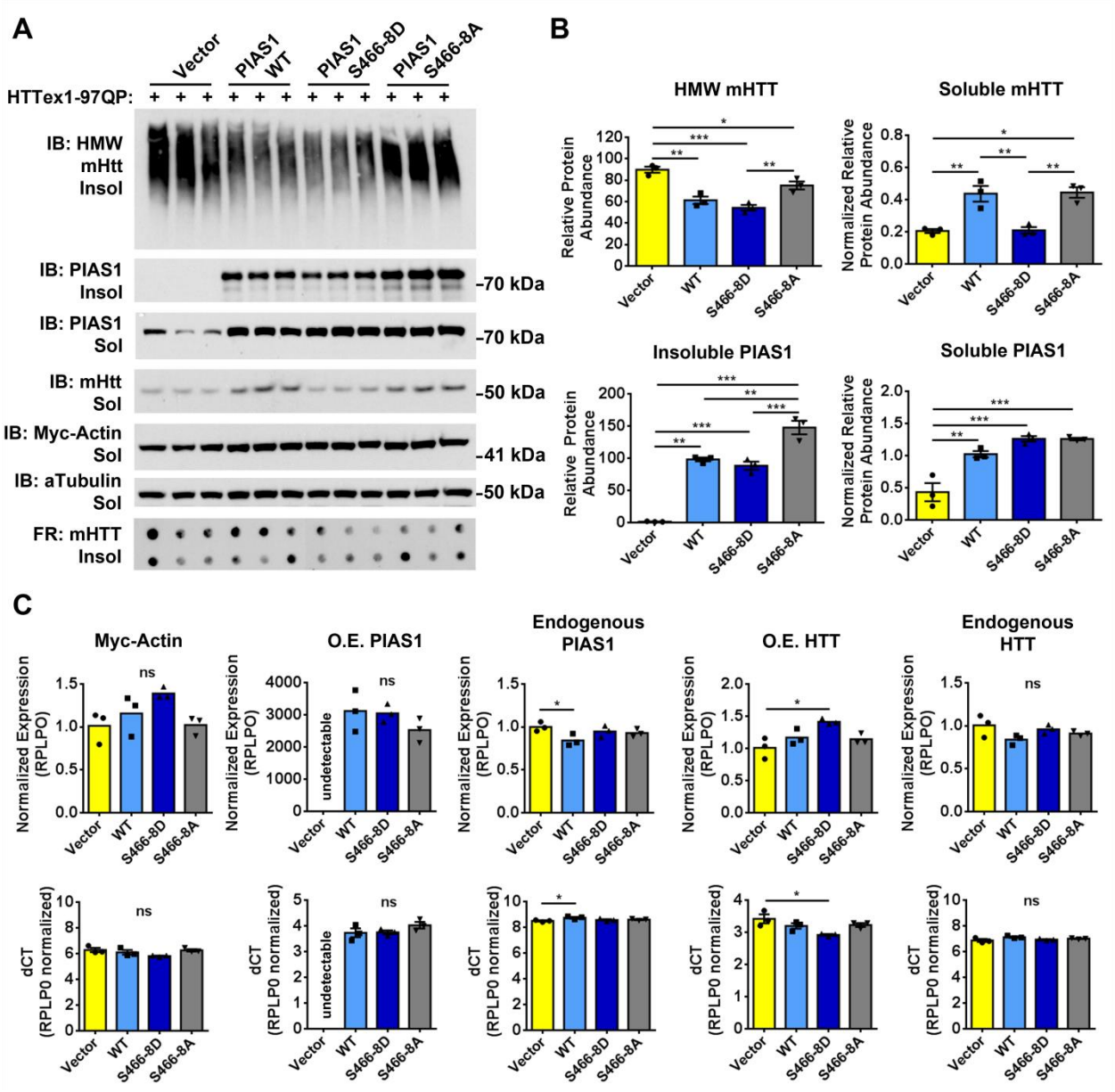

Figure 2.4: PIAS1 SIM may modulate mHTT solubility in striatal-like cells: A) Insoluble and Soluble Western Blot analysis and B) subsequent relative protein abundance from ST14A (rat, immortalized striatal cell type) cells co-transfected with PIAS1 phospho-SIM mutants and mHTTex1p showed an increase in PIAS1 S466-8A in the Insoluble fraction, corresponding to a significant increase in HMW mHTTex1p. C) qPCR analysis of CMV-driven over-expression (O.E.) constructs and endogenous *PIAS1* and *HTT* transcripts (Endog.) revealed a significant increase in endogenous *HTT* transcript. Western Blots were quantified by mean pixel value. All samples were analyzed by 1-way ANOVA followed by Tukey's multiple comparison test. *P<0.05, **P<0.01, ***P<0.001, ns=not significant, values represent means ± SEM.

mHTTex1p but did not affect levels of fibrillary or soluble monomeric mHTTex1p (1-Way ANOVA, post-hoc PIAS1vs.PIAS1 S466-8A $p>0.05$, Figure 2.4A, B). Interestingly, PIAS1 was increased in the Insoluble fraction in these samples further suggesting that the PIAS1 SIM is important for the subcellular localization or co-aggregation of PIAS1 (1-Way ANOVA $F(3,8)92.11$, post-hoc PIAS1vsPIAS1 S466-8A $p<0.01$). While the phospho-mimetic form of PIAS1 did not alter the levels of HMW mHTTex1p compared to WT PIAS1, it reduced levels of soluble, monomeric mHTTex1p (1-Way ANOVA, $F(3,8)=17.60$, post-hoc PIAS1vs.PIAS1 S466-8D $p<0.01$) indicating that the PIAS1 SIM also modulates conformational flux in a striatal cell line. Transcript levels assessed by qPCR analysis indicate that overexpression of PIAS1 may decrease endogenous PIAS1 levels (1-Way ANOVA, $F(3,8)=3.66$, $p>0.05$, post-hoc Vector vs. PIAS1 $p<0.05$) while PIAS1 phospho-mimetic slightly increased expression of mHTTex1p construct (1-Way ANOVA, $F(3,8)=5.58$, $p<0.05$) and therefore may be confounding accumulation results (Figure 2.4C).

PIAS1 Ligase domain may affect mHTTex1p accumulation in HEK293T cells

To begin investigating the consequence of ligase activity of PIAS1 on HTT accumulation, two previously reported Ligase-dead (LD) constructs were generated. The first construct contained a point mutation at cysteine 351 resulting in a serine substitution (C351S, (Lee et al., 2003)). This cysteine was previously reported to be crucial for interaction of PIAS1 with the SUMO E2 conjugating enzyme Ubc9 (Kahyo et al., 2001). Surrounding cysteine 351 are two additional cysteines, which also contribute significantly to ligase activity of PIAS1 (Figure 2.1, (Yurchenko et al., 2006)). Therefore, a second construct with three cysteine-to-serine substitutions was generated (3CS). To assess whether these mutations successfully

produced a Ligase-dead PIAS1 (PIAS1-LD) protein product, HEK293T cells were transfected and treated with protease inhibitor 5μm MG132 18 hours prior to harvest, to maximize retention of transiently SUMOylated proteins and soluble protein levels were assessed by western blot. PIAS1 itself is SUMOylated, potentially through autoSUMOylation (Alagu et al., 2018; Kotaja et al., 2002; Kumar et al., 2017) and presence of the LD mutations attenuated PIAS1 SUMOylation, strongly suggesting that PIAS1-LD constructs produce a dominant negative protein product of PIAS1 (Figure 2.5A).

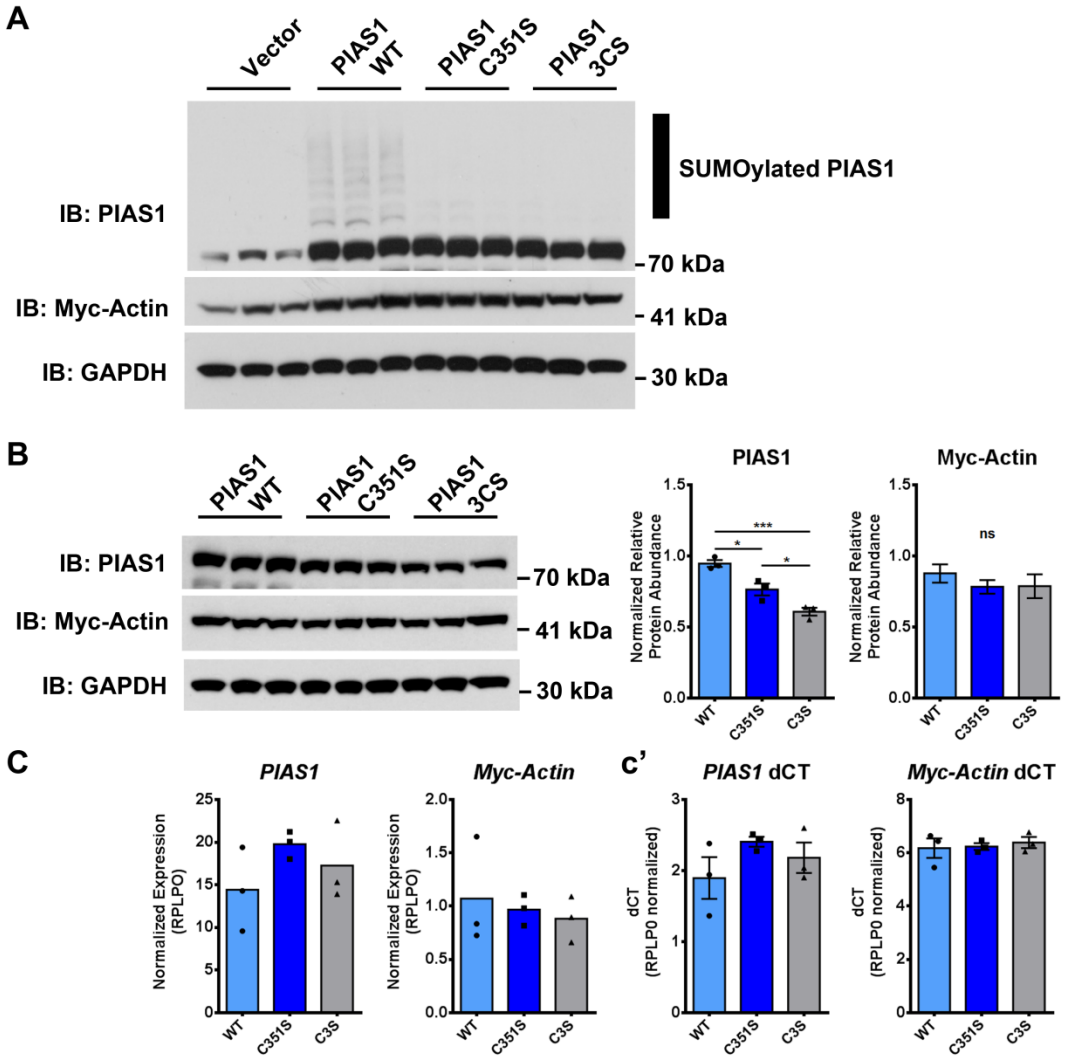

Figure 2.5: PIAS1 Ligase-Dead mutants produce a dominant-negative protein product: A) Assessment of soluble PIAS1-LD constructs showed lack of autoSUMOylation for both PIAS1 C351S and PIAS1 3CS. B) Assessment of whole-cell protein lysate and transcript expression levels of PIAS1-LD constructs. PIAS1-LD protein detected at lower levels than WT. C) qPCR and c') dCT values show constructs are transcriptionally expressed at the same level. Western Blots were quantified by mean pixel value. All samples were analyzed by 1-way ANOVA followed by Tukey's multiple comparison test. *P<0.05, **P<0.01, ***P<0.001, ns=not significant, values represent means ± SEM.

To test whether the PIAS1 Ligase domain contributes to accumulation of insoluble HMW mHTTex1p, HEK293T cells were transfected with either control or PIAS1-LD constructs together with mHTTex1p expressing constructs and assessed using Soluble/Insoluble fractionation. Preliminary data in HEK293T cells indicated that ligase activity may not affect accumulation of Insoluble HMW mHTTex1p but may affect levels of soluble monomeric mHTTex1p (Figure 2.6A, B). Overexpression of PIAS1-3CS, but not C351S, resulted in a significant decrease in soluble mHTTex1p levels (1-Way ANOVA, $F(3,8)=3.68$, post-hoc PIAS1vs.PIAS13CS $p<0.05$). However, levels of both PIAS1-LD protein products were significantly lower in both the Soluble (1-Way ANOVA, $F(3,8)=28.21$, $p<0.001$) and Insoluble (1-Way ANOVA, $F(3,8)=63.59$, $p<0.0001$) fractions indicating that PIAS1-LD protein may be preferentially cleared by the cell. Assessing PIAS1 protein levels without mHTTex1p overexpression in whole-cell lysate revealed a similar significant decrease with PIAS1-LD expression (1-Way ANOVA, $F(2, 6) = 27.79$, $p<0.001$, Figure 2.5B). This was not due to lower expression level as transcripts were assessed by qPCR and showed similar levels of expression (1-Way ANOVA, $F(2,6)=1.43$, $p>0.05$, Figure 2.5C, c'). Therefore, it was difficult to determine whether the PIAS1-LD mutants might have an impact on insoluble HMW mHTTex1p levels.

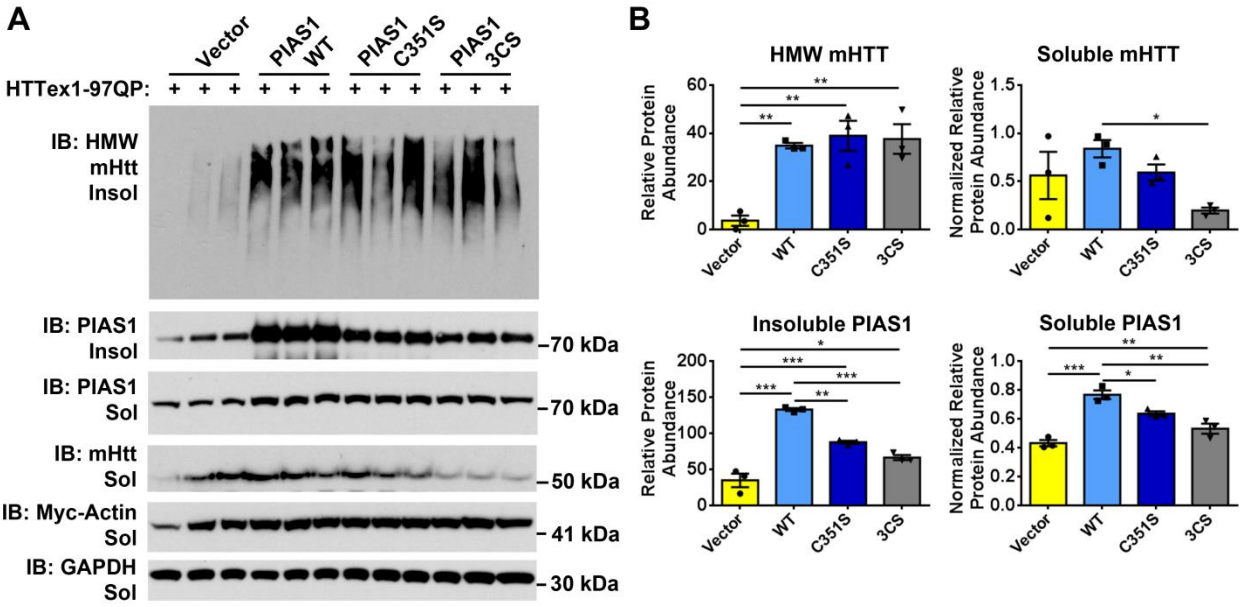

Figure 2.6: PIAS1 LD mutants confound mHTT assessment: A) Insoluble and Soluble Western Blot analysis and B) subsequent relative protein abundance from HEK293T cells co-transfected with reported PIAS1 LD mutants and expanded HTT exon1 without MG132 treatment showed significant decrease in PIAS1-LD protein products. Data confounded by PIAS1-LD protein levels such that PIAS1 LD constructs are significantly lower than WT. Western Blots were quantified by mean pixel value. All samples were analyzed by 1-way ANOVA followed by Tukey's multiple comparison test. *P<0.05, **P<0.01, ***P<0.001, ****P<0.0001, ns=not significant, values represent means ± SEM.

To address this potential confound, experiments were repeated and cells were this time treated with proteasome inhibitor MG132 to prevent protein clearance of dominant-negative PIAS1-LD (Figure 2.7A, B). Strikingly, even in the presence of MG132, PIAS1-LD protein products still showed minor but significant variations in insoluble PIAS1 protein abundance levels (1-Way ANOVA, $F(3,8)=315.9$, $p<0.0001$). No differences were observed in levels of insoluble HMW mHTTex1p (1-Way ANOVA, $F(3,8) = 3.20$, $p>0.05$) or soluble, monomeric mHTTex1p (1-Way ANOVA, $F(3,8) = 0.44$, $p>0.05$) in the presences of MG132 inhibitor (Figure 2.7A, MG132 panel). Interestingly, accumulation of insoluble HMW mHTTex1p was affected by DMSO control treatment in WT PIAS1 samples (1-Way ANOVA, $F(3,8)=4.60$, $p<0.05$). Due to these confounding variables, no conclusion about the effect of

PIAS1 ligase-activity on mHTTex1p accumulation could be derived using this transient transfection method.

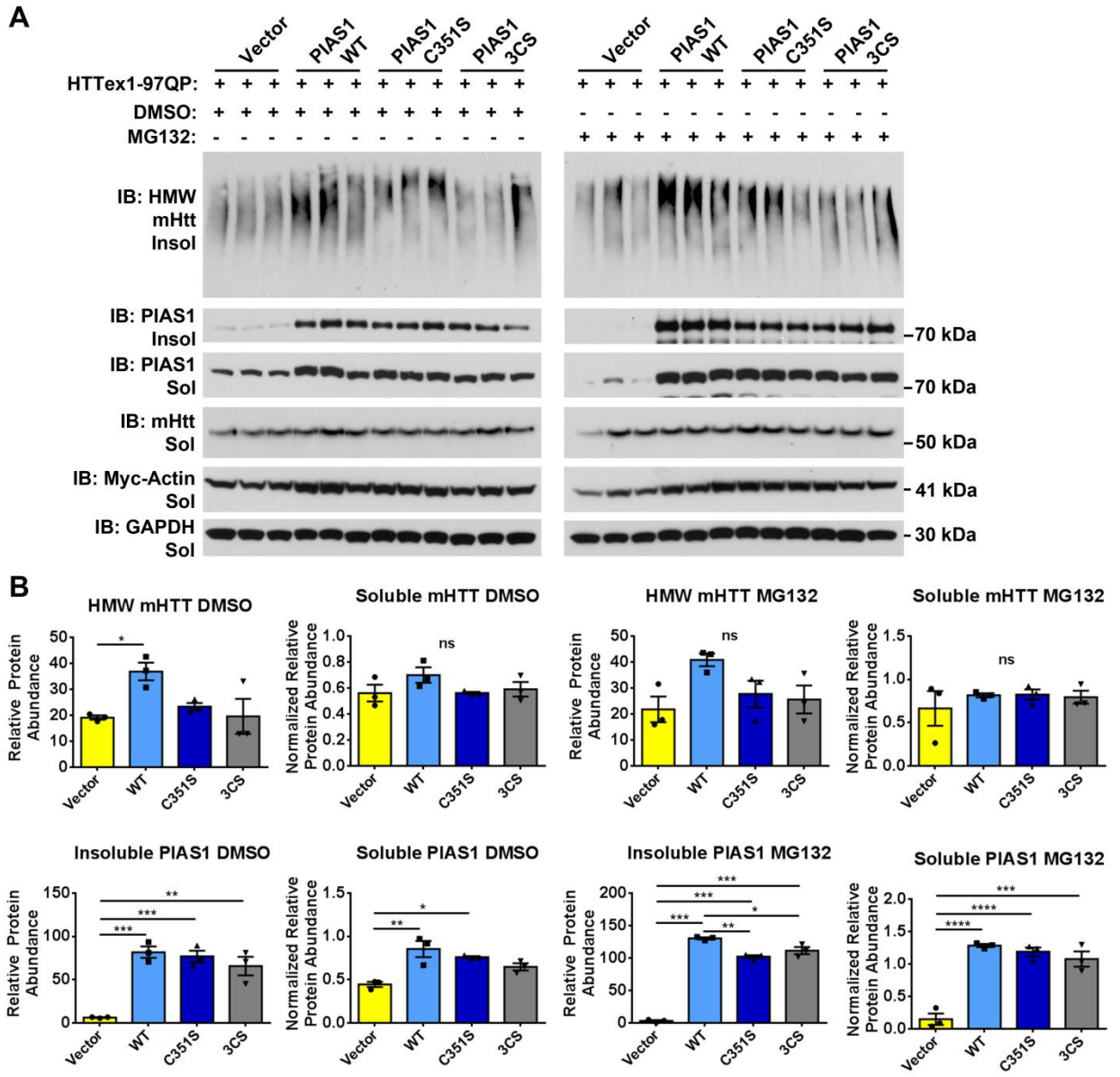

Figure 2.7: PIAS1 LD mutants confound mHTT assessment with MG132 treatment: A) Insoluble and Soluble Western Blot analysis and B) subsequent relative protein abundance from HEK293T cells co-transfected with PIAS1 LD mutants and mHTTex1p, with and without proteosomal inhibition with MG132. Data confounded by PIAS1-LD protein levels such that PIAS1 LD constructs are significantly lower than WT. Western Blots were quantified by mean pixel value. All samples were analyzed by 1-way ANOVA followed by Tukey's multiple comparison test. *P<0.05, **P<0.01, ***P<0.001, ****P<0.0001, ns=not significant, values represent means ± SEM.

DISCUSSION

While SUMOylated proteins as well as dysregulation of SUMO-associated proteostatic pathways are associated with neurodegenerative diseases, the exact functional contribution towards mediating homeostasis in disease states remains unclear. Specifically, how SUMO and SUMO-related machinery promote or prevent protein accumulation (e.g. mHTT) remains to be elucidated. Previously, we showed that SUMOylation with SUMO2 by PIAS1 increased the accumulation and aggregation potential of mHTT species (O'Rourke et al., 2013). Modulation of PIAS1 in cell culture and in the brain of HD mice significantly altered levels of accumulated mHTT (O'Rourke et al., 2013; Ochaba et al., 2016). Therefore, using PIAS1 and its SUMO-related functional domains as a target, I assessed if these domains were mediating mHTT accumulation.

The RING-domain within PIAS1 is critical for its function as an E3 SUMO ligase. This domain is also critical for the interaction between PIAS1 and E2 UBC9 (Kahyo et al., 2001). PIAS1 interaction with Ubc9 is mediated in part through the SIM domain following the RING domain. The creation of a ternary complex with a SUMO moiety through the PIAS1 SIM serves as an integral functional component in SUMOylation of target substrates (Mascle et al., 2013). Further, both of these domains are integral for tethering other SUMOylated proteins (Kotaja et al., 2002). Due to their significant role in mediating SUMOylation of target substrates, PIAS1 Ligase and SIM domains were assessed for their impact on mHTTex1p accumulation.

Overall, experiments presented here were confounded by effects of transient over-expression driven by the CMV-promoter. While PIAS1 mutant constructs had equivalent levels of transcript expression when expressed alone (Figures 2.2, 2.5), these constructs affected expression of both exogenous expression of mHTTex1p as well as endogenous *HTT* expression (Figures 2.3C, 2.4C). In turn, the increased expression of *mHTTex1p* could account for the observed differences in mHTTex1p protein levels (both soluble and insoluble levels). In the case of the PIAS1-LD constructs, protein products seemed to be preferentially degraded by the cell, preventing sufficient overexpression of dominant-negative PIAS1-LD, including when treated with proteasome inhibitor MG132 (Figure 2.6). Follow-up experiments blocking autophagy may provide information whether this process accounts for the increased clearance or whether some other mechanism is contributing to the reduced protein levels. However, further development of a cell-based assay is necessary to fully assess impact of PIAS1 functional domains on protein accumulation and SUMOylation. Alternative approaches include testing additional promoters that may be less sensitive to PIAS effects. However, the optimal approach would be to create endogenous mutations through CRISPR-mediated genome editing of the endogenous PIAS locus in both cell-based models and ultimately *in vivo* in mouse models of disease.

Although there are complications in interpretation, it appears that the PIAS1 SIM may be involved in modulating solubility of mHTTex1p in multiple cell lines, such that preventing phosphorylation of the SIM leads to an increase in insoluble mHTTex1p with a corresponding decrease in soluble mHTTex1p in human HEK293T cells (Figure 2.3). This may be a result of preventing SUMO binding to PIAS1 such that phosphorylation of SIMs

increases their affinity for SUMO (Anamika and Spyracopoulos, 2016; Cappadocia et al., 2015). This increased affinity may be in part due to increasing electrostatic interactions of SUMO moieties with the hydrophobic core of the SIM (Cappadocia et al., 2015) or potentially through mediating polarity of SUMO-SIM binding interactions (Gareau and Lima, 2010). For PIAS1 specifically, preventing phosphorylation of serines 466, 467, and 468 prevents SUMO binding (Stehmeier and Muller, 2009), which in turn may destabilize the ternary complex of PIAS1 with Ubc9 and SUMO (Kahyo et al., 2001; Mascle et al., 2013). Destabilizing this interaction could impair SUMOylation of PIAS1 substrates. This could suggest that modulation of mHTTex1p accumulation was due to preventing SUMOylation of PIAS1 target proteins (e.g. mHTT itself or another substrate). Alternatively, evidence exists supporting a function for SIM phosphorylation in specification of protein interaction with SUMO1 (Hecker et al., 2006). While this could suggest that our observations are due to preferential binding of one SUMO isoform over another to mediate accumulation of insoluble protein substrates, the overall selectivity of SIMs for specific SUMO isoforms requires further characterization (Cappadocia et al., 2015).

Interestingly, in striatal-derived rat ST14A cells, preventing phosphorylation of the PIAS1 SIM abrogated a PIAS1 effect on insoluble mHTT, but increased soluble mHTTex1p levels (Figure 2.4). The observed difference in PIAS1 effects between cell lines may in part be due to cell lineage (e.g. striatal vs. kidney) or species (e.g. rat vs. human). Cell type and lineage may result in a differential contribution of SUMO machinery towards maintaining proteostasis. Additional experiments investigating differences in protein homeostatic

pathways (e.g. autophagy and proteasome) in these cell lines and *in vivo* may aid in elucidating these differences.

SUMMARY AND NEXT STEPS

Together, data presented in this chapter present a first step to establish a system to understand how SUMO machinery, specifically the E3 SUMO ligase PIAS1, is modulating mHTTex1p solubility and aggregation. Using Soluble/Insoluble fractionation allows for a quantitative assessment of mHTTex1p conformers (Morozko et al., 2018; Ochaba et al., 2016), Chapter 1). This technique, coupled with informed mutagenesis of key residues or domains involving SUMO (including within the HTT protein itself) could aid in understanding how SUMO may be contributing to solubility dynamics or modulating accumulation of target proteins. While aggregation dynamics observed in this chapter appear to have been affected by CMV-driven promoter effects, the data provides preliminary data showing that the SIM within PIAS1 may mediate HTT accumulation. Cell lines that avoid the use of transient overexpression constructs by using targeted gene editing techniques will need to be generated to fully assess the contribution of PIAS1 functional domains.

EXPERIMENTAL PROCEDURES

Cloning

Plasmids for PIAS1 functional domain studies were generated by Genscript. PIAS1 SIM domain was modulated by mutating the phophorylatable series directly adjacent to the PIAS1 SIM to either alanines (inactivating) or aspartic acids (activating) generating PIAS1

S466-8A or PIAS1 S466-8D constructs (Stehmeier and Muller, 2009). PIAS1 ring domain was targeted by site-specific mutagenesis of cysteine 351 to serine (C351S) or cysteines 346, 351, and 356 to serines (3CS) to yield ligase-dead PIAS1 (PIAS1-LD) as previously characterized (Lee et al., 2003; Yurchenko et al., 2006). Mutant huntingtin exon1 protein (mHTTex1p) and myc-actin constructs were used as previous (O'Rourke et al., 2013). All constructs were under CMV-driven promoter.

Cell Culture

Human, HEK293T cells were cultured in Dulbecco's Modified Eagle Medium (DMEM) with High glucose supplemented to 10% FBS at 37°C. Cells were transfected using 1.5 µl Lipofectamine 2000 at ~45% confluency with 2 µg of cDNA plus 1/10th myc-actin as a transfection and expression control on day 2. Media was changed 24 hours post transfection (day 3) and cells will be allowed to grow to ~95% confluency (~44 hours after transfection, day 4). Rat, ST14A striatal-derived (Ehrlich et al., 2001) cells were similarly cultured but grown at 33°C, transfected as above at ~45-50% confluency and allowed to grow to ~90% confluency prior to harvest on day 4.

Soluble/Insoluble Fractionation

Soluble and Insoluble fractionation was performed on cell samples in lysis buffer containing 10 mM Tris (pH 7.4), 1% Triton X-100, 150 mM NaCl, 10% glycerol, and 0.2 mM PMSF, and supplemented with protease inhibitors and NEM as previous (O'Rourke et al., 2013; Ochaba et al., 2016; Ochaba et al., 2018). Samples were lysed for 60 minutes on ice followed by a 20 minute centrifugation at 15,000 xg at 4°C. Supernatant served as Soluble

fraction. Pellet was re-suspended in lysis buffer supplemented to 4% SDS as the Insoluble fraction. Insoluble samples were sonicated for 30 seconds at 40% amplitude and boiled for 30 minutes. Protein fractions will be quantified using Lowry protein assay (Bio-Rad).

Western Blot and SDS-PAGE

Soluble protein lysates were resolved on 4-12% Bis-Tris Poly-Acrylamide gels while Insoluble protein lysates were resolved on 3-8% Tris-Acetate Poly-Acrylamide followed by transfer onto a nitrocellulose membrane. The following primary antibodies were used: anti-HTT (Millipore MAB5492) to detect HTTex1p, anti-PIAS1 (Cell Signaling 3550S), anti-PIAS1 (Invitrogen 39-6600), Anti-myc (Millipore 05-419), and anti-GAPDH (Novus Biologicals NB100-56875) and assessed using HRP-conjugated secondaries, ECL reagent (Thermo, 34580, 34076), and exposure to X-Ray film. Western blots were quantified by determining the mean pixel intensity using Scion Image processing software. Soluble and whole cell samples were normalized to house-keeping protein (GAPDH) prior to statistical analysis. Insoluble protein was quantified as relative protein abundance.

Filter Retardation Assay

To analyze insoluble, fibrillar mHTT species, filter retardation assays were performed (Wanker et al., 1999). 30 µg of Insoluble protein lysate was suspended in 200 µL of 2% SDS and boiled for 5 minutes. Samples were applied to a dot blot apparatus (Bio-Rad) and filtered through 0.2 µm cellulose-acetate membrane. Membrane was washed twice with 0.1% SDS solution and blocked in 5% non-fat milk dissolved in TBST for 1 hour at room temperature followed by incubation in primary antibody (Anti-HTT Viva Biosciences

VB3130) to detect insoluble mHTT fibrils overnight at 4°C. Protein was detected using ECL reagent and exposure to radiogram.

RNA purification and qPCR

Transfected cells were harvested on day 4 using 1 ml TRIzol reagent (Invitrogen, 15596026) per well of a 6-well dish. Cells were washed once with sterile 1x PBS prior to harvest in TRIzol reagent. RNA was extracted according to manufacturer's protocol and purified using RNeasy Mini kit (Qiagen, 74106). Residual DNA was removed by DNase treatment incorporated into RNEasy protocol as per manufacturer's suggestion. Random hexamer primers were used with 1 µg RNA per sample to reverse synthesize cDNA. Final synthesized cDNA was diluted 1:5 in DEPC treated water and stored at -20°C until use. The following primers were used to detect endogenous and exogenous transcripts:

endogenous human *PIAS1* (F: CGAAGTTCACTGCGCTTGCG, R: GTTCGTGTTTGCGTCCGTGC), endogenous human full-length *HTT* (F: CTCTGGTGTCAGATACTGCTGC, R: CTCCTCTTCTCCAGACATCTGG), endogenous human *RPLP0* (F: TGGTCATCCAGCAGGTGTTCGA, R: ACAGACACTGGCAACATTGCGG), endogenous rat *Pias1* (F: CAACAGTCTGAGGGAGAGCCAT, R: TTAATCTGGGATGGGGTGGGAG), endogenous rat full-length *Htt* (F: GCAGGGCTTTCCAGTCTGTGTT, R: CCTCTCAGCCTCTTGTTCCACA), endogenous rat *Rplp0* (F: GGCCCGAGAAGACCTCTTTCTT, R: CATGTTCAGCAGTGTGGCTTCG), exogenous *PIAS1* (F: CGTGTACGGTGGGAGGTCTA, R: TTAGTTCCGCACTGTCCGCC), exogenous *myc-actin* (F: CGTGTACGGTGGGAGGTCTA, R: CCGCCAGATCCTCTTCTGAGA), exogenous *HTT* (F: CGTGTACGGTGGGAGGTCTA, R:

GCTTTTCCAGGGTCGCCATG). Data presented as Fold-Change relative to Vector control (or *PIAS1-WT* for *PIAS1* overexpression assessment).

Statistical analysis

All data represented as mean ± SEM with a p value of $p<0.05$ considered statistically significant. Analyses were completed in GraphPad Prism™ software. Pixel intensity values were obtained from western blots and subjected to 1-way ANOVA to assess differences in protein levels. Statistical analysis using 1-way ANOVA was completed on the delta CT (dCT) values obtained from qPCR reactions normalized to RPLP0. All 1-way ANOVAs were followed by Tukey's multiple comparisons test.

CHAPTER 3

PIAS1 Serves as a SUMO E3 Ligase for PNKP and Modulates its Enzymatic Activity in Huntington's Disease Patient iPSC-Derived Neurons

SUMMARY

As a SUMO E3 ligase, PIAS1 modulates mHTT accumulation, potentially through non-covalent interactions mediated by the PIAS1-SIM (Chapter 2). While KD of Pias1 in the rapidly progressing R6/2 Huntington's disease (HD) mouse model reduced accumulation of mHTT and was behaviorally beneficial, PIAS1 has multiple cellular roles and may contribute to HD pathogenesis through alternative mechanisms. Previous studies relied on overexpression in immortalized cell culture or mice expressing a pathogenic, toxic fragment of human mHTT. Therefore, understanding the function of PIAS1 in the endogenous genomic disease context may reveal additional molecular contributions towards mediating disease pathogenesis. We therefore utilized human induced pluripotent stem cells (iPSCs) from control and HD patients and CRISPR-mediated genome editing to reduce endogenous *PIAS1*. These iPSCs were differentiated into medium spiny neurons (MSNs), the most overtly affected cell type in HD, permitting experimental manipulation of an otherwise inaccessible, post-mitotic cell type. This allowed us to begin elucidating neuron-specific functions of PIAS1 and how these may be perturbed by endogenous full-length mHTT in human cells. Here we show that PIAS1 is a component of the transcription-coupled repair complex, a DNA damage repair mechanism that safe-guards the genomic integrity of actively transcribing genes. Further, genetic reduction of PIAS1 in iPSC-derived MSNs restored mHTT-perturbed enzymatic activity of the TCR enzyme PNKP. We provide

experimental evidence that PIAS1 is a SUMO E3 ligase for PNKP *in vitro* and may modulate endogenous PNKP SUMOylation in neurons. Increased PNKP activity also corresponded to increased genomic integrity. Overall, data presented in this chapter presents the first evidence that PIAS1 serves as an E3 ligase mediating DNA damage repair processes in post-mitotic neurons and suggests that therapeutic reduction of PIAS1 could increase genomic stability in the HD brain.

INTRODUCTION

We previously showed that Small Ubiquitin-like Modifier (SUMO) modifies the huntingtin (HTT) protein and potentially mediates solubility and degradation (Steffan et al., 2004). SUMOylation plays an integral role in maintaining protein homeostasis (proteostasis) which is dysregulated in numerous neurodegenerative diseases, including HD (Liebelt and Vertegaal, 2016). SUMOylation is involved in many neuronal-specific processes including localization of metabotropic glutamate receptors, functionality of voltage-gated ion channels, and axonal trafficking by either directly modifying target substrates or mediating interactions with binding partners (Henley et al., 2018; Schorova and Martin, 2016). However, SUMOylation contributes broadly to overall cellular homeostasis in dividing cells by modulating protein-protein interactions and maintaining cellular homeostasis through mediating biological processes such as protein clearance pathways and DNA damage repair (DDR) cascades (Liebelt and Vertegaal, 2016; Schwertman et al., 2016). PIAS1 has defined roles in many different processes as a SUMO E3 ligase, including DNA repair (Galanty et al., 2009; Gibbs-Seymour et al., 2015). For HTT, PIAS1 serves as a SUMO E3 ligase by enhancing its SUMOylation which in part may

contribute to accumulation of insoluble mHTT protein (O'Rourke et al., 2013; Ochaba et al., 2016). Importantly, PIAS1 is the most expressed PIAS isoform in the human caudate, suggesting a potential region-specific function of this isoform in the striatum (Human Protein Atlas). However, the specific functional contribution of PIAS1 towards disease associated pathways in the brain is unknown.

An inverse relationship between the number of repeats within the *HTT* gene and age-of-onset (AO) is observed, though with great variability (Langbehn et al., 2004). It was recently shown that this variability in part is linked to genetic modifiers involved in DNA damage repair (DDR) pathways (Bettencourt et al., 2016; Flower et al., 2019; GeM-HD, 2015; Moss et al., 2017). The HTT protein itself has been identified as a scaffold for DDR proteins. Specifically, HTT interacts with components of the base excision repair (BER) and transcription coupled repair (TCR) complexes, suggesting that mHTT protein may be preventing appropriate repair in the brain (Gao et al., 2019; Maiuri et al., 2017). Indeed, presence of mHTT protein perturbs enzymatic activity of the end-processing enzyme PNKP with impaired activity corresponding with a decrease in genomic stability (Gao et al., 2019). This suggested that modulating activity of TCR processes may be therapeutically beneficial. Since DDR mechanisms rely heavily on post-translational modifications such as SUMO, and HTT itself is a SUMO substrate, it is possible that PIAS1 may be participating in these repair pathways in neurons as a SUMO E3 ligase.

In HD, the medium spiny neurons (MSNs) of the striatum and projection neurons of the cerebral cortex are specifically affected and degenerate (Ross and Tabrizi, 2011; Rub et al.,

2016; Zuccato et al., 2010). While many animal models are available to study HD, induced pluripotent stem cells (iPSC) allow us to study the disease within the human endogenous genomic context. HD iPSCs have already been informative in elucidating early aspects of transcriptional dysregulation (Consortium, 2017), nuclear/cytoplasmic transport deficits (Gasset-Rosa et al., 2017; Grima et al., 2017), neurodevelopmental changes (Consortium, 2017; Mathkar et al., 2019; Mattis et al., 2015), and deficits in DDR mechanisms (Gao et al., 2019) in HD. Therefore, they provide a powerful tool for studying HD-associated mechanisms in a human, neuronal context.

To begin to identify cellular mechanisms utilizing PIAS1 that contribute to HD pathogenesis we used HD patient iPSC-derived MSNs and CRISPR-Cas9 gene editing to knock-down (KD) *PIAS1*. After identifying PIAS1 as a binding partner of HTT within the TCR complex, and due to PIAS1's previously established functions in DDR, we assessed if PIAS1 was modulating repair activity in iPSC-derived MSNs. Genetic reduction of PIAS1 rescued mHTT-perturbed enzymatic activity of the repair enzyme PNKP. We now show that PIAS1 is a SUMO E3 ligase for PNKP and that rescued enzymatic activity corresponded with an increase in genomic stability of actively transcribing genes. Our data further supports a role for SUMOylation in maintaining neuronal homeostasis in neurodegenerative disease and defines PIAS1 as a key component of the DNA damage repair pathway in neurons.

RESULTS

Generation of PIAS1 KD in control and HD iPSCs using CRISPR-CAS9 genome editing

To investigate the impact of PIAS1 in HD neurons, KD of PIAS1 by creation of an in-del in the PIAS1 locus of the genome was performed using CRISPR-Cas9 genome editing technology. Clones were generated by targeting exon 2 of the PIAS1 locus (Figure 3.1A) and tested by T7EI digestion of PCR fragments (data not shown). Several clones that were positive in the T7EI assay were then validated for in-dels by genomic DNA sequencing. The specific mutation was shown to be a deletion in the 33Q and an insertion in the 66Q iPSC clones (Figure 3.1B, D) and both produced shortened transcripts that resulted in significantly reduced PIAS1 protein product as assessed by western blot ($p<0.05$, Figure 3.1C, E). iPSC clones were assessed by immunofluorescence for pluripotency (Figure 3.2B). Lines were determined to be karyotypically normal and selected for follow-up differentiation and functional studies (data not shown). Next, the differentiation capability into neurons was assessed by differentiation through a 37 day protocol to derive MSNs (Figure 3.2A). Cell lines showed comparable DARPP32 and BCL-11B co-staining, and MAP-2 staining at the end of differentiation indicating successful differentiation (Figure 3.2C) and reveals that PIAS1 reduction does not influence differentiation into neurons.

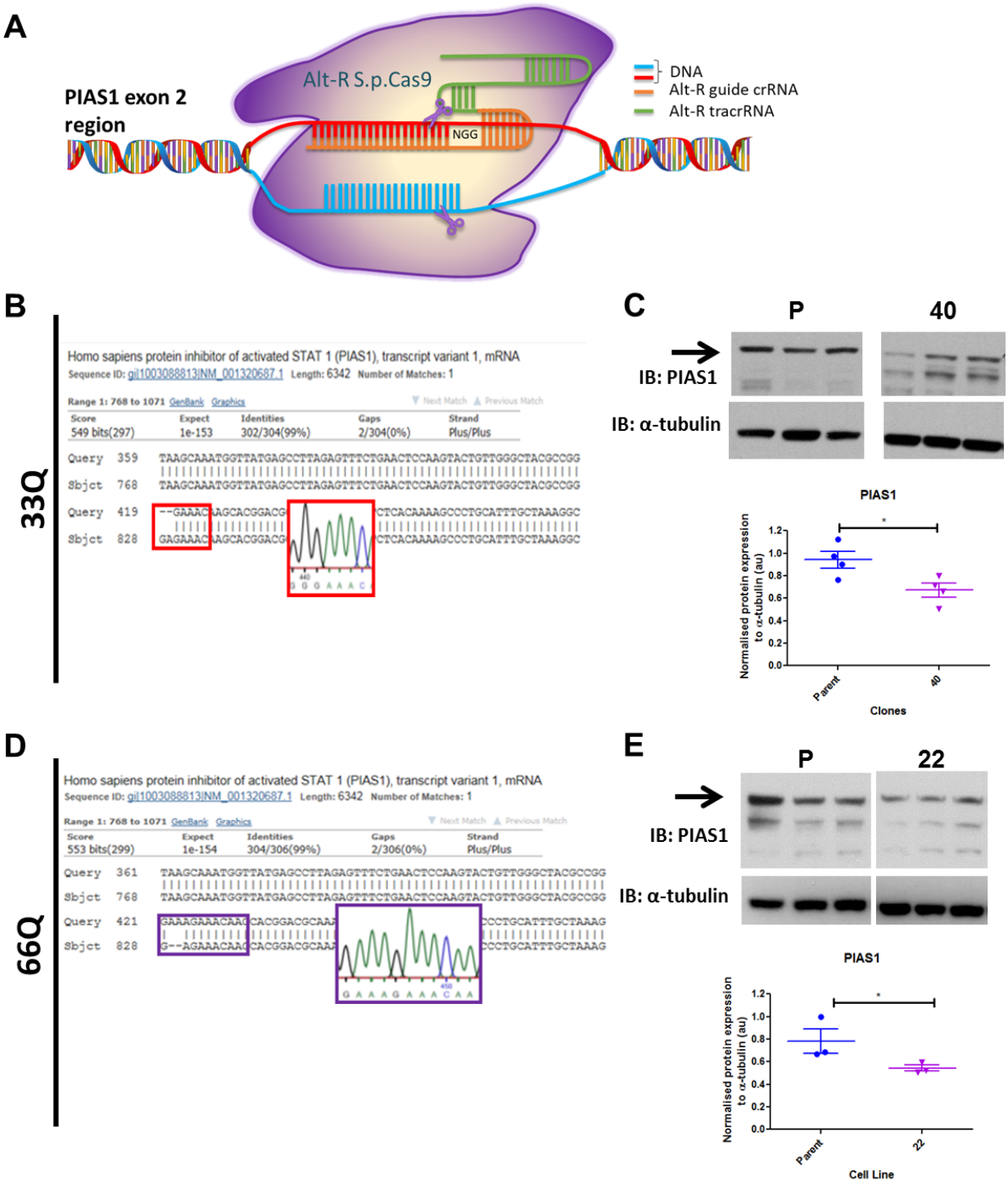
A
PIAS1 exon 2 region
Alt-R S.p.Cas9
NGG
DNA
Alt-R guide crRNA
Alt-R tracrRNA
B
33Q
Homo sapiens protein inhibitor of activated STAT 1 (PIAS1), transcript variant 1, mRNA
Sequence ID: gil1003088813|NM_001320687.1 Length: 6342 Number of Matches: 1
Range 1: 768 to 1071 GenBank Graphics
Score Expect Identities Gaps Strand
549 bits(297) 1e-153 302/304(99%) 2/304(0%) Plus/Plus
Query 359 TAAGCAAATGGTTATGAGCCTTAGAGTTTCTGAACTCCAAGTACTGTTGGGCTACGCCGG
Sbjct 768 TAAGCAAATGGTTATGAGCCTTAGAGTTTCTGAACTCCAAGTACTGTTGGGCTACGCCGG
Query 419 --GAAACAAGCACGGACG CTCACAAAAGCCCTGCATTTGCTAAAGGC
Sbjct 828 GAGAAACAAGCACGGACG CTCACAAAAGCCCTGCATTTGCTAAAGGC
C
P
40
IB: PIAS1
IB: α-tubulin
PIAS1
Normalised protein expression to α-tubulin (au)
Parent
40
Clones
D
66Q
Homo sapiens protein inhibitor of activated STAT 1 (PIAS1), transcript variant 1, mRNA
Sequence ID: gil1003088813|NM_001320687.1 Length: 6342 Number of Matches: 1
Range 1: 768 to 1071 GenBank Graphics
Score Expect Identities Gaps Strand
553 bits(299) 1e-154 304/306(99%) 2/306(0%) Plus/Plus
Query 361 TAAGCAAATGGTTATGAGCCTTAGAGTTTCTGAACTCCAAGTACTGTTGGGCTACGCCGG
Sbjct 768 TAAGCAAATGGTTATGAGCCTTAGAGTTTCTGAACTCCAAGTACTGTTGGGCTACGCCGG
Query 421 GAAAGAAACAAG CACGGACGCAAA CCCTGCATTTGCTAAAG
Sbjct 828 G--AGAAACAAG CACGGACGCAAA CCCTGCATTTGCTAAAG
E
P
22
IB: PIAS1
IB: α-tubulin
PIAS1
Normalised protein expression to α-tubulin (au)
Parent
22
Cell Line

Figure 3.1: CRISPR-Cas9 was used to reduce PIAS1 expression in iPSC. A) Schematic showing CRISPR-Cas9 design to create an in-del mutation at the PIAS1 locus in exon 2. B) 33n1 Clone 40 PIAS1 sequence highlighting the mutation a deletion in 33n1 Clone 40. C) Western blots showing PIAS1 expression in iPSCs that have been modified at the PIAS1 locus by CRISPR-Cas9 in 33Q and quantification of the PIAS1 expression normalized to α-tubulin. D) 66n4 Clone 22 PIAS1 sequence highlighting the mutation an insertion in 66n4 clone 22. E) Western blots showing PIAS1 expression in iPSCs that have been modified at the PIAS1 locus by CRISPR-Cas9 in 66Q and quantification of the PIAS1 expression normalized to α-tubulin. P = parental line. Arrows shows band quantified. 1-Way ANOVA, * $p<0.05$. Values represented as means ± SEM and individual values. Data and figure generated by Charlene Smith-Geater, PhD, Thompson lab.

PIAS1 is part of the TCR complex along with HTT and modulates PNKP activity

We previously showed that PIAS1 and HTT interact (O'Rourke et al., 2013) and that KD of PIAS1 modulated accumulation of mHTT *in vitro* and *in vivo* as well as additional HD-associated molecular readouts *in vivo* suggesting a functional, molecular association between PIAS1 and HTT in the brain (O'Rourke et al., 2013; Ochaba et al., 2016). More recently, we identified HTT as a member of the transcription-coupled repair complex (TCR) together with PNKP and RNA Pol2A in collaboration with the Sarkar lab (Gao et al., 2019). Presence of the CAG-repeat expansion perturbed function of the TCR complex, specifically PNKP activity, leading to a decrease in genomic stability. Since PIAS1 has a well characterized function in mediating DDR pathways through SUMOylation (Galanty et al., 2009; Gibbs-Seymour et al., 2015; Schwertman et al., 2016), we hypothesized that PIAS1 may also be part of the TCR complex through its interaction with HTT. To test this hypothesis, endogenous HTT was co-immunoprecipitated from nuclear extracts of SH-SY5Y cells and precipitated complex was analyzed by western blot. PIAS1 was co-precipitated with HTT along with PNKP and RNA Pol2A, suggesting that PIAS1 is a component of the TCR complex in neuronal-like cells (Figure 3.3A). Therefore, given that mHTT perturbs PNKP enzymatic activity in iPSC-derived MSNs (Gao et al., 2019) and PIAS1 is a component

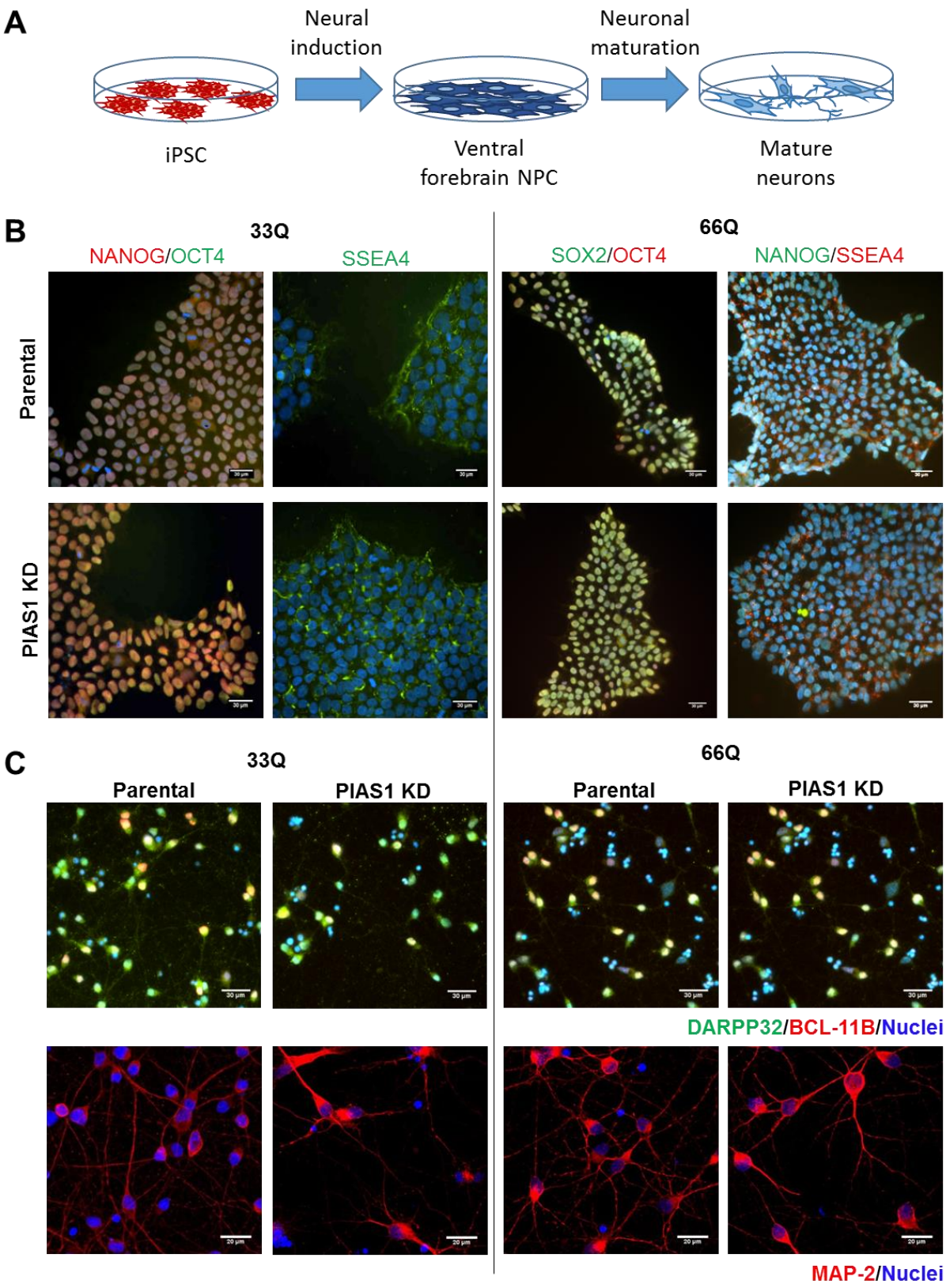
A
Neural induction
Neuronal maturation
iPSC
Ventral forebrain NPC
Mature neurons
B
33Q
66Q
NANOG/OCT4
SSEA4
SOX2/OCT4
NANOG/SSEA4
Parental
PIAS1 KD
C
33Q
66Q
Parental
PIAS1 KD
Parental
PIAS1 KD
DARPP32/BCL-11B/Nuclei
MAP-2/Nuclei

Figure 3.2: CRISPR edited HD-iPSC lines differentiate into neurons. A) Schematic of 37 day differentiation paradigm to make neurons enriched for medium spiny neurons. B) Staining for pluripotency markers (NANOG, OCT4, SOX2 and SSEA4 in gene edited clones shows no effect on pluripotency with levels the same between parental line and PIAS1 KD. C) Immunofluorescence for medium spiny neuronal markers DARPP32 and BCL-11B showing no effect on differentiation in control or PIAS1 KD neurons Parental neurons or gene edited neurons PIAS1 KD. Cells became MAP-2 positive neurons after the 37 day differentiation Scalebar = 30 μm for top panels and 20 μm for bottom panels. Data and figure generated by Charlene Smith-Geater, PhD, Thompson lab.

of the TCR complex, we investigated whether activity was altered in the CRISPR-derived PIAS1 KD iPSCs-derived MSNs. Excitingly, nuclear PNKP activity was increased in both the control (33Q) and HD (66Q) iPSC derived neurons upon PIAS1 KD (Figure 3.3B) and in the 66Q line, PIAS1 KD restored PNKP activity to almost control levels. This impact on PNKP enzymatic activity strongly suggested that PIAS1 is contributing to the TCR response to DNA damage in neurons.

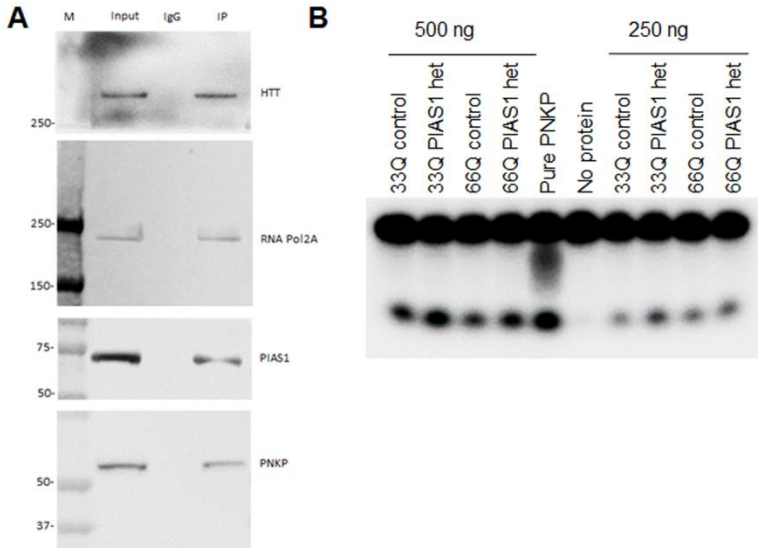

Figure 3.3: PIAS1 is part of the TCR complex and modulates PNKP enzymatic activity. A) Immunoprecipitation of the nuclear extract from SY5Y cells with HTT antibody identifies PIAS1 as an interactor of HTT as well as members of the transcription coupled repair complex, PNKP and RNApol2A. B) Nuclear PNKP activity assay shows increase of PNKP enzyme activity PIAS1 knockdown. These measurements were repeated 3-4 times and consistently showed increased PNKP activity. Data and figure generated in collaboration with Sarkar lab, UTMB.

PNKP is SUMOylated

The striking effect PIAS1 KD had on PNKP enzymatic activity suggested that PNKP may be a substrate for SUMOylation. Presence of one or more SUMOylation consensus sites (ψKXE, where ψ is a hydrophobic amino acid) can be used to predict if a protein may be modified by SUMO (Cappadocia and Lima, 2017) with E3 ligases in the SUMOylation cascade conferring specificity to target substrates (Figure 3.4A). The SUMOplot™ bioinformatics tool from Abgent was used to identify probable receptor lysines that fall within predicted SUMO-motifs. Several probable SUMO consensus motifs (11 total) in both the N and C terminus of human PNKP were identified (Figure 3.4B). Many of these lysines were highly conserved in mammals and lower vertebrates (Figure 3.4C), further supporting their potential for SUMOylation and suggesting that PNKP SUMOylation may be an important evolutionary contribution to PNKP function.

To test if PNKP is SUMOylated, a cell-based SUMOylation assay was used as described (O'Rourke et al., 2013). A Myc-tagged PNKP construct was co-expressed with either His-SUMO1 or His-SUMO2 constructs in HeLa cells. Lysates were processed using denaturing conditions and protein analyzed by western blotting for predicted motility shift of modified substrate. His-purification of SUMOylated proteins was completed using magnetic cobalt Dynabeads in 6M Guanidine lysis buffer followed by stringent washes in 6M Urea. Data shows that PNKP is SUMOylated by both SUMO1 and SUMO2 by at least two SUMO moieties as observed by predicted motility shift detected by both anti-PNKP and anti-Myc antibodies (Figure 3.5A, B). Additional laddering at higher molecular weights suggests further

polySUMOylation or subsequent polyUbiquitylation. Together with computational data, the in-cell SUMOylation data supports PNKP as a bona fide SUMO substrate.

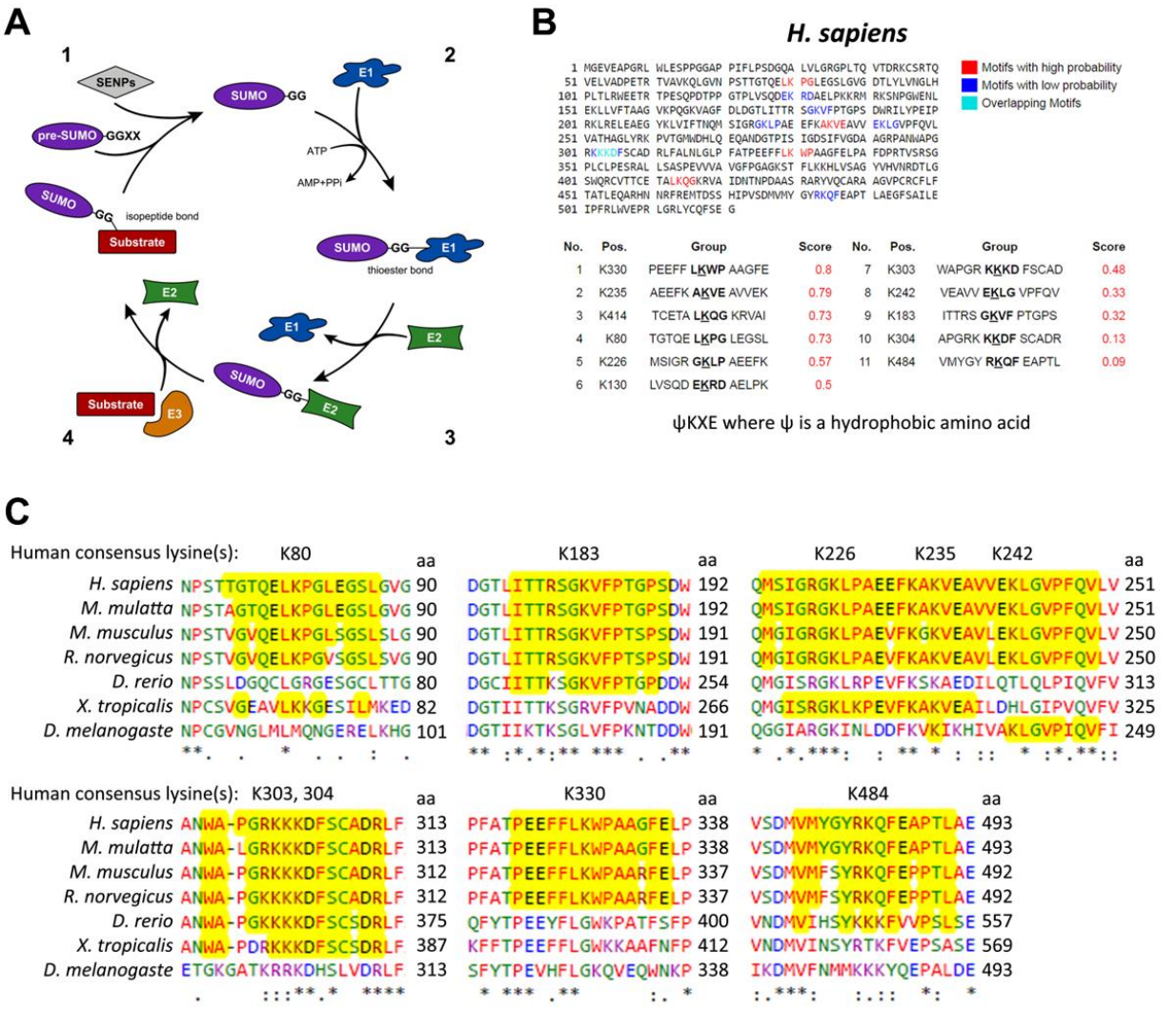

Figure 3.4: PNKP may be a substrate for SUMOylation. A) SUMO is covalently linked to target substrates through a four-step enzymatic pathway: 1) SUMO processing by SUMO-specific proteases (SENPs), 2) activation of SUMO by E1 activating enzymes, 3) SUMO transfer onto E2 conjugating enzyme followed by 4) transfer to E3 ligase to conjugate SUMO moiety onto target substrate. B) Human PNKP is predicted to be SUMOylated at numerous lysine residues by Abgent SUMOplot™. C) Several predicted PNKP SUMO consensus sites are highly conserved in mammals and lower vertebrates. Human lysines are listed with corresponding alignments from Clustal Omega™. Yellow highlights conserved residues (compared to human) if consensus site was predicted by SUMOplot™.

PIAS1 is a SUMO E3 Ligase for PNKP

Since PNKP is a substrate for SUMOylation and PIAS1 reduction modulated PNKP enzymatic activity in HD neurons, we next tested whether PIAS1 may serve as a SUMO E3 ligase for PNKP. First, the interaction between PIAS1 and PNKP was confirmed in HeLa cells used for the SUMOylation assay using co-immunoprecipitation. A specific interaction between PNKP and endogenous PIAS1 in HeLa cells was observed (Figure 3.6A).

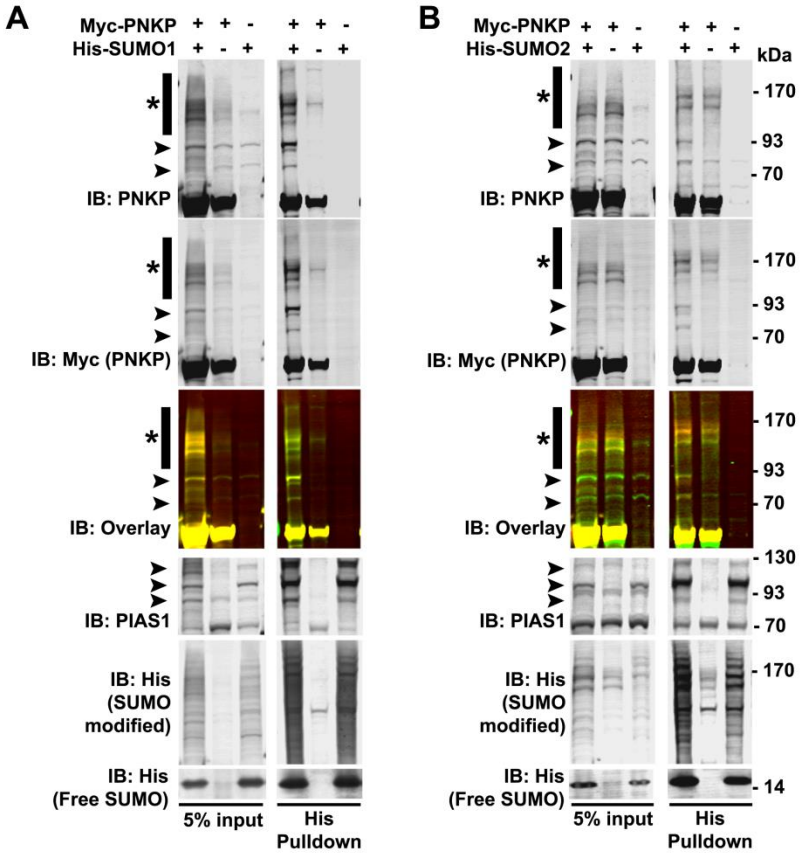

Figure 3.5: PNKP is SUMOylated and may be a substrate for STUbL activity *in vitro*. PNKP is SUMOylated by A) SUMO1 and B) SUMO2 as shown using in-cell SUMOylation assay HeLa cell-lysates assessed under denaturing conditions. Black arrowheads indicate corresponding molecular weight shift of SUMOylated substrate by numerous SUMO moieties. SUMOylated PIAS1 serves as a positive control (Alagu et al., 2018). High molecular weight laddering after denaturing pulldown suggests PNKP is modified beyond two SUMO moieties (Indicated by Asterisk). Overlay shows immunoreactivity of modified species with both anti-PNKP and anti-Myc antibodies.

Second, to assess if PIAS1 modulates PNKP SUMOylation, in-cell SUMOylation assays were repeated, with increased or decreased PIAS1. An siRNA against PIAS1 was co-transfected along with Myc-PNKP and His-SUMO1 to reduce PIAS1 (siPIAS1). Knock-down of PIAS1 ($p<0.0001$) caused a significant decrease in PNKP SUMOylation by SUMO1 ($p<0.01$, Figure 3.6B). To complement PIAS1 KD, PIAS1 overexpression under SUMO-limiting conditions was assessed. To detect facilitation of SUMOylated PNKP by PIAS1, Myc-PNKP was co-expressed in Hela cells with limited His-SUMO1 which reduced baseline levels of SUMOylated PNKP (1-Way ANOVAs, 1xSUMO $F(2, 6) = 24.34$, $p<0.01$, 2xSUMO $F(2, 6) = 369.40$, $p<0.0001$, Figure 3.6C) to allow detection of an enhancing effect. With PIAS1 overexpression, a significant increase in PNKP SUMOylation was observed (1-Way ANOVAs, 1xSUMO $F(2, 6) = 24.34$, $p<0.01$, 2xSUMO $F(2, 6) = 369.40$, $p<0.0001$). Together, data suggests that PIAS1 SUMOylates PNKP with SUMO1.

To determine if PIAS1 similarly enhances PNKP SUMO-2 modification, the same experiments were carried out with His-SUMO2 instead of His-SUMO1. With PIAS1 KD ($p<0.0001$), a significant reduction in SUMO2 modified PNKP by two SUMO2 moieties was detected ($p<0.01$, Figure 3.7A). Overexpression of PIAS1 under SUMO-limiting conditions again showed a significant enhancement of PNKP SUMOylation by SUMO2 (1-Way ANOVAs, 1xSUMO $F(2, 6) = 14.60$, $p<0.05$; 2xSUMO $F(2, 6) = 10.90$, $p<0.05$, Figure 3.7B). Together, these data support PIAS1 as a probable E3 ligase for PNKP by both SUMO1 and SUMO2.

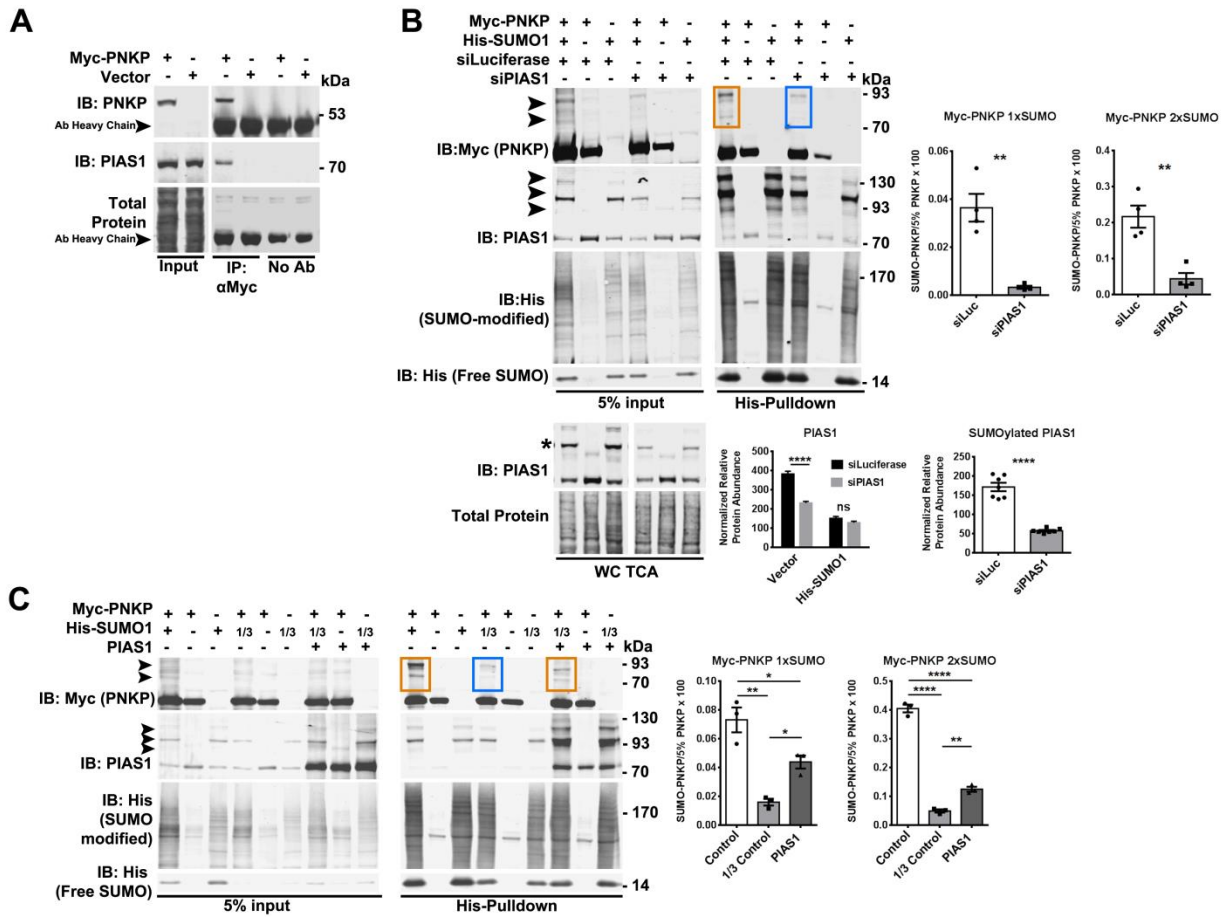

Figure 3.6: SUMO1 PNKP modification is mediated by PIAS1 *in vitro*. A) HeLa cells transfected with myc-PNKP and subjected with co-immunoprecipitation assay with anti-myc antibody shows specific interaction between myc-PNKP and endogenous PIAS1 in this cell type. Arrowheads represent antibody heavy chains. B) Significant KD of PIAS1 with siRNA (siPIAS1) shows a reduction in SUMOylated PNKP by His-SUMO1. C) Under SUMO-limiting conditions (1/3 normal input), PIAS1 overexpression significantly increases PNKP SUMOylation by His-SUMO1. Astrisk represent SUMOylated PIAS1. *p<0.01, **p<0.001, ***p<0.001, ****p<0.0001, ns= not significant, values represent means ± SEM.

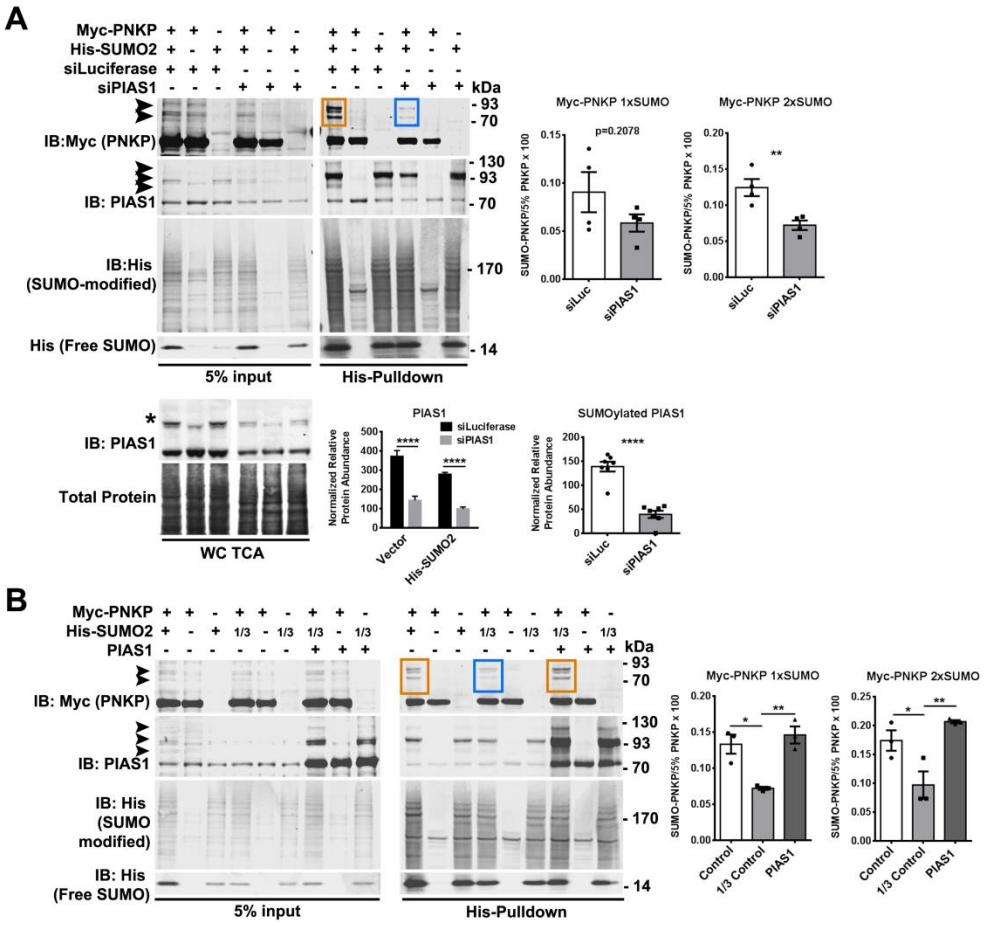

Figure 3.7: SUMO2 PNKP modification is mediated by PIAS1 *in vitro*. A) Significant knock-down of PIAS1 with siRNA (siPIAS1) shows a reduction in SUMOylated PNKP by His-SUMO2. B) Under SUMO-limiting conditions (1/3 normal input), PIAS1 over expression significantly increases PNKP SUMOylation by His-SUMO2. *p<0.01, **p<0.001, ***p<0.001, ****p<0.0001, ns= not significant, values represent means ± SEM.

mHTT may influence PNKP SUMOylation

To assess if the presence of the expanded CAG repeat in HTT impacts PNKP SUMOylation and if PNKP is SUMOylated endogenously, protein extracts from iPSC-differentiated MSNs were generated and evaluated using a co-immunoprecipitation assay capturing endogenous SUMO2/3-modified proteins (Figure 3.8). Prior to harvest, cells were treated with 50µm of inhibitor PR619 to prevent deSUMOylation and 200 µM hydrogen peroxide for 2 hours to additionally assess if inducing DNA damage impacted PNKP SUMOylation.

However, assessment of damage levels by marker γH2AX indicated that hydrogen peroxide treatment did not increase damage levels in this setting (Figure 3.8B), therefore treated samples were considered as biological replicates for analysis. Immunoblot of PNKP following co-immunoprecipitation of SUMO-2/3-ylated proteins from differentiated iPSCs showed high molecular weight bands that were PNKP immunoreactive, consistent with endogenous PNKP SUMOylation in human neurons (Figure 3.8A). This signal appeared increased in HD 66Q neurons, suggesting that presence of expanded mHTT increased PNKP

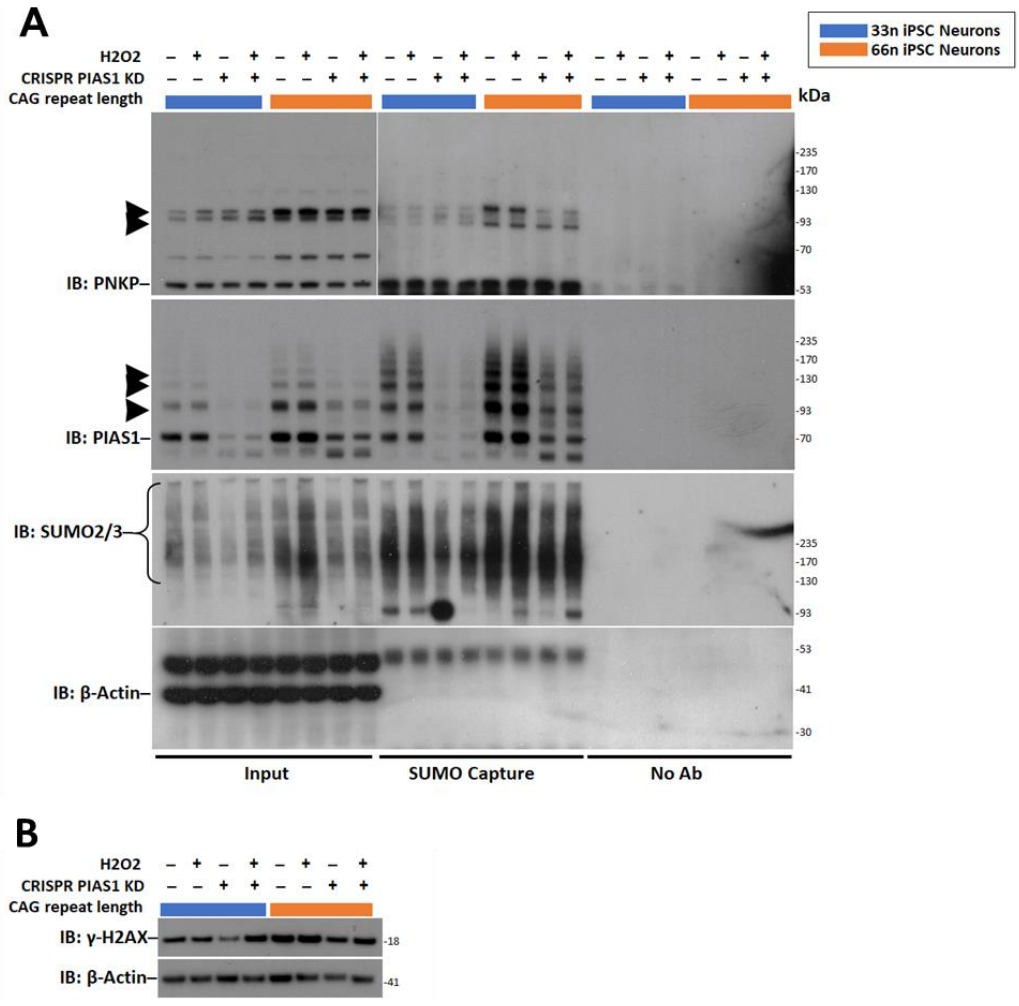

Figure 3.8: mHTT may affect endogenous PNKP SUMOylation. A) SUMO 2/3 Co-Immunoprecipitation assay precipitated endogenous unmodified PNKP and higher molecular weight PNKP suggesting endogenous PNKP SUMOylation in iPSC-derived neurons. KD of PIAS1 suggests reduction in high molecular weight PNKP signal. Endogenous SUMOylated PIAS1 served as a control for enrichment of SUMOylated proteins. B) DNA damage levels indicated by γH2AX immunostaining suggest no increase in damage levels with H2O2 treatment in these cells. β-Actin served as a relative loading control for whole cell lysate input samples. Data and figure generated by Marketta Kachemov, Thompson lab.

SUMOylation which was then decreased in the 66Q PIAS1 KD neurons. It is therefore possible that PIAS1 is modulating endogenous PNKP SUMOylaton in neurons, with KD restoring mHTT-mediated aberrant SUMOylation. Endogenous SUMOylated PIAS1 was also detected in SUMO-2/3 co-immunoprecipitation with a general increase in unmodified and SUMOylated PIAS1 in HD iPSC-derived neurons compared to control. Importantly, an overall accumulation in SUMOylated proteins was seen in HD neurons compared to control 33Q neurons, with a return towards control levels upon PIAS1 KD. Altogether, these findings suggest that PNKP is SUMOylated endogenously, that this SUMOylation may be modulated by PIAS1 in neurons, and that there may be aberrant SUMOylation in the presence of full-length mHTT. Of note, co-immunoprecipitation was performed with an antibody that preferentially recognizes SUMO2/3 over SUMO1, thus likely favoring the capture of polySUMOylated substrates over monoSUMOylated proteins and suggesting polySUMOylation of PNKP.

DISCUSSION

We previously reported that KD of PIAS1 has therapeutic potential for an HD mouse model (Ochaba et al., 2016). Therefore, we further investigated the molecular mechanisms associated with PIAS1 in HD by utilizing human iPSC derived cell models from a control

and HD patient. Using CRISPR-mediated gene editing, we provide evidence here that PIAS1 mediates DNA damage repair mechanisms in HD. DNA damage repair mechanisms have recently been shown to contribute to age of onset (AO) of HD (Bettencourt et al., 2016; Flower et al., 2019; GeM-HD, 2015; Moss et al., 2017) and affect somatic expansion of the HTT CAG-repeat (Goold et al., 2019; Pinto et al., 2013; Tome et al., 2013). HTT itself has been shown to play a role in repair mechanisms and we have recently reported that mHTT impacts enzymatic activity of repair enzyme PNKP in iPSC-derived MSNs from HD patients (Gao et al., 2019; Maiuri et al., 2017). Here we show that PNKP and PIAS1 interact in numerous cell types, that PIAS1 is a component of a TCR complex, and that PIAS1 is a SUMO E3 ligase for the repair enzyme PNKP and modulates its activity in neurons. Further, we provide evidence that PNKP is SUMOylated in neurons endogenously and this may be perturbed by HTT PolyQ expansion. Since decreased PNKP activity previously corresponded with decrease genomic integrity (Gao et al., 2019), rescue of activity with PIAS1 KD may serve to increase integrity of actively transcribing genes.

Other post-translational modifications for PNKP have been reported. For instance, phosphorylation of PNKP at S114 and S126 by ATM or DNA-PK regulates activation of PNKP enzymatic activity (Segal-Raz et al., 2011; Zolner et al., 2011). Ubiquitination of PNKP may prevent phosphorylation and serve as a degron signal for clearance by the ubiquitin proteasome system (UPS) suggesting that multiple PTMs may be affecting function and fate of PNKP (Parsons et al., 2012). PNKP had also previously been reported as a SUMO substrate in proteomic screens (Hendriks et al., 2017; Uzoma et al., 2018). Here we report

the first experimental validation that PNKP is SUMOylated endogenously in neurons and identify PIAS1 as an E3 SUMO ligase.

Genetic reduction of PIAS1 in HD iPSCs rescued perturbed DNA damage repair enzymatic activity of PNKP. PIAS1 and PIAS4 have well defined, canonical roles in the recruitment and eviction of DDR factors through SUMOylation (Schwertman et al., 2016). It is therefore possible that PIAS1 is recruiting PNKP to the sites of damaged DNA in a SUMO-dependent manner as SUMOylation often serves to recruit DNA damage repair factors to the sites of lesioned DNA. This might be in conjunction with activation of PNKP through ATM/DNA-PK mediated phosphorylation (Segal-Raz et al., 2011; Zolner et al., 2011). Cross-talk between phosphorylation and SUMOylation is well established, such that phosphorylation often primes substrates for SUMOylation by providing the negatively charged surrounding residues necessary for adequate SUMOylation and phosphorylation-dependent SUMOylation motifs (PDSM) have been well characterized (Hendriks et al., 2017; Hietakangas et al., 2006). However, while identified as a SUMO substrate, PNKP was not shown to be a co-modified (dual Phospho-SUMO modified) substrate in a recent proteomic screen and top probability consensus motifs (Figure 3.4) do not fit the characterized PDSM (Hendriks et al., 2017; Hietakangas et al., 2006). Alternatively, PIAS1 SUMOylation may be blocking phosphorylation of PNKP similar to reported ubiquitination, resulting in premature clearance of PNKP (Parsons et al., 2012). Knock-down of PIAS1 would therefore potentially facilitate PNKP phosphorylation and activation.

Instead of competing with ubiquitin, SUMOylation of PNKP could be serving as a primer for subsequent ubiquitination. SUMOylation of repair factors at DNA lesions can serve as a degradation signal in collaboration with ubiquitin signaling. The SUMO-targeted ubiquitin ligase (STUbL) RNF4 targets DNA repair factors that have been polySUMOylated to mark them for degradation with ubiquitin (Galanty et al., 2012; Kumar et al., 2017; Tatham et al., 2008). Failure of RNF4 to ubiquitinylate SUMOylated substrates leads to delayed eviction of DNA damage sites and inefficient repair (Galanty et al., 2012). Alternatively, premature eviction would prevent adequate repair suggesting that an ideal balance for retention and eviction needs to be maintained to ensure genomic stability. Therefore, due to the presence of HMW modifications (e.g. polySUMOylation) identified in our in-cell SUMOylation assay (Figure 3.5), PNKP SUMOylation may serve as a degradation signal for STUbL RNF4 as observed for other PIAS SUMO substrates (Gibbs-Seymour et al., 2015; Luo et al., 2012). Supporting this possibility is the observed immunoreactivity for PNKP from the SUMO2/3 co-immunoprecipitation assay such that modification by SUMO2/3 serves as a signal for STUbL activity (Sun et al., 2007). Therefore, we hypothesize that PIAS1 imbalance in HD may lead to expedited eviction from repair sites resulting in inefficient repair by removing repair factors prematurely (Figure 3.9). PIAS1 reduction could therefore serve as a molecular brake-pad, delaying PNKP eviction from repair sites long enough for enzymatic activity to effectively prep lesioned DNA for repair. This may serve as an alternative pathway for PNKP clearance to PNKP ubiquitination (Parsons et al., 2012), such that after PNKP is activated by phosphorylation, subsequent SUMOylation may trigger further signaling cascades for clearance after efficient repair. Further analysis testing these

hypotheses including cross-talk between other known PNKP post-translational modifications are the focus of future studies.

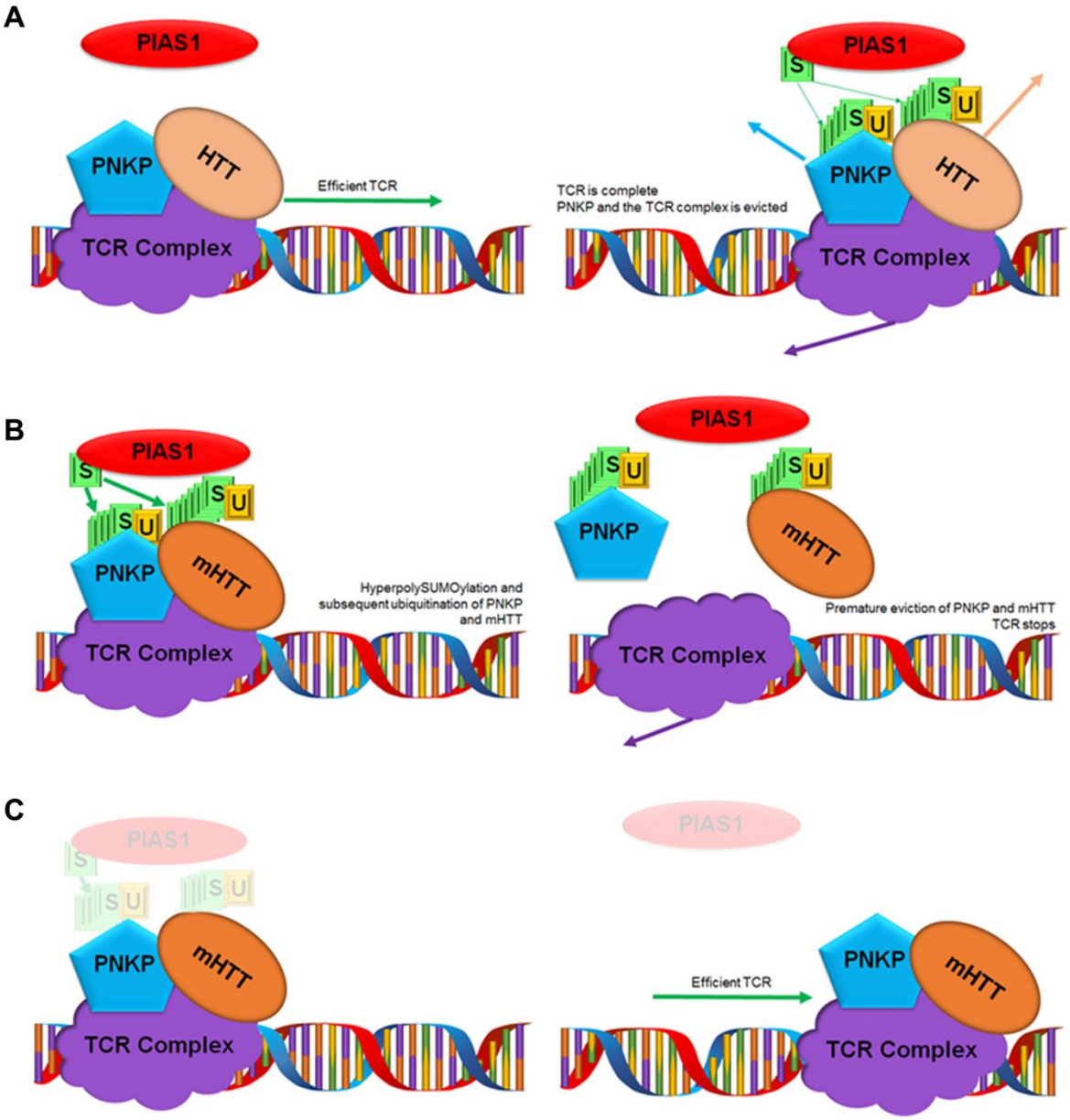

Figure 3.9: PIAS1 may play a role in evicting the TCR complex. A) In control cells, PIAS1 may SUMOylate PNKP and potentially other members of the TCR complex including HTT to cause eviction from the DNA. B) In HD, PIAS1 may hyperSUMoylate PNKP and maybe mHTT in the complex and cause premature eviction from the DNA and halting of DNA TCR. C) We hypothesize that PIAS1 knockdown prevents this premature eviction in HD and TCR happens without interruption. Figure generated by Charlene Smith-Geater, PhD, Thompson lab.

SUMMARY AND NEXT STEPS

Consistent with the defined role of PIAS1 in DDR pathways, data presented here provide the first evidence that PIAS1 is serving as an E3 SUMO ligase mediating DNA repair in post-mitotic neurons. Rescue of perturbed enzymatic activity of PNKP suggests that activity of PNKP is reduced by PIAS1 SUMOylation. The functional consequence of PNKP SUMOylation, however, remains unknown. Therefore, studies addressing our hypothesis that SUMOylation is mediating localization and clearance of PNKP and TCR proteins at damage sites will be carried out in future studies. The functional interplay between PNKP phosphorylation and SUMOylation can similarly be assessed by determining if one modification requires the other. With an impact on activity of DNA repair in neurons, it is possibly that PIAS1 is mediating repair pathways in the brain through SUMOylation. To investigate this possibility, we assessed Pnkp activity and transcriptional profiles in the knock-in, zQ175 mouse model with Pias1 KD, the results of which are detailed in Chapter 4. Overall, data here presents the first evidence that PIAS1 is mediating repair pathways in neurons through SUMOylation and highlight the importance of targeting disease-specific homeostatic imbalances for effective therapeutic design.

EXPERIMENTAL PROCEDURES

iPSC culture and CRISPR modification

iPSCs were cultured in mTESR1 on hESC-qualified Matrigel and passaged using Versene dissociation. Once at 70% confluence, iPSCs were pre-treated with 10 μM Y27632 dihydrochloride Rho kinase inhibitor for 1 hour to prevent cell death at single cell suspension. Cells were transfected with the CRISPR/CAS9 RNP complex and a pEF1α-

puromycin plasmid to allow for selection of successfully transfected colonies. CRISPR-guide RNA CAS9 ribonucleic acid protein complex was made as follows: both guide RNAs, Alt-R CRISPR-CAS9 crRNA for targeting the PIAS1 locus and the Alt-R tracR RNA were mixed with Nucleic acid duplex buffer (all IDT Technologies) to a final concentration of 1 μM and heated to 95^{o}C for 5 minutes in a thermocycler and allowed to cool to room temperature. CAS9 protein (IDT) is diluted to 1 μM in Optimem medium (Life Technologies) and combined with the duplex in the following amounts per transfection 2.4 μl of Alt-R Guide RNA duplex, 1.7 μl of 1 μM CAS9 protein and made up to 5 μl with PBS (with Ca^{2+} and Mg^{2+}) and incubated at room temperature for 20 minutes. Cells were prepared to a single cell suspension with Versene treatment for 5-10 minutes at 37^{o}C and then removed and replaced with mTESR1, cells were pipetted into a single cell suspension using a P1000 and collected by centrifuge at 200 *xg* for 90 seconds. Cells were resuspended in 100 μl per transfection of Nucleofector solution II for hESC 1 μg of pmaxGFP plasmid (Lonza) and 1 μg of pEF1α-puro were added and 5 μl of the RNP complex were added to each cuvette with 100 μl of cell suspension. Cells were nucleofected using an AMAXA Nucleofector II device on program B-016. Cells were transferred to a 15 ml conical and mTESR supplemented with CloneR (Stem Cell Technologies) and 1 μM azidothymidine (AZT - Tocris) and 10 μM Y27632 dihydrochloride. Cells were plated between 4 wells of a 6 well plate on hESC-qualified Matrigel. One day after transfection, AZT was removed and cells were treated with 200 ng/ml puromycin for 48 hours with a daily media change. Clones were picked 24 hours after puromycin was removed by removing medium and treating cells for 30 seconds with Versene at 37^{o}C. Cells were placed in mTESR and colonies were picked using a P200 pipette tip and replated in a 12 well plate 1 colony per well in mTESR1 supplemented with

CloneR. Cells were maintained in CloneR for 2 more days and then cells were maintained as above to collect enough cells for genomic DNA isolation and freezing back stocks.

Validation of CRISPR clones

iPSCs were pelleted and snap frozen in liquid nitrogen. Genomic DNA was extracted from the cells using the QIAGEN genomic DNA extraction kit (Qiagen). PCR across the region of interest containing potential in-dels was performed using the KAPA Hi-Fi PCR kit (VENDOR) following manufacturer's protocol. Formation of DNA heteroduplexes was performed by heating the double stranded DNA PCR product to 98^{o}C and then cooling 1^{o}C every 30 seconds to re-anneal DNA strands. Annealed products were then digested with the T7EI enzyme (NEB) and subsequently run on a 1% agarose TAE gel for assessment. Protein was harvested from frozen cell pellets of the clones using RIPA lysis buffer and run on a 4-12% Bis Tris polyacrylamide gel and transferred to 0.45 μm Nitrocellulose, blocked with Starting block (Invitrogen) and probed for PIAS1 (Cell signaling #3550S) and α-tubulin (Sigma T6079200). PCR products were cloned into the pGEM-T-easy cloning vector (Promega) and sequenced at Eurofins using T7 and SP6 enzymes. Sequences were analyzed on NCBI BLAST.

iPSC differentiation

iPSC were maintained as above. Once they reached 60-70% confluency, neuronal differentiation was started. iPSC colonies were washed with PBS (without Ca^{2+}/Mg^{2+}) and then switched into SLI medium (ADF supplemented with 2 mM Glutamax™, 2% B27 without vitamin A, 10 μM SB431542, 1 μM LDN 193189 and 1.5 μM IWR1) this is day 0.

Medium was changed daily and at day 4, cells were passaged 1:2. Cells were pre-treated for 1 hour at 37°C with 10 μM Y27632 dihydrochloride, then washed with PBS (without Ca^{2+}/Mg^{2+}) and dissociated using Stempro Accutase (Life Technologies) at 37°C for 5 minutes. Cells were re-plated in SLI medium containing 10 μM Y27632 dihydrochloride onto hESC-qualified Matrigel (Corning) and switched into SLI medium on day 5. Cells were passaged on day 8 as above in a ratio of 1:2 and replated in LIA medium (ADF supplemented with 2 mM Glutamax™, 2% B27 without vitamin A, 0.2 μM LDN 193189, 1.5 μM IWR1 and 20 ng/ml Activin A) containing 10 μM Y27632 dihydrochloride. Daily medium changes were performed with LIA medium until day 16. Cells were replated as before but plated into SCM1 (ADF supplemented with 2 mM Glutamax™, 2% B27 supplement, 2 μM PD 0332991 (Tocris, USA), a CDK4/6 inhibitor, 10 μM DAPT (Tocris, USA), 10 ng/ml brain-derived neurotrophic factor (BDNF, Peprotech), 10 μM Forskolin, 3 μM CHIR 99021, 300 μM γ-amino butyric acid (GABA, all Tocris), supplemented with $CaCl_2$ to final concentration of 1.8 mM) and 200 μM Ascorbic acid (both Sigma-Aldrich) for neuronal differentiation on nitric acid (Fisher Scientific) washed borosilicate 13 mm glass coverslips (VWR) pre-treated with 100 μg/ml poly-D-lysine hydrobromide (Sigma Aldrich) and hESC-qualified Matrigel and plated at a density of 80 x 10^3 cells/cm^2. Half medium change was performed on day 21. On day 23 medium was changed to SCM2 medium (1:1 ADF:Neurobasal A supplemented with 2 mM Glutamax™, 2% B27 supplement, 2 μM PD 0332991, 10 ng/ml BDNF, 3 μM CHIR 99021, 1.8 mM $CaCl_2$ and 200 μM Ascorbic acid). 50% media changes were then performed every 2-3 days until harvest at day 37.

PNKP enzymatic activity measurements

3'-phosphatase PNKP enzymatic activity from nuclear and mitochondrial extracts was performed as previously described (Chakraborty et al., 2015; Gao et al., 2019). A 3'-phosphate oligo (51-mer), 32P-labeled, containing a single strand break was used to assess activity by measuring the amount of released 3' phosphate from radio-labeled substrate as analyzed by 20% Urea-PAGE and PhosphorImager. The percent of phosphate release was represented as compared to total radiolabeled substrate (as 100).

Immunofluorescence

Cells for immunofluorescence were cultured on 13 mm borosilicate round coverslips and fixed after being washed with PBS pH 7.4 in 4% paraformaldehyde (Electron microscopy) for 10 minutes at room temperature. Coverslips were washed three times with PBS and then stored at 4^{o}C until staining. Primary antibody incubation was performed overnight at 4^{o}C, antibodies and permeabilization and blocking solution was specific per stain and detailed in Table 3.1. Secondary antibodies used were Alexa-Fluor IgG highly cross adsorbed antibodies resuspended at 1:1000 (Life Technologies) in blocking solution and used for 1 hour at room temperature in the dark. Nuclei were co-stained with Hoechst (Sigma #33342) for 10 minutes in the dark in PBS. Washed with PBS and then mounted using Fluoromount G (Fisher Scientific). Cells were imaged on either Nikon TE fluorescent microscope or the Olympus FV3000RS confocal laser scanning microscope. For synapse images, Z-stack images were obtained with 0.5 μm increments and maximum intensity projections generated. They were analyzed using Cell Profiler for staining intensity per image and number of cells were counted in ImageJ.

HeLa Cell Culture

HeLa cells were cultured in Dulbecco's Modified Eagle Medium (DMEM) with High glucose supplemented to 10% fetal bovine serum (FBS) at 37°C. Cells were transfected with cDNA plasmid and/or siRNA (PIAS1 knock-down) using Lipofectamine 2000 at ~60% confluency. Media was changed 24 hours post transfection. Cells were harvested 44 hours post transfection. *PIAS1* siRNA sense sequence: AUCACCUCACUUGUCCGACUGUUU.

Plasmids

Myc-PNKP construct was generous gift from the Sarkar lab. PIAS1, His-SUMO-1 and SUMO-2 were used as previously described (O'Rourke et al., 2013) as were pcDNA containing HTTex1p with 25QP or 97QP (Steffan et al., 2004) and HTT 586aa fragment with 25QP or 137QP (O'Rourke et al., 2013).

Denaturing SUMOylation Assay

HeLa cells were lysed under denaturing conditions in a buffer containing 6M guanidine HCl, 100 mM NaH2PO4 pH 7.8, and 10 mM Tris-HCl pH 7.8. Lysed cells were sonicated for 30 seconds at 40% amplitude. 5% lysis volume was removed for TCA precipitation. Remaining volume was used for His-purification under denaturing conditions by incubating lysed samples in lysis buffer together with His-isolation Dynabeads (Invitrogen, 10103D) for 1 hour at room temperature while rotating. Samples were washed twice in 8M urea with 100 mM NaH2PO4 pH 7.8, and 10 mM Tris-HCl pH 7.8, once in 8M urea with 100 mM NaH2PO4 pH 6.3, and 10 mM Tris-HCl pH 6.3 and once in 1X PBS. Beads were resuspended in loading buffer (1.6x loading dye, 1x reducing) and boiled for 10 minutes prior to western blot

analysis. Whole-cell, 5% loading input was assessed using TCA precipitation. Sample 5% inputs in 6M guanidine lysis buffer were incubated in an equal volume of cold, 20% TCA and incubated on ice for 30 minutes. Precipitates were centrifuged at 18,000xg for 15 minutes at 4°C. Supernatant was discarded and protein pellet was washed in ice-cold acetone followed by subsequent centrifugation at 18,000xg for 15 minutes at 4°C. Protein pellet was resuspended in loading buffer, pH was adjusted to basic with Tris-HCl pH 8, and samples were boiled for 10 minutes prior to western blot analysis.

Co-Immunoprecipitation Assays

HeLa and differentiated iPS cells were lysed in buffer containing 20 mM Tris-HCl pH 7.5, 137 mM NaCl, 5 mM EDTA, 1% NP40 alternative, and 10% glycerol (Pierce Protease Inhibitor tablet, 0.2 mM NaF, 1:1000 dilution of inhibitor cocktails 2 & 3, 0.2 mM butyric acid, 5 mM nicotinamide, 1 mM PMSF, 1ug/uL aprotinin, 1ug/uL leupeptin, and 25 mM n-ethylmaleimide). HeLa cell Co-immunoprecipitations were carried out using 1 ug α-Myc tag antibody in lysis buffer without glycerol. Samples (400ug) were incubated for 1 hour together with α-Myc tag antibody at 4°C while rotating. Dynabeads M280 (Invitrogen, 11201D) were then added to samples and rotated for 30 minutes at room temperature. Beads were washed 3x using a magnetic rack and lysis buffer without glycerol. For assessment of endogenous SUMOylated proteins in iPSCs, neuron pellets were lysed in lysis buffer (above) containing several deSUMOylation and phosphatase inhibitors (above). Pellets in lysis buffer were sonicated three times at 40% amplitude in 10 second intervals. A Bradford assay was then performed to assess protein concentration levels in lysates. Co-immunoprecipitation was carried out using an antibody against SUMO-2/3 (MBL M114-3).

Protein G Dynabeads (Invitrogen, 10004D) were pre-washed three times with lysis buffer without glycerol (above) and 1 ug of SUMO2/3 antibody was pre-bound to 30 uL of magnetic Dynabeads Protein G (Invitrogen, 10004D) for 1 hour at 4°C while rotating in lysis buffer without glycerol. Replicates of each sample, omitting antibody, served as no-antibody negative controls. Following antibody-bead pre-incubation, 200 ug of lysate was added to each IP and incubated overnight at 4°C while rotating in 500 ul lysis buffer. The following day, samples were washed three times each with 500 ul lysis buffer without glycerol. Protein was eluted from the beads in 1x reducing loading dye and boiled for 5 minutes. SUMO elution was separated from the beads using a magnetic rack, collected, and analyzed by western blot.

SDS-PAGE and Western Blot

Cell lysates and precipitated were assessed on 4-12% Bis-Tris PAGE gels and transferred onto 0.45 μm PVDF-FL or PVDF. For LiCor assessed membranes, prior to blocking, total protein was assessed using Revert total protein stain (LI-COR Biosciences 926-11016) and imaged using Odyssey CLx imager. Membranes were blocked in Intercept starting block (LI-COR Biosciences 927-60010) for 1 hour prior to incubation in primary antibodies overnight at 4°C. Goat-α-Rabbit secondary (IRDye 800CW or 680LR, LI-COR), goat- α-Mouse IgG secondary (IRDye 800CW or 680LR, LI-COR), and donkey- α-Goat (IRDye 800CW, LI-COR) were used to detect proteins. For assessment of PIAS1 KD and SUMOylated Co-immunoprecipitated proteins, membranes were assessed using chemiluminescence with either goat-anti-mouse (Jackson Laboratories #115035146) or

goat-anti-rabbit (Thermo scientific # 31460) HRP-conjugated secondaries and SuperSignal™ West Pico substrate (Thermo Scientific #34580) captured on X-ray film.

Antibodies

α-PNKP (Origene AP16044PU-N), α-PNK (Novus NBP1-87257), α-Myc tag (Millipore 05-419), α-Penta His tag (Qiagen 34600), α-PIAS1 (Cell Signaling #3550S), α-HTT (clone 5526, Abcam ab109115), Anti-α-Tubulin (Sigma T6079200), α-DARPP-32 (Abcam ab40801), α-CTIP2 (Abcam ab18465), α-FOXP1 (Abcam ab16645), and α-MAP2 (Millipore MAB3418) primaries were used. Goat- α-Rabbit (LI-COR Biosciences IRDye 800CW 926-32211 or 680RD 926-68071), goat- α-Mouse (LI-COR Biosciences IRDye 800CW 926-32210 or IRDye 680RD 926-68070), donkey- α -Goat (LI-COR Biosciences IRDye 800CW 926-32214), goat- α-mouse HRP (Jackson Laboratories #115035146), and goat- α-rabbit HRP (Thermo scientific # 31460) secondaries were used.

Statistical analysis

All data represented as mean ± SEM with a p value of $p<0.05$ considered statistically significant. Analyses were completed in GraphPad Prism™ software. Chemiluminescent pixel intensity values were obtained from western blots and normalized to α-Tubulin. IR-fluorescent intensity values were obtained using Li-Cor imaging software, Image Studio and normalized to total protein stain. SUMO-modified species of PNKP were quantified by normalizing to abundance of 5% input from the same western and multiplying by 100. 1-way ANOVA was used to assess differences in protein levels followed by Tukey's multiple comparisons test.

CHAPTER 3

TABLES

Table 3.1: Immunofluorescent staining protocols for iPSC QC

Antibody	Host	Source	Cat number	Co-stain	Permeabil-ization	Block	Concen-tration
DARPP32	Rabbit	Abcam	ab40801	CTIP2	0.3%Triton-X in PBS 10 minutes	2% Goat serum 3% BSA 0.1% Triton X PBS 1 hour RT	1:200
CTIP2	Rat	Abcam	ab18465	DARPP32			1:500
SYN	Mouse	Abcam	ab8049	PSD95	N/A	2% Goat serum 3% BSA 0.05% Tween PBS	1:200
PSD95	Goat	Abcam	ab12093	SYN			1:500
FOXP1	Rabbit	Abcam	ab16645	MAP2	0.3% Triton X PBS 10 minutes	10% Goat serum 1% BSA 0.1% TritonX PBS	1:1000
MAP2	Mouse	Millipore	MAB3418	FOXP1			1:1000

CHAPTER 4

Pias1 reduction modulates DNA damage repair and neuronal transcription in the zQ175 mouse model of HD

SUMMARY OF CHAPTER 4

Genetic modifiers that influence Huntington's disease (HD) age of onset have recently been identified. The majority of these modifiers have critical roles in DNA damage repair (DDR) pathways, mechanisms which rely strongly on signaling cascades and post translational modification such as ubiquitin and SUMO. Further, the Huntingtin (HTT) protein itself scaffolds DDR proteins and this scaffolding function may be impaired in HD. We previously showed that the E3 SUMO ligase PIAS1 enhances SUMOylation of the HTT protein and that reduction of Pias1 modulated disease associated phenotypes in the rapidly progressing R6/2 mouse model of HD. PIAS1 modifies other SUMO-substrates which participate in DDR pathways, including PNKP which is dysregulated by mHTT and modulated by PIAS1 in HD-patient iPSC-derived neurons, which may promote genomic stability (Chapter 3). Therefore, we investigated whether Pias1 also modulates DNA repair pathways and transcriptional networks in the striatum of a full-length, knock-in mouse model of HD (zQ175) to further elucidate the functional contributions of Pias1, SUMO, and DDR towards disease-associated mechanisms. Pias1 knock-down (KD) did not exert significant effects on either behavior or accumulation of insoluble mHTT protein in zQ175 mice. However, pre-symptomatic Pias1 KD did alter levels of the DNA damage marker γH2AX and restored enzymatic activity of Pnkp in striatum of zQ175 mice at 8 months of age, similar to the effect on PNKP observed in human HD neurons. Transcriptome analysis by mRNAseq

shows a significant normalization of disease-associated transcriptional networks and modules encompassing DNA damage repair mechanisms, synaptic transmission, and mRNA processing, suggesting that Pias1 may modulate neuronal health by mediating transcription. Together, these data suggest that Pias1 may influence DDR pathways and modulate molecular HD outcomes related to neuronal function *in vivo*.

INTRODUCTION

DNA damage repair (DDR) has been established as either an underlying cause of neurodegenerative disease (McKinnon, 2017) or as a contributor towards neurodegenerative disease pathogenesis as a disease modifier (Maiuri et al., 2019). Recently, groundbreaking work in the HD field identified genetic variants in the DNA repair genes *FAN1, MSH3,* and *MLH1* in human Huntington's disease (HD) patients associated with altered age-of-onset (AO) and disease progression, (GeM-HD, 2015; Lee et al., 2017; Moss et al., 2017). Huntington's disease is a monogenic disorder, caused by an expanded trinucleotide repeat expansion (CAG) within the *Huntingtin (HTT)* gene and inherited in an autosomal dominant manner (Group, 1993). The presence of the mutation exhibits nearly complete penetrance. The size of the repeat expansion is inversely correlated with AO in adult-onset HD patients, with CAG-repeat length accounting for about 50% of the observed AO (Langbehn et al., 2004). The identification of genetic variants that contribute to AO variance seen between HD patients with the same repeat size provided insight into mechanisms that may contribute to disease pathogenesis. Defining *FAN1, MSH3,* and *MLH1* (Bettencourt et al., 2016; Flower et al., 2019; GeM-HD, 2015; Lee et al., 2017; Moss et al.,

2017) as disease modifiers in HD strengthened the link between DNA damage repair and the neurodegenerative process.

We recently showed, in collaboration with the Sarkar lab, that transcription-coupled repair (TCR) is impaired in HD, with the huntingtin protein (HTT) itself serving as a scaffold for the TCR complex (Gao et al., 2019). In HD model systems, the presence of mutant expanded huntingtin protein (mHTT) directly perturbed enzymatic end-processing activity of DNA repair protein PNKP (Gao et al., 2019), a component of the base excision repair (BER) and TCR pathways (Chakraborty et al., 2016; Chakraborty et al., 2015). This data suggested that the loss of specific types of DNA repair mechanisms may enhance disease pathogenesis as a direct consequence of mHTT expression. Given that DNA repair associated genetic variants mediating AO of HD and dysfunctional DNA repair pathways are implicated in other neurodegenerative diseases (McKinnon, 2017), there is a need to understand the underlying mechanism of how either deficient or inappropriate repair might contribute to disease pathogenesis.

Post-translational modifications, including by small ubiquitin like modifier (SUMO), are integral signaling components that participate in numerous cellular processes and dysregulation of SUMOylation is associated with neurodegenerative diseases including HD (Liebelt and Vertegaal, 2016; Princz and Tavernarakis, 2019; Vijayakumaran and Pountney, 2018). The HTT protein is SUMOylated and SUMOylation may contribute to solubility and aggregation potential of the mHTT protein (Steffan et al., 2004). We previously identified PIAS1 as a specific E3 ligase that enhances SUMOylation of HTT (O'Rourke et al., 2013).

Insoluble Pias1 was found to aberrantly accumulate in the striatum of the R6/2 mouse model of HD and viral miRNA-mediated knock-down (KD) of Pias1 in R6/2 striata was beneficial to behavior and reduced accumulation of insoluble mHTT, SUMO-modified, and Ubiquitin-modified proteins (Ochaba et al., 2016). In addition to mediating accumulation of insoluble proteins, Pias1 KD in R6/2 mice increased levels of the pre-synaptic marker synaptophysin and normalized the aberrant, inflammatory profile observed in the mice. This in part may have been through Pias1's function as a negative regulator of NfkB signaling (Liu and Shuai, 2008; Ochaba et al., 2016). However, the precise mechanistic contributions of Pias1 in HD pathogenesis are not yet defined.

In addition to SUMOylating the HTT protein (O'Rourke et al., 2013) and serving as a negative regulator of inflammation (Liu and Shuai, 2008), PIAS1 is also a SUMO E3 ligase in DDR pathways. SUMO serves as an integral signaling component for DDR pathways (Schwertman et al., 2016). Specifically, SUMOylation by PIAS1 may serve to recruit repair factors (Galanty et al., 2009) or mark them for eviction or clearance (Gibbs-Seymour et al., 2015). More recently, we identified a function of PIAS1 in mediating repair-related enzymatic activity of PNKP in HD patient iPSC-derived medium spiny neurons following genome editing to reduce PIAS1 levels (Chapter 3). In collaboration with the Sarkar lab, the TCR complex contained PIAS1 along with HTT, PNKP, and RNA polymerase 2A, defining a new role for PIAS1 in mediating DDR mechanisms. PNKP is SUMOylated by PIAS1 in HD neurons and this SUMOylation was elevated at baseline in patient neurons (Chapter 3). Knock-down of PIAS1 rescued perturbed PNKP enzymatic activity and reduced endogenous PNKP SUMOylation.

We next wished to investigate the possibility that DDR pathways (specifically Pnkp) and other molecular readouts (e.g. mHTT accumulation), might be influenced by Pias1 KD in a full-length and slowly progressing zQ175 knock-in mouse model of HD. The zQ175 mouse expresses the human expanded repeat region encoded by exon 1 within the endogenous murine *Htt* locus, producing a chimeric mHTT protein (Menalled et al., 2012). These animals have a more subtle disease progression compared to the rapidly progressing, fragment R6/2 mouse model. Due to their underlying molecular differences and the ability to assess zQ175 animals in a pre-symptomatic stage and over longer time frames, we utilized this model to assess the temporal contribution of Pias1 in disease. These animals also have perturbed Pnkp enzymatic activity, similar to HD-patient derived neurons (Gao et al., 2019). Further, zQ175 animals have a well-established transcriptional profile (Langfelder et al., 2016). Pias1 regulates transcription including that mediated by NfkB and p53 in addition to several neuronal specific transcription factors (Table 2, (Rytinki et al., 2009)). Therefore, we assessed behavioral and molecular phenotypes including transcription, Pnkp activity, and accumulation of insoluble high molecular weight (HMW) mHTT with Pias1 KD in these animals.

Using the same viral approach as described for R6/2 mice (Ochaba et al., 2016) in collaboration with the Davidson lab, we evaluated Pias1 reduction by intrastriatal injection of zQ175 mice at pre-symptomatic and symptomatic disease stages and assessed the impact of this reduction over time. Pias1 KD did not alter the majority of behavioral readouts nor did it modulate accumulation of insoluble mHTT in most groups assessed, suggesting that Pias1 may not primarily be modulating mHTT aggregation in these animals.

Of note, Pias1 did not aberrantly accumulate in the insoluble fraction in these mice. However, we did observe a rescue in Pnkp enzymatic activity at 8 months of age with pre-symptomatic KD of Pias1. Additionally, genotype-associated transcriptional profiles were normalized with pre-symptomatic Pias1 KD, specifically in genes enriched for processes involved in neuronal and synaptic function. Compared to established transcriptional modules of a zQ175 allelic series (Langfelder et al., 2016), pre-symptomatic Pias1 KD also rescued disease-associated DDR-related modules, suggesting that Pias1 mediates repair pathways *in vivo*. Therefore, data presented in this chapter further defines Pias1 as a modulatory component of the TCR pathway and regulator of transcriptional networks associated with neuronal function in the context of HD *in vivo*.

RESULTS

Pre-symptomatic Pias1 KD may modulate behavioral phenotypes in zQ175 mice

Heterozygote zQ175 mice exhibit behavioral deficits starting around 7 months of age (Menalled et al., 2012). For this study we designated 2.5 months of age as "pre-symptomatic" and 7.5 months of age as "symptomatic" and a timeline for behavioral and molecular assessments of miPias1.3 treatment at both pre-symptomatic and symptomatic stages was developed (Figure 4.1B). Male and female heterozygote (Het/zQ175) or wild-type (WT) littermates were treated with either a miRNA against *Pias1* (miPias1.3) or a control, scrambled miRNA (miSafe) through bilateral stereotaxic striatal injections of AAV2/1 as described ((Ochaba et al., 2016), Figure 4.1C). The GFP viral reporter can be detected 11 months after injection suggesting continued expression of transduced constructs and long-term feasibility of viral delivery method (Figure 4.1D).

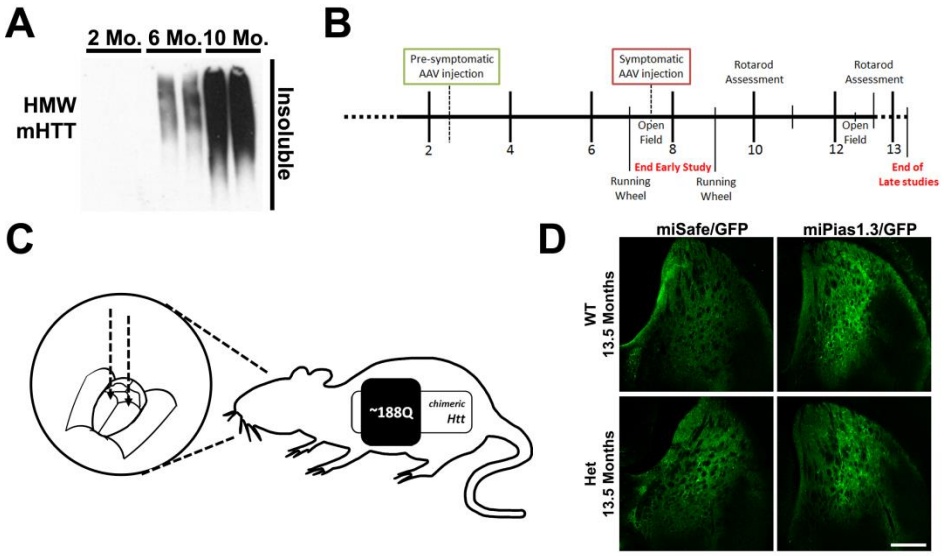

Figure 4.1: Experimental design for modulating Pias1 in zQ175 mice. A) HMW Insoluble mHTT is detectable by 6 months of age, and increases with age allowing for molecular assessment of mHTT accumulation after onset of symptoms in this model. B) Time-line for pre-symptomatic and symptomatic injections of AAV2/1 miRNA, behavior, and sacrifice dates. C) Schematic for bilateral stereotaxic injections into the striatum of zQ175 mice. D) GFP viral reporter is present 11 months post-injection, indicating continued presence of successful transduction. Scale bar 500μm

First, pre-symptomatic miPias1.3 treated animals were assessed behaviorally until 13.5 months of age prior to sacrifice (Figure 4.2A, Direction 1). Open field, previously reported to detect genotype differences in zQ175 mice, was used to assess motor and anxiety measures (Menalled et al., 2012). A running wheel task was used to assess motor deficits as described (Hickey et al., 2008). Accelerating Rotarod task was also performed as it was previously reported to detect genotype differences in zQ175 heterozygous mice (Menalled et al., 2012). Body weights were recorded. Statistical outputs for open field, Rotarod, and body weights are detailed in Table 4.1. Overall, animals exhibited genotype-related deficits with little to no impact observed for miPias1.3 treated animals (Figure 4.3).

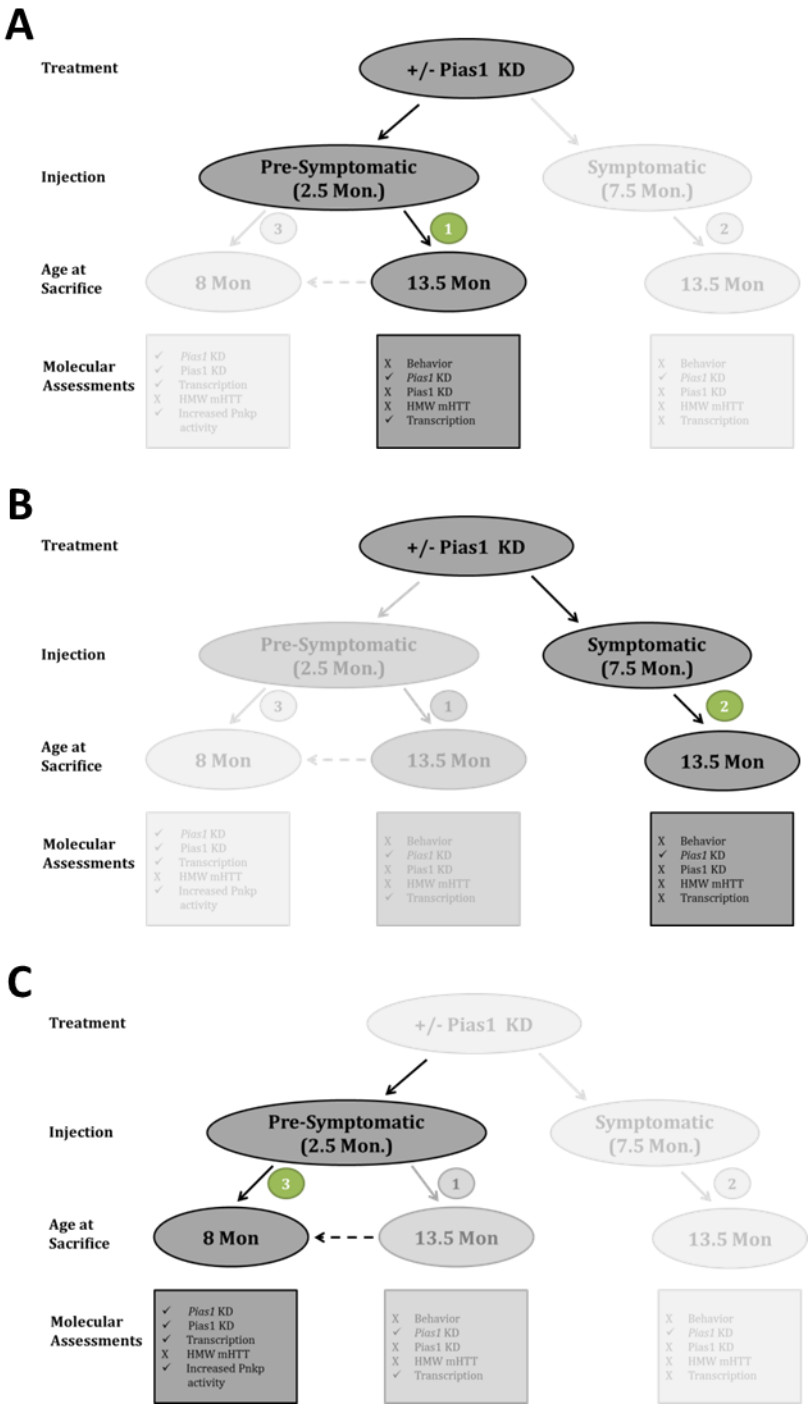

Figure 4.2: Flow chart summary of zQ175 Pias1 KD experimental groups, study progression, and overall findings. A) Direction 1 pre-symptomatic KD assessed at 13.5 months of age had robust transcriptional changes but no reduced Pias1 protein. B) Direction 2 symptomatic KD assessed at 13.5 months of age had few molecular changes. C) Direction 3 informed from direction 1 for pre-symptomatic KD assessed at an earlier time point (8 months) to assess molecular readouts associated with reduced Pias1 protein.

Open field task: To assess motor deficits and anxiety, the open field task was performed at 7.5 and 12.5 months of age and analyzed by Ethovision™ video tracking software. Deficits in total distance traveled were previously reported at 7.5 months of age for zQ175 heterozygous mice (Menalled et al., 2012). At 7.5 months of age, both zQ175 males and females had significantly less distance traveled with slower velocity. This was retained analyzing both genders combined with no effect of Pias1 KD treatment observed (Table 4.1, Figure 4.3A). These data support a clear zQ175 motor deficit but miPias1.3 treatment had no effect on motor behavior in these animals at 7.5 months of age. No effects were observed for percent of time spent in center zone for any group indicating a lack of anxiety phenotype in these animals that was not affected by miPias1.3 treatment. At 12.5 months of age, zQ175 motor deficits were no longer observed and there was no miPias1.3 treatment effect (Figure 4.3B). No anxiety phenotype was observed for percent time spent in center zone. Loss of genotype effect is common in these animals at later ages (Menalled et al., 2012) and overall Pias1 KD did not affect these behavioral readouts.

Rotarod: Rotarod detects genotype differences starting at 7.5 months of age in zQ175 mice (Menalled et al., 2012). No overt miPias1.3 treatment effects were observed for either males or females in latency to fall in this study (Figure 4.3C, Table 4.1). Specifically assessing latency to fall at 9.5 months of age, both males and females showed a significant genotype effect that was retained when combined, indicating that zQ175 mice had a decreased latency to fall (Figure 4.3C). No treatment effect was observed for either sex when analyzed separately or for males and females combined. Interestingly, at 12.5 months of age, male heterozygote animals with miPias1.3 treatment may have had a slight rescue in

latency to fall as observed by a significant interaction detected by 2-way ANOVA (Interaction, $F(1, 26) = 4.473$, $p<0.05$). This effect was not observed in females and only the genotype effect was observed analyzing the combined group (Genotype: $F(1, 53) = 9.958$, $p<0.01$, Figure 4.3C), further suggesting that miPias1.3 treatment does not affect motor phenotypes in these animals.

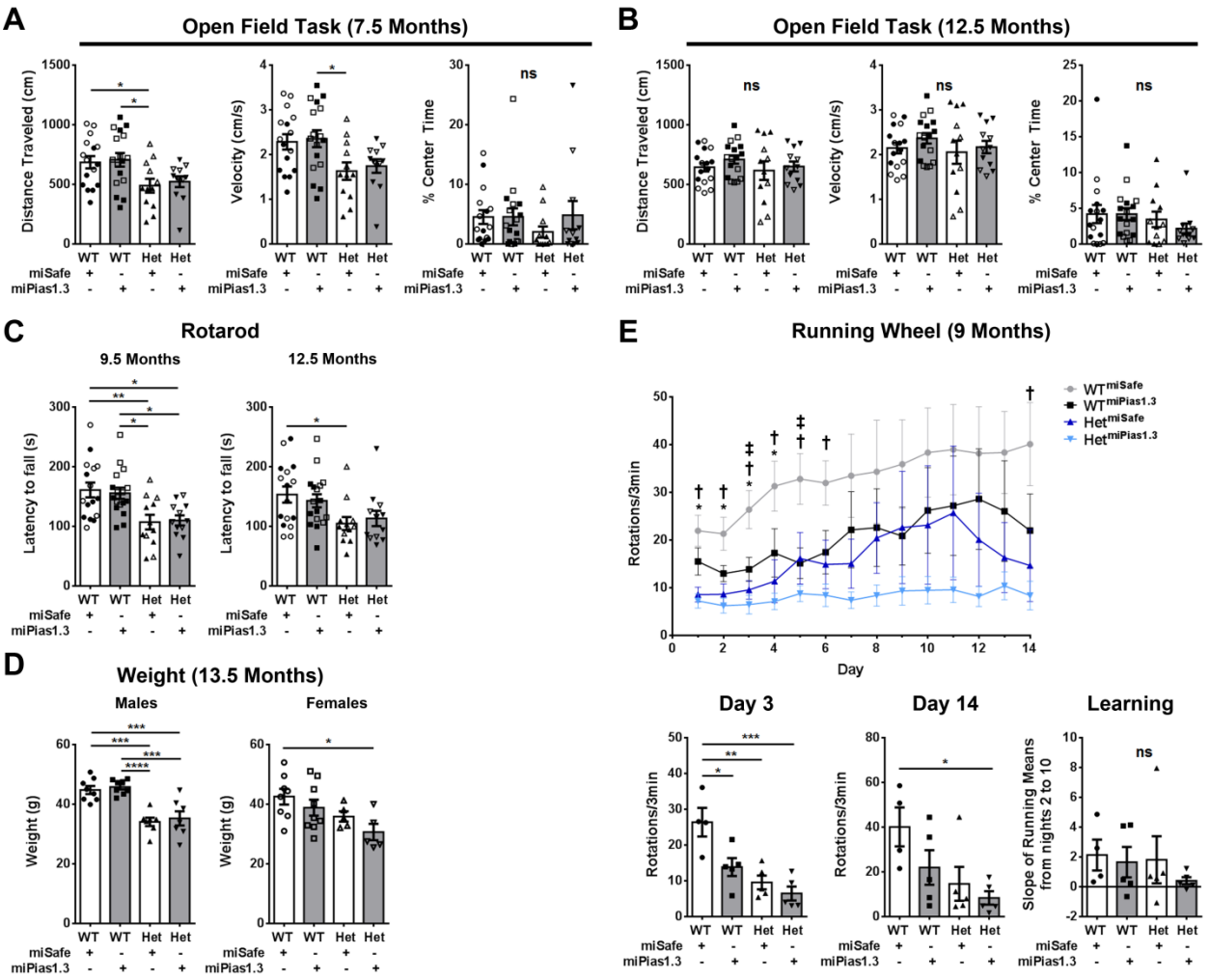

Figure 4.3: Pre-symptomatic Pias1 KD may exacerbate motor deficits in zQ175 mice. A) open field task at 7.5 months of age for combined group shows significant genotype effect for distance traveled and velocity but not % center time. B) No differences were detected in open field task at 12.5 months of age. Rotarod at C) 9.5 months of age and 12.5 months of age shows significant genotype effects. D) Male mice show genotype effect in body weight while female heterozygotes treated with miPias1.3 have a deficit in weight gain. E) Running wheel task at 9 months of age in males suggests a negative impact on motor tasks with miPias1.3 treatment but with no effect on motor learning. Genotype effects were observed for day 1 ($F(1, 15) = 21.620$, $p<0.001$), day 2 ($F(1, 15) = 19.320$, $p<0,001$), day 3 ($F(1, 15) = 22.230$, $p<0.001$), day 4 ($F(1, 15) = 12.230$, $p<0.01$), day 5 ($F(1, 15) = 7.879$, $p<0.05$), day 6 ($F(1, 15) = 9.265$, $p<0.001$), day 7 ($F(1, 15) = 6.986$, $p<0.05$), day 12 ($F(1, 15) = 4.887$, $p<0.05$), day 13 ($F(1, 15) = 5.751$, $p<0.05$), and day 14 ($F(1, 15) = 7.883$, $p<0.05$). Treatment effects were observed for day 3 ($F(1, 15) = 9.243$, $p<0.01$) and Day 5 ($F(1, 15) = 9.339$, $p<0.01$) Open symbols represent female mice. All samples were analyzed by 2-way ANOVA followed by Tukey's multiple comparison test. ns=not significant, *p<0.05, **p<0.01, ***p<0.001, ****p<0.0001, values represent means ± SEM. Shaded bars represent miPias1.3 treated animals. For running wheel: ‡ = $p<0.05$ WT^{miSafe} vs $WT^{miPias1.3}$, * = $p<0.05$ WT^{miSafe} vs Het^{miSafe}, † = $p<0.05$ WT^{miSafe} vs $Het^{miPias1.3}$

Body weight: zQ175 heterozygous animals reliably show decreased body weight (Menalled et al., 2012). Male zQ175 animals had significantly lower body weights than their WT counterparts with Pias1 KD not altering this genotype effect (Table 4.1, Figure 4.3D). In female animals, only a decrease in weight was observed for miPias1.3 treated zQ175 animals, but with no significant treatment effect (Treatment: $F(1, 23) = 2.592$, $p>0.05$). Overall, males showed a significant genotype effect while female zQ175 animals did not show a genotype effect but may have decreased body weight with Pias1 KD.

Running Wheel: The running wheel task allows for uninterrupted, voluntary assessment of motor function and motor learning (Hickey et al., 2008). Therefore, males were assessed at 9 months of age for two weeks. Females were not analyzed due to the influence of estrus cycle on running wheel activity (Hickey et al., 2008). Running wheel data trends suggest a promotion of motor deficits in mice treated with miPias1.3 in both WT and zQ175 mice

compared to miSafe-treated controls, but with no significant treatment effect over time (Treatment: $F(3, 15) = 3.257$, $p>0.05$, Figure 4.3E). Overall, miPias1.3 treated zQ175 mice performed worse throughout the task and WT animals with miPias1.3 treatment showed a significant reduction in wheel-usage at days 3 and 5, suggesting a negative impact on this task with miPias1.3 treatment on WT and HD mice at this age (Figure 4.3E).

The running wheel task can also be used to assess motor learning based on the slope of mean running between days 2 and 10 (Hickey et al., 2008). Using this analysis, no differences in motor learning were observed between our groups (Genotype, $F(1, 15) = 0.510$, $p>0.05$; Treatment, $F(1, 15) = 0.741$, $p>0.05$, Figure 4.3E). Overall, running wheel data may suggest an exacerbation in motor deficits in zQ175 animals and a decreased usage effect in WT animals with miPias1.3 pre-symptomatic treatment when assessed at 9 months of age, with no effect on motor learning.

Pias1 knock-down affects formation of HMW mHTT in pre-symptomatic treated female zQ175 mice

Next, we assessed formation of insoluble HMW mHTT after sacrifice at 13.5 months of age, a molecular readout modulated in cell culture and R6/2 mice by Pias1 (O'Rourke et al., 2013; Ochaba et al., 2016). In zQ175 mice, this species can be detected at 6 months of age, accumulating over time in zQ175 heterozygotes similar to the HMW insoluble mHTTex1p species observed in R6/2 mice (Chapter 1, Figure 4.1A). First, to evaluate KD efficiency, mRNA was harvested from GFP-positive microdisected striata to quantify levels of *Pias1* transcript. *Pias1* levels were significantly reduced in both zQ175 and WT animals with pre-

symptomatic KD as assessed by qPCR, being about -0.5 to -0.6 fold less than control groups (Males: $F(1, 11) = 52.800$, $p<0.0001$, Females: $F(1, 10) = 73.160$, $p<0.0001$), indicating successful reduction by *Pias1* miRNA (Figure 4.4A, D). To assess KD effect on Pias1 protein levels and levels of accumulated, insoluble mHTT species, Soluble/Insoluble fractionation was performed as described (Ochaba et al., 2016; Ochaba et al., 2018) and assessed by western blot. In males, no differences in Pias1 protein levels were detected in any group in both Insoluble (Treatment: $F(1, 8) = 3.709$, $p>0,05$, Genotype: $F(1, 8) = 0.069$, $p>0.05$) and Soluble (Treatment: $F(1, 8) = 0.533$, $p>0.05$, Genotype: $F(1, 8) = 0.104$, $p>0,05$) fractions (Figure 4.4B, C). GFP was detected in all animals, suggesting successful viral transduction. In zQ175 males, HMW mHTT was not modulated with miPias1.3 treatment, unlike that observed previously in R6/2 animals ($p>0.05$, (Ochaba et al., 2016)). This may have been due to insufficient reduction in Pias1 protein levels or lack of accumulation of Pias1 in the insoluble fraction of zQ175 animals as reduction of insoluble Pias1 previously corresponded with a decrease in HMW mHTT accumulation (Ochaba et al., 2016). A decline in mHTT protein levels is associated with disease progression in knock-in HD mice (Franich et al., 2018). To determine if Pias1 KD affected this genotype-associated decline, Soluble, full-length HTT (FL HTT) protein was quantified using D7F7 antibody (Cell signaling #5656S). FL-HTT was significantly reduced in zQ175 males compared to WT ($F(1, 8) = 39.600$, $p<0.001$), but no miPias1.3 treatment effect was observed ($F(1, 8) = 0.935$, $p>0.05$, Figure 4.4B, b'), suggesting that Pias1 did not impact age-associated decline of mHTT.

In female animals, Pias1 protein was also not significantly reduced in any group for either the Insoluble ($F(1, 10) = 4.464$, $p>0.05$) or Soluble fractions ($F(1, 10) = 2.512$, $p>0.05$, Figure 4.4E, F), however, insoluble HMW mHTT was significantly increased in females with miPias1.3 treatment ($p<0.05$). No treatment effect was observed on levels of soluble, FL HTT ($F(1, 10) = 1.879$, $p>0.05$) but similar to males, showed a significant reduction in zQ175 mice ($F(1, 10) = 43.570$, $p<0.0001$, Figure 4.4E, F). Therefore, Pias1 KD may have influenced the accumulation of insoluble, HMW mHTT in females only.

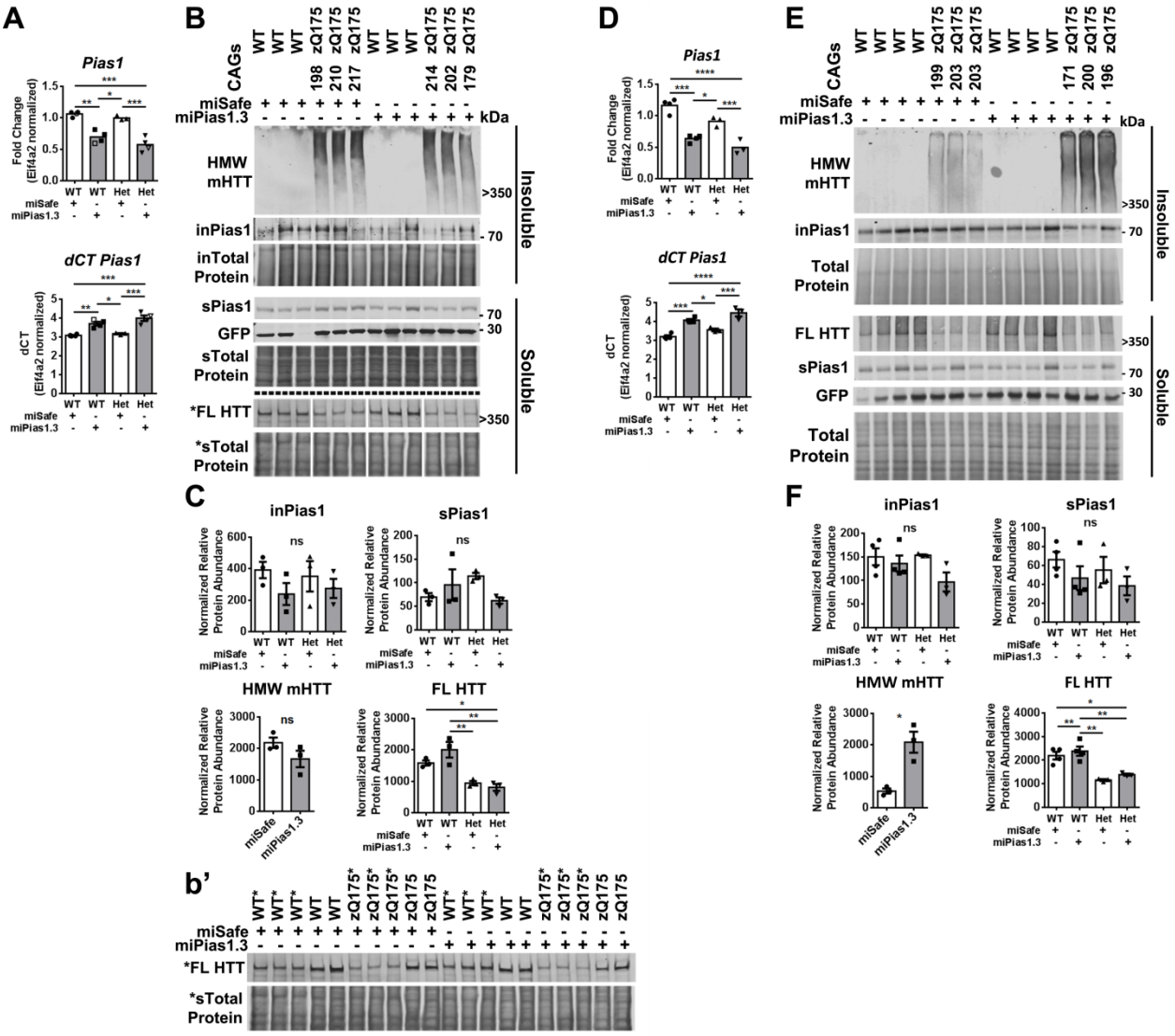

Figure 4.4: Pre-symptomatic Pias1KD does not affect mHTT accumulation at 13.5 months of age. A) qPCR analysis of mRNA harvested from male GFP+ microdisected striata shows significant reduction in levels of *Pias1* transcript with miPias1.3 treatment. Solid symbols for qPCR represent samples used for later mRNAseq analysis. B) Western blot analysis of Soluble/Insoluble fractionation of striatal tissue and C) quantification from male mice shows insufficient reduction of Pias1 protein in both fractions. HMW insoluble mHTT remains unchanged with treatment. Soluble Full length (FL) HTT shows a significant genotype effect with no treatment effect, b') *samples used for representative image and quantitative analysis due to observed batch effect. *Samples all processed from the same batch. D) qPCR analysis of mRNA harvested from female GFP+ microdisected striata shows significant reduction in levels of *Pias1* transcript with miPias1.3 treatment. E) Western blot analysis of Soluble/Insoluble fractionation and F) quantification of striatal tissue from female mice shows insufficient reduction of Pias1 protein in both fractions. HMW insoluble mHTT significantly increased with treatment. Soluble Full length (FL) HTT shows a significant genotype effect with no treatment effect. Protein normalized to total protein stain. Normalized relative protein abundances for all samples were analyzed by 2-way ANOVA followed by Tukey's multiple comparison test. ns = not significant, *$p<0.05$. **$p<0.01$, ***$p<0.001$, ****$p<0.0001$, values represent means ± SEM. Shaded bars represent miPias1.3 treated animals.

Reducing *Pias1* differentially modulates the transcriptional landscape in zQ175 mice

Pias1 is well established to function as a regulator of transcription (Rytinki et al., 2009) including serving as a negative regulator of inflammatory transcriptional response through binding of NfkB (Liu et al., 2005). Pias1 also serves as an E3 SUMO ligase for several transcription factors that regulate neuronal transcription, suggesting that KD of Pias1 could have an impact on the transcriptional profile in the brain (Table 2, (Estruch et al., 2016; Gregoire and Yang, 2005; Riquelme et al., 2006; Tai et al., 2016)). Therefore, with significant KD at the transcript level, we hypothesized that miPias1.3 treatment would impact the transcriptome in zQ175 mice.

Transcriptomic analysis was carried out on GFP-positive striatal regions harvested from pre-symptomatic male mice representing four conditions: WT miSafe, WT miPias1.3, Het miSafe, and Het miPias1.3 with three mice each per condition. Total RNA was isolated using

Trizol extraction and purified using RNeasy columns (Qiagen) for mRNAseq analysis. Data of completed mRNAseq analysis will be deposited to GEO. After QC, mapping, and quantification, normalized gene expression values were used for exploratory analysis. Principal component analysis (PCA) revealed a clear separation between the groups; both genotype and treatment conditions showed distinct separation along PC1 and PC2, representing the maximal variance among samples (Figure 4.5A). These data recapitulate known transcriptional deficits in HD mice and human patients and indicate that reduction of *Pias1* has a substantial, and reproducible, impact on gene expression in both HD and WT mice. Statistical analysis of differentially expressed genes (DEGs) was performed using DEseq2 (Love et al., 2014) and a significance threshold was set at a 10% FDR. Overall, WT animals had a higher number of dysregulated genes with miPias1.3 treatment than zQ175 animals (1438 for WT and 759 for ZQ175, Figure 4.5B). Of these, 279 DEGs were in common with miPias1.3 treatment between genotypes (Figure 4.5C). Interestingly, the majority of these shared genes modulated by Pias1 were inversely regulated based on genotype, supporting a unique role for Pias1 in the context of mHTT expression. These shared DEGs were analyzed using Gene Ontology (GO, GOrilla (Eden et al., 2009)) enrichment analysis to assess specific biological processes (Figure 4.5D). Data revealed top processes related to synaptic vesicle and neurotransmitter release, suggesting that Pias1 is differentially modulating neuronal function based on disease context. Remaining DEGs were unique to either WT or zQ175 mice when treated with miPias1.3. These genotype-specific changes were further analyzed using GO and Ingenuity Pathway Analysis (IPA) for upstream regulators by assessing all DEGs mediated by Pias1 KD for each genotype, with each showing unique enrichment terms (Figure 4.5E, G). GO analysis of WT animals with

Pias1 KD revealed processes related to cellular defense mechanisms and immune responses. Upstream regulators suggest inhibition of immune related processes with *Pias1* KD (Figure 4.5E, F), consistent with the well-defined function of Pias1 as a negative regulator of the NfkB inflammatory pathway (Shuai and Liu, 2005). GO analysis of zQ175 animals with *Pias1* KD showed enrichment for genes involved in cellular communication, neuronal transmission, and development (Figure 4.5G). IPA analysis revealed upstream pathways associated with HTT and neuronal trophic support (Figure 4.5G). Overall, analysis of genotype-specific transcriptional dysregulation with miPias1.3 treatment suggests that Pias1 may be differentially mediating pathways in zQ175 mice compared to WT mice. In WT animals, networks appear to be centered around immune and cellular defense functions while in zQ175, networks are associated with neuronal function.

Due to the differential impact of miPias1.3 treatment in zQ175 mice compared to WT, we next examined the effect of treatment on genotype-specific dysregulated genes. A unique set of DEGs was generated when comparing zQ175 miPias1.3 DEGs to those from control WT and zQ175 animals. Analyzing these genotype-filtered DEGs by GO and IPA revealed that *Pias1* KD normalized genotype-associated changes in genes involved in neuronal function and health (Figure 4.5I, J). These included trans-synaptic signaling, synaptic transmission, and nervous system development suggesting a normalizing effect for *Pias1* KD on aberrant disease associated gene transcription with an inverse fold change observed for most DEGs (Figure 4.5K). Together, transcriptomic profiling of miPias1.3 treated zQ175 animals suggests that Pias1 is contributing to neuronal function in HD mice.

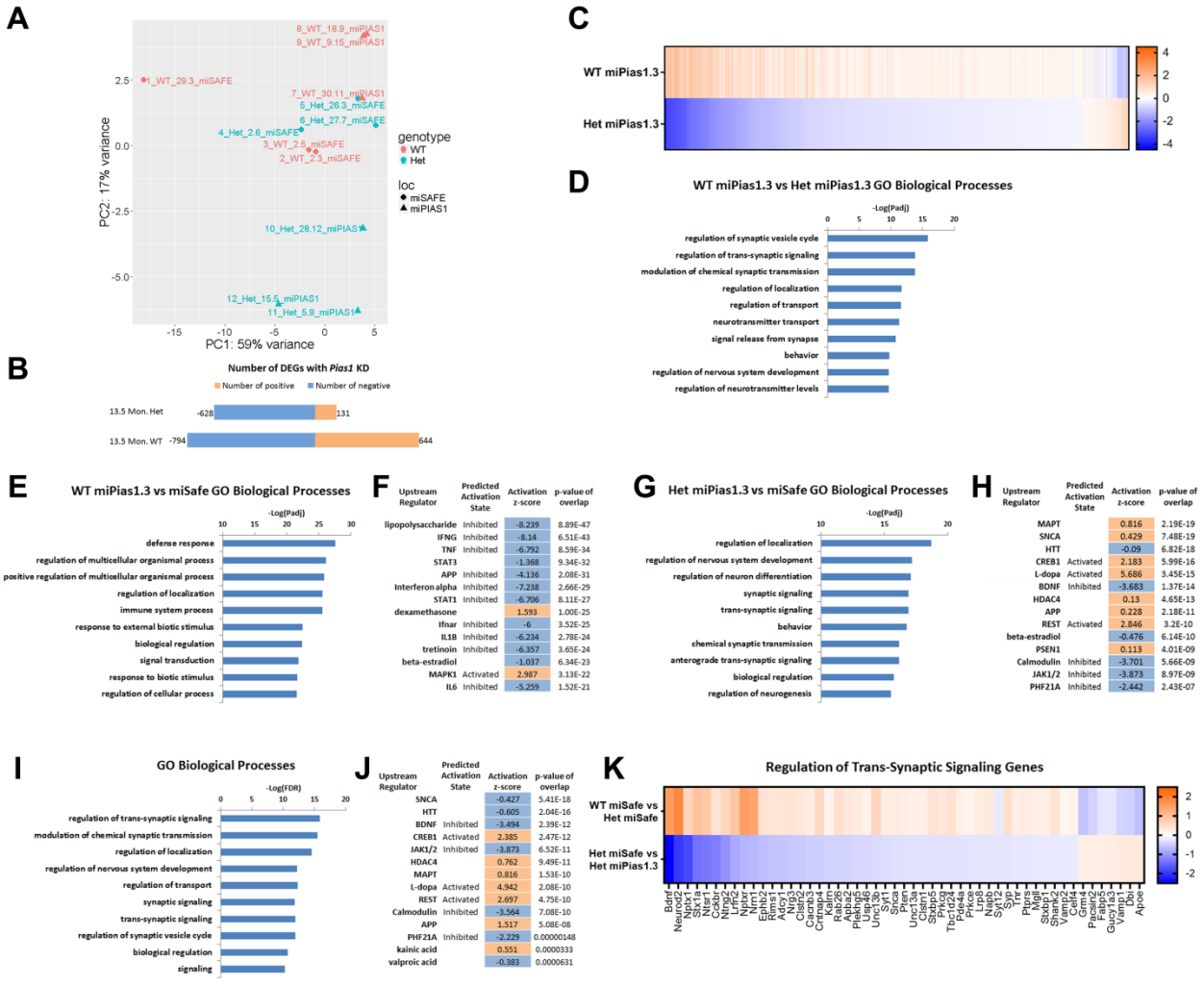

Figure 4.5: Pre-symptomatic Pias1 KD rescues neuronal function-related transcriptional dysregulation in zQ175 mice at 13.5 months of age. A) PCA of normalized gene expression values shows separation by both treatment and genotype. B) Number of DEGs with miPias1.3 treatment in WT and zQ175 mice. C) Overlap of 279 genes dysregulated with miPias1.3 treatment in WT and zQ175 mice enrich for D) GO biological processes associated with neuronal function. E) GO enrichment analysis of WT miPias1.3 vs miSafe treated animals shows modulation of immune and cellular defense processes and corresponding F) IPA upstream analysis suggests inhibition of immune related regulators. G) GO enrichment analysis of Het miPias1.3 vs miSafe treated animals shows modulation of synaptic signaling and development related processes and corresponding H) IPA upstream analysis suggests modulation of neuronal and disease-related regulators with miPias1.3 treatment. I) GO enrichment analysis and fold change of rescued, genotype-associated DEGs reveals enrichment for synaptic and neuronal functional processes and J) corresponding IPA upstream analysis similarly shows modulation of neuronal and disease-related regulators. K) Fold change heatmap indicating normalizing effect of miPias1.3 treatment on genotype-associated DEGs. Sequencing completed by UCI GHTF, analysis assisted by Ryan Lim, PhD, and Jie Wu, PhD, Thompson Lab.

Transcriptional analysis was done on mRNA extracted from male striata. Therefore, to determine if miPias1.3 treatment was similarly affecting transcriptional readouts in zQ175 females, mRNA was assessed using qPCR on several genes that were normalized with miPias1.3 treatment in males (Table 4.3). The house-keeping gene *Eif4a2* was used to normalize gene expression as it does not have a genotype effect in zQ175 mice (Southwell et al., 2016) and consistently remained unchanged in our mRNAseq dataset. In males, qPCR confirmed data obtained by mRNAseq showing a significant normalization effect with *Pias1* KD on genotype-associated DEGs for levels of *Bdnf*, *NeuroD1*, *NeuroD2*, *Syn1*, and *Syn2*, (Figure 4.6A). In females, however, levels of *Bdnf* remained statistically unaffected by miPias1.3 treatment with high variability within groups. Levels of *NeuroD1* and *NeuroD2* showed a significant increase in expression with *Pias1* KD, unlike in males, which showed a decrease with KD (Figure 4.6B). Levels of *Syn1* and *Syn2* were unaffected by miPias1.3 treatment or genotype in females (Figure 4.6B). While data suggests a differential effect on transcription in a gender-specific manner, transcriptional qPCR data supports the hypothesis that Pias1 has a regulatory role in synaptic and neuronal function by modulating *NeuroD1* and *NeuroD2* in both sexes and other neuronal genes in males. Gender-specific consequences of differential expression and accumulation of HMW mHTT remain to be explored. It is noteworthy that the vast majority of transcriptomic studies in R6/2 mice have been carried out in males, and previous transcriptional profiling in zQ175 mice removed gender-associated variation (Langfelder et al., 2016). Moreover, the majority of the findings correspond with gene changes found in human HD brain (Hodges et al., 2006).

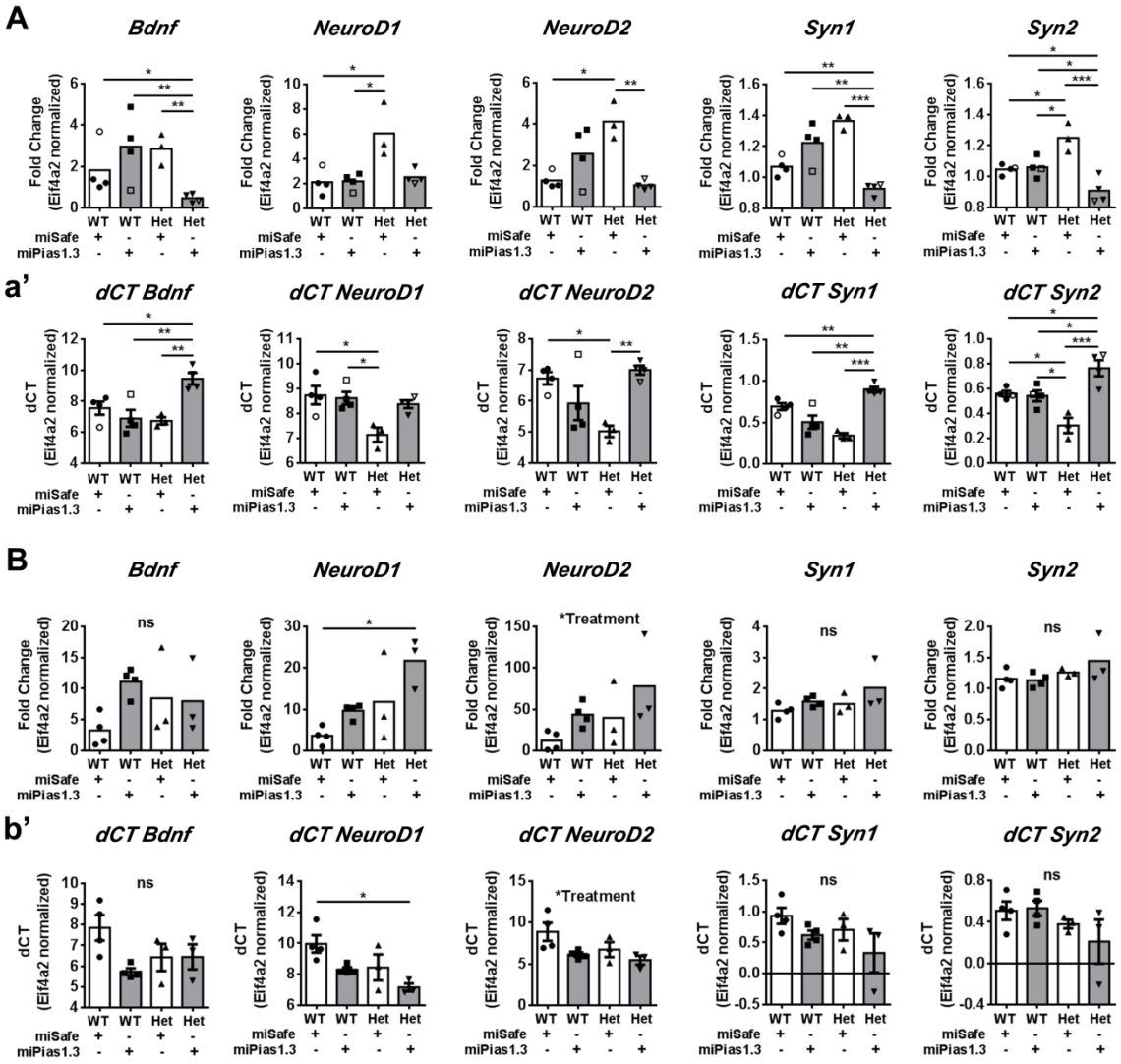

Figure 4.6: qPCR analysis to validate mRNAseq identified genes for pre-symptomatic miPias1.3 treatment assessed at 13.5 months of age. A) Fold change and a') dCT values for male mice show significant treatment and interaction effects for miPias1.3 treated Hets reproducing normalizing effect seen in mRNAseq data. Solid symbols represent animals used for mRNAseq analysis: *Bdnf* (Interaction: $F(1, 11) = 15.090$, $p<0.01$), *NeuroD1* (Interaction: $F(1, 11) = 5.740$, $p<0.05$), *NeuroD2* (Interaction: $F(1, 11) = 17.340$, $p<0.01$), *Syn1* (Interaction: $F(1, 11) = 48.480$, $p<0.0001$), and *Syn2* (Interaction: $F(1, 11) = 22.780$, $p<0.001$). B) Fold change and b') dCT values for female mice show significant treatment effect for *NeuroD1* and *NeuroD2* but inverse of effect seen in males: *Bdnf* (Treatment: $F(1, 10) = 3.886$, $p>0.05$), *NeuroD1* (Treatment: $F(1, 10) = 8.699$, $p<0.05$) and *NeuroD2* (Treatment: $F(1, 10) = 6.309$, $p<0.05$), *Syn1* (Treatment: $F(1, 10) = 3.851$, $p>0.05$), and *Syn2* (Treatment: $F(1, 10) = 0.410$, $p>0.05$). All samples were analyzed by 2-way ANOVA followed by Tukey's multiple comparison test. ns = not significant , *p<0.05, **p<0.01, ***P<0.0001, values represent means ± SEM. Shaded bars represent miPias1.3 treated animals.

Inflammation is impacted by pre-symptomatic Pias1 reduction

We previously showed that Pias1 KD decreased the number of microglia in the striatum of R6/2 mice. Given the enrichment of pathways involved in defense-responses in WT animals treated with miPias1.3, we evaluated inflammatory signatures. Microglia activation in mouse striata was monitored by counting the number of cells and measuring cell-body diameter of Iba1+ microglia using confocal microscopy and Imaris automatic analysis software. Microglia with cell body diameters of greater than 7 μm were considered reactive (Watson et al., 2012). Images were taken at 20x magnification from GFP+ regions of the striatum, representing virally transduced, Pias1 reduced regions. Pias1 KD in zQ175 males appeared to return cells towards resting state by 13.5 months of age (Diameter: $F(13, 112)=194.900$, $p<0.0001$). However, post-hoc analysis failed to reach significance for Het miPias1.3 treated animals compared to other groups. Further, no difference in the number of microglia was observed (Genotype: $F(1, 8) = 0.023$, $p>0.05$, Figure 4.7A, B). Interestingly, miPias1.3 treatment in WT animals significantly increased the number of reactive microglia in the striatum based on cell-body diameter (Figure 4.7B). This is consistent with the observed mRNAseq GO analysis, with enrichment in pathways associated with cellular defense in WT animals only compared to zQ175 mice. We further measured inflammatory markers that we previously reported were affected by Pias1 KD in R6/2 mice (NfkB and Il-6) by western blot (Figure 4.7C). Soluble levels of NfkB significantly increased in zQ175 mice treated with miPias1.3 (Genotype: $F(1, 8) = 14.820$, $p<0.01$), with no signal being detected in the Insoluble fraction (data not shown) unlike what was observed in R6/2 mice with KD (Ochaba et al., 2016). Further, levels of total Il-6 remained

unchanged (Treatment: $F(1, 8) = 1.810$, $p>0.05$), indicating a potential differential baseline inflammatory signature from the initial R6/2 study that may be strain specific.

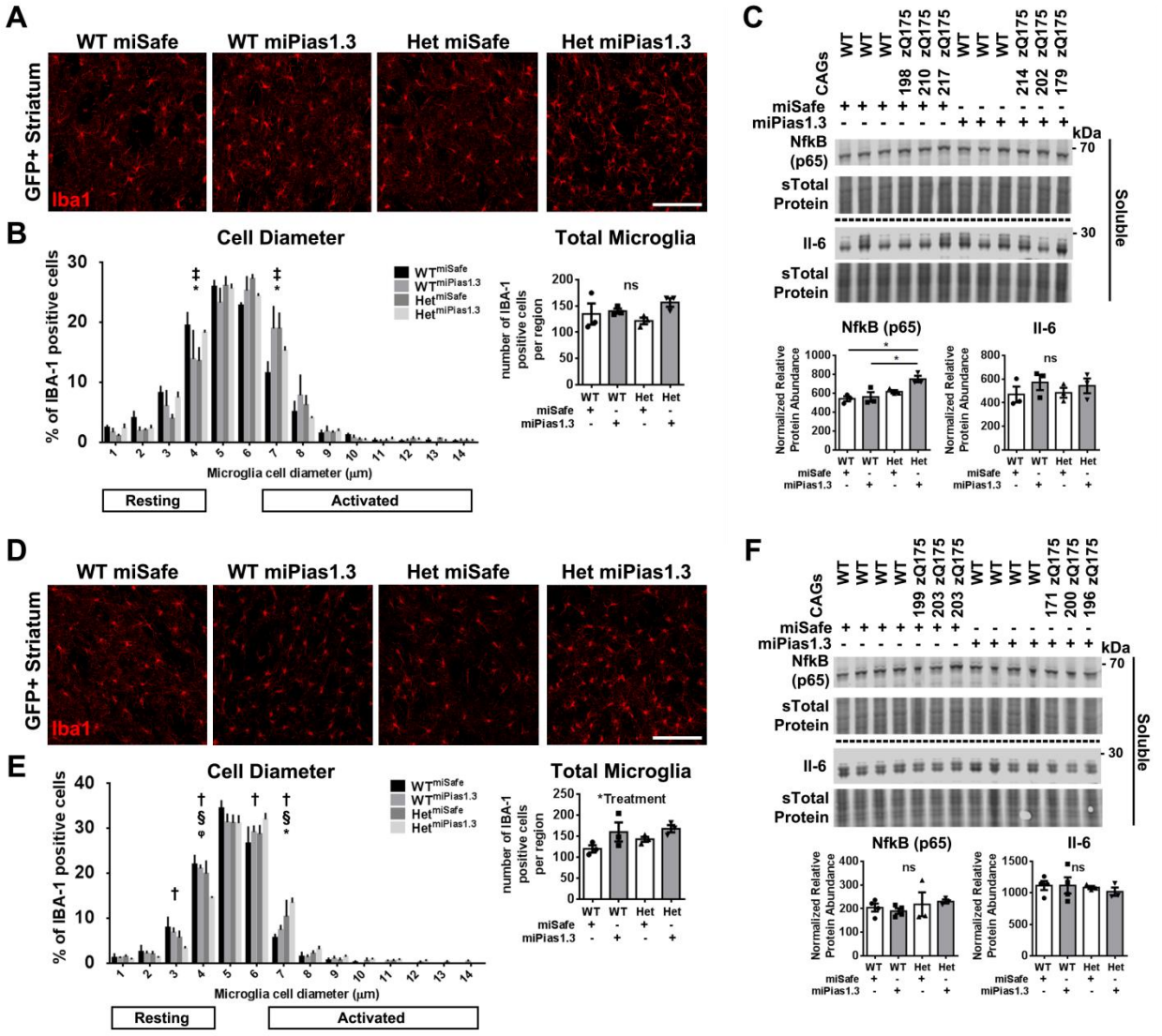

Figure 4.7: Pre-symptomatic Pias1 KD modulates immune response. Confocal analysis of Iba1+ microglia in striatum of male mice with pre-symptomatic knock-down of Pias1 (n=3). A) Representative images from the GFP+ region of 13.5 mon. old male mice. B) Cell body diameter analysis and cell count from male mice quantified using Bitplane Imaris automated software to detect cell bodies. C) Western blot from soluble striatal fraction shows significant increase in inflammatory regulator NfkB but not in cytokine Il-6 in males. D) Representative images from the GFP+ region of 13.5 mon. old female mice. E) Cell body diameter analysis and cell count from female mice quantified using Bitplane Imaris automated software to detect cell bodies. F) Western blot from soluble striatal fraction shows no changes in inflammatory markers in females. Protein normalized to total protein stain. Normalized relative protein abundances for all samples were analyzed by 2-way ANOVA followed by Tukey's multiple comparison test. ns = not significant, *p<0.05, values represent means ± SEM. For cell body diameter: ‡ = p<0.05 WT^{miSafe} vs $WT^{miPias1.3}$, * = p<0.05 WT^{miSafe} vs Het^{miSafe}, † = p<0.05 WT^{miSafe} vs $Het^{miPias1.3}$, # = p<0.05 $WT^{miPias1.3}$ vs Het^{miSafe}, § = p<0.05 $WT^{miPias1.3}$ vs $Het^{miPias1.3}$, $^{\varphi}$ = p<0.05 Het^{miSafe} vs $Het^{miPias1.3}$

Interestingly, female zQ175 animals treated with miPias1.3 showed an increase in microglial activation (Diameter: $F(13, 112) = 397.100$, $p<0.0001$), but with only a slight treatment affect in total number of microglia (Treatment: $F(1, 8) = 6.095$, $p<0.05$, Figure 4.7D, E). Inflammatory markers remained unchanged by western blot (NfkB: Treatment, $F(1, 10) = 0.004$, $p>0.05$; Il-6: Treatment, $F(1, 9) = 0.013$, $p>0.05$, Figure 4.7F). Taken together, the data suggest that Pias1 influences molecular networks associated with neuronal function in zQ175 mice, which may be independent of behavioral or protein homeostasis readouts at the 13.5 month long-term time point.

Symptomatic Pias1 KD does not affect zQ175 behavior or HMW HTT accumulation

We next asked whether Pias1 miRNA treatment after onset of symptoms in zQ175 mice could alter behavioral or molecular phenotypes (Figure 4.2B, Direction 2). Symptomatic Pias1 KD animals (injections at 7.5 months of age in collaboration with the Davidson lab, Figure 4.1B) were also subjected to a battery of assays as described above for pre-symptomatic mice. Mice were evaluated for behavior following viral injections until they

were sacrificed at 13.5 months of age to match the pre-symptomatic cohort. Statistical outputs for open field, Rotarod, and body weights are detailed in Table 4.2.

Behavior: For open field task at 12.5 months of age, no significant differences were detected between groups for distance traveled or velocity (Figure 4.8A). This data is consistent with the lack of a genotype effect in the pre-symptomatic cohort assessed with this task at 12.5 months of age and as observed previously for these animals (Menalled et al., 2012). No differences were detected for males or females for percent of time in center separately but combined, animals showed a significant difference, suggesting that this cohort of zQ175 mice may have had increased anxiety ($F(2, 44) = 3.380$, $p<0.05$, Figure 4.8A). However, post-hoc analysis failed to reveal the source of significance.

To assess additional deficits in motor movements, accelerating Rotarod task was performed at 9.5 and 12.5 months of age (Figure 4.8B). At 9.5 months of age, zQ175 animals had a significant decrease in latency to fall that was primarily observed in the females only as males alone did not show any significant difference in latency to fall between the groups (Table 4.2). Pias1 KD had no effect on latency to fall at 9.5 months of age. At 12.5 months of age, no differences in latency to fall were detected for males and females separately, but combined showed a significant difference suggesting a slight decrease in latency to fall for zQ175 mice (Combined: $F(2, 43) = 3.576$, $p<0.05$). However, post-hoc analysis failed to show significance between groups with combined animals further suggesting that miPias1.3 treatment did not affect behavioral readouts in zQ175 mice (Figure 4.8B).

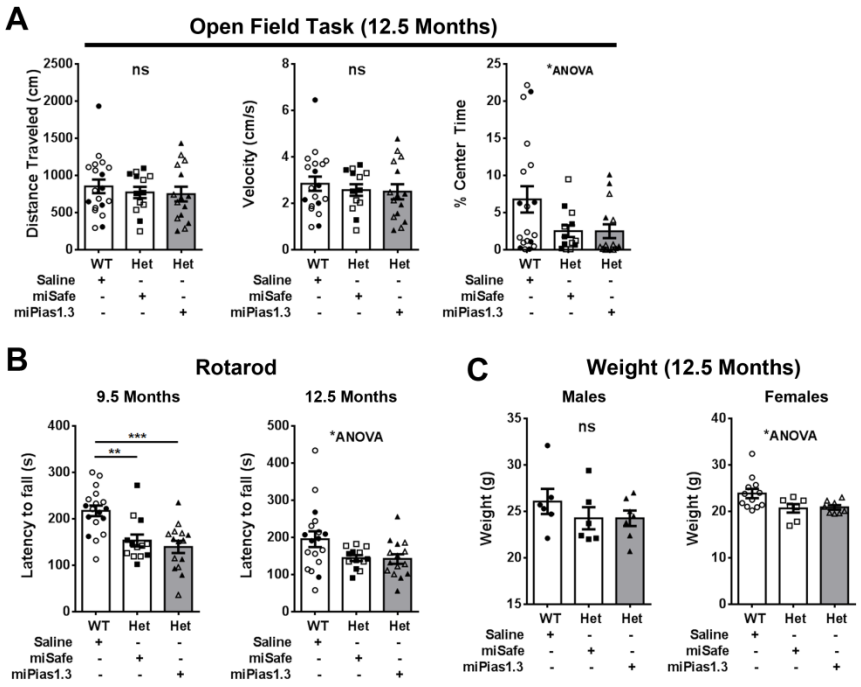

Figure 4.8: Symptomatic Pias1 KD has no effect on behavior in zQ175 mice. A) Open field task at 12.5 months of age for combined group shows no effect for distance traveled and velocity but with a significant difference in % center time by 1-Way ANOVA, with no post-hoc reaching significance. B) Rotarod at 9.5 months of age and 12.5 months of age shows significant genotype effects but no treatment effects. C) No differences were detected in body weight at 8 months of age. Open symbols represent female mice. All samples were analyzed by 1-way ANOVA followed by Tukey's multiple comparison test. ns=not significant, *p<0.05, **p<0.01, ***p<0.001, values represent means ± SEM. Shaded bars represent miPias1.3 treated animals. Data generated in collaboration with Davidson lab, CHOP.

Body weight was also recorded for these animals and assessed separately due to the previously observed differences based on gender in these animals (Menalled et al., 2012). Males did not show any differences in body weight at 12.5 months of age even though decreased body weight is typical in zQ175 mice at this age (Menalled et al., 2012). For females, 1-way ANOVA suggested a significant genotype effect indicating decreased body weight ($F(2, 24) = 4.226$, $p<0.05$) but with post-hoc analysis again failing to reveal significance (Figure 4.8C). Symptomatic Pias1 KD did not affect body weights. Taken

together, behavioral data suggest that symptomatic miPias1.3 treatment does not affect behavioral readouts in zQ175 mice.

HMW mHTT: First, KD efficiency was assessed by measuring levels of *Pias1* transcript from GFP-positive microdissected striata at 13.5 months of age. A significant reduction by about -0.5 to -0.6 fold in levels of *Pias1* transcript, assessed by qPCR, in both females ($F(2, 8) = 70.210$, $p<0.0001$) and males ($F(2, 9) = 13.410$, $p<0.01$) was observed (Figure 4.9A, D), indicating successful reduction by *Pias1* miRNA. Similar to previous cohorts, striata from symptomatic miPias1.3 treated animals were also assessed by Soluble/Insoluble fractionation (Figure 4.9). A significant reduction of Pias1 was observed in the Soluble fraction in females only (Figure 4.9E, F, Females: $F(2,11)=14.510$, $p<0.001$; Males: $F(2, 9) = 1.165$, $p>0.05$). Insoluble Pias1 was not altered (Females: $F(2, 11) = 3.262$, $p>0.05$; Males: $F(2, 9) = 0.730$, $p>0.05$) and HMW mHTT was not affected in symptomatic miPias1.3-treated animals (Females: $p>0.05$, males: $p>0.05$). There were significantly lower levels of soluble FL HTT in zQ175 mice, independent of miPias1.3 treatment in both females ($F(2, 11) = 19.830$, $p<0.001$) and males ($F(2, 9) = 12.060$, $p<0.01$, Figure 4.9B, E), again suggesting that Pias1 is not modulating age-associated decline of mHTT protein. Together, these data suggest that targeting Pias1 symptomatically in these zQ175 mice does not affect accumulation of insoluble mHTT species, even with successful reduction of Pias1 protein in females.

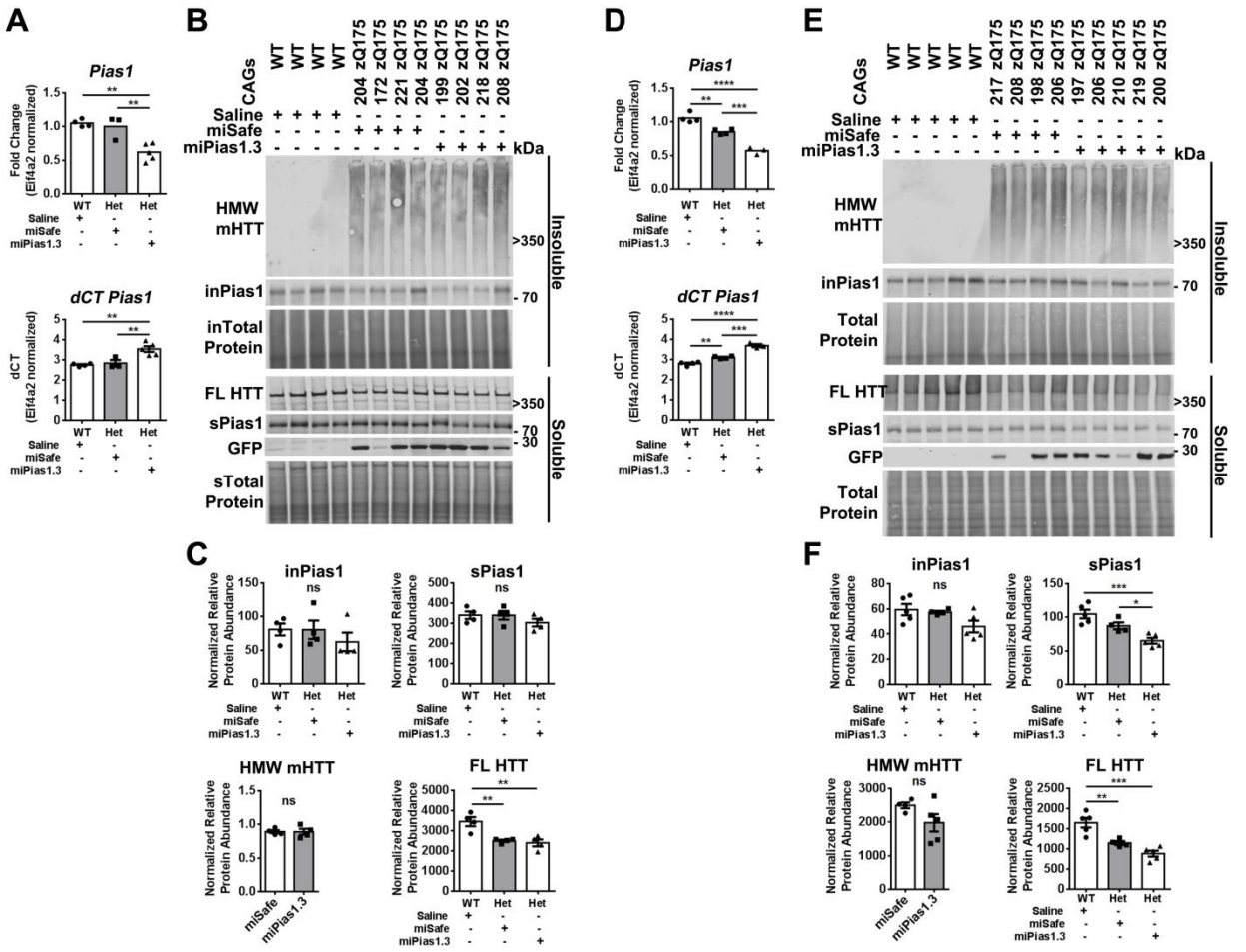

Figure 4.9: Symptomatic Pias1 KD does not affect mHTT accumulation at 13.5 months of age. A) qPCR analysis of mRNA harvested from male GFP+ microdisected striata shows significant reduction in levels of *Pias1* transcript with miPias1.3 treatment. B) Western blot analysis and C) quantification of Soluble/Insoluble fractionation of striatal tissue from male mice shows insufficient reduction of Pias1 protein in both fractions. HMW insoluble mHTT remains unchanged with treatment. Soluble Full length (FL) HTT shows a significant genotype effect with no treatment effect. D) qPCR analysis of mRNA harvested from female GFP+ microdisected striata shows significant reduction in levels of *Pias1* transcript with miPias1.3 treatment as well as a significant genotype effect compared to WT vehicle control mice. E) Western blot analysis and F) quantification of Soluble/Insoluble fractionation of striatal tissue from female mice shows insufficient reduction of insoluble Pias1 protein but significant reduction of soluble Pias1 levels with miPias1.3 treatment. HMW insoluble mHTT remains unchanged with treatment. Soluble Full length (FL) HTT shows a significant genotype effect with no treatment effect. Protein normalized to total protein stain. Normalized relative protein abundances for all samples were analyzed by 1-way ANOVA followed by Tukey's multiple comparison test. ns = not significant, *p<0.05. **p<0.01, ***p<0.001, ****p<0.0001, values represent means ± SEM. Shaded bars represent miPias1.3 treated animals.

Microglial activation: Similar to pre-symptomatic Pias1 KD animals, symptomatic-treated mice were assessed for microglial activation and inflammatory markers. Male zQ175 animals with symptomatic miPias1.3 treatment had a significant increase in activated microglia based on cell body diameter ($F(13,84)=150.500$, $p<0.0001$) as well as an increase in the number of microglia detected suggesting that miPias1.3 treatment in symptomatic zQ175 animals increased microglial activity in the striatum ($F(2,6)=7.870$, $p<0.05$, Figure 4.10A, B). This suggested that targeting Pias1 symptomatically may have induced an immune response as opposed to reducing one (compared to pre-symptomatic treated males, Figure 4.7B). However, no changes in inflammatory markers were detected in the Soluble protein fraction assessed by western blot (NfkB: $F(2, 9) = 2.588$, $p>0.05$; Il-6: $F(2, 9) = 0.202$, $p>0.05$, Figure 4.10C). For females, a significant increase in soluble levels of NfkB was observed in zQ175 mice treated with miPias1.3 (NfkB: $F(2, 9) = 9.610$, $p<0.01$; Il-6: $F(2, 11) = 2.818$, $p>0.05$, Figure 4.10D), which had not been observed with pre-symptomatic KD (Figure 4.7F), also suggesting an increased inflammatory response. Insoluble NfkB was not detected (data not shown). Taken together these data suggest that Pias1 may have different functional consequences towards specific neuroinflammatory responses during different disease stages.

In summary, for both pre-symptomatic and symptomatic mice, Pias1 reduction in general did not modulate behavior or insoluble HMW HTT species. Modest modulatory effects on inflammatory responses were observed with both symptomatic and pre-symptomatic KD with symptomatic reduction potentially increasing an inflammatory response in zQ175 males. However, Pias1 protein levels were not significantly reduced with KD for most

groups when assessed at 13.5 months of age, potentially reflecting disruptions in protein clearance or compensatory responses. Importantly, Pias1 did not accumulate in the insoluble fraction as was observed in R6/2 mice (Ochaba et al., 2016). These data suggest that either Pias1 modulation does not impact these outcomes in zQ175 animals or that the concordant accumulation of insoluble Pias1 and activation of Pias1 specific inflammatory responses is a necessary component for impacting either behavior or aberrant protein homeostasis in HD animals.

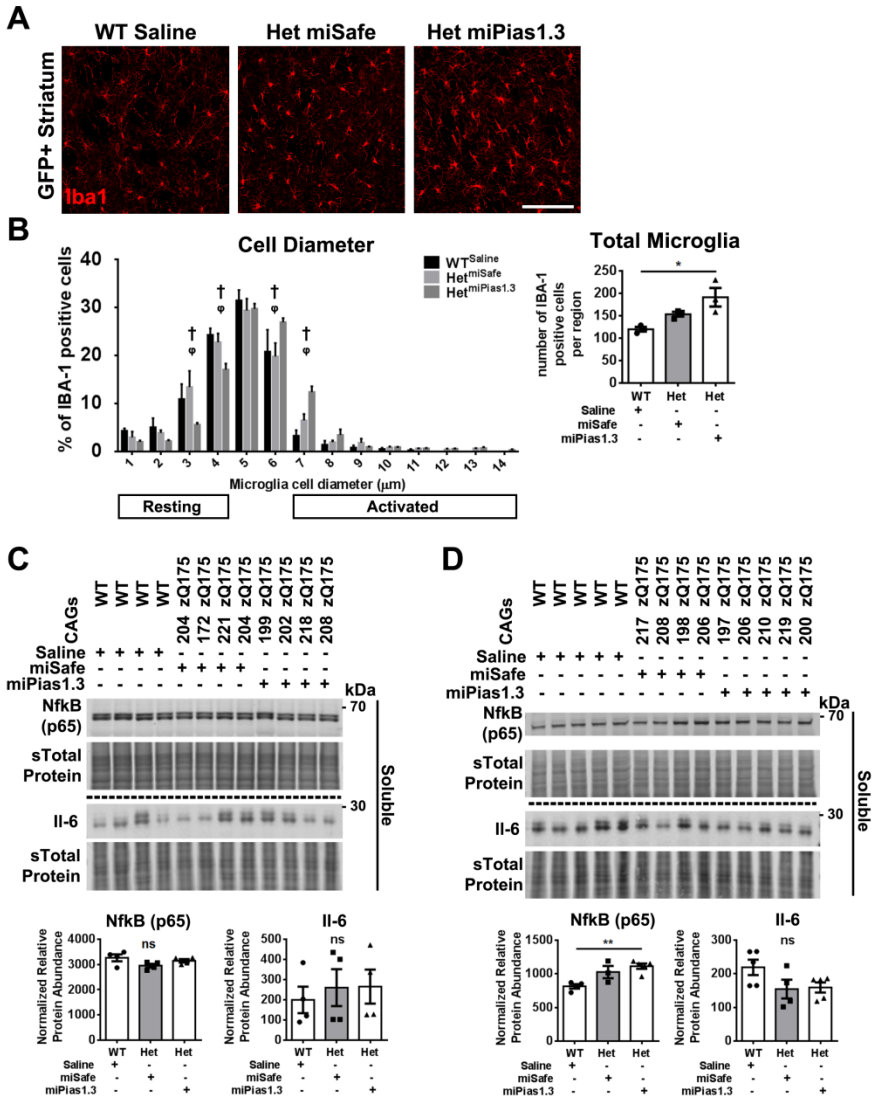

Figure 4.10: Symptomatic Pias1 KD modulates immune response. Confocal analysis of Iba1+ microglia in striatum of male mice with symptomatic knock-down of Pias1 (n=3). A) Representative images from the GFP+ region of 13 mon. old male mice. B) Cell body diameter analysis and cell count from male mice quantified using Bitplane Imaris automated software to detect cell bodies. Western blot from C) male soluble striatal fraction effects on inflammatory regulator NfkB and cytokine Il-6 with miPias1.3 treatment. D) Female western blot analysis shows significant elevation in NfkB but no change in Il-6. Protein normalized to total protein stain. Normalized relative protein abundances for all samples were analyzed by 1-way ANOVA followed by Tukey's multiple comparison test. ns = not significant, *p<0.05, values represent means ± SEM. Shaded bars represent miPias1.3 treated animals. For cell body diameter: ‡ = p<0.05 WT^{miSafe} vs $WT^{miPIAS1.3}$, * = p<0.05 WT^{miSafe} vs Het^{miSafe}, † = p<0.05 WT^{miSafe} vs $Het^{miPIAS1.3}$, # = p<0.05 $WT^{miPIAS1.3}$ vs Het^{miSafe}, § = p<0.05 $WT^{miPias1.3}$ vs $Het^{miPias1.3}$, $^{\varphi}$ = p<0.05 Het^{miSafe} vs $Het^{miPias1.3}$

Assessing pre-symptomatic Pias1 KD at 8 months of age reveals additional molecular modulation

To further understand molecular mechanisms impacted by Pias1KD and inform results from the 13.5 month-old study, we evaluated mice at an earlier time point of 8 months of age, just after symptomatic phenotypes emerge (Menalled et al., 2012). We repeated pre-symptomatic treatment with miPias1.3 and miSafe with a small cohort of animals at 2.5 months of age and aged mice to 8 months, specifically to evaluate biochemical and molecular readouts (Figure 4.2, Direction 3). A Saline/vehicle control was included in female mice to control for viral delivery method. Behavior was evaluated primarily as a mode of enrichment to ensure that molecular readouts were not confounded by lack of trophic support (Mattson et al., 2004) and for consistency with the longer term studies.

Behavioral analysis of pre-symptomatic Pias1 KD at 8 months

The same battery of behavioral tasks was carried out as above. Open field was completed at 7.5 months of age with running wheel task performed at 7 months before sacrifice. Body weights were also recorded. A summary of statistical analysis for open field and body

weights are shown in Table 4.1 (Figure 4.11A, B). The smaller cohort size may account, in part, for the lack of observed genotype effects for these readouts.

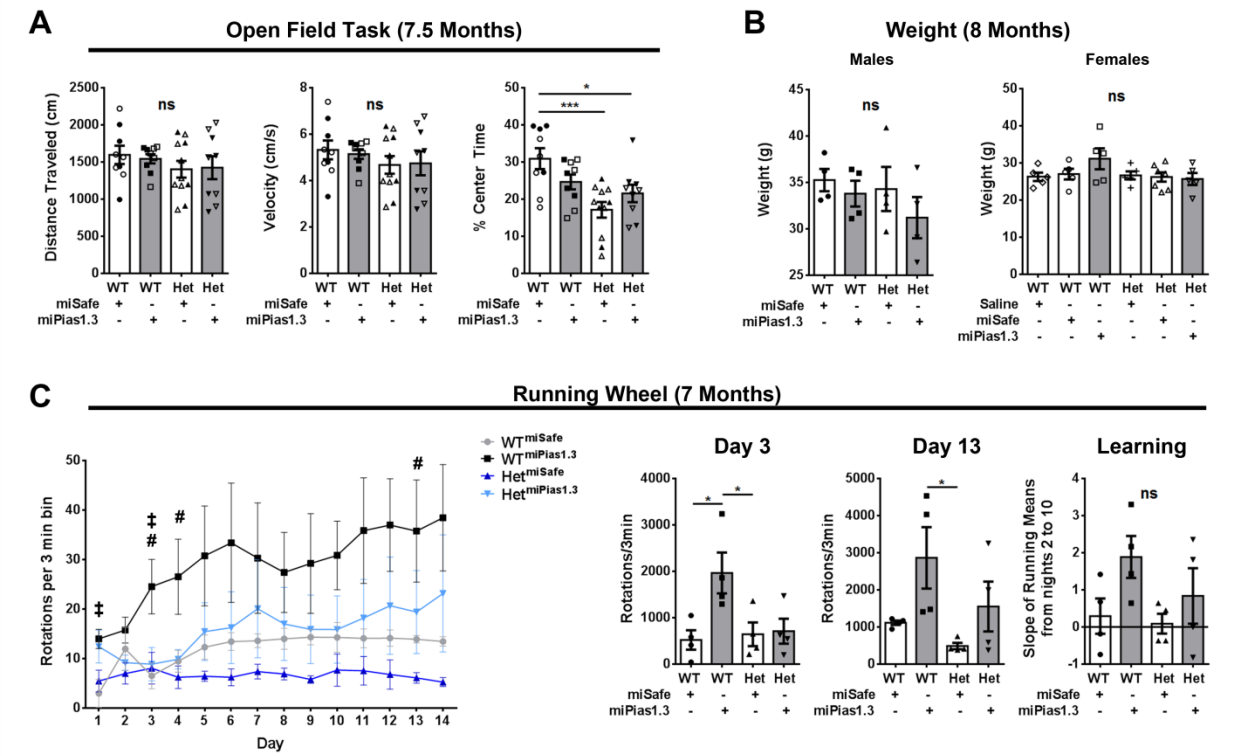

Figure 4.11: Pre-symptomatic Pias1 KD may rescue early motor deficits in zQ175 mice. A) open field task at 7.5 months of age for combined group shows no effect for distance traveled and velocity but a significant genotype effect for % center time. B) No differences were detected in body weight at 8 months of age. C) Running wheel task at 7 months of age in males suggests a significant increase in motor activity with miPias1.3 treatment in at least WT animals but with no effect on motor learning. Significant treatment effects were observed on day 1 ($F(1, 12) = 11.840$, $p<0.01$), day 3 ($F(1, 12) = 6.053$, $p<0.05$), day 4 ($F(1, 12) = 6.019$, $p<0.05$), day 5 ($F(1, 12) = 5.292$, $p<0.05$), day 10 ($F(1, 12) = 5.390$, $p<0.05$), day 11 ($F(1, 12) = 5.646$, $p<0.05$), day 12 ($F(1, 12) = 6.882$, $p<0.05$), day 13 ($F(1, 12) = 6.921$, $p<0.05$), and day 14 ($F(1, 12) = 7.148$, $p<0.5$). A significant interaction was detected on day 3 ($F(1, 12) = 5.045$, $p<0.5$). A significant genotype effect was detected on day 4 ($F(1, 12) = 5.566$, $p<0.05$). Open symbols represent female mice. All samples were analyzed by 2-way ANOVA followed by Tukey's multiple comparison test. ns=not significant, *p<0.05, **p<0.01, ***p<0.001, values represent means ± SEM. Shaded bars represent miPias1.3 treated animals. For running wheel: ‡ = $p<0.05$ WT^{miSafe} vs $WT^{miPias1.3}$, # = $p<0.05$ $WT^{miPias1.3}$ vs Het^{miSafe}

The running wheel apparatus has a finite number of animals that can be tested at a time due to single housing. Therefore, groups of male mice were of comparable size to the cohort assessed at 9 months of age and data was similarly processed (Figure 4.11C). In contrast to mice tested at 9 months of age, which showed some additional impairment in this task with Pias1KD, at this earlier time point, KD increased running wheel usage. Specifically, a significant treatment effect (Treatment: $F(3, 12) = 3.526$, $p<0.05$) was observed with WT animals treated with miPias1.3 showing an apparent increase in usage of the running wheel over time compared to WT control treated animals. A similar trend was observed between zQ175 miSafe and miPias1.3 treated animals over time. No differences were detected in motor learning (Genotype: $F (1, 12) = 1.339$, $p>0.05$; Treatment, $F(1, 12) = 4.663$, $p>0.05$). Overall, data suggests that miPias1.3 treatment led to increased usage of the running wheel and increased motor capabilities in at least WT animals and potentially zQ175 animals at this time point (7 months, Figure 4.11C). Therefore, miPias1.3 pre-symptomatic treatment may have differential effects on behavior during different stages of disease pathogenesis.

Bodyweight was recorded and assessed as in previous cohort until 8 months of age. No differences in weight gain were detected for either genotype or treatment by 8 months of age. However, at 8 months of age, zQ175 mice only exhibit minor deficits in body weight (Menalled et al., 2012). It is possible that this cohort of animals had not begun showing detectable genotype effects with this analysis by time of sacrifice.

Pias1 does not affect formation of HMW mHTT or alter microglial activation at 8 months of age

Striata from male mice were assessed at 8 months of age for levels of Pias1 and accumulated mHTT using Soluble/Insoluble fractionation and western blotting (Figure 4.12) to determine whether an earlier time point might reveal changes in protein homeostasis. Unlike pre-symptomatic animals assessed at 13.5 months of age, Pias1 protein levels were significantly reduced in the Soluble fraction in both WT and HD zQ175 males treated with miPias1.3 (Treatment: $F(1, 10) = 76.120$, $p<0.0001$). Insoluble Pias1 levels also showed a significant treatment effect suggesting reduction of this species ($F(1, 10) = 12.920$, $p<0.01$) but only between control WT animals and miPias1.3 treated zQ175 as revealed by post-hoc analysis. Levels of insoluble Pias1 were not elevated in untreated zQ175 animals at this age, similar to 13.5 month old animals. We next assessed formation of the insoluble HMW mHTT species in this younger cohort of pre-symptomatic miPias1.3 treated animals. Significant reduction of Pias1 still did not affect formation of insoluble HMW mHTT accumulated species ($p>0.05$). zQ175 animals again had significantly reduced levels of soluble FL HTT compared to WT animals (Genotype: $F(1, 10) = 31.990$, $p<0.0001$), and a modest treatment effect of reduced FL HTT in zQ175 mice was observed with miPias1.3 treatment (Treatment: $F(1, 10) = 7.564$, $p<0.05$).

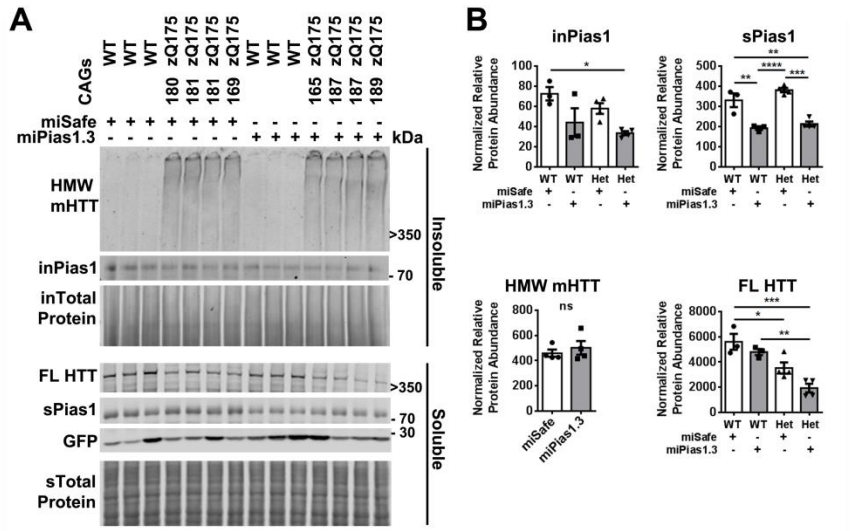

Figure 4.12: Pre-symptomatic PIias1 KD does not affect mHTT accumulation at 8 months of age. A) Western blot analysis and B) quantification of Soluble/Insoluble fractionation of striatal tissue from male mice shows significant reduction of Pias1 protein in both fractions. HMW insoluble mHTT remains unchanged with treatment at this age. Soluble Full length (FL) HTT shows a significant genotype effect with a slight treatment effect observed with zQ175 animals having significantly less FL HTT than WT with miPias1.3 treatment. Protein normalized to total protein stain. Normalized relative protein abundances for all samples were analyzed by 2-way ANOVA followed by Tukey's multiple comparison test. ns = not significant, *p<0.05. **p<0.01, ***p<0.001, ****p<0.0001, values represent means ± SEM. Shaded bars represent miPias1.3 treated animals.

Given the modest effect of miPias1.3 treatment on microglia in older animals, we assessed cell body diameter and total number of microglia in females at 8 months of age. A saline treatment control group was included in this analysis to determine if inflammatory effects could arise from viral delivery. Using the same analysis as above on Iba1+ cells, there was no effect of miPias1.3 treatment on microglial activation in these animals. Interestingly, saline WT and zQ175 control groups appeared to have more reactive microglia than viral treated WT and zQ175 groups based on cell body diameter ($F(13, 168) = 477.500$, $p<0.0001$, Figure 4.13A, B), potentially confounding the data. No difference in number of microglia was observed for either genotype ($F(1, 12) = 0.026$, $p>0.05$) or treatment ($F(2, 12) = 0.234$, $p>0.05$, Figure 4.13B). Due to these confounding variables, no conclusion

regarding microglial activation in these animals could be made using this analysis. Due to cohort size, male animals were not assessed using this assay, rather, inflammatory markers were analyzed by western blot on male tissues (Figure 4.13C). Soluble levels of NfkB were significantly altered in males with miPias1.3 treatment in a genotype dependent manner (Treatment: $F(1, 10) = 6.564$, $p<0.05$; Interaction: $F(1, 10) = 30.850$, $p<0.001$) such that, WT animals with Pias1 KD had less soluble NfkB: an effect that was not observed at 13.5 months of age (Figure 4.7C). For levels of soluble Il-6, a slight increase in WT treated animals and a slight decrease in zQ175 treated animals was observed (Interaction: $F(1, 10) = 8.932$, $p<0.05$) but with no significant treatment effect (Treatment: $F(1, 10) = 0.108$, $p>0.05$). Therefore, Pias1 appears to modulate some inflammatory responses in a genotype-dependent manner but may have differential impact depending on disease stage.

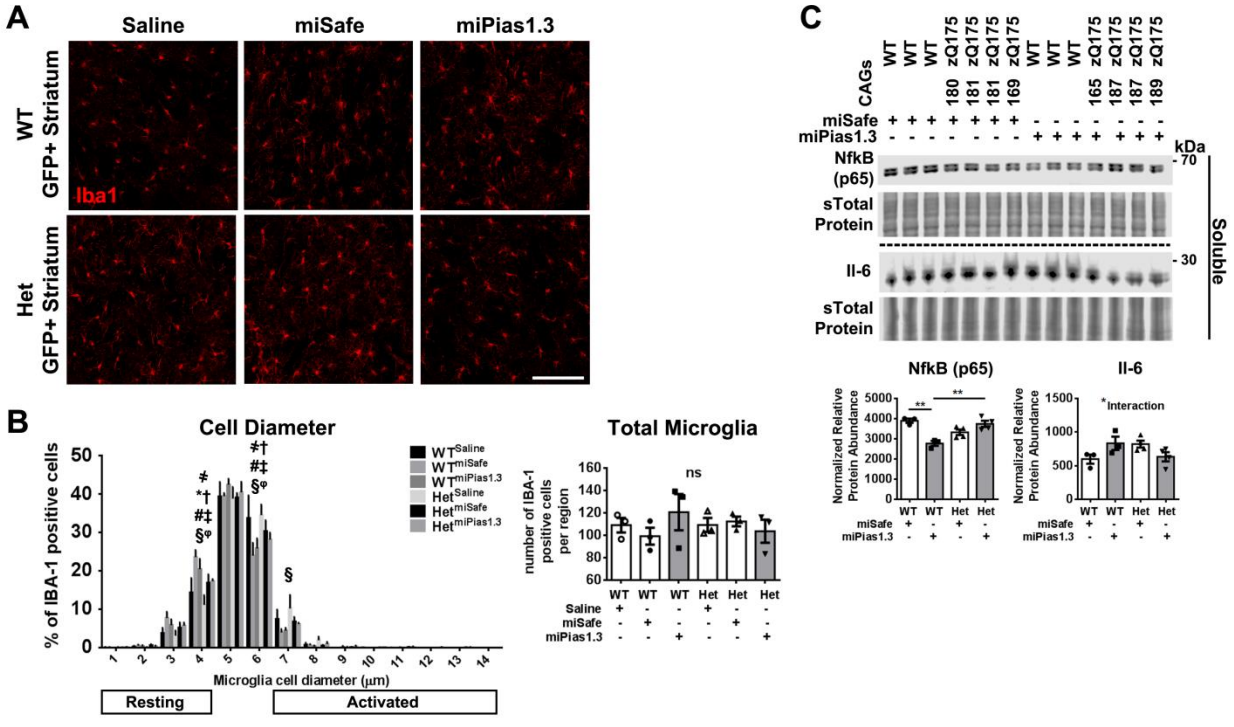

Figure 4.13: Pre-symptomatic Pias1 KD does not modulate immune response in younger mice. Confocal analysis of Iba1+ microglia in striatum of female mice with pre-symptomatic knock-down of Pias1 (n=3). A) Representative images from the GFP+ region of 8 mon. old female mice. B) Cell body diameter analysis and cell count from female mice quantified using Bitplane Imaris automated software to detect cell bodies. C) Western blot from soluble striatal fraction shows significant effects on inflammatory regulator NfkB and cytokine Il-6 in males with miPias1.3 treatment. Protein normalized to total protein stain. Normalized relative protein abundances for all samples were analyzed by 2-way ANOVA followed by Tukey's multiple comparison test. ns = not significant, *p<0.05, **p<0.01, values represent means ± SEM. Shaded bars represent miPias1.3 treated animals. For cell body diameter: ≠ = WT^{Saline} vs WT^{miSafe}, * = p<0.05 WT^{miSafe} vs Het^{miSafe}, † = p<0.05 WT^{miSafe} vs $Het^{miPias1.3}$, # = p<0.05 Het^{Saline} vs $Het^{miPias1.3}$, ‡ = p<0.05 WT^{Saline} vs $WT^{miPias1.3}$, § = p<0.05 WT^{miSafe} vs Het^{Saline}, ᵠ = p<0.05 $WT^{miPias1}$ vs Het^{Saline}

Transcriptional changes by Pias1 reduction appear to be temporally regulated

Pias1 KD strongly affected the transcriptional landscape at 13.5 months of age, even without significant reduction at the protein level. Therefore, mRNAseq was also carried out as above at 8 months of age when a significant reduction in Pias1 protein levels were detected following Pias1 KD. PCA for these younger animals showed less separation with genotype as anticipated given that disease is progressive compared to 13.5 month-old animals (Figure 4.5A, 4.14A). Treatment also showed less separation than older mice. This difference may be due to time between miPias1.3 treatment and sacrifice as compared to data from 13.5-month old animals or alternatively, as disease progresses, effect sizes may become more pronounced. Supporting these possibilities, fewer DEGs were observed to be affected by *Pias1* KD in both WT and zQ175 mice as compared to the older animals (Figure 4.14B). Of these, only a small overlap of 22 shared dysregulated genes between the age groups for zQ175 mice with miPias1.3 treatment was observed (Figure 4.14B, C). All 22 of these genes were similarly dysregulated with miPias1.3 treatment (Figure 4.14D). GO enrichment and IPA analysis for all DEGs revealed regulation of biological processes and neurogenesis in WT animals treated with miPias1.3 (Figure 4.14E) but only intracellular

signal transduction as a process significantly impacted by *Pias1* reduction in zQ175 treated animals (Figure 4.14G). Interestingly, IPA upstream analysis in WT treated animals showed an enrichment for similar regulators compared to older zQ175 animals treated with miPias1.3 such at HTT, CREB1, L-dopa, SNCA, and BDNF (Figure 4.5E, Figure 4.14F). While some of these regulators were also enrichened in 8-month old zQ175 mice with treatment (e.g. CREB1, BDNF), there was less overlap compared to 13.5 month-old treated zQ175 animals (Figures 4.5G, 4.14H) suggesting either a different or smaller impact on transcription with less treatment time or stage of disease progression.

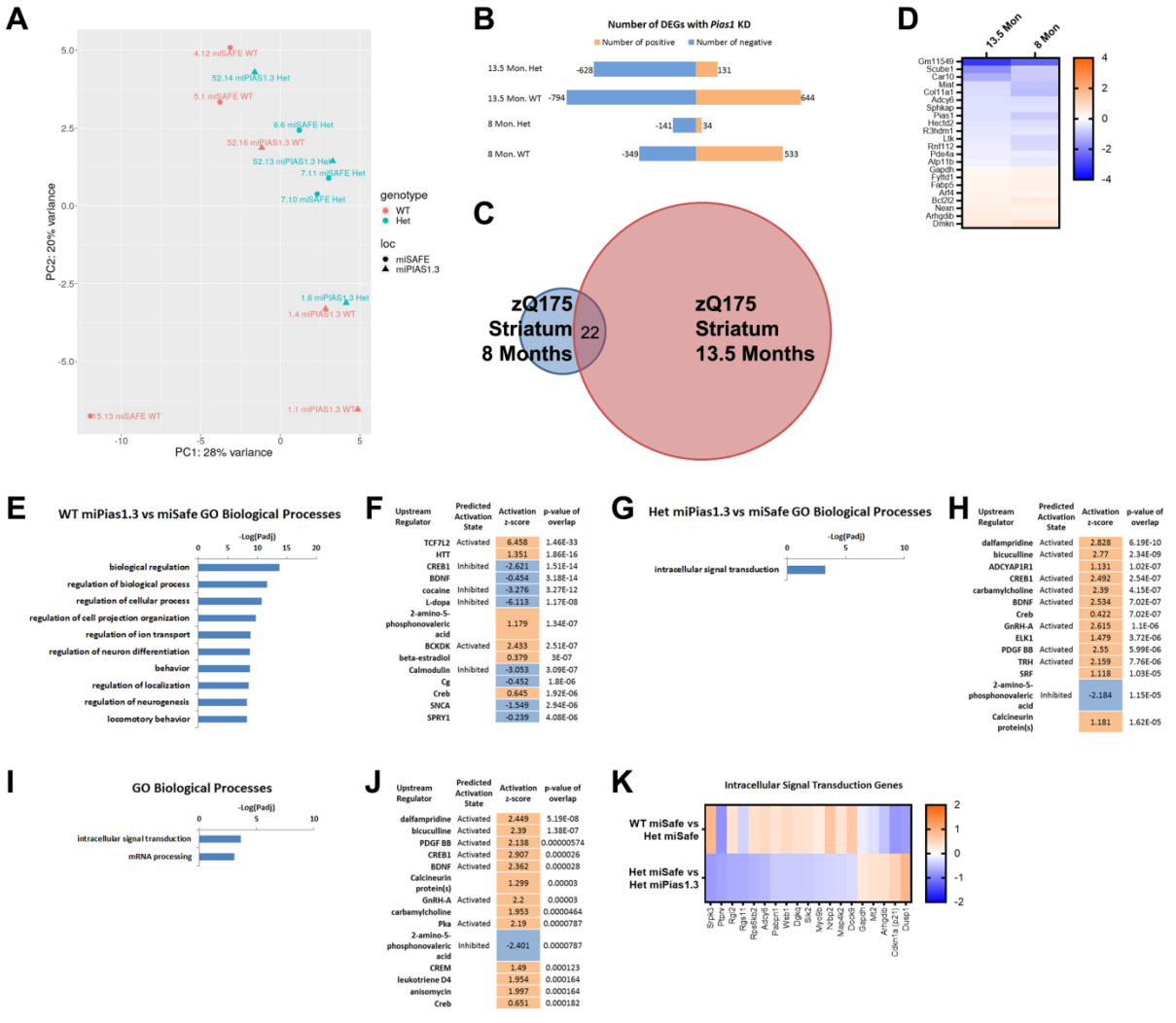

Figure 4.14: Pre-symptomatic Pias1 KD has minimal effect on transcriptional landscape at 8 months of age. A) PCA of normalized gene expression values shows separation of WT treated animals. B) 8 month-old zQ175 mice with miPias1.3 treatment have fewer measured DEGs compared to 13.5 month-old pre-symptomatic treated animals with C) minimal overlap of 22 DEGs observed between cohorts. D) Fold change heatmap of 22 shared DEGs between age groups shows similar modulation with miPias1.3 treatment. E) GO enrichment analysis of WT miPias1.3 vs miSafe treated animals shows modulation of biological processes including localization and development-related processes and F) corresponding IPA upstream analysis suggests modulation of neuronal and disease-related regulators with miPias1.3 treatment at this age in WT animals. G) GO enrichment analysis of Het miPias1.3 vs miSafe treated animals shows modulation of only intracellular signal transduction with corresponding H) IPA upstream analysis. H) GO enrichment analysis of rescued, genotype-associated DEGs reveals enrichment for intracellular signaling and mRNA processing only with J) corresponding IPA upstream analysis. K) Fold change heatmap indicating normalizing effect of miPias1.3 treatment on genotype-associated DEGs. Sequencing completed by UCI GHTF, analysis assisted by Ryan Lim, PhD, and Jie Wu, PhD, Thompson Lab.

Only 175 genes were dysregulated in zQ175 animals with miPias1.3 treatment at this age. Of these, 119 were associated with genotype. When analyzing the effect of miPias1.3 treatment on these 119 genotype-specific DEGs, processing of mRNA was also significantly enriched by GO analysis in the 8 month-old zQ175 animals (Figure 4.14I). Upstream IPA regulator analysis of genotype-associated DEGs normalized with KD (119), revealed similar upstream processes to those detected when all DEGs in zQ175 mice with KD were assessed (175). This suggests that *Pias1* may be primarily regulating disease-associated transcriptional networks at this age (Figure 4.14H, J). The majority of genotype-dysregulated genes that are altered in expression by miPias1.3 treatment again showed inverse fold changes suggesting a normalizing effect on aberrant HD-associated transcription (Figure 4.14K). Together, transcriptional analysis at 8 months of age revealed a smaller impact of *Pias1* KD in both WT and zQ175 mice suggesting that length of KD treatment or stage of disease greatly influences modulation of transcriptional profiles in

these animals, but that *Pias1* KD does appear to also have a normalizing effect on transcriptionally dysregulated genes in HD mice.

Pias1 KD consistently modulates *Bcl2l2* expression levels independent of age or disease stage

As described above, 22 Pias1 KD-dysregulated genes in zQ175 animals overlapped between age groups (Figure 4.14D). Within these overlapping genes, *Rnf112* and *Pde4a* were of interest, as these were both dysregulated in male zQ175 mice at 13.5 months of age and normalized with pre-symptomatic Pias1 KD as determined by mRNAseq (Table 4.3). *Rnf112*, also known as Neurolastin, encodes a GTPase that functions in neurogenesis (Lomash et al., 2015). *Pde4*a is a SUMO substrate that mediates cAMP signaling cascades by hydrolyzing cyclic nucleotides. Members of the Pde4 family play a role in mediating Darpp-32 signaling cascades and memory in the brain (Havekes et al., 2016; Kuroiwa et al., 2012). A third gene of interest that was modulated at both 8 months of age and 13.5 months of age in males with pre-symptomatic Pias1 KD, but did not show a normalizing effect, was *Bcl2l2*. Instead, pre-symptomatic Pias1 KD consistently resulted in an increase in *Bcl2l2* expression, regardless of age assessed (Table 4.3). *Bcl2l2*, (also known as *Bcl-w*), is a member of the Bcl-2 protein family. This family has multiple members that comprise two self-antagonizing functions: pro-survival and pro-death pathways through maintenance of mitochondrial dynamics (Aouacheria et al., 2017). *Bcl2l2* is a pro-survival member of the Bcl-2 family that has been implicated in neuronal survival after injury (Courchesne et al., 2011; Simon et al., 2016). Therefore, due to their potential roles in mediating neuronal function, development, and survival, transcript levels of gene targets *Rnf112, Pde4a,* and

Bcl2l2 were assessed in 13.5-month old cohorts of animals with either pre-symptomatic or symptomatic *Pias1* KD by qPCR (Table 4.4).

Pre-symptomatic KD, 13.5 months of age: Levels of *Rnf112* were significantly reduced in treated male zQ175 mice, similar to that observed in mRNAseq data (Figure 4.15A). Interestingly, there was no significant difference in levels of *Rnf112* transcript in pre-symptomatic female mice (Figure 4.15B). For *Pde4a*, a significant reduction in transcript levels was again observed in male zQ175 animals only, corresponding with mRNAseq data. This affect was not observed in females and may be due to sex-related differences in Pde4 isoforms previously reported after neuroinflammatory insult (Johansson et al., 2012). *Bcl2l2* was significantly increased in males by mRNAseq and in females by qPCR (Figure 4.16B) with miPias1.3 treatment. Therefore, for pre-symptomatic KD, only *Bcl2l2* was modulated in both males and females at 13.5 months of age of the genes assessed.

Symptomatic KD, 13.5 month of age: We also evaluated this set of genes in symptomatically treated mice. No differences were observed for gene targets *Rnf112* and *Pde4a* (Figure 4.16C, D). Levels of *Bcl2l2*, however, showed a slightly rescued genotype effect in males ($F(2, 9) = 5.951$, $p<0.05$), suggesting an increase in zQ175-treated mice consistent with other cohorts (Figure 4.15A, B, C). In symptomatic treated females, levels of *Bcl2l2* remained statistically unchanged though with a trend similar to that of males ($F(2, 8) = 1.199$, $p>0.05$) (Figure 4.15D). Overall, qPCR data suggests that *Bcl2l2* is consistently modulated by Pias1 independent of age and animal gender, potentially supporting a role for Pias1 in this pro-survival pathway (Figure 4.15, Table 4.4).

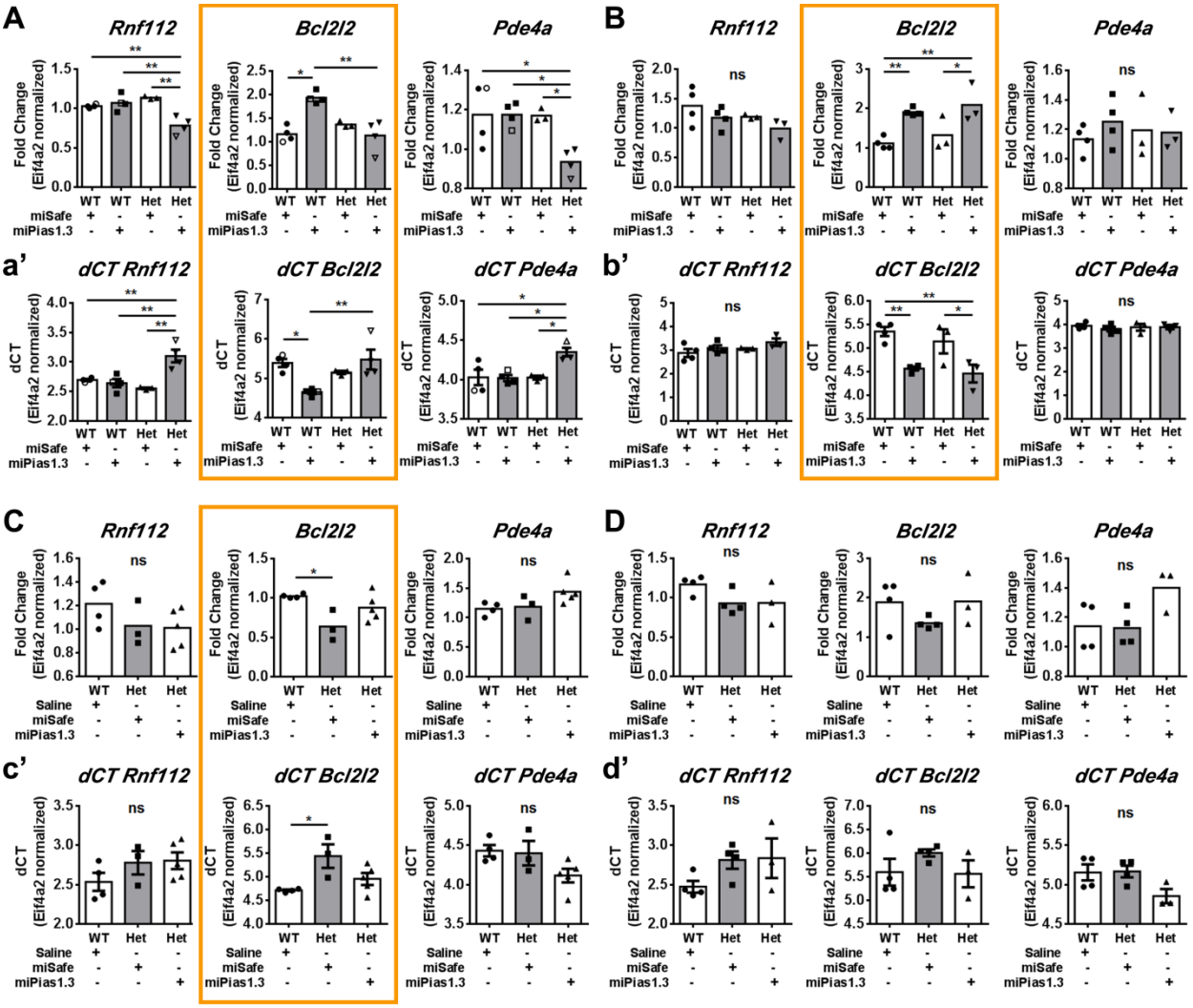

Figure 4.15: qPCR analysis on top mRNAseq identified genes. A) Fold change and a') dCT values for male mice validate mRNAseq data. Solid symbols represent animals used for mRNAseq analysis: *Rnf112* (Interaction: $F(1, 11) = 18.510$, $p<0.01$), *Bcl2l2* (Interaction: $F(1, 11) = 12.600$, $p<0.01$), *Pde4a* (Interaction: $F(1, 11) = 6.553$, $p<0.05$). B) Fold change and b') dCT values for female mice show significant treatment effect for *Bcl2l2*: *Rnf112* (Treatment: $F(1, 10) = 3.017$, $p>0.05$), *Bcl2l2* (Treatment: $F(1, 10) = 25.090$, $p<0.001$), *Pde4a* (Treatment: $F(1, 10) = 0.422$, $p>0.05$). C) Fold change and c') dCT values for symptomatic treated male mice show significant rescue effect on *Bcl2l2* levels: *Rnf112* ($F(2, 9) = 1.561$, $p>0.05$), *Bcl2l2* ($F(2, 9) = 5.951$, $p<0.05$), *Pde4a* ($F(2, 9) = 3.380$, $p>0.05$). D) Fold change and d') dCT values for symptomatic-treated zQ175 female mice show no significant differences but with trending increases in *Bcl2l2* and *Pde4a* in Hets with miPias1.3 treatment: *Rnf112* ($F(2, 8) = 2.097$, $p>0.05$), *Bcl2l2* ($F(2, 8) = 1.199$, $p>0.05$), *Pde4a* (: $F(2, 8) = 3.460$, $p>0.05$). All samples for pre-symptomatic treated animals were analyzed by 2-way ANOVA followed by Tukey's multiple comparison test. All samples for symptomatic treated animals were analyzed by 1-way ANOVA followed by Tukey's multiple comparison test. ns = not significant, *$p<0.05$, **$p<0.01$, values represent means ± SEM. Shaded bars represent miPias1.3 treated animals.

Pias1 KD rescues disease-associated transcriptional modules including DNA damage

We next compared our zQ175 transcriptional profiles to a previously established transcriptome from an allelic series derived from zQ175 mice (Langfelder et al., 2016) and compared Pias1 signatures on defined disease-associated profiles. For this analysis, the combined data from both the 13.5 and 8-month old pre-symptomatic KD cohorts were compared to RNAseq data from the zQ175 allelic series. First, we looked at gene expression changes between zQ175 and WT without treatment; a scatter plot of Z scores calculated using the log2FC from each dataset showed strong concordance with previously established transcriptional dysregulation ($R=0.72$, $p<0.0001$) supporting a robust transcriptional phenotype for zQ175 animals between datasets (Figure 4.16A). To assess the impact of Pias1 KD per a genotype, we employed the same scatterplot and correlation analysis comparing zQ175 treated animals with WT treated animals. A significant, negative concordance was observed ($R=-0.02$, $p<0.05$), further supporting a disease-specific function and impact of *Pias1* modulation in HD (Figure 4.16B).

To determine the impact of miPias1.3 treatment on previously established, disease gene networks, our datasets were analyzed against disease correlated co-expression modules identified in the allelic series (Langfelder et al., 2016). KD of *Pias1* significantly rescued M11, M20, and M39 modules while having a modest but not significant rescue in others (M2, M25, M34, M1, M10, M43, M46) and slightly but not significantly exacerbating M7 and M9 modules (Figure 4.16C, Table 4.5). Of interest, significant rescues in both M20 and M39 support a role for *Pias1* regulating DNA damage repair pathways through p53 signaling and ubiquitination pathways respectfully (Galanty et al., 2009). M11 module is glial and

immune response related, further implicating Pias1 KD in neuroinflammatory responses. The remaining co-expression modules that are modestly rescued by *Pias1* KD are enriched for genes involved in synaptic function and Huntington's disease associated pathways (Table 4.5). The slightly exacerbated M52 module confirms the negative regulatory role of *Pias1* in modulating NfkB inflammatory pathways, with KD potentially further activating this module (Liu et al., 2005). Interestingly, both M7 and M9 exacerbated modules suggests a worsening of neuronal signaling in response to oxidative stress, synaptic transmission, and cell death. This was unexpected due to the normalization effect observed in our previous analysis for synaptic-related functions but may suggest Pias1 is serving to counterbalance disease-associated signaling insults. Overall, data further supports that KD of *Pias1* impacts neuronal function and synaptic components, as well as inflammatory regulation. Our data for genotype effects highly correlates with previously published zQ175 transcriptional data and the analysis revealed a significant impact on disease-associated DNA damage repair pathways with *Pias1* modulation in HD.

Pias1 modulates Pnkp enzymatic activity for effective DNA repair at 8 months of age

In Chapter 3, we showed that PIAS1 can serve as an E3 ligase for PNKP and that genetic reduction of PIAS1 in human iPSCs differentiated into medium spiny neurons rescued mHTT-perturbed enzymatic activity of PNKP. That data provided new evidence for PIAS1 as a SUMO E3 ligase that selectively modulates DNA damage repair pathways in neurons. Given those results and transcriptomic data above showing that Pias1 KD rescues DNA damage-associated disease modules in HD mice (M20 and M39), we analyzed enzymatic activity of Pnkp *in vivo.* Activity was assessed using 32P-labeled 3'-phosphate-containin

oligo substrate and Pnkp-containing tissue lysates from GFP+ regions of 8-month old zQ175 WT and zQ175 females treated with Saline, miSafe, or miPias1.3 pre-symptomatically. HD animals recapitulated reduced enzymatic activity of Pnkp (Gao et al., 2019), and excitingly, miPias1.3 treatment rescued this perturbed activity (Figure 4.17A) similar to that observed in human neurons (Chapter 3). Together *in vivo* data provides additional evidence for a role for Pias1 in DNA damage repair pathways in the brain.

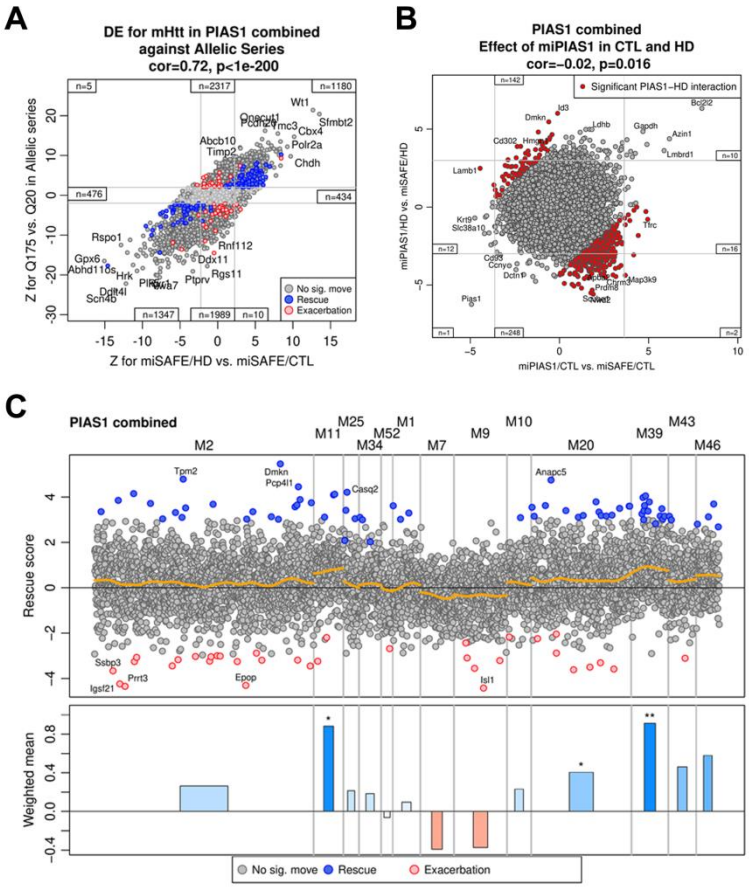

Figure 4.16: Pre-symptomatic Pias1 KD rescues disease-associated modules from zQ175 allelic series. A) Disease signatures from our zQ175 data has high concordance with published allelic series (Langfelder et al., 2016). B) Slight anticorrelation is observed in genes changed between WT and Het miPias1.3 treated vs miSafe treated animals; suggesting disease-specific functional impact with modulation of PIAS1. C) Manhattan plot of rescue score from combined mRNAseq data sets shows rescue and exacerbation of disease-associated transcriptional modules. Analysis and figure completed by Peter Langfelder, PhD, Yang lab, UCLA.

Pias1 KD affects levels of DNA damage at different ages in zQ175 mice

Given the rescue of Pnkp enzymatic activity *in vivo* with miPias1.3 treatment and the significant rescue in DNA damage disease-associated zQ175 transcriptional modules, we assessed levels of the DNA damage marker γH2AX and Pnkp protein levels by western blot in all cohorts of zQ175 pre-symptomatic and symptomatic treated animals. In the 8 month-old animals, a significant interaction was detected in levels of γH2AX, suggesting a disease-dependent functional consequence of modulating Pias1 (Interaction: $F(1, 10) = 26.940$, $p<0.001$). Specifically, levels were increased at baseline in zQ175 control mice and significantly decreased with miPias1.3 treatment. For WT animals, a potential increase in levels of γH2AX was detected after KD (Figure 4.17B). Pnkp was detected in the Soluble fraction only and was unchanged (Genotype: $F(1, 9) = 0.040$, $p>0.05$; Treatment: $F(1, 9) = 0.970$, $p>0.05$, Figure 4.17B).

In 13.5-month old mice with pre-symptomatic miPias1.3 treatment, no significant treatment effects in levels of γH2AX were detected in either male (Treatment: $F(1, 8) = 2.843$, $p>0.05$) or female (Treatment: $F(1, 10) = 1.675$, $p>0.05$) animals (Figure 4.18C, D). No genotype effects were observed (Males: $F(1, 8) = 1.379$, $p>0.05$; Females: $F(1, 10) = 1.379$, $p>0.05$). Levels of Pnkp were unchanged in male mice (Genotype: $F(1, 8) = 0.001$, $p>0.05$; Treatment: $F(1, 8) = 0.552$, $p>0.05$) but showed a significant interaction in female mice (Interaction: $F(1, 9) = 8.001$, $p<0.05$, Figure 4.17D). However, post-hoc analysis failed to reveal source of this interaction.

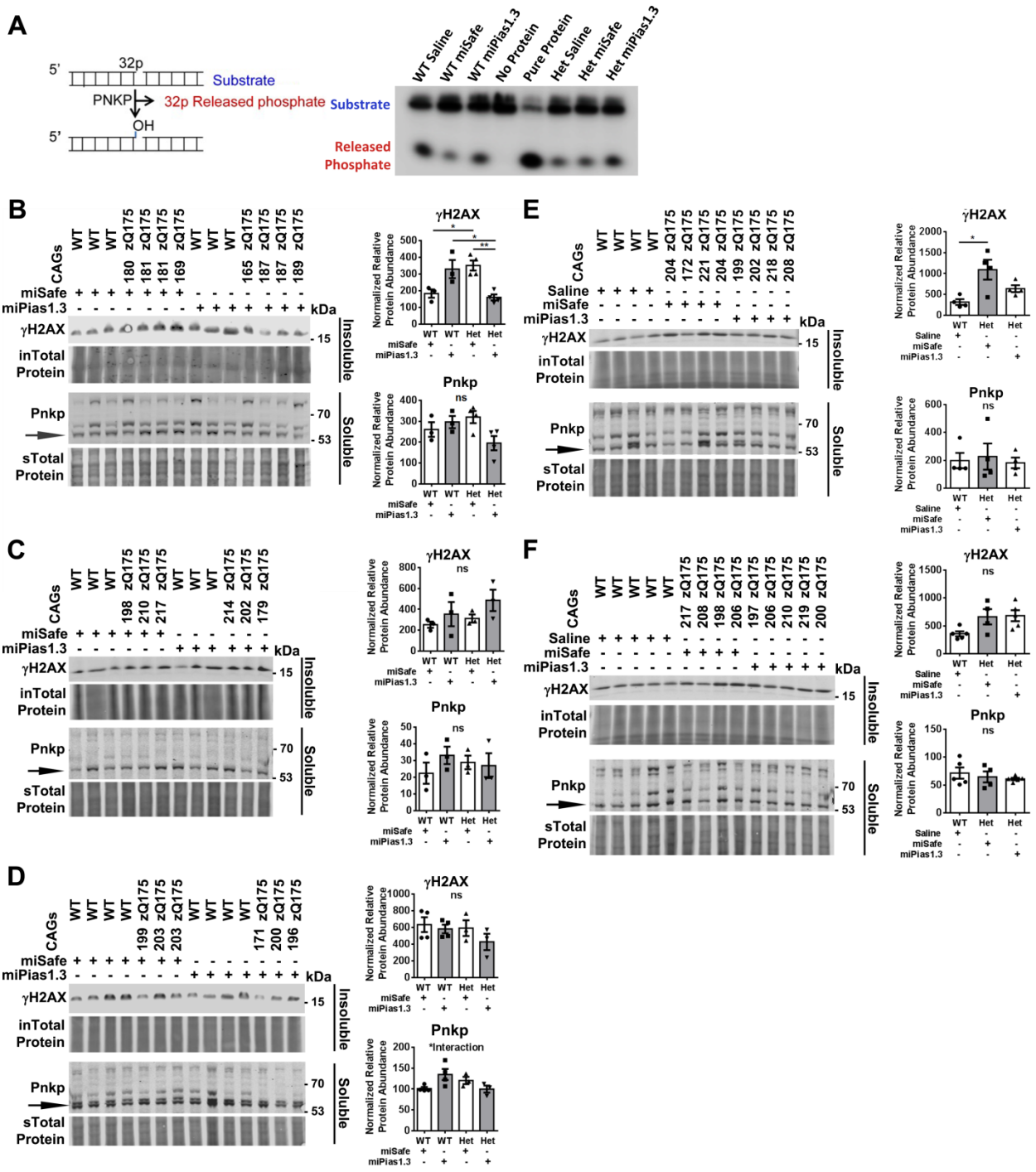
A
5'
32p
Substrate
PNKP
32p Released phosphate
OH
5'
WT Saline
WT miSafe
WT miPias1.3
No Protein
Pure Protein
Het Saline
Het miSafe
Het miPias1.3
Substrate
Released Phosphate
B
C
D
E
F
CAGs
miSafe
miPias1.3
kDa
γH2AX
inTotal Protein
Pnkp
sTotal Protein
Insoluble
Soluble
Normalized Relative Protein Abundance
ns
*Interaction
WT
Het
Saline

Figure 4.17: Pias1KD effects DNA damage repair in zQ175 mice. A) mHTT-perturbed enzymatic activity of repair enzyme PNKP in the striatum is rescued with Pias1 KD. Western blot analysis of Soluble/Insoluble fractionation of striatal tissue from B) 8 month-old male mice with pre-symptomatic miPias1.3 treatment. C) 13.5 month-old male mice with pre-symptomatic treatment. D) 13.5 month-old female mice with pre-symptomatic treatment. E) 13.5 month-old male mice with symptomatic treatment. F) 13.5 month-old female mice with symptomatic treatment. Black arrows indicated quantified Pnkp protein band which corresponds to unmodified positive control of overexpressed Pnkp (not shown). Higher bands are suggested to be post-translational modifications of Pnkp as observed in Chapter 3. Protein normalized to total protein stain. Normalized relative protein abundances for all samples for pre-symptomatic treated animals were analyzed by 2-way ANOVA followed by Tukey's multiple comparison test. All samples for symptomatic treated animals were analyzed by 1-way ANOVA followed by Tukey's multiple comparison test. ns = not significant, *$p<0.05$, **$p<0.01$, values represent means ± SEM. Shaded bars represent miPias1.3 treated animals. Panel A data and figure generated in collaboration with Sarkar lab, UTMB.

In 13.5-month old mice with symptomatic miPias1.3 treatment, more γH2AX was observed in zQ175 males at 13.5 months of age ($F(2, 9) = 6.742$, $p<0.05$) with levels of damage in miPias1.3 treated zQ175 mice being statistically insignificant from control WT animals, suggesting a rescue in accrued DNA damage (Figure 4.17E). This affect was not observed in female mice ($F(2, 11) = 3.849$, $p>0.05$, Figure 4.17F). Levels of Pnkp remained unchanged in this cohort (Males: $F(2, 9) = 0.119$, $p>0.05$; Females: $F(2, 11) = 0.490$, $p>0.05$). Symptomatic miPias1.3 treatment in zQ175 mice may therefore rescue accrued DNA strand breaks in males only. Further assessment of DNA damage repair pathways remains to be assessed as perturbation of PNKP enzymatic activity results in hyperactivation of ATM-mediated signaling (Gao et al., 2019). Reducing Pias1 in these animals did not impact the level of detectable, unmodified Pnkp protein.

DISCUSSION

Here we investigated the molecular impact of Pias1 reduction in the striatum of the knock-in zQ175 mouse model of HD to address the temporal contribution of Pias1 towards HD pathogenesis in different disease stages and in the context of full-length mHTT. Further, we investigated the molecular contribution of Pias1 to DNA damage repair *in vivo* to compare to our data obtained in human neurons (Chapter 3). We now show that Pias1 KD rescues mHTT-associated perturbation of Pnkp enzymatic activity in two models of HD: Human patient, iPSC-derived medium spiny neurons and a full-length KI mouse model (Figure 3.X, Figure 4.18) and normalizes aberrant genotype-associated transcriptional profiles *in vivo*. Since impaired Pnkp activity previously corresponded to decreased genomic integrity in HD neurons (Gao et al., 2019), observed normalization effect may be due to increased stability of normalized genes. Levels of Pnkp remained unchanged with KD however, suggesting that SUMOylation may not mediate clearance. Pias1 may therefore either be modulating subcellular localization or recruitment of Pnkp through SUMOylation or SUMOylation may prevent activation without directly influencing clearance of this repair factor (Chapter 3). While the functional contribution of PNKP SUMOylation remains to be elucidated, Pias1 KD also rescued DNA damage related transcriptional modules associated with disease. Together this data suggests that Pias1 is modulating a conserved DDR mechanism in response to transcription-linked genomic instability in the brain.

Pias1 serves as a negative inhibitor of NfkB signaling (Liu et al., 2005). In R6/2 mice, Pias1 KD restored perturbed localization of NfkB and normalized inflammatory responses (Ochaba et al., 2016). In our current study, Pias1 modestly impacted inflammatory

readouts in older zQ175 mice. With pre-symptomatic treatment, Pias1 KD may have in part restored resting state of microglia in male mice with a corresponding increase in soluble NfkB. With symptomatic treatment, an opposite effect was observed for microglial activation, potentially suggesting a shift in inflammatory balance during symptomatic disease stages that is exacerbated with Pias1 KD. However, baseline inflammatory profiles may have influenced the impact of Pias1 KD in zQ175 mice. A key biochemical difference observed between zQ175 mice and R6/2 mice was the lack of a HD-associated increase in insoluble/nuclear Pias1 in zQ175 mouse striatum. In R6/2 mice, Pias1 was significantly increased in the Insoluble fraction and miPias1.3 treatment specifically reduced insoluble Pias1 protein levels only (Ochaba et al., 2016). Reduction in this species specifically corresponded to normalization of inflammatory profiles and was accompanied by a decrease in insoluble accumulated HMW mHTT. No increased insoluble Pias1 was observed in zQ175 mice compared to WT controls in any group assessed (Figures 4.4, 4.9, 4.13). Additionally, no insoluble NfkB was detected (data not shown). Therefore, it is possible that zQ175 mice display a differential baseline of Pias1 activity/function based on localization as compared to the R6/2 mouse model. This difference may be why levels of insoluble Pias1 remained unchanged in zQ175 mice with KD and in part, might account for the lack of impact observed on behavior and HMW mHTT accumulation. Further, this difference might have potentially influenced the modest impact on inflammatory readouts in this study. Future studies will investigate the functional contributions of insoluble versus soluble Pias1 on molecular pathways, particularly inflammatory networks.

Modulating Pias1 in pre-symptomatic zQ175 mice strongly impacted synaptic networks at 13.5 months of age at the transcriptional level. Synaptic abnormalities in HD patients have been well characterized, with changes often preceding neuronal degeneration and likely accounting for some of the earliest, cognitive and psychiatry symptoms observed during disease pathogenesis (Nithianantharajah and Hannan, 2013). As a result of an imbalance between excitatory and inhibitory neurotransmission, HD mice have alterations in number of GABAergic, glutamatergic, and dopaminergic receptors (Nithianantharajah and Hannan, 2013). zQ175 mice also have altered neurotransmission and synaptic vesicle release (Chen et al., 2018; Heikkinen et al., 2012). This may be due to a loss of Htt function as conditional cortical knock-out of Htt impairs synaptic formation and maturation (McKinstry et al., 2014). Further, Htt is localized at post-synaptic spines, interacts with synaptic-associated proteins, and functions in vesicular trafficking of Bdnf (Gauthier et al., 2004; Nithianantharajah and Hannan, 2013). Indeed, loss of Bdnf decreases trophic support necessary for activity-dependent dendritic spine strengthening thereby affecting synaptic plasticity (Bramham and Messaoudi, 2005; Jia et al., 2010), with exogenous Bdnf providing neuroprotective affects in HD animals (Lynch et al., 2007). In the current study, levels of *Bdnf* transcript were elevated in control zQ175 mice compared to control WT animals at 13.5 months of age. This is consistent with the zQ175 allelic series transcriptional profile (Langfelder et al., 2016) and may represent a compensatory overexpression for decreased trophic support in HD animals relatively early in disease. With Pias1 KD, levels of *Bdnf* transcript decreased, suggesting a normalizing impact on aberrant transcription.

Transcription of *Bdnf* was not the only normalizing affect observed for Pias1 KD in our mRNAseq analysis. Looking further, biological processes enriched from GO analysis such as regulation of trans-synaptic signaling and modulation of chemical synaptic transmission were genotype-specific networks modulated by Pias1 KD. Specifically, the DEGs that were contributing to these processes in our data set showed a majority with inverse fold changes with Pias1 KD compared to control zQ175 mice, suggesting that miPias1.3 treatment normalized aberrant transcription associated with disease progression in these animals (Figure 4.5). We hypothesize this may be in part due to facilitated repair of key neuronal genes. Therefore, increasing activity of Pnkp and thereby DNA repair with Pias1 KD may have a direct impact on genomic stability in zQ175 mice. Increased genomic integrity would then facilitate neuronal health and promote synaptogenesis or strengthen existing synapses. Direct measurements of genomic integrity of normalized genes will allow testing of this hypothesis. Additionally, assessing stability of the *HTT* CAG-repeat expansion in zQ175 mice will determine if modulating Pias1 and subsequently TCR impacts expansion propensity.

An alternative mechanism is that SUMOylation of transcription factors for synaptic genes may be modulated by Pias1 KD. Pias1 serves as an E3 ligase for neuronal transcription factors ((Estruch et al., 2016; Gregoire and Yang, 2005; Riquelme et al., 2006; Tai et al., 2016), Table 2) including CREB whose activity is impaired by the mHTT containing TCR complex (Chen et al., 2014; Gao et al., 2019). Indeed, CREB was consistently regulated with Pias1 KD at both 8 and 13.5 months of age as determined by IPA upstream analysis (Figure 4.5, Figure 4.15), supporting this possibility. Mef2a is also SUMOylated by PIAS1, with

SUMOylation serving to repress transcription of genes such as *synaptotagmin1* (*Syt1*) which itself is SUMOylated (Gregoire and Yang, 2005; Matsuzaki et al., 2015; Riquelme et al., 2006; Yamada et al., 2013). SUMOylated Mef2a increases the number of PSD95-positive dendritic claws while also suppressing orphaned presynaptic sites, suggesting that SUMOylated Mef2a contributes to synapse maturation during development (Shalizi et al., 2006; Yamada et al., 2013). Interestingly, levels of *Syt1* in our mRNAseq data were decreased with Pias1 KD in zQ175 mice at 13.5 months of age, opposite to what would have been expected if there was a decrease in Mef2a SUMOylation by Pias1 (Yamada et al., 2013). No change in *Mef2a* transcription was observed in with Pias1 KD in any group, indicating we may not have affected expression as opposed to function or localization mediated through SUMOylation of transcription factors. Further, some transcription factors may be uncharacterized SUMO substrates. Therefore, it remains possible that Pias1 KD is mediating synaptic function in zQ175 striatum by directly affecting SUMOylation of transcription factors required to facilitate production of protein products needed for synaptic maturation. Directly targeting SUMOylation of these transcription factors may account in part for the observed impact on transcriptional networks associated with synaptic function (Figure 4.5, Figure 4.15). Analysis of transcription factors associated with synaptic transcription will need to be assessed at the protein level to determine if this mechanism is contributing to the observed transcriptional impact of Pias1 KD on synaptic networks.

Finally, Pias1 may also directly modulate SUMOylation of proteins involved in synaptic development, function, and health. SUMOylation can modulate synaptic activity by

dynamically mediating protein subcellular distribution and function (see (Schorova and Martin, 2016) and (Henley et al., 2018) for comprehensive reviews). Several synaptic proteins themselves are SUMOylated which often associates with repressive functional consequences and therefore has been attributed to a potential neuroprotective effect to prevent excitotoxic events in response to neuronal injury ((Peters et al., 2017), Table 3). This highlights the importance of maintaining SUMO-related proteostatic balance to ensure cellular survival. Supporting this, overexpression of SUMO1 in the mouse brain leads to impairments in learning and memory associated with reduction in synaptic transmission and presynaptic function (Matsuzaki et al., 2015). Though the direct mechanism is unclear, imbalance in the SUMO landscape in the brain leads to neuronal malfunction and suggests a potential direct impact on synaptic health with reduction of an E3 ligase promoting SUMOylation. Signaling feedback may then result in observed transcriptional changes. Whether or not Pias1 directly modulates localization or SUMOylation of these proteins remains to be investigated. Overall, KD of Pias1 significantly impacted synaptic and neuronal gene networks, highlighting a potential modulatory function of Pias1 towards mediating HD-associated synaptic malfunction (Nithianantharajah and Hannan, 2013).

The most consistently regulated gene assessed with Pias1 KD in zQ175 mice was *Bcl2l2*, also known as *Bcl-w*, which could suggest that Pias1 may mediate apoptotic and survival pathways in the brain. *Bcl2l2* is a member of the *Bcl-2* family of genes that serve as fate determinants by having dual, antagonizing functions (Youle and Strasser, 2008). Some family members such as Bax and Puma are pro-apoptotic while others including Bcl-2, Bcl2l2, and Bcl-xL have anti-apoptotic function. These family members antagonize each

other either directly or indirectly with the pro-death members preventing Bax-mediated cytochrome-c release from the mitochondria (Wei et al., 2001; Yang et al., 1997; Youle and Strasser, 2008). If the balance of pro and anti-apoptotic family members shifts towards the former, Bax is free to bind to the mitochondrial outer membrane and trigger caspase-mediated apoptosis (Dewson and Kluck, 2009; Jurgensmeier et al., 1998). Due to this intricate balance of pro-death and pro-survival signals, the ratio of Bax-to-Bcl-2 is often used as a metric for evaluating apoptosis potential (Kilbride and Prehn, 2013; Korsmeyer, 1999; Oltvai et al., 1993). Together, these family members in part dictate the fate of neuronal development, connections, and survival (Akhtar et al., 2004). Future studies into the balance of Bax and Bcl2l2 proteins in zQ175 mice with Pias1 KD would further test this hypothesis.

It is exciting that of the genes assessed, *Bcl2l2* specifically was elevated with miPias1.3 treatment in zQ175 mice since the presence of Bcl2l2 in the axons of sensory neurons is critical for their survival under trophic deprivation (Courchesne et al., 2011; Simon et al., 2016). This balances the observation that Bax mediates axonal degradation (Nikolaev et al., 2009) as well as neuronal death during development (Deckwerth et al., 1996) with decreases in trophic support. Indeed, there are neuroprotective roles for the pro-survival side of the Bcl-2 family in nervous system development and brain or spinal cord after injury, including loss of neurotrophic support (i.e. Bdnf, Ngf, etc., (Anilkumar and Prehn, 2014)). BDNF deficiency is a hallmark of HD (Ferrer et al., 2000; Zuccato and Cattaneo, 2009). Further, dysregulation of the Bcl-2 family has been well documented in numerous models of HD (Sassone et al., 2013). Therefore, inducing expression of pro-survival *Bcl2l2*

with Pias1 KD may counterbalance the decreased trophic support seen within the HD striatum, ultimately promoting neuronal survival and strengthening sensory axons.

The observed differences between pre-symptomatic and symptomatic KD of Pias1 in this study suggest that Pias1 may have different functional contributions towards HD pathogenesis dependent on disease stage. The characterized embryonic lethality of *Pias1* knock-out mice highlights an important role in development, particularly in angiogenesis (Constanzo et al., 2016), indicating that targeting Pias1 at different ages may have specific functional outcomes. Our data suggests that Pias1 may contribute to compensatory mechanisms attempting to maintain neuronal homeostasis under genotoxic stress in neurodegenerative disease (Vanni et al., 2019). Overall, we saw significant *Pias1* KD at all stages tested at the transcript level. For symptomatic-treated animals, we only observed significant Pias1 KD at the protein level in the soluble fraction of female striatal lysates. At 13.5 months of age, no reduction in Pias1 protein levels were observed for pre-symptomatic treated animals, suggesting a compensatory proteostatic mechanism to combat the reduced production of *Pias1* transcript. These findings suggest that an optimal window for targeting Pias1 mediated mechanisms may be at earlier disease stages. Even with no observed changes in Pias1 protein at 13.5 months of age, reduced level of *Pias1* transcript was observed along with robust transcriptional changes in both WT and zQ175 mice. Seeing that significant reduction in Pias1 protein was observed at our earlier time-point, data suggests a long-term, rippling effect of Pias1 KD in these animals during aging which could be considered for future therapeutic studies.

SUMMARY AND NEXT STEPS

Intrastriatal viral KD of Pias1 in the long term, knock-in zQ175 mouse model of HD restored Pnkp enzymatic activity and normalized disease-associated transcriptional dysregulation in these animals. Overall, Pias1 KD had little to no effect on behavioral readouts in zQ175 animals. Pre-symptomatic KD specifically had the strongest effect on molecular readouts, suggesting that targeting Pias1 in this disease stage could aid in restoring homeostatic balance. Unexpectedly, Pias1 KD had little effect on accumulation of HMW mHTT suggesting that Pias1 and SUMOylation may not be mediating solubility or aggregation propensity of mHTT in this disease context, potentially due to lack of impact on levels of insoluble Pias1 with KD. The robust and cross-model impact on Pnkp enzymatic activity, however, provides evidence that Pias1 may be mediating DDR *in vivo.* Future experiments to elucidate the exact modulatory mechanism of Pias1 on synaptic structure and function remain to be completed. Such experiments would include high resolution microscopy to visualize synaptic structures with Pias1 KD as well as proteomic analysis of SUMO-containing synaptosomes to assess potential direct mechanisms. Further, assessing levels and chromatin binding of SUMO-targeted transcription factors that mediate synaptic transcription would identify indirect mechanisms for Pias1 mediating synaptic structure and function. Finally, assessing the functional impact of modulating pro-survival gene *Bcl2l2,* such as assessing caspase activation or the balance of Bcl-2 protein family members, may further elucidate how Pias1 KD could be neuroprotective and a viable therapeutic target for treatment of HD.

EXPERIMENTAL PROCEDURES

Animals

Knock-in, zQ175 mice were obtained from CHDI colony, bred in house, genotyped, and aged to approximately 13.5 months of age. CAG repeat sizing of genomic DNA harvested from tails was performed by Laragen. Experiments were carried out in strict accordance with the Guide for the Care and Use of Laboratory Animals of the NIH and an approved animal research protocol by the Institutional Animal Care and Use Committee (IACUC) at the University of California, Irvine. Animals were humanely euthanized by an over injection of Euthasol followed by whole body perfusion with 1x-PBS and cervical dislocation.

Surgery

At 2.5 months of age and 7.5 months of age, zQ175 mice were anesthetized using isoflurane and underwent bilateral intrastriatal injections using a dual injection stereotaxic apparatus (coordinates 0.01 mm caudal to bregma, 0.2 mm right/left of midline, 0.345 pocket to 0.325 mm ventral to pial surface) as previous (Ochaba et al., 2016). 5 µl of AAV2/1 virus containing miPIAS1.3 CMVeGFP or miSAFE CMVeGFP at ~ 3e12 vg/ml was injected using a Hamilton syringe at a rate of 0.5 µl/min. Syringe was left in place for 5 minutes after each injection to ensure complete ejection of viral solution into brain region. Animals were allowed to recover for 1 week under observation prior to beginning behavioral analysis.

Behavioral Paradigms

For zQ175 PIAS1 pre-symptomatic knock-down cohorts, animal body weights were measured weekly over the course of the studies. Motor deficits were assessed by a running

wheel (0297-0521-D60; Columbus Instruments) at 7 or 9 months of age months of age depending on date of sacrifice. Running wheel usage was constantly monitored over two weeks and collected in three minute bins using Multi-Device System software 24-Channel Version 1.55 (160640; Columbus instruments). Data from dark phase only was analyzed for significance over the two week period. Motor learning was calculated as previously described (Hickey et al., 2008). Briefly, slopes were calculated using formula $(Y_2-Y_1)/(X_2-X_1)$ where Y_2 is wheel usage per bin on night 10 and X_2 is 10 (night 10), and Y_1 is wheel usage per bin on night 2 with X_1 as 2.

Rotarod was also used to assess motor deficits in these mice using an accelerating apparatus (Dual Species Economex Rota-Rod; 0207-003M; Columbus Instruments) at 9.5 and 12.5 months of age under blinded conditions. Animals were tested over two days with four trial runs each day consisting of 5 minute trial periods. The first trial for each test day was used as a training trial and not used in final calculations. The latency to fall for the three final trials on day 2 of testing were averaged and analyzed for significance.

To assess impairments in anxiety, and as an additional motor task, animals were subjected to open field test at 7.5 months of age and 12.5 months of age when applicable. Mice were allowed to explore an empty open field box for 5 minutes. Activity during these five minutes was recorded and analyzed automatically using Ethovision™ Software by determining time spent in the center and on the periphery of the open field in addition to average velocity and distance traveled over the 5 minute test period. Velocity and distance

traveled during the open field trials were used as measures of motor performance while percent time spent in center was used as a measure of anxiety.

Immunofluorescence protocol

Brain tissue samples used for immunofluorescence were from animals humanely sacrificed as described above. 40μm coronal brain slices from flash frozen, previously preserved hemispheres were washed three times in 1xPBS and then blocked in 5% goat serum with 0.2% Triton-X blocking solution for 1 hour at room temperature. After blocking, slices were incubated in primary antibody in blocking solution overnight while rocking at 4°C. The following day, slices were washed 3 times in 1xPBS followed by incubation in secondary antibody in blocking solution for 1 hour at room temperature. Slices were washed a final 3 times with 1x PBS prior to mounting on slides using fluoromount mounting media and imaged using confocal microscopy. The following antibodies were used: anti-Iba1 (Wako Pure Chemicals Industries 27030) and DAPI was used as a nuclear stain. To measure microglia number and cell body diameter, Imaris Bitplane analysis software was run using region-growing spot detection analysis on Iba1+ cells.

Tissue and cell protein lysis, quantification, and Western Blot analysis

Flash frozen brain tissue was prepared as previous (Ochaba et al., 2016; Ochaba et al., 2018). Protein fractions were quantified using detergent compatible (DC) protein assay (Bio-Rad). Soluble protein lysates were resolved on 4-12% Bis-Tris Poly-Acrylamide gels and transferred onto either 0.45μM or 0.2μM nitrocellulose membrane depending on size of proteins of interest (smaller proteins on 0.2μM). Insoluble protein lysates were resolved

on 3-8% Tris-Acetate Poly-Acrylamide gels and transferred onto 0.45μM nitrocellulose membrane. Membranes were blocked in Odessey starting block (Li-Cor) for 1 hour at room temperature and probed in primary antibody overnight at 4°C in blocking supplemented to 0.5% tween. Secondary IR-fluorophore antibodies were used and detected using a Li-Cor Odyssey CLx system. IR fluorescence imaging was used for quantitative analysis with detected protein levels normalized to Revert Li-Cor whole-protein stain prior to statistical analysis. Antibodies used for analysis were anti-PIAS1 (Cell Signaling 3550S), anti-HTT (Millipore MAB5492, HMW mHTT), anti-HTT (Cell Signaling 5656S, clone D7F7 for FL-HTT), anti-GFP (Living Colors, Clontech Laboratories 632381), anti-NfkB (Cell Signaling 8242S), anti-Il-6 (Mouse specific, Cell Signaling 12912T), anti-PNKP (Novus Biologicals NBP1-87257), and anti-γH2AX (Millipore 05-636).

RNA purification, qPCR, mRNASeq

GFP+ flash frozen brain regions were homogenized in TRIzol reagent (Invitrogen) and RNA was extracted according to manufacturer's protocol and purified using RNEasy Mini kit (QIAGEN). Residual DNA was removed by DNase treatment incorporated into RNEasy protocol as per manufacturer's suggestion. RNA was submitted for mRNAseq as described previously (Vashishtha et al., 2013). Differentially expressed genes were generated using DEseq2 (Love et al., 2014) and a significance threshold was set at a 10% FDR. Enrichment analysis was completed using GOrilla (Eden et al., 2009) and Ingenuity Pathway Analysis software. To confirm differentially regulated genes identified in mRNAseq studies, reverse transcription was performed using SuperScript 3 First-strand synthesis system according to manufacturer's protocol (Invitrogen) from harvested and purified RNA. Both oligo (dT)

and random hexamer primers were used in a 1:1 ratio. Final synthesized cDNA was diluted to 5ng/ul in DEPC treated water and stored at -20°C until use. Primers used for qPCR were: *Eif4a2* (F: GTGGACTGGCTCACGGAGAAAA, R: AGAACACGGCTTGACCCTGATC), *Pias1* (F: CTGCACAGACTGTGACGAGATAC, R: CGCTACCTGATGCTCCAATGTG), *NeuroD2* (F: GCTACTCCAAGACGCAGAAGCT, R: CACAGAGTCTGCACGTAGGACA), *NeuroD1* (F: CCTTGCTACTCCAAGACCCAGA, R: TTGCAGAGCGTCTGTACGAAGG), *Bdnf* (F: TCGTTCCTTTCGAGTTAGCC, R: TTGGTAAACGGCACAAAAC), *Pde4a* (F: CCGTGTTCACAGACCTGGAGAT, R: GGTGGTTCTCAAGCACAGACTC), *Syn1* (F: TATGCCACTGCTGAGCCCTTCA, R: ATGGCAATCTGCTCAAGCATAGC), *Syn2* (F: CCTGCTCTGAAATGTTTGGTGGC, R: TCTGTCCTCCACTTGGTGTTCC), *Rnf112* (F: AAGTGGAAGCCGCCAAGAAGGA, R: AGGAGGTTCCTCATCGTGTCAG), *Bcl2l2* (F: CAAGTGCAGGATTGGATGGTGG, R: CTGTCCTCACTGATGCCCAGTT).

Pnkp enzymatic activity

3'-phosphatase PNKP enzymatic activity from nuclear and mitochondrial extracts was performed as previously described (Chakraborty et al., 2015; Gao et al., 2019). A 3'-phosphate oligo (51-mer), 32P-labeled, containing a single strand break was used to assess activity by measuring the amount of released 3' phosphate from radio-labeled substrate as analyzed by 20% Urea-PAGE and PhosphorImager. The percent of phosphate release was represented as compared to total radiolabeled substrate (as 100).

Statistical Analysis

All data represented as mean ± SEM with a p value of $p<0.05$ considered statistically significant. Analyses were completed in GraphPad Prism software. IR-fluorescent intensity values were obtained from western blots using Li-Cor imaging software, Image Studio and normalized to total protein stain, Revert. Normalized protein abundance levels were the subjected to 2-way ANOVA to assess changes in protein levels with the exception of HMW mHTT analysis which was with Student's unpaired 2-tailed t-test. Statistical analysis was completed of the delta CT (dCT) values obtained from qPCR reactions normalized to *Eif4a2*. All 2-way ANOVAs were followed by Tukey's multiple comparisons test.

CHAPTER 4

TABLES

Table 4.1: Statistical outputs for zQ175 pre-symptomatic Pias1 KD cohorts.

Age at Sac	Behavioral task	n (m,f,c)	Genotype effect	Treatment effect	Interaction
13.5	Open Field 7.5 Mon. (Distance Traveled)	7-8, 5-9, 12-17	M: F(1, 26) = 6.420, p<0.05 F: F(1, 23) = 7.911, p<0.01 C: F(1, 51) = 13.080, p<0.001	M: F(1, 26) = 2.845, p>0.05 F: F(1, 23) = 2.814, p>0.05 C: F(1, 51) = 0.898, p>0.05	M: F(1, 26) = 0.012, p>0.05 F: F(1, 23) = 0.012, p>0.05 C: F(1, 51) = 0.0651, p>0.05
13.5	Open Field 7.5 Mon. (Velocity)	7-8, 5-9, 12-17	M: F(1, 26) = 6.420, p<0.05 F: F(1, 23) = 7.911, p<0.01 C: F(1, 53) = 11.900, p<0.01	M: F(1, 26) = 2.845, p>0.05 F: F(1, 23) = 2.814, p>0.05 C: F(1, 53) = 0.253, p>0.05	M: F(1, 26) = 0.012, p>0.05 F: F(1, 23) = 0.012, p>0.05 C: F (1, 53) = 0.013, p>0.05
13.5	Open Field 7.5 Mon. (Center time)	7-8, 5-9, 12-17	M: F(1, 26) = 0.099, p>0.05 F: F(1, 23) = 0.204, p>0.05 C: F(1, 53) = 0.526, p>0.05	M: F(1, 26) = 1.039, p>0.05 F: F(1, 23) = 0.033, p>0.05 C: F(1, 53) = 0.850, p>0.05	M: F(1, 26) = 1.070, p>0.05 F: F(1, 23) = 0.049, p>0.05 C: F(1, 53) = 0.822, p>0.05
13.5	Open Field 12.5 Mon. (Distance Traveled)	7-8, 5-9, 12-17	M: F(1, 26) = 0.302, p>0.05 F: F(1, 23) = 1.311, p>0.05 C: F(1, 53) = 0.831, p>0.05	M: F(1, 26) = 0.156, p>0.05 F: F(1, 23) = 1.617, p>0.05 C: F(1, 53) = 1.091, p>0.05	M: F(1, 26) = 0.681, p>0.05 F: F(1, 23) = 0.146, p>0.05 C: F(1, 53) = 0.104, p>0.05
13.5	Open Field 12.5 Mon. (Velocity)	7-8, 5-9, 12-17	M: F(1, 26) = 0.302, p>0.05 F: F(1, 23) = 1.311, p>0.05 C: F(1, 53) = 0.831, p>0.05	M: F(1, 26) = 0.156, p>0.05 F: F(1, 23) = 1.617, p>0.05 C: F(1, 53) = 1.091, p>0.05	M: F(1, 26) = 0.681, p>0.05 F: F(1, 23) = 0.146, p>0.05 C: F(1, 53) = 0.104, p>0.05
13.5	Open Field 12.5 Mon. (Center time)	7-8, 5-9, 12-17	M: F(1, 26) = 0.615, p>0.05 F: F(1, 23) = 3.092, p>0.05 C: F(1, 53) = 1.802, p>0.05	M: F(1, 26) = 0.553, p>0.05 F: F(1, 23) = 0.013, p>0.05 C: F(1, 53) = 0.388, p>0.05	M: F(1, 26) = 0.185, p>0.05 F: F(1, 23) = 0.202, p>0.05 C: F(1, 53) = 0.397, p>0.05
13.5	Rotarod (9.5 Mon.)	7-8, 5-9, 12-17	M: F(1, 26) = 11.030, p<0.01 F: F(1, 23) = 9.185, p<0.01 C: F(1, 53) = 20.290, p<0.0001	M: F(1, 26) = 0.232, p>0.05 F: F(1, 23) = 0.007, p>0.05 C: F(1, 53) = 0.014, p>0.05	M: F(1, 26) = 0.748, p>0.05 F: F(1, 23) = 0.006, p>0.05 C: F(1, 53) = 0.135, p>0.05
13.5	Rotarod (12.5 Mon.)	7-8, 5-9, 12-17	M: F(1, 26) = 6.476, p<0.05 F: F(1, 23) = 3.206, p>0.05 C: F(1, 53) = 9.958, p<0.01	M: F(1, 26) = 0.046, p>0.05 F: F(1, 23) = 0.040, p>0.05 C: F(1, 53) = 0.006, p>0.05	M:F(1, 26) = 4.473, p<0.05 F: F(1, 23) = 0.857, p>0.05 C: F(1, 53) = 0.590, p>0.05
13.5	Weight (13.5 Mon)	7-8, 5-9	M: F(1, 26) = 47.110, p<0.0001 F: F(1, 23) = 7.078, p<0.05	M: F(1, 26) = 0.492, p>0.05 F: F(1, 23) = 2.592, p>0.05	M: F(1, 26) = 0.002, p>0.05 F: F(1, 23) = 0.075, p>0.05
8	Open Field 7.5 Mon. (Distance Traveled)	4, 5-7, 9-11	M: F(1, 12) = 0.655, p>0.05 F: F(1, 26) = 3.010, p>0.05 C: F(1, 34) = 1.750, p>0.05	M: F(1, 12) = 0.102, p>0.05 F: F(2, 26) = 0.638, p>0.05 C: F(1, 34) = 0.019, p>0.5	M: F(1, 12) = 0.062, p>0.05 F: F(2, 26) = 0.495, p>0.05 C: F (1, 34) = 0.099, p>0.05
8	Open Field 7.5 Mon. (Velocity)	4, 5-7, 9-11	M: F(1, 12) = 0.655, p>0.05 F: F(1, 26) = 3.010, p>0.05 C: F(1, 34) = 1.750, p>0.05	M: F(1, 12) = 0.102, p>0.05 F: F(2, 26) = 0.638, p>0.05 C: F(1, 34) = 0.019, p>0.5	M: F(1, 12) = 0.062, p>0.05 F: F(2, 26) = 0.495, p>0.05 C: F(1, 34) = 0.099, p>0.05
8	Open Field 7.5 Mon. (Center time)	4, 5-7, 9-11	M: F(1, 12) = 7.958, p<0.05 F: F(1, 26) = 7.219, p<0.05 C: F(1, 34) = 13.090, p<0.001	M: F(1, 12) = 0.316, p>0.05 F: F(2, 26) = 0.220, p>0.05 C: F(1, 34) = 0.160, p>0.05	M: F(1, 12) = 6.434, p<0.05 F: F(2, 26) = 0.263, p>0.05 C: F(1, 34) = 5.259, p<0.05
8	Weight (8 Mon)	4, 5-7	M: F(1,12)=0.907, p>0.05 F: F(1,26)=2.143, p>0.05	M: F(1,12)=1.491, p>0.05 F: F(2,26)=0.846, p>0.05	M: F(1, 12) = 0.196, p>0.05 F: F(2, 26) = 1.687, p>0.05

All groups and tasks analyzed by 2-way ANOVA followed by Tukey's multiple comparison test. $p<0.05$ considered statistically significant. m=males, f=females, c=combined.

Table 4.2: Statistical outputs for zQ175 Symptomatic Pias1 KD cohorts.

Behavioral task	n (m,f,c)	1-way ANOVA
Open Field 12.5 Mon. (Distance Traveled)	6-7, 7-13, 13-19	M: $F(2, 16) = 0.377$, $p>0.05$ F: $F(2, 25) = 0.304$, $p>0.05$ C: $F(2, 44) = 0.385$, $p>0.05$
Open Field 12.5 Mon. (Velocity)	6-7, 7-13, 13-19	M: $F(2, 16) = 0.378$, $p>0.05$ F: $F(2, 25) = 0.304$, $p>0.05$ C: $F(2, 44) = 0.381$, $p>0.05$)
Open Field 12.5 Mon. (Center time)	6-7, 7-13, 13-19	M: $F(2, 16) = 0.751$, $p>0.05$ F: $F(2, 25) = 2.580$, $p>0.05$ C: $F(2, 44) = 3.380$, $p<0.05$
Rotarod (9.5 Mon.)	6-7, 7-12, 13-18	M: $F(2, 16) = 2.736$, $p>0.05$ F: $F(2, 24) = 9.256$, $p<0.01$ C: $F(2, 43) = 12.09$, $p<0.0001$
Rotarod (12.5 Mon.)	6-7, 7-12, 13-18	M: $F(2, 16) = 2.087$, $p>0.05$ F: $F(2, 24) = 1.580$, $p>0.05$ C: $F(2, 43) = 3.576$, $p<0.05$
Weight (12.5 Mon)	6-7, 7-12	M: $F(2, 16) = 0.843$, $p>0.05$ F: $F(2, 24) = 4.226$, $p<0.05$

All groups and tasks analyzed by 1-way ANOVA followed by Tukey's multiple comparison test. $p<0.05$ considered statistically significant. m=males, f=females, c=combined.

Table 4.3: Top Pias1 KD- modulated DEGs in pre-symptomatic miPias1.3 treated animals used for RT-qPCR

Gene	13.5 months FC Het w/KD	8 Months FC Het w/KD	Pathway/Function
BDNF	-2.492*	n/a	Neurotrophic growth factor
Neurod2	-1.965*	n/a	Neuronal transcription factor
Neurod1	-1.133*	n/a	Neuronal transcription factor
Syn1	-0.456*	n/a	Synaptic vesicle pathway
Syn2	-0.295*	n/a	Synaptic vesicle pathway
Rnf112	-0.296*	-0.629	Neurogenesis, protection against oxidative stress-induced damage
Pde4a	-0.281*	-0.303	cAMP signaling
Bcl2l2	0.315	0.506	Survival of NGF- and BDNF-dependent neurons

Asterisk indicates normalized genotype DEG with Pias1 KD

Table 4.4: Summary heat map of Pias1 KD effect on transcriptional targets in zQ175 heterozygote animals

Gene	8 Mon. zQ175 Pre-Symp miPias1.3	13.5 Mon. zQ175 Pre-Symp miPias1.3 male	13.5 Mon. zQ175 Pre-Symp miPias1.3 female	13.5 Mon. zQ175 Symp miPias1.3 male	13.5 Mon. zQ175 Symp miPias1.3 female
Rnf112	Treatment	Treatment	No Difference	No Difference	No Difference
Bcl2l2	Treatment	Treatment	Treatment	Genotype	No Difference
Pde4a	Treatment	Treatment	No Difference	No Difference	No Difference

(Orange = elevated, blue = decreased)

Table 4.5: disease associated transcriptional modules affected by Pias1 KD in zQ175 mice

Module	GO Term(s)	IPA Term(s)	Enrichment Term(s)	Pias1 KD effect	Significant
M11	Ensheathment of neurons Fatty acid biosynthetic process	Endothelin-1 signaling LPS/IL-1 inhibition of RXR Signaling by Rho family GTPase	Oligodendrocyte Astrocyte probable	rescue	Y
M20	Cell division Protocadherin beta Zinc finger, CH2H-like	p53 signaling Brca1 in DNA damage response	Glial marker p53 immune pathway	rescue	Y
M39	Protocadherin beta Microtubule cytoskeleton Ubl conjucation pathway	DNA break repair by NHEJ Signaling by Rho family GTPases Protein ubiquitination pathway	Oligodendrocyte	rescue	Y
M2	Protein kinase ATP binding site GTPase regulator activity Synapse	GPCR signaling cAMP signaling Huntington's disease signaling	Neuron probable Postsynaptic density proteins	rescue	N
M25	Leucine-rich repeat Reg. neuron differentiation	Glutamate receptor signaling Gαi signaling Huntington's disease signaling	Autism associated Neuron probable	rescue	N
M34	Regulation of transcription Chromatin modification Protocadherin gamma	LPS-stimulated MAPK signaling FGF signaling Huntington's disease signaling	Immune pathway	rescue	N
M1	Purine nucleotide binding Cellular protein localization Ubl conjugation pathway	Protein ubiquitination pathway tRNA charging Huntington's disease signaling	Neuron Postsynaptic density proteins	rescue	N
M10	Ubl conjugation pathway Chaperonin TCP-1 conserved site Zinc finger, CH2H-like	Sonic hedgehog signaling RAN signaling Amyloid processing	Down in Alzheimer's CA1 Nuclear proteins	rescue	N
M43	Fatty acid catabolic process	Fatty Acid β-oxidation I LPS/IL-1 Inhibition of RXR 14-3-3 mediated signaling	Postsynaptic density proteins Mitochondria	rescue	N
M46	Protocadherin gamma Zinc finger, CH2H-like	IL-22 signaling Glucocorticoid signaling	Nuclear proteins	rescue	N
M52	Transmembrane region VEGF receptor activity	NF-κB signaling Protein kinase A signaling	JAX disease genes Astrocyte probable	Exacer-bation	N
M7	Cell death Oligodendrocyte cell fate	Death receptor signaling Phospholipase C signaling Axonal guidance signaling	Oligodendrocyte Putamen local marker	Exacer-bation	N
M9	Mitochondrion Protein transport Translation elongation factor	Nrf2 oxidative stress response Serotonin degradation	Postsynaptic density proteins Mitochondria	Exacer-bation	N

CHAPTER 5

Restoration of Pnkp Activity by Pias1 Reduction in R6/2 and Potential Relationship to Somatic Repeat Expansion

SUMMARY OF CHAPTER 5

Pias1 is a SUMO E3 ligase that can modulate molecular and behavioral phenotypes in the R6/2 transgenic mouse model of Huntington's disease (HD). PIAS1 can also modulate DNA damage repair pathways in human patient iPSC-derived medium spiny neurons and in the striatum of the zQ175 knock-in mouse model of HD (Chapters 3 and 4). Specifically, PIAS1 SUMOylates the DNA repair factor PNKP, an enzyme in the transcription-coupled repair complex scaffolded by the huntingtin protein. Mutant huntingtin-associated perturbation of PNKP enzymatic activity was rescued with PIAS1 knock-down in both models and normalized aberrant transcriptional profiles, suggesting an impact on genomic stability. However, due to the extreme length of CAG-repeat in zQ175 mice, somatic repeat expansion could not be assessed in these animals due to technical limitations for resolution of repeat sizes. Therefore, given the previously reported impact on R6/2 pathogenesis with Pias1 knock-down and our robust, cross-model modulatory effect on PNKP activity, Pias1 modulation of Pnkp and DNA damage-associated mechanisms in R6/2 mice was assessed. Pias1 knock-down similarly rescued perturbed Pnkp activity in R6/2 mice, and data shows a potential reduction of somatic CAG repeat expansion in the striatum. Taken together, data in this dissertation suggest that Pias1 is an integral component of the transcription-coupled repair complex and response in multiple models of HD, and may contribute towards transcriptional dysregulation and somatic repeat expansion within the disease context.

INTRODUCTION

The typical age of adult-onset for HD is between 35 and 50 years of age with an inverse relationship existing between the length of the CAG repeat and age of onset. However, CAG length only accounts for 40-50% of the variance in the age of onset (AO) for adult-onset HD patients; variance is also influenced by genetic or environmental factors (Langbehn et al., 2004; Wexler et al., 2004).

Recent genome-wide association studies (GWAS) identified genetic variants that correlated with either a delay of AO or exacerbation of AO as positive or negative modifiers respectfully (Bettencourt et al., 2016; Flower et al., 2019; GeM-HD, 2015; Lee et al., 2017; Moss et al., 2017). These variants were primarily identified as components of DNA damage repair (DDR) pathways suggesting that genomic stability contributes to onset of HD. Indeed, one of the potential pathogenic features of HD is a propensity for somatic CAG-repeat instability in the striatum, observed in both human and mouse HD brain (Lee et al., 2011; Shelbourne et al., 2007); e.g. the number of CAG-repeats in the brain exhibits increased length mosaicism over time (Lee et al., 2011; Telenius et al., 1994) with greater expansion in postmortem cortex significantly correlating with earlier onset of HD in human patients (Swami et al., 2009). Expansion is attributed to decreased genomic stability of the CAG-repeat and DNA damage repair (DDR) pathways are implicated in mediating this instability (Jones et al., 2017; Schmidt and Pearson, 2016). Supporting this, two disease modifiers with genetic variants found in GWAS from HD patients were *MLH1* and *MSH3,* genes involved in mismatch repair (MMR) and previously linked to somatic repeat expansion (Flower et al., 2019; Lee et al., 2017; Moss et al., 2017). Another genetic modifier

of AO identified in the GWAS was FAN1, a DDR nuclease in the Fanconi Anemia, inter-strand crosslink repair pathway (Bettencourt et al., 2016). Recently, FAN1 has been shown to prevent somatic repeat expansion including that of *HTT* (Goold et al., 2019; Zhao and Usdin, 2018), further linking DDR responses to somatic repeat expansion and disease pathogenesis.

We recently showed that PNKP enzymatic activity is perturbed by expanded mutant HTT protein (mHTT, (Gao et al., 2019)). PNKP is a DNA-end processing enzyme that is a component of the base excision repair (BER) and transcription-coupled repair (TCR) pathways (Chakraborty et al., 2016; Chakraborty et al., 2015; Jilani et al., 1999). Our recent data shows that PIAS1 is a SUMO E3 ligase for PNKP and is a component of the TCR complex together with HTT (Chapter 3). Further, reduction of PIAS1 in both human iPSC-derived MSNs and striatum of zQ175 HD knock-in (KI) mice rescued mHTT-associated perturbed enzymatic activity of PNKP (Chapter 3, Chapter 4). PIAS1 is an E3 SUMO ligase that modulates DDR repair mechanisms, including the Fanconi Anemia pathway (Gibbs-Seymour et al., 2015), through SUMOylation of repair factors (Schwertman et al., 2016; Su et al., 2019) to either aid in recruitment or eviction of DDR components. PIAS1 was also identified as an E3 ligase enhancing SUMOylation of the HTT protein itself, with SUMOylation potentially modulating aggregation propensity of the mHTT protein (O'Rourke et al., 2013; Steffan et al., 2004). HTT serves as a scaffold for DDR complexes (Gao et al., 2019; Maiuri et al., 2017), with both PNKP and PIAS1 being binding partners within this complex, potentially through a SUMO-mediated mechanism (Chapter 3). Overall, PIAS1 knock-down (KD) in these models normalized aberrant transcriptional

profiles suggesting a neuroprotective role for modulating PIAS1-involved mechanisms at key disease stages (Chapter 3, Chapter 4).

We previously reported that Pias1 can modulate disease progression in a rapidly progressing mouse model of HD, the R6/2 model (Ochaba et al., 2016). R6/2 mice differ from zQ715 in that the HD phenotype is caused by expression of a mutant exon-1 human *HTT* fragment transgene instead of a knock-in (KI) mutation at the endogenous murine *Htt* locus (zQ175, (Brooks and Dunnett, 2015; Menalled and Brunner, 2014)). The R6/2 mouse model is overtly symptomatic at very early ages (e.g. 5-8 weeks) (Carter et al., 1999; Mangiarini et al., 1996) compared to the more subtle, long term symptomatic progression of the zQ175 model (Menalled et al., 2012). Previously, insoluble Pias1 was found to be increased in R6/2 striatum and KD of Pias1 in the striatum decreased this species and rescued HD-associated motor behavioral deficits, reduced accumulation of insoluble mHTT protein, and normalized an aberrant inflammatory profile (Ochaba et al., 2016). Therefore, because of the robust impact of Pias1 KD in the R6/2 mouse model (Ochaba et al., 2016) and our data showing a cross-model, and conserved impact of PIAS1 KD on PNKP enzymatic activity (Chapter 3, Chapter 4), we assessed whether Pias1 could also modulate Pnkp activity in R6/2 mice. Further, we examined whether Pias1 had an effect on somatic CAG repeat expansion of the R6/2 transgene to determine if modulating DNA repair activity *in vivo*, via a Pias1-mediated mechanism, could affect instability of the *HTT* CAG repeat.

Here I show that Pias1 KD in R6/2 mice rescued perturbed Pnkp enzymatic activity in both the nuclear and mitochondrial fractions of R6/2 mouse striata. Excitingly, a significant but modest reduction in somatic repeat expansion of the R6/2 transgene was observed. Due to the modest degree of reduction in expansion, no conclusions could be made about translational impact of stabilizing the CAG-repeat, however the data provides preliminary evidence that modulating Pias1-mediated DNA repair *in vivo* may have direct consequences on a key modifier of HD onset and progression. Interestingly, data also suggest that the neuroinflammatory profile in HD animals may have been an important component of a subset of previously observed phenotypic consequences of Pias1 KD in the R6/2 model.

RESULTS

miPias1.3 treatment does not reproduce behavioral rescue in R6/2 mice

To evaluate Pias1 reduction in R6/2 mice, we used the same parameters as our published study (Ochaba et al., 2016) and previous zQ175 studies (Chapter 4), using bilateral intrastriatal injections of the same AAV2/1 containing either miPias1.3 or control miSafe. Animals were injected at 5 weeks of age and behavior was recorded until sacrifice at 10 weeks of age (Figure 5.1A). In this study, baseline measures differed and miPias1.3 treated R6/2 mice did not show rescued behavior as previously recorded (Ochaba et al., 2016). Only a significant genotype effect was observed for grip strength at 6 weeks ($F(1, 36) = 36.660$, $p<0.0001$) and 8 weeks of age ($F(1, 35) = 31.730$, $p<0.0001$) with no significant treatment effect (Week 6: $F(1, 36) = 4.054$, $p>0.05$; Week 8: $F(1, 35) = 0.722$, $p>0.05$, Figure 5.1B). A slight genotype effect was observed for pole test with a significant interaction detected at 6 weeks of age suggesting a partial rescue of time to descend with miPias1.3

treatment (Genotype: F (1, 36) = 4.268, p<0.05; Interaction: F(1, 36) = 5.192, p<0.05, Figure 5.1C). This interaction was lost by 8 weeks of age, with only a significant genotype effect observed (Genotype: F(1, 35) = 16.510, p<0.001; Treatment: F(1, 35) = 2.846, p>0.05).

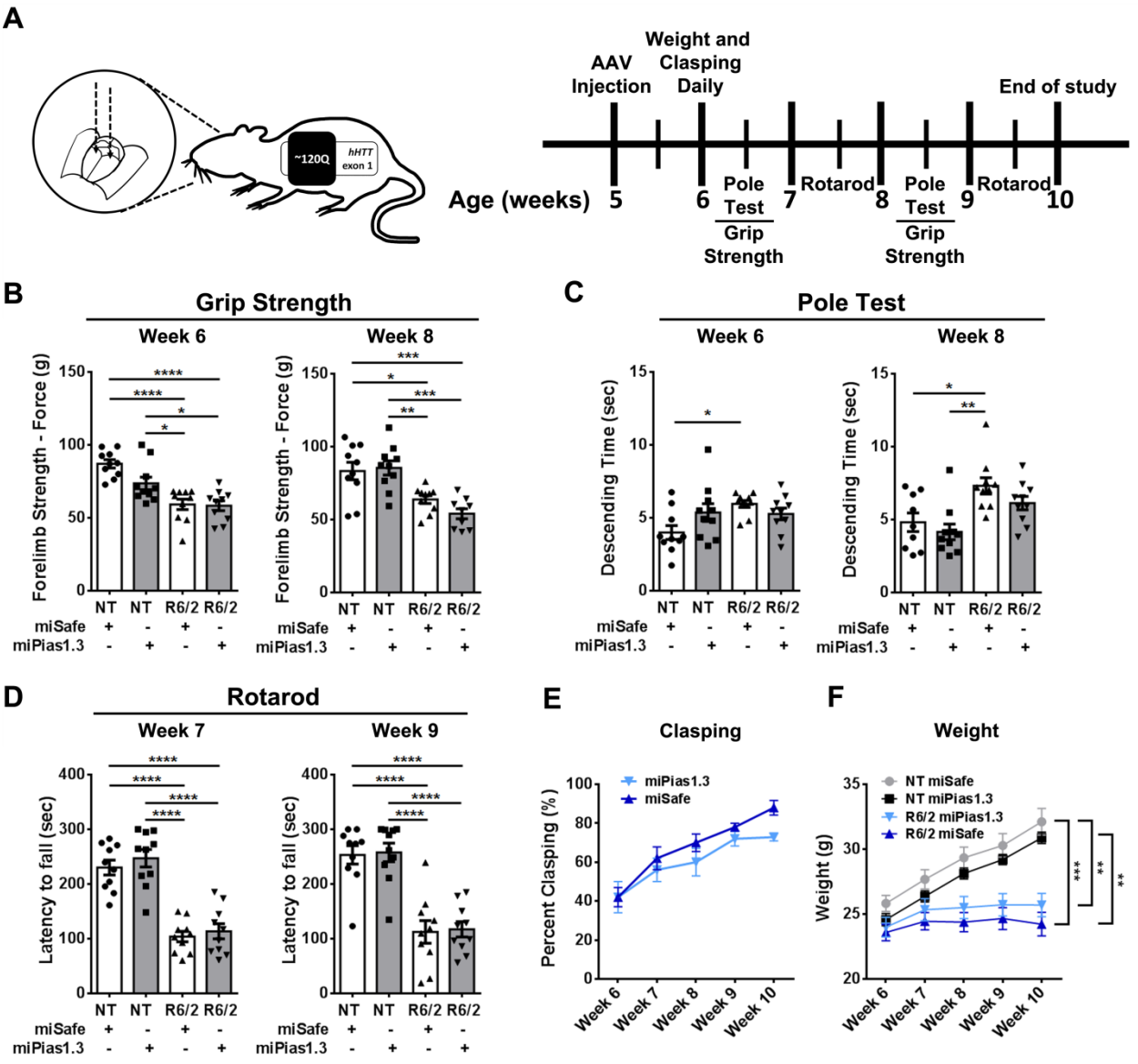

Figure 5.1: Pias1 KD does not rescue behavior in R6/2 mice. A) Experimental design and timeline for modulating Pias1 in R6/2 mice. Significant genotype effects observed for B) Grip strength, C) Pole test, and D) Rotarod at all ages tested. E) No difference in percent clasping with miPias1.3 treatment. F) Significant genotype for weight observed. All samples were analyzed by 2-way ANOVA followed by Tukey's multiple comparison test. ns=not significant, *p<0.05, **p<0.01, ***p<0.001, ****p<0.0001, values represent means ± SEM. Shaded bars represent miPias1.3 treated animals.

Similar genotype-only results were observed for Rotarod at 7 weeks of age (Genotype: $F(1, 36) = 93.120$, $p<0.0001$; Treatment: $F(1, 36) = 0.969$, $p>0.05$) and 9 weeks of age (Genotype: $F(1, 36) = 66.490$, $p<0.0001$; Treatment: $F(1, 36) = 0.074$, $p>0.05$, Figure 5.1D). For Clasping, no differences were observed between control R6/2 animals and miPias1.3 treated animals in percent clasping (Figure 5.1E). A clear body weight genotype effect was observed as described ((Ochaba et al., 2016); Genotype: $F (1, 36) = 59.620$, $p<0.0001$; Treatment: $F (1, 36) = 0.020$, $p>0.05$, Figure 5.1F) with R6/2 mice exhibiting less weight gain over time. Together, these data suggest that miPias1.3 treatment in this cohort of R6/2 animals did not rescue or modulate behavior as previously reported (Ochaba et al., 2016). However, R6/2 behavior overall appeared more subtle compared to previous results independent of treatment.

Molecular readouts not altered by Pias1 KD in R6/2 mice

We next evaluated whether we modulated the molecular landscape of R6/2 animals with miPias1.3 treatment. We previously showed that levels of insoluble Pias1, but not soluble PIAS1, were elevated in R6/2 mice and that knock-down of Pias1 restored these levels to that of NT animals. (Ochaba et al., 2016). Therefore, soluble and insoluble levels of Pias1 were assessed using Soluble/Insoluble fractionation (Ochaba et al., 2016; Ochaba et al., 2018) by western blot. Interestingly, in this cohort of R6/2 animals, no significant increase in insoluble Pias1 protein levels was observed in untreated R6/2 mice (Figure 5.2A). Instead, R6/2 mice had significantly less insoluble Pias1 (Genotype: $F(1, 10) = 51.230$, $p<0.0001$) with only a KD treatment effect being observed in NT treated mice (Treatment: $F(1, 10) = 12.210$, $p<0.01$), in contrast to what had previously been seen in NT mice. A

significant decrease in Pias1 levels with miPias1.3 treatment in R6/2 mice was observed in the Soluble fraction with no effect observed in NT mice with treatment (Interaction: $F(1, 10) = 25.360$, $p<0.001$). Assessing levels of *Pias1* transcript by qPCR showed successful, significant reduction of *Pias1* in both NT and R6/2 animals (Treatment: $F(1, 11) = 49.91$, $p<0.0001$, Figure 5.2B). Unexpectedly, a significant genotype effect between NT and R6/2 mice was also observed (Genotype: $F(1, 11) = 10.370$, $p<0.01$) with R6/2 control animals having less *Pias1* expression at baseline compared to NT control animals. This effect was not observed previously and may in part explain the baseline differences in Pias1 levels as detected by western blot. Therefore, Soluble/Insoluble fractionation analysis reveals differential levels of Pias1 at baseline between NT and R6/2 animals as well as a differential impact of miPias1.3 treatment in a genotype-dependent manner as compared to our previously published results modulating Pias1 in this animal model (Ochaba et al., 2016). These differences in baseline may, in part, explain differences in behavioral and molecular outcomes with Pias1 KD in these animals.

High molecular weight (HMW) insoluble mHTT exon-1 protein (mHTTex1p) species was previously modulated by Pias1 both *in vitro* (O'Rourke et al., 2013) and *in vivo* in the R6/2 model (Ochaba et al., 2016). Assessing formation of this species, miPias1.3 treatment in this cohort did not significantly modulate HMW mHTTex1p formation compared to miSafe treated R6/2 mice, though with an observed trending decrease ($p>0.05$, Figure 5.2A). This was consistent with the lack of change in insoluble Pias1 levels in these animals as reduction in this Pias1 species previously corresponded to a significant decrease in HMW mHTT (Ochaba et al., 2016). Levels of soluble monomeric transgene protein product from

R6/2 mice decrease with age ((Morozko et al., 2018), Chapter 1). Monomeric mHTTex1p was not detected at 10 weeks of age (data not shown), indicating that the majority of transgene product had shifted towards the insoluble fraction and that miPias1.3 treatment did not affect levels of this mHTTex1p species similar to what was previously observed (Ochaba et al., 2016).

Pias1 has an important role in inflammation. In our previous studies, inflammatory responses were noted; in particular, changes in NfkB (p65) localization and increased Il-6 cytokine levels were observed. However, in this study, these inflammatory responses were not mounted nor were they altered by Pias1 reduction. For instance, protein levels of NfkB did not change in a genotype-dependent manner (Genotype: $F(1, 10) = 0.050$, $p>0.05$), and were not affected by miPias1.3 treatment in this cohort (Treatment: $F(1, 10) = 0.140$, $p>0.05$, Figure 5.2C). Further, NfkB was only detected in the soluble fraction suggesting a different inflammatory profile in these animals. Il-6 levels were significantly reduced in these R6/2 mice, regardless of treatment, as detected by western blot (Genotype: $F(1, 10) = 16.940$, $p<0.01$, Figure 5.2C). This cytokine was previously shown by a Meso Scale Discovery panel to be elevated in R6/2 mice and restored to NT baseline levels by miPias1.3 treatment (Ochaba et al., 2016). No treatment effect was observed in this current cohort of R6/2 miPias1.3 treated animals using an antibody which similarly detects total levels of soluble Il-6 (Treatment: $F(1, 10) = 0.111$, $p>0.05$). Together, these data suggest that the baseline inflammatory background was distinctly different in this cohort of animals compared to previously published studies.

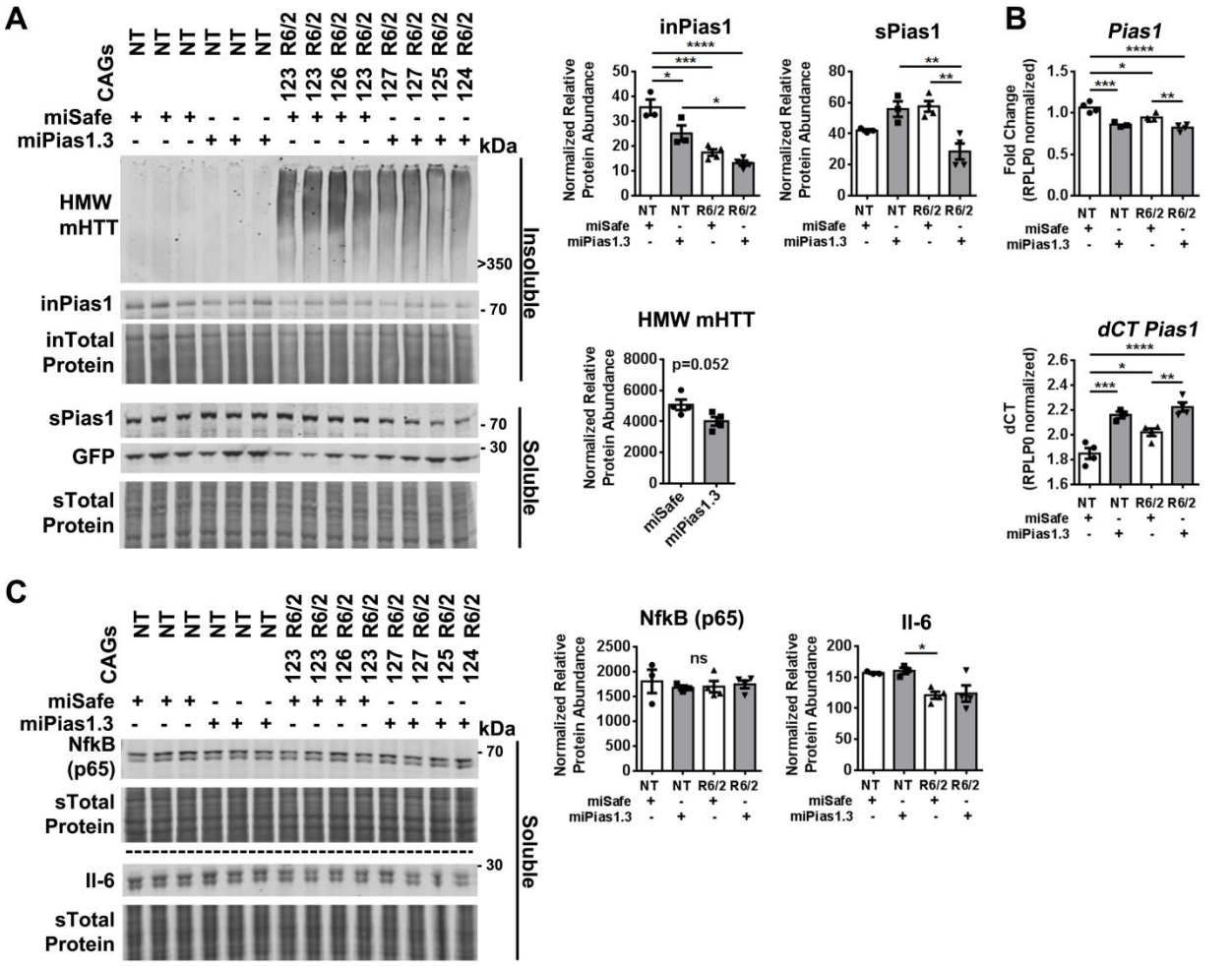

Figure 5.2: Pias1 knockdown does not affect mHTT accumulation. A) Soluble/Insoluble fractionation of striatal tissue shows significant reduction of soluble Pias1 only. HMW insoluble mHTT remains statistically unchanged with treatment. B) qPCR analysis shows significant reduction in levels of *Pias1* transcript with KD. C) Western blot shows no change in NfkB protein abundance with miPias1.3 treatment and reveals that Il-6 levels are significantly lower in R6/2 mice from this cohort. Protein normalized to total protein stain. Normalized relative protein abundances for all samples were analyzed by 2-way ANOVA followed by Tukey's multiple comparison test. ns = not significant, *p<0.05. **p<0.01, ***p<0.001, ****p<0.0001, values represent means ± SEM. Shaded bars represent miPias1.3 treated animals.

Pnkp enzymatic activity is modulated by Pias1 in R6/2 mice

Although baseline behavior and HMW mHTTex1p accumulation were not affected by Pias1 KD, we assessed if the DDR function of Pias1 was modulated in these animals. We examined the effect of Pias1 KD on Pnkp activity as described for zQ175 mice (Chapter 4). Enzymatic

activity of Pnkp was assessed from both the nuclear and mitochondrial extracts harvested from GFP+ regions of microdissected striata. In R6/2 animals, a noticeable reduction in Pnkp activity was observed in both extracts. Nuclear and mitochondrial activity deficits were rescued with miPias1.3 treatment (Figure 5.3A, B), reproducing modulatory phenotypes of Pias1 observed in zQ175 mice and human iPSC-derived neurons. These data suggest a robust and conserved function for Pias1 in modulating transcription-coupled repair mechanisms in distinctly different mouse models of HD and in human, patient cells.

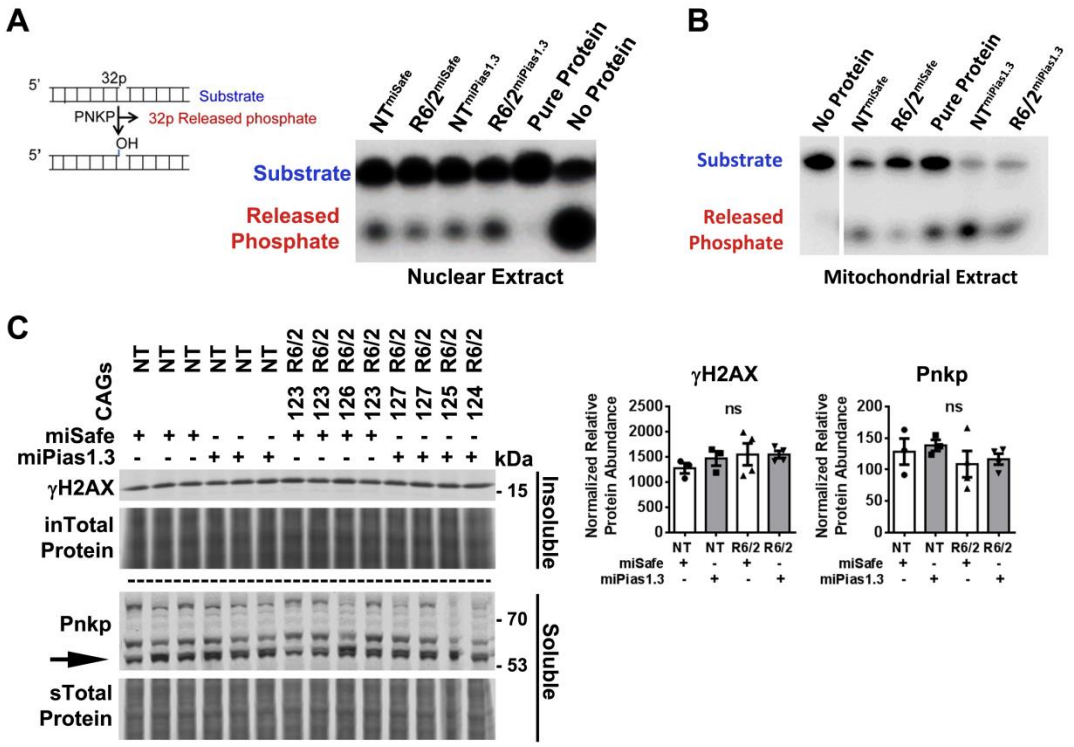

Figure 5.3: Pias1 modulated Pnkp enzymatic activity but not DNA damage levels in R6/2 mice. Decreased Pnkp activity in R6/2 mice is rescued by miPias1.3 treatment in both the A) nucelar and B) mitochondrial extract. C) Western blot analysis of Soluble/Insoluble fractionation of striatal tissue showed not significant difference in levels of DNA damage marker γH2AX and unmodified Pnkp, with Pias1 KD. Black arrow indicated quantified Pnkp protein band which corresponds to unmodified positive control of overexpressed Pnkp (not shown). Higher bands are suggested to be post-translational modifications of Pnkp as observed in Chapter 3. Protein normalized to total protein stain. Normalized relative protein abundances for all samples were analyzed by 2-way ANOVA followed by Tukey's multiple comparison test. ns = not significant, values represent means ± SEM. Shaded bars represent miPias1.3 treated animals. Panels A and B data and figure generated in collaboration with Sarkar lab, UTMB.

Rescued Pnkp activity previously corresponded to decreased levels of the DNA damage marker γH2AX in 8-month old zQ175 mice, suggesting an impact on total levels of DNA damage overall (Chapter 4). In R6/2 mice treated with miPias1.3, no significant difference in abundance of γH2AX was observed by western blot (Genotype: $F(1, 10) = 1.308$, $p>0.05$; Treatment: $F(1, 10) = 0.388$, $p>0.05$) in R6/2 mice (Figure 5.3C). The lack of genotype effect was unexpected as levels of γH2AX have previously been shown to be elevated in R6/2 mice as compared to NT in the striatum (Enokido et al., 2010; Illuzzi et al., 2009). Levels of unmodified PNKP similarly were unaffected (Genotype: $F(1, 10) = 1.625$, $p>0.05$; Treatment: $F(1, 10) = 0.296$, $p>0.05$, Figure 5.3C).

Pias1 modulates key transcriptional targets in R6/2 mice

A robust effect on specific dysregulated genes in zQ175 mice following miPias1.3 treatment was observed (Chapter 4), therefore I assessed a subset of those genes following Pias1 modulation in R6/2 (Figure 5.4). Besides *Bdnf,* these genes were not previously detected as altered in 12 week old R6/2 mice (Jacobsen et al., 2017; Vashishtha et al., 2013). The most robustly modified gene in zQ175 was *Bcl2l2*; in R6/2 mice, miPias1.3 treatment resulted in a significant increase in *Bcl2l2* expression in the NT animals (Treatment: $F(1, 11) = 10.660$, $p<0.01$) with a trending increase in R6/2 treated animals. *Bcl2l2* was increased in pre-symptomatically treated zQ175 animals by mRNASeq as well (Chapter 4, Table 5.1).

Synaptic vesicle component genes *Syn1* and *Syn2* were shown to be modulated by Pias1, with pre-symptomatic KD reducing zQ175 genotype-associated aberrantly elevated transcription (Chapter 4,). In R6/2 animals, levels of *Syn1* were significantly increased with

miPias1.3 treatment (Treatment: $F(1, 11) = 9.603$, $p<0.05$) but showed no significant genotype effect (Genotype: $F(1, 11) = 1.336$, $p>0.05$). For *Syn2*, both a significant genotype and treatment effect was observed (Genotype: $F(1, 11) = 10.820$, $p<0.01$; Treatment: $F(1, 11) = 6.749$, $p<0.05$) but with post-hoc analysis only indicating a difference between NT Pias1 KD and control R6/2 animals. Therefore, Pias1 may also modulate synaptic transcriptional profiles in R6/2 mice.

The neurotrophic growth factor *Bdnf* was significantly modulated by Pias1 at the transcriptional level in pre-symptomatic treated zQ175 animals. In R6/2 mice, miPias1.3 treatment significantly increased levels of *Bdnf* in NT animals and trended in R6/2 animals (Treatment: $F (1, 11) = 12.56$, $p<0.01$) with a significant genotype effect also observed ($F(1, 11) = 8.065$, $p<0.05$). Additional genes arising from mRNASeq data in zQ175 mice were evaluated (Table 5.1), however were not significantly altered by Pias1 KD in R6/2 mice. Given that levels of *Bcl2l2* were consistently elevated with Pias1 KD in the majority of animal groups assessed, these data strongly suggest there may be an underlying pro-survival pathway that is modulated by Pias1 in the brain ((Aouacheria et al., 2017), Figure 5.4, Table 5.1) and can be further explored.

Somatic repeat expansion is reduced in R6/2 mice with Pias1 KD

DNA damage repair genes modulate CAG repeat instability in animal models of HD (Schmidt and Pearson, 2016). Further, the human GWAS-identified Age-of-Onset modifier *FAN1*, a cross-link DDR gene, stabilizes the *HTT CAG* repeat to modify disease progression in patient-derived neurons (Goold et al., 2019). Given that we have observed Pias1

modulating repair activity in Pnkp in three models of HD, in collaboration with Vanessa Wheeler's group, we evaluated whether increasing repair activity in R6/2 mice had any impact on somatic repeat expansion in the striatum with miPias1.3 treatment.

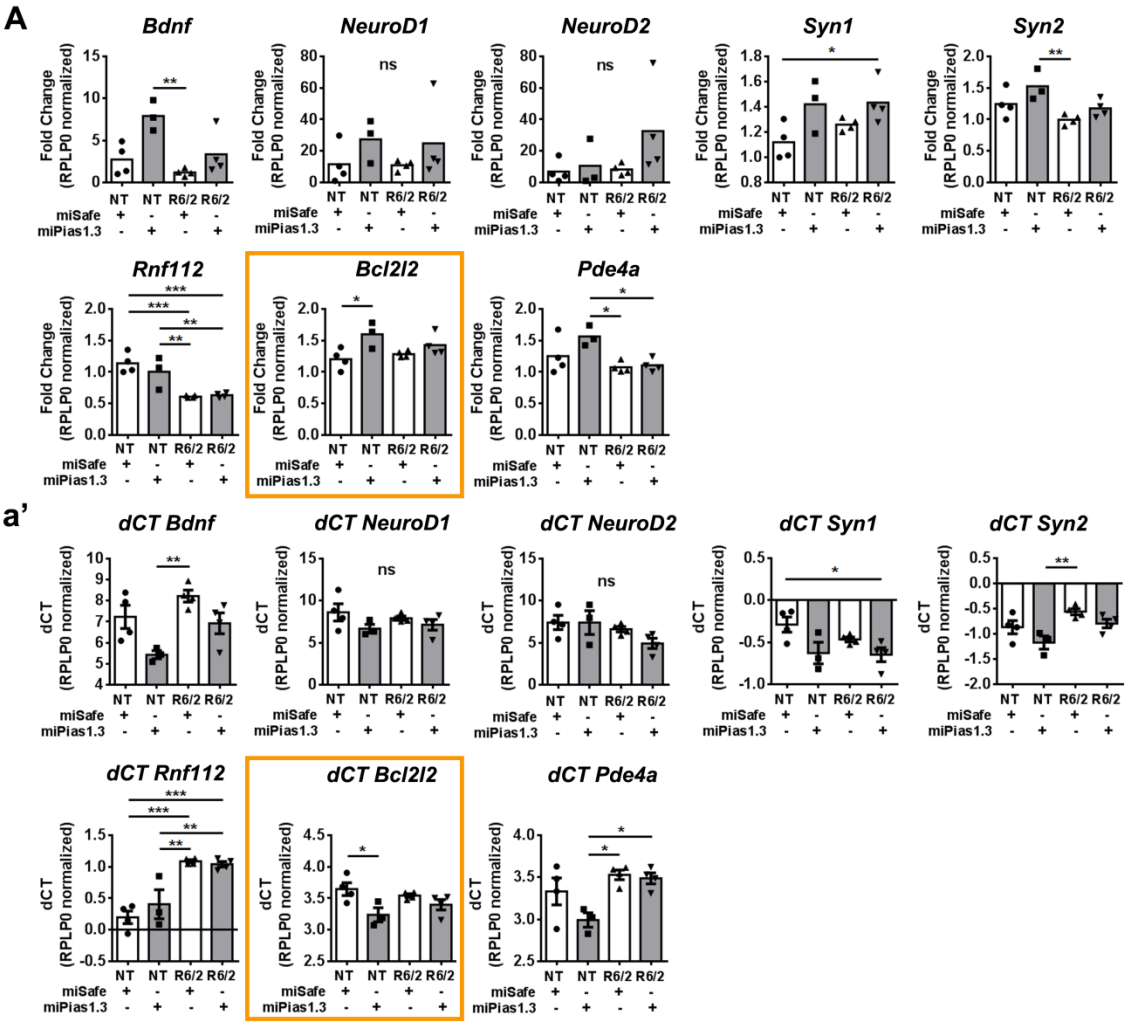

Figure 5.4: qPCR analysis on top mRNAseq identified genes identified in Chapter 4 for R6/2 miPias1.3 treated mice. A) Fold change and a') dCT values for mice show significant genotype and treatment effects for miPias1.3 treated animals. Mice show significant treatment effect for *Bcl2l2, Syn1, Syn2*, and *Bdnf*. *Rnf112* (Genotype: F (1, 11) = 50.720, p<0.0001; Treatment: F(1, 11) = 0.562, p>0.05), *Pde4a* (Genotype: F (1, 11) = 10.990, p<0.01; Treatment: F(1, 11) = 3.350, p>0.05), *NeuroD1* (Genotype: F (1, 11) = 0.032, p>0.05; Treatment: F(1, 11) = 3.803, p>0.05), *NeuroD2* (Genotype: F(1, 11) = 4.215, p>0.05; Treatment: F(1, 11) = 1.099, p>0.05). All samples were analyzed by 2-way ANOVA followed by Tukey's multiple comparison test. ns = not significant, *p<0.05, **p<0.01, ***P<0.0001, values represent means ± SEM. Shaded bars represent miPias1.3 treated animals.

Genomic DNA (gDNA) from R6/2 mice was harvested from the same GFP+ microdissected striatal tissue used for mRNA purification and assessed as previously described (Lee et al., 2010). Somatic repeat expansion was determined using ABI GeneMapper and expansion indexes using threshold factors of 0%, 10%, and 20% were calculated. R6/2 mice with Pias1 KD had significantly smaller expansion indexes at all peak thresholds measured (0%: $p<0.01$, 10%: $p<0.01$, 20%: $p<0.01$) strongly suggesting a positive effect on expansion that is sustained with more stringent analyses (Figure 5.5A, C). The significantly smaller expansion indexes in miPias1.3 treated R6/2 mice compared to miSafe treated animals was not due to general variation in CAG-repeat length as no significant difference was observed in repeat size measured from tail gDNA ($p>0.05$) and from modal striatal allele from expansion analysis ($p>0.05$, Figure 5.5B). Therefore, Pias1 KD lead to a modest but significant decrease in somatic repeat expansion in the striatum of R6/2 mice that may be associated with restoration of Pnkp activity. This supports previous observations that DDR mechanisms are contributing to genomic stability and suggests that TCR may also be a driving factor for promoting somatic repeat expansion in the striatum.

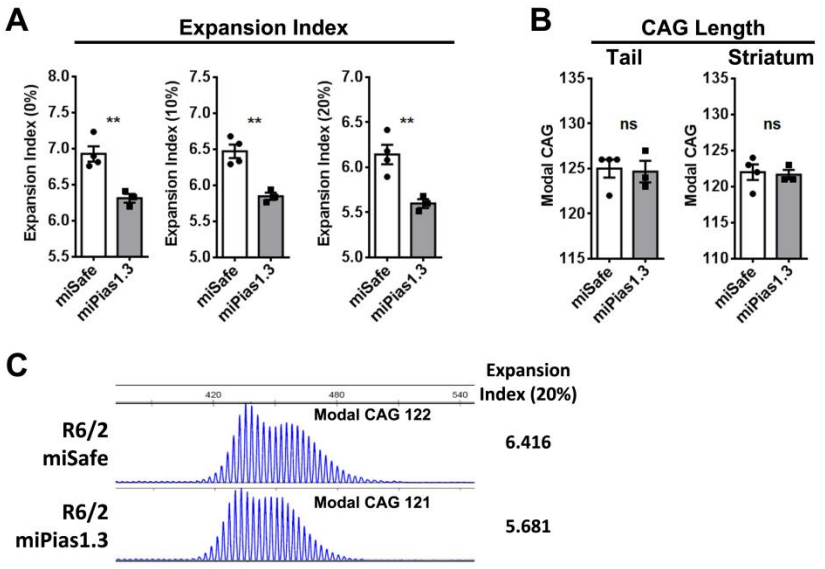

Figure 5.5: Pias1 knock-down results in smaller expansion indexes in R6/2 mice. A) R6/2 measured expansion indexes from PCR traces obtained from amplifying genomic *HTT* CAG repeat are significantly smaller in miPias1.3 treated R6/2 mice at all peak thresholds analyzed. B) Modal CAG repeat length not significantly different between groups in both tail and striatum. C) Representative PCR peak traces from ABI GeneMapper shows smaller expansion in miPias1.3 treated animal. Expansion indexes analyzed by Student's unpaired 2-tailed t-test. ns = not significant, values represent means ± SEM. Shaded bars represent miPias1.3 treated animals. Data generated in collaboration with Wheeler lab, MGH.

DISCUSSION

We previously showed that PIAS1 KD rescued perturbed enzymatic activity of PNKP in two models of HD: Human HD patient, iPCS-derived MSNs and zQ175 mouse striatum (Chapter 3, Chapter 4). Here we show that this modulatory effect is reproduced in a third model of HD; the R6/2. Even though all three models have different molecular profiles and represent different stages of disease progression and development, data presented here suggest a robust, conserved mechanism in modulating DDR pathways in neurons for PIAS1. Together, data from all three models supports a function for PIAS1 in DDR mechanisms in the brain with high translational impact for targeting PIAS1 to modulate these pathways in HD. With KD serving to normalize aberrant transcription associated with HD in the zQ175 mice and facilitating enzymatic activity of the TCR repair complex, it is possible that PIAS1 is participating in inappropriate DNA repair within the HD context (Shelbourne et al., 2007). Therefore, homeostatic imbalance may result in initially beneficial or compensatory mechanisms shifting to promote detrimental outcomes (Vanni et al., 2019). Supporting this hypothesis is the observation that Pias1 KD differentially impacted transcriptional networks in WT and zQ175 mice (Chapter 4), suggesting that normal homeostatic function of Pias1 during aging may be different from that under neurodegenerative disease-associated insults and that appropriately targeting Pias1 in HD may restore balance.

Excitingly, I provide preliminary evidence here for a potential direct consequence of Pias1 mediated DDR pathways in the brain and specifically within the context of CAG-repeat associated neurodegenerative diseases. Together with rescue of Pnkp enzymatic activity, I also observed a statistically significant decrease in the expansion indexes for transgene CAG-repeat length with miPias1.3 treatment (Figure 5.3, Figure 5.5). This reduction in expansion was significant, but modest, potentially representing a variation of only a few repeats. The ultimate impact of this reduction is therefore not yet known and impact of the modest change may be masked by the rapid progression of symptomology in the R6/2 mouse model. Assessing repeat length and stability in a long-term model of HD (i.e. the zQ175 or Q140) may aid in elucidating the molecular impact of reducing somatic expansion with Pias1 modulation.

DNA damage repair mechanisms have been previously linked to CAG repeat instability and somatic repeat expansion (Kovtun et al., 2007; Mollersen et al., 2012). Notably, repair of oxidized nucleotides through the base-excision repair (BER) pathway is linked to somatic expansion of the HD-associated CAG repeat in mice, suggesting that normal repair processes may contribute to detrimental outcomes in disease contexts when under oxidative stress (Kovtun et al., 2007; Mollersen et al., 2012). Genes involved in mismatch repair pathways (MMR) also promote somatic repeat expansion (Dragileva et al., 2009; Gonitel et al., 2008; Kovalenko et al., 2012; Shelbourne et al., 2007; Wheeler et al., 2003), likely as a consequence of DNA instability or inappropriate repair (Gonitel et al., 2008; Shelbourne et al., 2007). This could be caused by slippage of DNA to produce unusual structures or formation of DNA:RNA hybrid structures known as R-loops (Schmidt and

Pearson, 2016). While formation of unusual DNA structures is common in replicating cells, in neurons they can form as a consequence of active transcription and subsequent misalignment of the CAG-repeat or hybridization of the transcribing RNA strand (Reddy et al., 2011; Slean et al., 2013). Indeed, MMR has been shown to have a preference for actively transcribing genes (Huang and Li, 2018). Therefore, MMR may inappropriately repair these structures in a manner that produces a few new repeat units at a time, leading to incremental expansion over time (Schmidt and Pearson, 2016). Indeed, a genetic variant within MMR gene *MSH3* that resulted in decreased expression corresponded with reduced somatic expansion, delayed onset, and slower disease progression (Flower et al., 2019; Moss et al., 2017). It is important to note, however, that while active MMR facilitates somatic repeat expansion, recent work investigating FAN1, a known HD genetic variant AO modifier, supports a role for active and appropriate repair in stabilizing the CAG repeat region (Goold et al., 2019; Zhao and Usdin, 2018). Therefore, a protective role for adequate repair has also been established.

Interestingly, the most recent GWAS completed on HD patients showed that the length of uninterrupted CAG repeats predominately predicts AO rather than translational length of expanded polyglutamine stretch (with glutamine also being coded by CAA, (GeM-HD, 2019)). Therefore, the length of the uninterrupted CAG may dictate its propensity for somatic expansion due to instability within the striatum as interruptions increase trinucleotide repeat stability (Pearson et al., 1998). Indeed, somatic expansion has been long been suggested to correlate with the regional vulnerability seen in diseases like HD (i.e. MSNs, striatum) where the disease-associated mutation is ubiquitously expressed, yet

only specific tissues are affected (Pearson et al., 2005; van Eyk and Richards, 2012). In HD, this effect was suggested early on where larger somatic repeat expansion was observed in the striatum versus the cerebellum which is less affected by disease (Kennedy and Shelbourne, 2000; Telenius et al., 1994). Tissue-specific expansion occurs early on in disease pathogenesis, with brain regions showing earlier expansion being the most overtly affected over time (Kennedy et al., 2003; Lee et al., 2011) and regional expression of DDR genes corresponding to observed increases in repeat expansion (Mason et al., 2014). Therefore, understanding the modest impact miPias1.3 treatment is having on somatic expansion may have a novel and significant translational impact for modulating disease progression or AO of HD.

Even though we saw a significant impact on DDR activity and CAG-repeat stability, we unexpectedly observed significant differences in behavioral and molecular readouts in R6/2 mice at baseline and with Pias1 KD compared to our previously published results (Ochaba et al., 2016). This is likely due to the molecular differences at baseline between these groups. The functional consequence of the lack of initially increased Pias1 in the Insoluble fraction in these current animals is not clear, although suggests that Pias1 responses were altered to start and therefore did not change inflammatory readouts or presence of HMW insoluble mHTTex1p. Further, levels of soluble Pias1 were previously not affected by miPias1.3 treatment unlike our current observations (Figure 5.2A, (Ochaba et al., 2016)). Insoluble HMW mHTTex1p species tracks with disease progression in R6/2 mice ((Morozko et al., 2018), Chapter 1) and rescued behavioral deficits corresponding to reduced insoluble Pias1 were observed when this mHTTex1p species was significantly

reduced (Ochaba et al., 2016). Our current data therefore, may explain the lack of behavioral impact with Pias1 KD as neither of these Insoluble species were altered in this study (Figure 5.2A).

These differences in protein homeostasis and behavioral readouts between studies may in part be explained by the striking differences in inflammatory markers observed. Pias1 has a canonical function in modulating inflammation through NfkB signaling, such that Pias1 binds to NfkB to prevent transcription of pro-inflammatory gene targets (Liu and Shuai, 2008). Therefore, in R6/2 mice, perturbed translocation of NfkB was suggested to be caused by Pias1 accumulation in the Insoluble/nuclear fraction with KD reducing insoluble levels of Pias1 specifically. Previous observed results were associated with a restoration of NfkB localization and subsequent lack of inhibition towards associated signaling cascades which resulted in normalization of perturbed inflammatory cytokine profile (Ochaba et al., 2016). In this current study, there was no detectable NfkB in the Insoluble fraction and Pias1 KD did not alter this profile (data not shown), suggesting that even though mice express mHTT, their Pias1-mediated inflammatory responses were altered. Similarly, levels of soluble cytokine Il-6 in control R6/2 animals observed in this study were not elevated and miPias1.3 had no significant effect (Figure 5.2B). With this current data, it is apparent that previous cohorts of animals may have had an elevated inflammatory environment at baseline, therefore utilizing Pias1's inhibitory function in an attempt to counterbalance neuroinflammation. While purely speculative, due to the difference in time when experiments were completed, it is possible that environment and/or microbiome differences in the cohorts of mice may have contributed to differences in inflammatory

baseline between studies (Castillo et al., 2019; Sherwin et al., 2018). Specifically, composition of the microbiome has been reported to be highly variable between breeding centers or vendors (Hufeldt et al., 2010) and it is possible that over the time between the R6/2 studies, conditions changed within the vivarium.

Overall, the data presented here supports a function for Pias1 in mediating genome integrity in the brain, especially in the context of HD. This function may be independent from serving as an inhibitor of inflammatory cascades and reflect a *dual role* for Pias1 in inflammation and as a SUMO E3 ligase for DDR pathways (Galanty et al., 2009; Gibbs-Seymour et al., 2015). PIAS1 KD restored activity of repair protein PNKP in three models, including human patient-derived neurons and in two drastically different mouse models of HD. In R6/2 mice, this increased activity corresponded to a decrease in somatic repeat expansion, suggesting that facilitating TCR stabilized the CAG repeat. And while future studies remain to be carried out to investigate the specific functional consequence of PNKP SUMOylation as well as the pathogenic impact of CAG-repeat stability in HD animal models with Pias1 KD, we have defined a new role for Pias1 modulating HD pathogenesis through DNA damage repair mechanisms.

EXPERIMENTAL PROCEDURES

Animals

R6/2 mice were obtained from Jackson Laboratories. Initial CAG repeat sizing of genomic DNA harvested from tails was performed by Laragen. Experiments were carried out in strict accordance with the Guide for the Care and Use of Laboratory Animals of the NIH and

an approved animal research protocol by the Institutional Animal Care and Use Committee (IACUC) at the University of California, Irvine. Animals were humanely euthanized by an injection of Euthasol at 10 weeks followed by cardiac perfusion with PBS then decapitation. Brain tissue used for biochemical assessment was flash-frozen in liquid nitrogen and stored at -80°C until further use. Striatal tissue was microdissected for GFP+ region using Night Sea fluorescent lamp at time of harvest, prior to freezing.

Surgery

At 5 weeks of age, R6/2 mice were anesthetized using isoflurane and underwent bilateral intrastriatal injections using a dual injection stereotaxic apparatus (coordinates 0.01 mm caudal to bregma, 0.2 mm right/left of midline, 0.345 pocket to 0.325 mm ventral to pial surface). 5 µl of AAV2/1 virus containing miPias1.3 CMVeGFP or miSAFE CMVeGFP at ~ 3e12 vg/ml, purified as described (Ochaba et al., 2016), was injected using a Hamilton syringe at a rate of 0.5 µl/min. Syringe was left in place for 5 minutes after each injection to ensure complete ejection of viral solution into brain region. Animals were allowed to recover for 1 week under observation prior to beginning behavioral analysis.

Behavioral Paradigms

Motor deficits were assessed in pole test, Rotarod, and grip strength assays as described (Ochaba et al., 2016). For pole test, mice were tested at 6, and 8 weeks of age for their ability to descend a vertical pole (1 cm in diameter, 60 cm high) by recording and averaging time to descend over four trials for analysis. Rotarod was carried out using an accelerating apparatus (Dual Species Economex Rota-Rod; 0207-003M; Columbus Instruments) at 7and

9 weeks of age. Animals were trained on Rotarod for 5 minutes on day 1 and tested the following day by an accelerating assay recording and averaging time to fall for three, 5-minute trials test day.

Grip strength was assessed 6 and 8 weeks of age to measure forelimb strength using a meshed force gauge which retained the peak force applied (IITC Life Science instrument, Woodland Hills, CA) and averaging the top 4 strongest pulls of 5 trials in grams of force applied to the meter. Dyskinesia was assessed by recording percent of animals clasping from weeks 5-10 as described (Mangiarini et al., 1996) and body weights were recorded at the same time daily from weeks 5-10 and averaged for each week for statistical analysis.

Tissue and cell protein lysis, quantification, and Western Blot analysis

Flash frozen brain tissue was prepared as previous (Ochaba et al., 2016; Ochaba et al., 2018). Protein fractions were quantified using detergent compatible (DC) protein assay (Bio-Rad). Soluble and Insoluble protein lysates were resolved on either 3-8% or 4-12% Bis-Tris Poly-Acrylamide gels and transferred onto either 0.45μM or 0.2μM nitrocellulose membrane depending on size of proteins of interest (smaller proteins with 4-12% on 0.2μM). Insoluble protein lysates were resolved on 3-8% Tris-Acetate Poly-Acrylamide gels and transferred onto 0.45μM nitrocellulose membrane to assess formation of HMW mHTT species. Membranes were blocked in Odessey starting block (Li-Cor) for 1 hour at room temperature and probed in primary antibody overnight at 4°C in blocking supplemented to 0.5% tween. Secondary IR-fluorophore antibodies were used and detected using a Li-Cor Odyssey CLx system and Image Studio software. IR fluorescence imaging was used for

quantitative analysis with detected protein levels normalized to Revert Li-Cor whole-protein stain prior to statistical analysis. Antibodies used for analysis were anti-Pias1 (Cell Signaling 3550S), anti-HTT (Millipore MAB5492, HMW mHTT), anti-HTT (Cell Signaling 5656S, clone D7F7 for FL-HTT), anti-GFP (Living Colors, Clontech Laboratories 632381), anti-NfkB (Cell Signaling 8242S), anti-Il-6 (Cell Signaling 12912T), anti-PNKP (Novus Biologicals NBP1-87257), and anti-γH2AX (Millipore 05-636).

RNA purification and qPCR

GFP+ flash frozen brain regions were homogenized in TRIzol reagent (Invitrogen) and RNA was extracted according to manufacturer's protocol and purified using RNEasy Mini kit (QIAGEN). Residual DNA was removed by DNase treatment incorporated into RNEasy protocol as per manufacturer's suggestion. Reverse transcription was performed using SuperScript 3 First-strand synthesis system according to manufacturer's protocol (Invitrogen) from harvested and purified RNA. Both oligo (dT) and random hexamer primers were used in a 1:1 ratio using a total of 500 ng RNA per sample. Final synthesized cDNA was diluted to 5ng/ul in DEPC treated water and stored at -20°C until use. *Rplp0* was used as the normalizing house-keeping gene as previous (PMID: 30452420). qPCR primers:
Rplp0 (F: GCTTCGTGTTCACCAAGGAGGA, R: GTCCTAGACCAGTGTTCTGAGC),
Pias1 (F: CTGCACAGACTGTGACGAGATAC, R: CGCTACCTGATGCTCCAATGTG),
NeuroD2 (F: GCTACTCCAAGACGCAGAAGCT, R: CACAGAGTCTGCACGTAGGACA),
NeuroD1 (F: CCTTGCTACTCCAAGACCCAGA, R: TTGCAGAGCGTCTGTACGAAGG),
Bdnf (F: TCGTTCCTTTCGAGTTAGCC, R: TTGGTAAACGGCACAAAAC),
Pde4a (F: CCGTGTTCACAGACCTGGAGAT, R: GGTGGTTCTCAAGCACAGACTC),

Syn1 (F: TATGCCACTGCTGAGCCCTTCA, R: ATGGCAATCTGCTCAAGCATAGC),

Syn2 (F: CCTGCTCTGAAATGTTTGGTGGC, R: TCTGTCCTCCACTTGGTGTTCC),

Rnf112 (F: AAGTGGAAGCCGCCAAGAAGGA, R: AGGAGGTTCCTCATCGTGTCAG),

Bcl2l2 (F: CAAGTGCAGGATTGGATGGTGG, R: CTGTCCTCACTGATGCCCAGTT).

PNKP enzymatic activity

3'-phosphatase PNKP enzymatic activity from nuclear and mitochondrial extracts was performed as previously described (Chakraborty et al., 2015; Gao et al., 2019). A 3'-phosphate oligo (51-mer), 32P-labeled, containing a single strand break was used to assess activity by measuring the amount of released 3' phosphate from radio-labeled substrate as analyzed by 20% Urea-PAGE and PhosphorImager. The percent of phosphate release was represented as compared to total radiolabeled substrate (as 100).

Genomic DNA purification and Somatic Expansion Measurement

Genomic DNA (gDNA) was harvested for TRIzol interphase from tissue samples processed for RNA extraction as per manufacturers protocol. Bulk striatal gDNA was subjected to PCR amplification as previously described (Lee et al., 2010) using *Htt* CAG repeat–specific primers. Products were analyzed with ABI GeneMapper. PCR product traces were evaluated for somatic expansion by assessing cluster of peaks that differ by a single CAG repeat unit with the modal allele representing the designated base striatal CAG repeat length. Expansion indexes were calculated as previously described using threshold factors of 0%, 10%, and 20% to distinguish peaks from noise (Lee et al., 2010). Data was collected and analyzed blind.

Statistical Analysis

All data represented as mean ± SEM with a p value of $p<0.05$ considered statistically significant. Analyses were completed in GraphPad Prism software. IR-flourescent intensity values were obtained from western blots using Li-Cor imaging software (Image Studio) and subjected to 2-way ANOVA to assess changes in protein levels with the exception of HMW mHTT analysis which was with Student's unpaired 2-tailed t-test. Statistical analysis was completed of the delta CT (dCT) values obtained from qPCR reactions normalized to *Rplp0*. All 2-way ANOVAs were followed by Tukey's multiple comparisons test. Somatic expansion was analyzed by comparing the expansion indexes with designated peak thresholds between miSafe and miPias1.3 treated R6/2 animals using Student's unpaired 2-tailed t-test.

CHAPTER 5

TABLES

Table 5.1: Summary heat map of Pias1 KD effect on transcriptional readouts in R6/2 and zQ175 heterozygote animals

Gene	R6/2 miPias1	8 Mon. zQ175 Pre-Symp miPias1.3	13.5 Mon. zQ175 Pre-Symp miPias1.3 male	13.5 Mon. zQ175 Pre-Symp miPias1.3 female	13.5 Mon. zQ175 Symp miPias1.3 male	13.5 Mon. zQ175 Symp miPias1.3 female
NeuroD1	No Difference	No Difference	Treatment	Treatment	n/a	n/a
NeuroD2	No Difference	No Difference	Treatment	Treatment	n/a	n/a
Syn1	Treatment	Genotype	Treatment	No Difference	n/a	n/a
Syn2	Treatment	Genotype	Treatment	No Difference	n/a	n/a
Bdnf	Treatment	Genotype	Treatment	No Difference	n/a	n/a
Rnf112	Genotype	Treatment	Treatment	No Difference	No Difference	No Difference
Bcl2l2	Treatment	Treatment	Treatment	Treatment	Genotype	No Difference
Pde4a	No Difference	Treatment	Treatment	No Difference	No Difference	No Difference

(Orange = elevated, blue = decreased)

DISSERTATION CONCLUDING REMARKS

Data presented in this dissertation provides the first mechanistic evidence for PIAS1 in modulating DNA damage repair pathways in the brain. In a normal, aging neuron, cellular processes exist to actively maintain cellular homeostasis and genomic integrity. Under neurodegenerative insults, these processes may be overcompensating or acting inappropriately in an attempt to maintain balance. Eventually they may become overwhelmed by disease insult and these normally neuroprotective mechanisms may tip the scale and become detrimental (Vanni et al., 2019). Therefore, my findings help elucidate how normal cellular processes are altered in HD and lay the foundation for understanding how targeting PIAS1 and DDR may restore balance, genomic integrity, and normalize aberrant transcription.

A long standing question exists as to how PIAS1 and SUMOylation may modulate mHTT solubility and accumulation. I provide preliminary evidence that this accumulation may be modulated through non-covalent interactions through the PIAS1 SIM (Chapter 2). This may occur through binding to HTT itself or from interaction with a highly SUMOylated complex. However, while promising, the use of transient overexpression constructs resulted in promoter-driven artifacts that precluded final interpretation. Moving forward, the generation of endogenously edited PIAS1 mutations will allow for investigation into the specific mechanistic contributions of different functional domains of PIAS1 towards protein accumulation and other readouts, without the impact of overexpression promoters.

Pias1 KD previously reduced accumulation of an insoluble HMW mHTT species in the rapidly progressing, symptomatic R6/2 mouse model (Ochaba et al., 2016). This species accumulates over time in R6/2 mice and tracks with behavioral deficits ((Morozko et al., 2018), Chapter 1). Interestingly, in zQ175 mice, Pias1 KD did not consistently modulate accumulation of this species which similarly accumulates over time (Chapter 4). In replicate R6/2 studies, baseline readouts differed but PIAS1 KD also did not have an effect on HMW species (Chapter 5). This was unexpected but may in part have been due to the lack of insoluble Pias1 protein accumulation at baseline or modulation of insoluble Pias1 with miPias1.3 treatment in these mice. While the exact function of insoluble Pias1 versus soluble Pias1 is unknown, these differences at baseline suggest that there were fundamentally different molecular processes utilizing Pias1 in these current animal cohorts and may, in part, explain the lack of impact on accumulation of insoluble HMW mHTT protein and HD-associated behavioral deficits. This functional difference may be related to Pias1's role in mediating inflammatory pathways since reduction in insoluble Pias1 previously corresponded to normalized inflammatory markers in R6/2 mice (Ochaba et al., 2016).

PIAS1 functions to counterbalance inflammatory cascades by inhibiting STAT1 and binding to NfkB in the nucleus. Indeed, reduction of Pias1 in WT animals showed enrichment for inflammatory and cellular defense related mechanisms in the brain at the mRNA level (Chapter 4). However, this was not observed in HD zQ175 animals. Further, repeating our previous study in R6/2 mice, animals displayed inherently different baseline inflammatory profiles between cohorts based on levels of NfkB, Il-6, and insoluble Pias1 at baseline

(Chapter 5). This raises the possibility that Pias1 may have several and separable functions in the brain, which may be differentially accessed depending on the pre-existing molecular landscape. In neurodegenerative diseases, neuroinflammation may be an integral pathological process that drives disease progression. Therefore, targeting PIAS1 to modulate immune responses may be therapeutically beneficial in that way. However, this landscape may be influenced in part by genetic background, the surrounding environment, and diet. There is an emerging awareness in the neurodegeneration field that environment may impact observed phenotypic differences.

Recent insights have been gained into the link between inflammatory diseases, including neurodegenerative diseases with neuroinflammatory components, and microbiome dysbiosis (Keshavarzian et al., 2015; Sherwin et al., 2018). Several pathways exist between the gastrointestinal tract and the nervous systems, providing an infrastructure for communication or the exchange of signaling molecules between the two (Bhattacharjee and Lukiw, 2013). The vascular system can also serve as a highway to deliver neurotoxic bacterial biproducts to the brain through the blood brain barrier. Therefore, microbiome dysbiosis may result in production of endotoxins (i.e. LPS) which circulate through the blood to reach the brain, triggering glial activation and protein aggregation (Castillo et al., 2019). These changes in microbiome composition may in part be due vivarium differences as laboratory mouse microbiome composition can vary based on environment (Hufeldt et al., 2010). Since dysbiosis has been related to neurodegenerative diseases (Castillo et al., 2019), different environments between the timing of experiments may have influenced the neuroinflammatory profile of individual animal cohorts. For future studies, it may be

beneficial to collect intestinal tissue or fecal matter at time of sacrifice to track differences in microbiome composition that could influence behavioral or molecular readouts.

While levels of insoluble Pias1 were unchanged with KD in zQ175 mice, and accumulation of HMW mHTT was not affected, soluble levels of Pias1 protein as well as *Pias1* transcript levels were significantly reduced. This corresponded with profound effects on transcriptional networks in mouse striatum (Chapter 4). Therefore, it is possible that modulating levels of soluble Pias1 specifically revealed additional molecular functions of Pias1 in the brain that had not been previously observed. However, the functional consequences of modulating these genes remain to be evaluated. At older ages, these genes were largely related to neuronal health and synaptic function. These genes could be affected by Pias1 mediated SUMOylation of transcription factors, thus altering their activity. Binding of transcription factors to transcription start sites with Pias1 KD can be assessed using chromatin-immunoprecipitation assays. Alternatively, Pias1 may be having a direct impact on SUMOylation of synaptic proteins. Assessing the SUMOylation status of synaptic compartments may help elucidate this direct effect. This is currently being pursued through use of SUMO-enrichment from striatum and striatal synaptosomes followed by proteomic profiling with and without Pias1 KD in HD animals. High-resolution microscopy will also help determine the structural impact of specific synaptic proteins with Pias1 KD. Finally, differentiated MSNs are electrophysiologically active (Telezhkin et al., 2016). Completing electrophysiology on these cells with PIAS1 KD, coupled with slice cultures from HD mice with Pias1 KD, could further elucidate the functional consequences of modulating these synaptic-related transcriptional networks in HD neurons and brain.

The most consistently regulated gene with Pias1 KD was *Bcl2l2,* part of the Bcl-2 family. The pro-apoptotic protein Bax is also a member of this family but instead contributes towards neuronal death under numerous sources of stress including excitoxic, oxidative, and trophic deprivation stressors (D'Orsi et al., 2012; Deckwerth et al., 1996). Seeing as upstream regulator ATM mediates DNA damage response as well as Bax-mediated pro-death pathways in conjunction with p53, it is possible that hyperactivation of ATM signaling due to sustained DNA damage in the HD brain might be triggering Bax mediated pro-death pathways (Chong et al., 2000; Gao et al., 2019; Gilman et al., 2003; Herzog et al., 1998; Martin and Liu, 2002). Bcl2l2/Bcl-w is a pro-survival bcl-2 family member, counter balancing Bax mediated mitochondrial malfunction and cytochrome c release (Youle and Strasser, 2008). With the profound impact Pias1 KD had on *Bcl2l2* transcript levels in zQ175 and R6/2 mice, it is possible that reducing Pias1 is supporting pro-survival pathways by increasing *Bcl2l2* expression. Several experiments can be carried out to assess this possibility. First, assessment of protein balance between Bax and Bcl2l2 protein levels will determine pro-survival balance in neurons with Pias1 KD. As the balance between pro-death and pro-life Bcl-2 family members is often used as a marker of apoptotic potential (Kilbride and Prehn, 2013; Korsmeyer, 1999; Oltvai et al., 1993), determining if the observed transcriptional effect of Pias1 KD on *Bcl2l2* affects protein level balance may further support a pro-survival mechanism. Second, levels of cytochrome c release can be assessed either by western blot or by immunofluorescent staining. Increased levels of cytochrome c could indicate a shift towards pro-death pathways. Third, experiments can assess mitochondrial integrity or malfunction can also be carried out. An ATP assay can be completed on neuronal tissue extract. Alterations in ATP production could indicate

mitochondrial malfunction, suggesting a deficit in mitochondrial integrity. Together, these experiments would help determine if Pias1 is mediating neuronal survival by regulating the bcl-2 family balance and dynamics.

Excitingly, reduction of PIAS1 rescued mHTT-impaired enzymatic activity of the end-processing enzyme PNKP in several models of HD (Chapters 3-5). This was likely due PIAS1's role as a SUMO E3 ligase for PNKP as I have now shown that PNKP is SUMOylated by PIAS1 (Chapter 3). The direct functional consequence of PNKP SUMOylation remains to be elucidated. Since KD of PIAS1 restored activity, it can be hypothesized that PNKP SUMOylation was preventing activity. This could be either by preventing activating phosphorylation of PNKP (Segal-Raz et al., 2011; Zolner et al., 2011) or by serving as an eviction signal for PNKP similar to other DDR repair factors that are PIAS1 SUMO substrates (Gibbs-Seymour et al., 2015; Luo et al., 2012). To investigate this, several experiments are currently underway. First, assessment of *in vivo* PNKP SUMOylation is currently being assessed. While endogenously SUMOylated PNKP was detected in human neurons, detecting PNKP SUMOylation in the complex environment of the brain will provide further evidence that PNKP SUMOylation may be modulating activity. Second, the target lysine(s) for PNKP SUMOylation will be identified. This will then allow for follow-up activity assays to assess the functional contribution of PNKP SUMOylation towards enzymatic activity. Third, as PNKP is phosphorylated to induce enzymatic activity (Segal-Raz et al., 2011; Zolner et al., 2011), the interplay and relationship between phosphorylation and SUMOylation will be assessed. This will be completed by assessing SUMOylation of non-phosphorylatable PNKP compared to phosphorylated PNKP. Fourth,

PNKP will be assessed for STUbL activity to determine if SUMOylation is serving as an eviction signal similar to what has previously been seen for other DDR proteins. The STUbL RNF4 is a likely candidate as it has been shown to work in close harmony with PIAS1 within repair processes (Gibbs-Seymour et al., 2015; Luo et al., 2012). Experiments knocking-down RNF4 will be completed to assess impact on PNKP SUMOylation, recruitment to repair sites, and clearance. These experiments will greatly aid in elucidating the functional consequences of PNKP SUMOylation.

Decreased PNKP activity previously corresponded to decreased genomic integrity of actively transcribing neuronal genes (Gao et al., 2019). With Pias1 KD in zQ175 mice, aberrant transcriptional profiles were normalized and in R6/2 mice, the CAG-repeat was moderately stabilized. This supports the hypothesis that facilitating appropriate repair of unstable genes, or genes obtaining DNA lesions arising from active transcription, may be neuroprotective. However, due to the rapidly progressing nature of the R6/2 mouse model, the physiological consequences of preventing somatic repeat expansion by only a few repeats remained elusive. Therefore, to understand the long-term contribution of PIAS1 towards stabilizing the *HTT* CAG-repeat, somatic repeat expansion will be assessed in knock-in HD animal models to compare to overall molecular landscape. For zQ175 mice, long-read sequencing technologies will be utilized as the length of the CAG-repeat in these animals is too long and unstable to assess expansion by conventional methods. Follow-up studies will include the use of PacBio™ Single Molecule, Real-Time Sequencing technology which allows for highly accurate, targeted sequencing of long regions including those of low complexity such as repeat expansions with high GC content (e.g. CAG-repeats). Further,

genomic integrity of genes normalized by pre-symptomatic Pias1 knock-down in zQ175 is currently being assessed by long-amplification qPCR. These genes are primarily synaptic and suggest that neuronal function may, in part, be modulated by maintaining genomic integrity of key genes required for neuronal function. These genes are likely accruing damage from active transcription and therefore may be overexpressed in a compensatory manner in an attempt to maintain function. With Pias1 KD serving to reduce this apparent, aberrant transcriptional profile in zQ175 mice, facilitating Pnkp activity may be promoting repair similar to what was observed in HD human neurons. Therefore, experiments directly assessing genomic integrity of several Pias1 KD-modulated genes are currently underway. Together, these studies will further establish how PIAS1 may be maintaining genomic stability and thereby neuronal function *in vivo*.

Overall, data presented in this dissertation sheds light on functional contributions of Pias1 towards HD pathogenesis in several different models of disease. These functional contributions may in part be modulated by baseline biochemical and inflammatory profiles and strongly suggest an ideal pre-symptomatic window for targeting HD-associated molecular readouts. Rescued activity of DNA damage repair processes and enhanced genomic integrity with PIAS1 KD defines a new function for PIAS1 in neurons and the brain. Given that modulating Pias1 at different disease stages differentially impacted molecular readouts, this data further highlights the importance of understanding the temporal effects on maintaining proteostatic balance that is perturbed by neurodegenerative processes.

REFERENCES

Abbotts, R., and Wilson, D.M., 3rd (2017). Coordination of DNA single strand break repair. Free radical biology & medicine 107, 228-244.

Abeywardana, T., and Pratt, M.R. (2015). Extent of inhibition of alpha-synuclein aggregation in vitro by SUMOylation is conjugation site- and SUMO isoform-selective. Biochemistry 54, 959-961.

Abner, C.W., and McKinnon, P.J. (2004). The DNA double-strand break response in the nervous system. DNA repair 3, 1141-1147.

Acharya, S., Foster, P.L., Brooks, P., and Fishel, R. (2003). The coordinated functions of the E. coli MutS and MutL proteins in mismatch repair. Molecular cell 12, 233-246.

Achour, M., Le Gras, S., Keime, C., Parmentier, F., Lejeune, F.X., Boutillier, A.L., Neri, C., Davidson, I., and Merienne, K. (2015). Neuronal identity genes regulated by super-enhancers are preferentially down-regulated in the striatum of Huntington's disease mice. Human molecular genetics 24, 3481-3496.

Aguilera, A., and Gomez-Gonzalez, B. (2017). DNA-RNA hybrids: the risks of DNA breakage during transcription. Nature structural & molecular biology 24, 439-443.

Akhtar, R.S., Ness, J.M., and Roth, K.A. (2004). Bcl-2 family regulation of neuronal development and neurodegeneration. Biochimica et biophysica acta 1644, 189-203.

Akita, M., Tak, Y.S., Shimura, T., Matsumoto, S., Okuda-Shimizu, Y., Shimizu, Y., Nishi, R., Saitoh, H., Iwai, S., Mori, T.*, et al.* (2015). SUMOylation of xeroderma pigmentosum group C protein regulates DNA damage recognition during nucleotide excision repair. Scientific reports 5, 10984.

Alagu, J., Itahana, Y., Sim, F., Chao, S.H., Bi, X., and Itahana, K. (2018). Tumor Suppressor p14ARF Enhances IFN-gamma-Activated Immune Response by Inhibiting PIAS1 via SUMOylation. J Immunol 201, 451-464.

Altmann, T., and Gennery, A.R. (2016). DNA ligase IV syndrome; a review. Orphanet journal of rare diseases 11, 137.

Anamika, and Spyracopoulos, L. (2016). Molecular Basis for Phosphorylation-dependent SUMO Recognition by the DNA Repair Protein RAP80. The Journal of biological chemistry 291, 4417-4428.

Anderson, D.B., Zanella, C.A., Henley, J.M., and Cimarosti, H. (2017). Sumoylation: Implications for Neurodegenerative Diseases. Advances in experimental medicine and biology 963, 261-281.

Anilkumar, U., and Prehn, J.H. (2014). Anti-apoptotic BCL-2 family proteins in acute neural injury. Frontiers in cellular neuroscience 8, 281.

Aouacheria, A., Baghdiguian, S., Lamb, H.M., Huska, J.D., Pineda, F.J., and Hardwick, J.M. (2017). Connecting mitochondrial dynamics and life-or-death events via Bcl-2 family proteins. Neurochemistry international 109, 141-161.

Arndt, J.R., Chaibva, M., and Legleiter, J. (2015). The emerging role of the first 17 amino acids of huntingtin in Huntington's disease. Biomolecular concepts 6, 33-46.

Au, K.G., Welsh, K., and Modrich, P. (1992). Initiation of methyl-directed mismatch repair. The Journal of biological chemistry 267, 12142-12148.

Barzilai, A. (2007). The contribution of the DNA damage response to neuronal viability. Antioxidants & redox signaling 9, 211-218.

Bates, G., Harper, P.S., and Jones, L. (2002). Huntington's disease, 3rd edn (Oxford ; New York: Oxford University Press).
Beerens, N., Hoeijmakers, J.H., Kanaar, R., Vermeulen, W., and Wyman, C. (2005). The CSB protein actively wraps DNA. The Journal of biological chemistry 280, 4722-4729.
Benn, C.L., Sun, T., Sadri-Vakili, G., McFarland, K.N., DiRocco, D.P., Yohrling, G.J., Clark, T.W., Bouzou, B., and Cha, J.H. (2008). Huntingtin modulates transcription, occupies gene promoters in vivo, and binds directly to DNA in a polyglutamine-dependent manner. The Journal of neuroscience : the official journal of the Society for Neuroscience 28, 10720-10733.
Benson, M.D., Li, Q.J., Kieckhafer, K., Dudek, D., Whorton, M.R., Sunahara, R.K., Iniguez-Lluhi, J.A., and Martens, J.R. (2007). SUMO modification regulates inactivation of the voltage-gated potassium channel Kv1.5. Proceedings of the National Academy of Sciences of the United States of America 104, 1805-1810.
Bettencourt, C., Hensman-Moss, D., Flower, M., Wiethoff, S., Brice, A., Goizet, C., Stevanin, G., Koutsis, G., Karadima, G., Panas, M.*, et al.* (2016). DNA repair pathways underlie a common genetic mechanism modulating onset in polyglutamine diseases. Annals of neurology 79, 983-990.
Bhattacharjee, S., and Lukiw, W.J. (2013). Alzheimer's disease and the microbiome. Frontiers in cellular neuroscience 7, 153.
Bibb, J.A., Yan, Z., Svenningsson, P., Snyder, G.L., Pieribone, V.A., Horiuchi, A., Nairn, A.C., Messer, A., and Greengard, P. (2000). Severe deficiencies in dopamine signaling in presymptomatic Huntington's disease mice. Proceedings of the National Academy of Sciences of the United States of America 97, 6809-6814.
Bogdanov, M.B., Andreassen, O.A., Dedeoglu, A., Ferrante, R.J., and Beal, M.F. (2001). Increased oxidative damage to DNA in a transgenic mouse model of Huntington's disease. Journal of neurochemistry 79, 1246-1249.
Bologna, S., Altmannova, V., Valtorta, E., Koenig, C., Liberali, P., Gentili, C., Anrather, D., Ammerer, G., Pelkmans, L., Krejci, L., and Ferrari, S. (2015). Sumoylation regulates EXO1 stability and processing of DNA damage. Cell Cycle 14, 2439-2450.
Bonnet, J., Devys, D., and Tora, L. (2014). Histone H2B ubiquitination: signaling not scrapping. Drug discovery today Technologies 12, e19-27.
Borden, K.L. (2002). Pondering the promyelocytic leukemia protein (PML) puzzle: possible functions for PML nuclear bodies. Molecular and cellular biology 22, 5259-5269.
Bossis, G., Malnou, C.E., Farras, R., Andermarcher, E., Hipskind, R., Rodriguez, M., Schmidt, D., Muller, S., Jariel-Encontre, I., and Piechaczyk, M. (2005). Down-regulation of c-Fos/c-Jun AP-1 dimer activity by sumoylation. Molecular and cellular biology 25, 6964-6979.
Bramham, C.R., and Messaoudi, E. (2005). BDNF function in adult synaptic plasticity: the synaptic consolidation hypothesis. Progress in neurobiology 76, 99-125.
Bras, J., Alonso, I., Barbot, C., Costa, M.M., Darwent, L., Orme, T., Sequeiros, J., Hardy, J., Coutinho, P., and Guerreiro, R. (2015). Mutations in PNKP cause recessive ataxia with oculomotor apraxia type 4. American journal of human genetics 96, 474-479.
Brooks, S.P., and Dunnett, S.B. (2015). Mouse Models of Huntington's Disease. Current topics in behavioral neurosciences 22, 101-133.
Brown, E.J., and Baltimore, D. (2003). Essential and dispensable roles of ATR in cell cycle arrest and genome maintenance. Genes & development 17, 615-628.

Browne, S.E., Bowling, A.C., MacGarvey, U., Baik, M.J., Berger, S.C., Muqit, M.M., Bird, E.D., and Beal, M.F. (1997). Oxidative damage and metabolic dysfunction in Huntington's disease: selective vulnerability of the basal ganglia. Annals of neurology 41, 646-653.

Bulley, S.J., Drew, C.J., and Morton, A.J. (2012). Direct Visualisation of Abnormal Dendritic Spine Morphology in the Hippocampus of the R6/2 Transgenic Mouse Model of Huntington's Disease. Journal of Huntington's disease 1, 267-273.

Bunting, S.F., Callen, E., Wong, N., Chen, H.T., Polato, F., Gunn, A., Bothmer, A., Feldhahn, N., Fernandez-Capetillo, O., Cao, L.*, et al.* (2010). 53BP1 inhibits homologous recombination in Brca1-deficient cells by blocking resection of DNA breaks. Cell 141, 243-254.

Cappadocia, L., and Lima, C.D. (2017). Ubiquitin-like Protein Conjugation: Structures, Chemistry, and Mechanism. Chemical reviews.

Cappadocia, L., Mascle, X.H., Bourdeau, V., Tremblay-Belzile, S., Chaker-Margot, M., Lussier-Price, M., Wada, J., Sakaguchi, K., Aubry, M., Ferbeyre, G., and Omichinski, J.G. (2015). Structural and functional characterization of the phosphorylation-dependent interaction between PML and SUMO1. Structure 23, 126-138.

Carter, R.J., Lione, L.A., Humby, T., Mangiarini, L., Mahal, A., Bates, G.P., Dunnett, S.B., and Morton, A.J. (1999). Characterization of progressive motor deficits in mice transgenic for the human Huntington's disease mutation. The Journal of neuroscience : the official journal of the Society for Neuroscience 19, 3248-3257.

Carty, N., Berson, N., Tillack, K., Thiede, C., Scholz, D., Kottig, K., Sedaghat, Y., Gabrysiak, C., Yohrling, G., von der Kammer, H.*, et al.* (2015). Characterization of HTT inclusion size, location, and timing in the zQ175 mouse model of Huntington's disease: an in vivo high-content imaging study. PloS one 10, e0123527.

Castillo, X., Castro-Obregon, S., Gutierrez-Becker, B., Gutierrez-Ospina, G., Karalis, N., Khalil, A.A., Lopez-Noguerola, J.S., Rodriguez, L.L., Martinez-Martinez, E., Perez-Cruz, C.*, et al.* (2019). Re-thinking the Etiological Framework of Neurodegeneration. Frontiers in neuroscience 13, 728.

Ceccaldi, R., Sarangi, P., and D'Andrea, A.D. (2016). The Fanconi anaemia pathway: new players and new functions. Nature reviews Molecular cell biology 17, 337-349.

Cha, J.H. (2007). Transcriptional signatures in Huntington's disease. Progress in neurobiology 83, 228-248.

Cha, J.H., Kosinski, C.M., Kerner, J.A., Alsdorf, S.A., Mangiarini, L., Davies, S.W., Penney, J.B., Bates, G.P., and Young, A.B. (1998). Altered brain neurotransmitter receptors in transgenic mice expressing a portion of an abnormal human huntington disease gene. Proceedings of the National Academy of Sciences of the United States of America 95, 6480-6485.

Chabrier, M.A., Cheng, D., Castello, N.A., Green, K.N., and LaFerla, F.M. (2014). Synergistic effects of amyloid-beta and wild-type human tau on dendritic spine loss in a floxed double transgenic model of Alzheimer's disease. Neurobiology of disease 64, 107-117.

Chakraborty, A., Tapryal, N., Venkova, T., Horikoshi, N., Pandita, R.K., Sarker, A.H., Sarkar, P.S., Pandita, T.K., and Hazra, T.K. (2016). Classical non-homologous end-joining pathway utilizes nascent RNA for error-free double-strand break repair of transcribed genes. Nature communications 7, 13049.

Chakraborty, A., Wakamiya, M., Venkova-Canova, T., Pandita, R.K., Aguilera-Aguirre, L., Sarker, A.H., Singh, D.K., Hosoki, K., Wood, T.G., Sharma, G.*, et al.* (2015). Neil2-null Mice Accumulate Oxidized DNA Bases in the Transcriptionally Active Sequences of the Genome and Are Susceptible to Innate Inflammation. The Journal of biological chemistry 290, 24636-24648.

Chamberlain, S.E., Gonzalez-Gonzalez, I.M., Wilkinson, K.A., Konopacki, F.A., Kantamneni, S., Henley, J.M., and Mellor, J.R. (2012). SUMOylation and phosphorylation of GluK2 regulate kainate receptor trafficking and synaptic plasticity. Nature neuroscience 15, 845-852.

Chao, H.W., Hong, C.J., Huang, T.N., Lin, Y.L., and Hsueh, Y.P. (2008). SUMOylation of the MAGUK protein CASK regulates dendritic spinogenesis. The Journal of cell biology 182, 141-155.

Chappell, C., Hanakahi, L.A., Karimi-Busheri, F., Weinfeld, M., and West, S.C. (2002). Involvement of human polynucleotide kinase in double-strand break repair by non-homologous end joining. The EMBO journal 21, 2827-2832.

Chechlacz, M., Vemuri, M.C., and Naegele, J.R. (2001). Role of DNA-dependent protein kinase in neuronal survival. Journal of neurochemistry 78, 141-154.

Chen, S., Yu, C., Rong, L., Li, C.H., Qin, X., Ryu, H., and Park, H. (2018). Altered Synaptic Vesicle Release and Ca(2+) Influx at Single Presynaptic Terminals of Cortical Neurons in a Knock-in Mouse Model of Huntington's Disease. Frontiers in molecular neuroscience 11, 478.

Chen, Y.C., Hsu, W.L., Ma, Y.L., Tai, D.J., and Lee, E.H. (2014). CREB SUMOylation by the E3 ligase PIAS1 enhances spatial memory. The Journal of neuroscience : the official journal of the Society for Neuroscience 34, 9574-9589.

Cheng, J., Huang, M., Zhu, Y., Xin, Y.J., Zhao, Y.K., Huang, J., Yu, J.X., Zhou, W.H., and Qiu, Z. (2014). SUMOylation of MeCP2 is essential for transcriptional repression and hippocampal synapse development. Journal of neurochemistry 128, 798-806.

Chinta, S.J., Woods, G., Rane, A., Demaria, M., Campisi, J., and Andersen, J.K. (2015). Cellular senescence and the aging brain. Experimental gerontology 68, 3-7.

Chiruvella, K.K., Liang, Z., and Wilson, T.E. (2013). Repair of double-strand breaks by end joining. Cold Spring Harbor perspectives in biology 5, a012757.

Choi, J.H., Park, J.Y., Park, S.P., Lee, H., Han, S., Park, K.H., and Suh, Y.H. (2016). Regulation of mGluR7 trafficking by SUMOylation in neurons. Neuropharmacology 102, 229-235.

Chong, M.J., Murray, M.R., Gosink, E.C., Russell, H.R., Srinivasan, A., Kapsetaki, M., Korsmeyer, S.J., and McKinnon, P.J. (2000). Atm and Bax cooperate in ionizing radiation-induced apoptosis in the central nervous system. Proceedings of the National Academy of Sciences of the United States of America 97, 889-894.

Chow, H.M., and Herrup, K. (2015). Genomic integrity and the ageing brain. Nature reviews Neuroscience 16, 672-684.

Choy, K.R., and Watters, D.J. (2018). Neurodegeneration in ataxia-telangiectasia: Multiple roles of ATM kinase in cellular homeostasis. Developmental dynamics : an official publication of the American Association of Anatomists 247, 33-46.

Chrzanowska, K.H., Gregorek, H., Dembowska-Baginska, B., Kalina, M.A., and Digweed, M. (2012). Nijmegen breakage syndrome (NBS). Orphanet journal of rare diseases 7, 13.

Consortium, H.i. (2017). Developmental alterations in Huntington's disease neural cells and pharmacological rescue in cells and mice. Nature neuroscience 20, 648-660.
Constanzo, J.D., Deng, M., Rindhe, S., Tang, K.J., Zhang, C.C., and Scaglioni, P.P. (2016). Pias1 is essential for erythroid and vascular development in the mouse embryo. Developmental biology 415, 98-110.
Courchesne, S.L., Karch, C., Pazyra-Murphy, M.F., and Segal, R.A. (2011). Sensory neuropathy attributable to loss of Bcl-w. The Journal of neuroscience : the official journal of the Society for Neuroscience 31, 1624-1634.
Craig, T.J., Anderson, D., Evans, A.J., Girach, F., and Henley, J.M. (2015). SUMOylation of Syntaxin1A regulates presynaptic endocytosis. Scientific reports 5, 17669.
Craig, T.J., Jaafari, N., Petrovic, M.M., Jacobs, S.C., Rubin, P.P., Mellor, J.R., and Henley, J.M. (2012). Homeostatic synaptic scaling is regulated by protein SUMOylation. The Journal of biological chemistry 287, 22781-22788.
Crouch, J.D., and Brosh, R.M., Jr. (2017). Mechanistic and biological considerations of oxidatively damaged DNA for helicase-dependent pathways of nucleic acid metabolism. Free radical biology & medicine 107, 245-257.
D'Orsi, B., Bonner, H., Tuffy, L.P., Dussmann, H., Woods, I., Courtney, M.J., Ward, M.W., and Prehn, J.H. (2012). Calpains are downstream effectors of bax-dependent excitotoxic apoptosis. The Journal of neuroscience : the official journal of the Society for Neuroscience 32, 1847-1858.
Dadke, S., Cotteret, S., Yip, S.C., Jaffer, Z.M., Haj, F., Ivanov, A., Rauscher, F., 3rd, Shuai, K., Ng, T., Neel, B.G., and Chernoff, J. (2007). Regulation of protein tyrosine phosphatase 1B by sumoylation. Nature cell biology 9, 80-85.
Dai, X.Q., Kolic, J., Marchi, P., Sipione, S., and Macdonald, P.E. (2009). SUMOylation regulates Kv2.1 and modulates pancreatic beta-cell excitability. Journal of cell science 122, 775-779.
Danielsen, J.R., Povlsen, L.K., Villumsen, B.H., Streicher, W., Nilsson, J., Wikstrom, M., Bekker-Jensen, S., and Mailand, N. (2012). DNA damage-inducible SUMOylation of HERC2 promotes RNF8 binding via a novel SUMO-binding Zinc finger. The Journal of cell biology 197, 179-187.
Datta, A., and Brosh, R.M., Jr. (2019). Holding All the Cards-How Fanconi Anemia Proteins Deal with Replication Stress and Preserve Genomic Stability. Genes 10.
Davies, S.W., Turmaine, M., Cozens, B.A., DiFiglia, M., Sharp, A.H., Ross, C.A., Scherzinger, E., Wanker, E.E., Mangiarini, L., and Bates, G.P. (1997). Formation of neuronal intranuclear inclusions underlies the neurological dysfunction in mice transgenic for the HD mutation. Cell 90, 537-548.
Deckwerth, T.L., Elliott, J.L., Knudson, C.M., Johnson, E.M., Jr., Snider, W.D., and Korsmeyer, S.J. (1996). BAX is required for neuronal death after trophic factor deprivation and during development. Neuron 17, 401-411.
Despras, E., Sittewelle, M., Pouvelle, C., Delrieu, N., Cordonnier, A.M., and Kannouche, P.L. (2016). Rad18-dependent SUMOylation of human specialized DNA polymerase eta is required to prevent under-replicated DNA. Nature communications 7, 13326.
Dewson, G., and Kluck, R.M. (2009). Mechanisms by which Bak and Bax permeabilise mitochondria during apoptosis. Journal of cell science 122, 2801-2808.

DiFiglia, M., Sapp, E., Chase, K.O., Davies, S.W., Bates, G.P., Vonsattel, J.P., and Aronin, N. (1997). Aggregation of huntingtin in neuronal intranuclear inclusions and dystrophic neurites in brain. Science 277, 1990-1993.

DiGiovanni, L.F., Mocle, A.J., Xia, J., and Truant, R. (2016). Huntingtin N17 domain is a reactive oxygen species sensor regulating huntingtin phosphorylation and localization. Human molecular genetics 25, 3937-3945.

Dorval, V., and Fraser, P.E. (2007). SUMO on the road to neurodegeneration. Biochimica et biophysica acta 1773, 694-706.

Dou, H., Huang, C., Singh, M., Carpenter, P.B., and Yeh, E.T. (2010). Regulation of DNA repair through deSUMOylation and SUMOylation of replication protein A complex. Molecular cell 39, 333-345.

Dragatsis, I., Levine, M.S., and Zeitlin, S. (2000). Inactivation of Hdh in the brain and testis results in progressive neurodegeneration and sterility in mice. Nature genetics 26, 300-306.

Dragileva, E., Hendricks, A., Teed, A., Gillis, T., Lopez, E.T., Friedberg, E.C., Kucherlapati, R., Edelmann, W., Lunetta, K.L., MacDonald, M.E., and Wheeler, V.C. (2009). Intergenerational and striatal CAG repeat instability in Huntington's disease knock-in mice involve different DNA repair genes. Neurobiology of disease 33, 37-47.

Dutting, E., Schroder-Kress, N., Sticht, H., and Enz, R. (2011). SUMO E3 ligases are expressed in the retina and regulate SUMOylation of the metabotropic glutamate receptor 8b. The Biochemical journal 435, 365-371.

Eden, E., Navon, R., Steinfeld, I., Lipson, D., and Yakhini, Z. (2009). GOrilla: a tool for discovery and visualization of enriched GO terms in ranked gene lists. BMC bioinformatics 10, 48.

Ehrlich, M.E., Conti, L., Toselli, M., Taglietti, L., Fiorillo, E., Taglietti, V., Ivkovic, S., Guinea, B., Tranberg, A., Sipione, S.*, et al.* (2001). ST14A cells have properties of a medium-size spiny neuron. Experimental neurology 167, 215-226.

Eisele, Y.S., Monteiro, C., Fearns, C., Encalada, S.E., Wiseman, R.L., Powers, E.T., and Kelly, J.W. (2015). Targeting protein aggregation for the treatment of degenerative diseases. Nature reviews Drug discovery 14, 759-780.

El-Khamisy, S.F., Katyal, S., Patel, P., Ju, L., McKinnon, P.J., and Caldecott, K.W. (2009). Synergistic decrease of DNA single-strand break repair rates in mouse neural cells lacking both Tdp1 and aprataxin. DNA repair 8, 760-766.

Enokido, Y., Tamura, T., Ito, H., Arumughan, A., Komuro, A., Shiwaku, H., Sone, M., Foulle, R., Sawada, H., Ishiguro, H.*, et al.* (2010). Mutant huntingtin impairs Ku70-mediated DNA repair. The Journal of cell biology 189, 425-443.

Estruch, S.B., Graham, S.A., Deriziotis, P., and Fisher, S.E. (2016). The language-related transcription factor FOXP2 is post-translationally modified with small ubiquitin-like modifiers. Scientific reports 6, 20911.

Fei, E., Jia, N., Yan, M., Ying, Z., Sun, Q., Wang, H., Zhang, T., Ma, X., Ding, H., Yao, X.*, et al.* (2006). SUMO-1 modification increases human SOD1 stability and aggregation. Biochemical and biophysical research communications 347, 406-412.

Feligioni, M., Nishimune, A., and Henley, J.M. (2009). Protein SUMOylation modulates calcium influx and glutamate release from presynaptic terminals. The European journal of neuroscience 29, 1348-1356.

Fernandez-Fernandez, M.R., Ferrer, I., and Lucas, J.J. (2011). Impaired ATF6alpha processing, decreased Rheb and neuronal cell cycle re-entry in Huntington's disease. Neurobiology of disease 41, 23-32.

Ferrer, I., Goutan, E., Marin, C., Rey, M.J., and Ribalta, T. (2000). Brain-derived neurotrophic factor in Huntington disease. Brain research 866, 257-261.

Fielder, E., von Zglinicki, T., and Jurk, D. (2017). The DNA Damage Response in Neurons: Die by Apoptosis or Survive in a Senescence-Like State? Journal of Alzheimer's disease : JAD 60, S107-S131.

Flower, M., Lomeikaite, V., Ciosi, M., Cumming, S., Morales, F., Lo, K., Hensman Moss, D., Jones, L., Holmans, P., Monckton, D.G., and Tabrizi, S.J. (2019). MSH3 modifies somatic instability and disease severity in Huntington's and myotonic dystrophy type 1. Brain : a journal of neurology.

Folch, J., Junyent, F., Verdaguer, E., Auladell, C., Pizarro, J.G., Beas-Zarate, C., Pallas, M., and Camins, A. (2012). Role of cell cycle re-entry in neurons: a common apoptotic mechanism of neuronal cell death. Neurotoxicity research 22, 195-207.

Foran, E., Bogush, A., Goffredo, M., Roncaglia, P., Gustincich, S., Pasinelli, P., and Trotti, D. (2011). Motor neuron impairment mediated by a sumoylated fragment of the glial glutamate transporter EAAT2. Glia 59, 1719-1731.

Foran, E., Rosenblum, L., Bogush, A., Pasinelli, P., and Trotti, D. (2014). Sumoylation of the astroglial glutamate transporter EAAT2 governs its intracellular compartmentalization. Glia 62, 1241-1253.

Franich, N.R., Basso, M., Andre, E.A., Ochaba, J., Kumar, A., Thein, S., Fote, G., Kachemov, M., Lau, A.L., Yeung, S.Y.*, et al.* (2018). Striatal Mutant Huntingtin Protein Levels Decline with Age in Homozygous Huntington's Disease Knock-In Mouse Models. Journal of Huntington's disease 7, 137-150.

Frank, K.M., Sharpless, N.E., Gao, Y., Sekiguchi, J.M., Ferguson, D.O., Zhu, C., Manis, J.P., Horner, J., DePinho, R.A., and Alt, F.W. (2000). DNA ligase IV deficiency in mice leads to defective neurogenesis and embryonic lethality via the p53 pathway. Molecular cell 5, 993-1002.

Frappart, P.O., Tong, W.M., Demuth, I., Radovanovic, I., Herceg, Z., Aguzzi, A., Digweed, M., and Wang, Z.Q. (2005). An essential function for NBS1 in the prevention of ataxia and cerebellar defects. Nature medicine 11, 538-544.

Freudenreich, C.H. (2018). R-loops: targets for nuclease cleavage and repeat instability. Current genetics 64, 789-794.

Galanty, Y., Belotserkovskaya, R., Coates, J., and Jackson, S.P. (2012). RNF4, a SUMO-targeted ubiquitin E3 ligase, promotes DNA double-strand break repair. Genes & development 26, 1179-1195.

Galanty, Y., Belotserkovskaya, R., Coates, J., Polo, S., Miller, K.M., and Jackson, S.P. (2009). Mammalian SUMO E3-ligases PIAS1 and PIAS4 promote responses to DNA double-strand breaks. Nature 462, 935-939.

Gao, R., Chakraborty, A., Geater, C., Pradhan, S., Gordon, K.L., Snowden, J., Yuan, S., Dickey, A.S., Choudhary, S., Ashizawa, T.*, et al.* (2019). Mutant huntingtin impairs PNKP and ATXN3, disrupting DNA repair and transcription. eLife 8.

Garcia-Rubio, M.L., Perez-Calero, C., Barroso, S.I., Tumini, E., Herrera-Moyano, E., Rosado, I.V., and Aguilera, A. (2015). The Fanconi Anemia Pathway Protects Genome Integrity from R-loops. PLoS genetics 11, e1005674.

Gareau, J.R., and Lima, C.D. (2010). The SUMO pathway: emerging mechanisms that shape specificity, conjugation and recognition. Nature reviews Molecular cell biology 11, 861-871.

Gasset-Rosa, F., Chillon-Marinas, C., Goginashvili, A., Atwal, R.S., Artates, J.W., Tabet, R., Wheeler, V.C., Bang, A.G., Cleveland, D.W., and Lagier-Tourenne, C. (2017). Polyglutamine-Expanded Huntingtin Exacerbates Age-Related Disruption of Nuclear Integrity and Nucleocytoplasmic Transport. Neuron 94, 48-57 e44.

Gauthier, L.R., Charrin, B.C., Borrell-Pages, M., Dompierre, J.P., Rangone, H., Cordelieres, F.P., De Mey, J., MacDonald, M.E., Lessmann, V., Humbert, S., and Saudou, F. (2004). Huntingtin controls neurotrophic support and survival of neurons by enhancing BDNF vesicular transport along microtubules. Cell 118, 127-138.

Geater, C., Hernandez, S., Thompson, L., and Mattis, V.B. (2018). Cellular Models: HD Patient-Derived Pluripotent Stem Cells. Methods Mol Biol 1780, 41-73.

GeM-HD (2015). Identification of Genetic Factors that Modify Clinical Onset of Huntington's Disease. Cell 162, 516-526.

GeM-HD (2019). CAG Repeat Not Polyglutamine Length Determines Timing of Huntington's Disease Onset. Cell 178, 887-900 e814.

Ghosh, H., Auguadri, L., Battaglia, S., Simone Thirouin, Z., Zemoura, K., Messner, S., Acuna, M.A., Wildner, H., Yevenes, G.E., Dieter, A.*, et al.* (2016). Several posttranslational modifications act in concert to regulate gephyrin scaffolding and GABAergic transmission. Nature communications 7, 13365.

Gibb, S.L., Boston-Howes, W., Lavina, Z.S., Gustincich, S., Brown, R.H., Jr., Pasinelli, P., and Trotti, D. (2007). A caspase-3-cleaved fragment of the glial glutamate transporter EAAT2 is sumoylated and targeted to promyelocytic leukemia nuclear bodies in mutant SOD1-linked amyotrophic lateral sclerosis. The Journal of biological chemistry 282, 32480-32490.

Gibbs-Seymour, I., Oka, Y., Rajendra, E., Weinert, B.T., Passmore, L.A., Patel, K.J., Olsen, J.V., Choudhary, C., Bekker-Jensen, S., and Mailand, N. (2015). Ubiquitin-SUMO circuitry controls activated fanconi anemia ID complex dosage in response to DNA damage. Molecular cell 57, 150-164.

Gil, J.M., and Rego, A.C. (2009). The R6 lines of transgenic mice: a model for screening new therapies for Huntington's disease. Brain research reviews 59, 410-431.

Gilman, C.P., Chan, S.L., Guo, Z., Zhu, X., Greig, N., and Mattson, M.P. (2003). p53 is present in synapses where it mediates mitochondrial dysfunction and synaptic degeneration in response to DNA damage, and oxidative and excitotoxic insults. Neuromolecular medicine 3, 159-172.

Girach, F., Craig, T.J., Rocca, D.L., and Henley, J.M. (2013). RIM1alpha SUMOylation is required for fast synaptic vesicle exocytosis. Cell reports 5, 1294-1301.

Giuliano, P., De Cristofaro, T., Affaitati, A., Pizzulo, G.M., Feliciello, A., Criscuolo, C., De Michele, G., Filla, A., Avvedimento, E.V., and Varrone, S. (2003). DNA damage induced by polyglutamine-expanded proteins. Human molecular genetics 12, 2301-2309.

Goh, A.M., Wibawa, P., Loi, S.M., Walterfang, M., Velakoulis, D., and Looi, J.C. (2018). Huntington's disease: Neuropsychiatric manifestations of Huntington's disease. Australasian psychiatry : bulletin of Royal Australian and New Zealand College of Psychiatrists 26, 366-375.

Gonitel, R., Moffitt, H., Sathasivam, K., Woodman, B., Detloff, P.J., Faull, R.L., and Bates, G.P. (2008). DNA instability in postmitotic neurons. Proceedings of the National Academy of Sciences of the United States of America 105, 3467-3472.

Goold, R., Flower, M., Moss, D.H., Medway, C., Wood-Kaczmar, A., Andre, R., Farshim, P., Bates, G.P., Holmans, P., Jones, L., and Tabrizi, S.J. (2019). FAN1 modifies Huntington's disease progression by stabilizing the expanded HTT CAG repeat. Human molecular genetics 28, 650-661.

Gregoire, S., and Yang, X.J. (2005). Association with class IIa histone deacetylases upregulates the sumoylation of MEF2 transcription factors. Molecular and cellular biology 25, 2273-2287.

Grima, J.C., Daigle, J.G., Arbez, N., Cunningham, K.C., Zhang, K., Ochaba, J., Geater, C., Morozko, E., Stocksdale, J., Glatzer, J.C., *et al.* (2017). Mutant Huntingtin Disrupts the Nuclear Pore Complex. Neuron 94, 93-107 e106.

Group, H.C.R. (1993). A novel gene containing a trinucleotide repeat that is expanded and unstable on Huntington's disease chromosomes. The Huntington's Disease Collaborative Research Group. Cell 72, 971-983.

Guo, C., Hildick, K.L., Luo, J., Dearden, L., Wilkinson, K.A., and Henley, J.M. (2013). SENP3-mediated deSUMOylation of dynamin-related protein 1 promotes cell death following ischaemia. The EMBO journal 32, 1514-1528.

Gutekunst, C.A., Li, S.H., Yi, H., Mulroy, J.S., Kuemmerle, S., Jones, R., Rye, D., Ferrante, R.J., Hersch, S.M., and Li, X.J. (1999). Nuclear and neuropil aggregates in Huntington's disease: relationship to neuropathology. The Journal of neuroscience : the official journal of the Society for Neuroscience 19, 2522-2534.

Han, Z.J., Feng, Y.H., Gu, B.H., Li, Y.M., and Chen, H. (2018). The post-translational modification, SUMOylation, and cancer (Review). International journal of oncology 52, 1081-1094.

Havekes, R., Park, A.J., Tolentino, R.E., Bruinenberg, V.M., Tudor, J.C., Lee, Y., Hansen, R.T., Guercio, L.A., Linton, E., Neves-Zaph, S.R., *et al.* (2016). Compartmentalized PDE4A5 Signaling Impairs Hippocampal Synaptic Plasticity and Long-Term Memory. The Journal of neuroscience : the official journal of the Society for Neuroscience 36, 8936-8946.

Hecker, C.M., Rabiller, M., Haglund, K., Bayer, P., and Dikic, I. (2006). Specification of SUMO1- and SUMO2-interacting motifs. The Journal of biological chemistry 281, 16117-16127.

Heikkinen, T., Lehtimaki, K., Vartiainen, N., Puolivali, J., Hendricks, S.J., Glaser, J.R., Bradaia, A., Wadel, K., Touller, C., Kontkanen, O., *et al.* (2012). Characterization of neurophysiological and behavioral changes, MRI brain volumetry and 1H MRS in zQ175 knock-in mouse model of Huntington's disease. PloS one 7, e50717.

Hendriks, I.A., Lyon, D., Young, C., Jensen, L.J., Vertegaal, A.C., and Nielsen, M.L. (2017). Site-specific mapping of the human SUMO proteome reveals co-modification with phosphorylation. Nature structural & molecular biology 24, 325-336.

Hendriks, I.A., Treffers, L.W., Verlaan-de Vries, M., Olsen, J.V., and Vertegaal, A.C. (2015). SUMO-2 Orchestrates Chromatin Modifiers in Response to DNA Damage. Cell reports.

Henley, J.M., Carmichael, R.E., and Wilkinson, K.A. (2018). Extranuclear SUMOylation in Neurons. Trends in neurosciences 41, 198-210.

Hershko, A., and Ciechanover, A. (1998). The ubiquitin system. Annual review of biochemistry 67, 425-479.
Herzog, K.H., Chong, M.J., Kapsetaki, M., Morgan, J.I., and McKinnon, P.J. (1998). Requirement for Atm in ionizing radiation-induced cell death in the developing central nervous system. Science 280, 1089-1091.
Hickey, M.A., Gallant, K., Gross, G.G., Levine, M.S., and Chesselet, M.F. (2005). Early behavioral deficits in R6/2 mice suitable for use in preclinical drug testing. Neurobiology of disease 20, 1-11.
Hickey, M.A., Kosmalska, A., Enayati, J., Cohen, R., Zeitlin, S., Levine, M.S., and Chesselet, M.F. (2008). Extensive early motor and non-motor behavioral deficits are followed by striatal neuronal loss in knock-in Huntington's disease mice. Neuroscience 157, 280-295.
Hietakangas, V., Anckar, J., Blomster, H.A., Fujimoto, M., Palvimo, J.J., Nakai, A., and Sistonen, L. (2006). PDSM, a motif for phosphorylation-dependent SUMO modification. Proceedings of the National Academy of Sciences of the United States of America 103, 45-50.
Hipp, M.S., Park, S.H., and Hartl, F.U. (2014). Proteostasis impairment in protein-misfolding and -aggregation diseases. Trends in cell biology 24, 506-514.
Hodges, A., Strand, A.D., Aragaki, A.K., Kuhn, A., Sengstag, T., Hughes, G., Elliston, L.A., Hartog, C., Goldstein, D.R., Thu, D.*, et al.* (2006). Regional and cellular gene expression changes in human Huntington's disease brain. Human molecular genetics 15, 965-977.
Hoffner, G., and Djian, P. (2014). Monomeric, oligomeric and polymeric proteins in huntington disease and other diseases of polyglutamine expansion. Brain sciences 4, 91-122.
Hoffner, G., and Djian, P. (2015). Polyglutamine Aggregation in Huntington Disease: Does Structure Determine Toxicity? Molecular neurobiology 52, 1297-1314.
Hu, L.Y., Chang, C.C., Huang, Y.S., Chou, W.C., Lin, Y.M., Ho, C.C., Chen, W.T., Shih, H.M., Hsiung, C.N., Wu, P.E., and Shen, C.Y. (2018). SUMOylation of XRCC1 activated by poly (ADP-ribosyl)ation regulates DNA repair. Human molecular genetics 27, 2306-2317.
Huang, Y., and Li, G.M. (2018). DNA mismatch repair preferentially safeguards actively transcribed genes. DNA repair 71, 82-86.
Hufeldt, M.R., Nielsen, D.S., Vogensen, F.K., Midtvedt, T., and Hansen, A.K. (2010). Variation in the gut microbiota of laboratory mice is related to both genetic and environmental factors. Comparative medicine 60, 336-347.
Hwang, S.P., and Lee, D.H. (2017). Autophagy mediates SUMO-induced degradation of a polyglutamine protein ataxin-3. Animal cells and systems 21, 169-176.
Illuzzi, J., Yerkes, S., Parekh-Olmedo, H., and Kmiec, E.B. (2009). DNA breakage and induction of DNA damage response proteins precede the appearance of visible mutant huntingtin aggregates. Journal of neuroscience research 87, 733-747.
Jacobs, A.L., and Schar, P. (2012). DNA glycosylases: in DNA repair and beyond. Chromosoma 121, 1-20.
Jacobsen, J.C., Erdin, S., Chiang, C., Hanscom, C., Handley, R.R., Barker, D.D., Stortchevoi, A., Blumenthal, I., Reid, S.J., Snell, R.G.*, et al.* (2017). Potential molecular consequences of transgene integration: The R6/2 mouse example. Scientific reports 7, 41120.

Janer, A., Werner, A., Takahashi-Fujigasaki, J., Daret, A., Fujigasaki, H., Takada, K., Duyckaerts, C., Brice, A., Dejean, A., and Sittler, A. (2010). SUMOylation attenuates the aggregation propensity and cellular toxicity of the polyglutamine expanded ataxin-7. Human molecular genetics 19, 181-195.

Jia, Y., Gall, C.M., and Lynch, G. (2010). Presynaptic BDNF promotes postsynaptic long-term potentiation in the dorsal striatum. The Journal of neuroscience : the official journal of the Society for Neuroscience 30, 14440-14445.

Jilani, A., Ramotar, D., Slack, C., Ong, C., Yang, X.M., Scherer, S.W., and Lasko, D.D. (1999). Molecular cloning of the human gene, PNKP, encoding a polynucleotide kinase 3'-phosphatase and evidence for its role in repair of DNA strand breaks caused by oxidative damage. The Journal of biological chemistry 274, 24176-24186.

Jinks-Robertson, S., and Bhagwat, A.S. (2014). Transcription-associated mutagenesis. Annual review of genetics 48, 341-359.

Johansson, E.M., Sanabra, C., and Mengod, G. (2012). Sex-related differences of cAMP-specific PDE4B3 mRNA in oligodendrocytes following systemic inflammation. Glia 60, 1815-1825.

Jones, L., Houlden, H., and Tabrizi, S.J. (2017). DNA repair in the trinucleotide repeat disorders. The Lancet Neurology 16, 88-96.

Jurgensmeier, J.M., Xie, Z., Deveraux, Q., Ellerby, L., Bredesen, D., and Reed, J.C. (1998). Bax directly induces release of cytochrome c from isolated mitochondria. Proceedings of the National Academy of Sciences of the United States of America 95, 4997-5002.

Kahyo, T., Nishida, T., and Yasuda, H. (2001). Involvement of PIAS1 in the sumoylation of tumor suppressor p53. Molecular cell 8, 713-718.

Kang, J., Gocke, C.B., and Yu, H. (2006). Phosphorylation-facilitated sumoylation of MEF2C negatively regulates its transcriptional activity. BMC biochemistry 7, 5.

Kang, J.S., Saunier, E.F., Akhurst, R.J., and Derynck, R. (2008). The type I TGF-beta receptor is covalently modified and regulated by sumoylation. Nature cell biology 10, 654-664.

Katchanov, J., Harms, C., Gertz, K., Hauck, L., Waeber, C., Hirt, L., Priller, J., von Harsdorf, R., Bruck, W., Hortnagl, H.*, et al.* (2001). Mild cerebral ischemia induces loss of cyclin-dependent kinase inhibitors and activation of cell cycle machinery before delayed neuronal cell death. The Journal of neuroscience : the official journal of the Society for Neuroscience 21, 5045-5053.

Katyal, S., el-Khamisy, S.F., Russell, H.R., Li, Y., Ju, L., Caldecott, K.W., and McKinnon, P.J. (2007). TDP1 facilitates chromosomal single-strand break repair in neurons and is neuroprotective in vivo. The EMBO journal 26, 4720-4731.

Kennedy, L., Evans, E., Chen, C.M., Craven, L., Detloff, P.J., Ennis, M., and Shelbourne, P.F. (2003). Dramatic tissue-specific mutation length increases are an early molecular event in Huntington disease pathogenesis. Human molecular genetics 12, 3359-3367.

Kennedy, L., and Shelbourne, P.F. (2000). Dramatic mutation instability in HD mouse striatum: does polyglutamine load contribute to cell-specific vulnerability in Huntington's disease? Human molecular genetics 9, 2539-2544.

Keshavarzian, A., Green, S.J., Engen, P.A., Voigt, R.M., Naqib, A., Forsyth, C.B., Mutlu, E., and Shannon, K.M. (2015). Colonic bacterial composition in Parkinson's disease. Movement disorders : official journal of the Movement Disorder Society 30, 1351-1360.

Kilbride, S.M., and Prehn, J.H. (2013). Central roles of apoptotic proteins in mitochondrial function. Oncogene 32, 2703-2711.

Kim, Y.M., Jang, W.H., Quezado, M.M., Oh, Y., Chung, K.C., Junn, E., and Mouradian, M.M. (2011). Proteasome inhibition induces alpha-synuclein SUMOylation and aggregate formation. Journal of the neurological sciences 307, 157-161.

Klapstein, G.J., Fisher, R.S., Zanjani, H., Cepeda, C., Jokel, E.S., Chesselet, M.F., and Levine, M.S. (2001). Electrophysiological and morphological changes in striatal spiny neurons in R6/2 Huntington's disease transgenic mice. Journal of neurophysiology 86, 2667-2677.

Klein Douwel, D., Boonen, R.A., Long, D.T., Szypowska, A.A., Raschle, M., Walter, J.C., and Knipscheer, P. (2014). XPF-ERCC1 acts in Unhooking DNA interstrand crosslinks in cooperation with FANCD2 and FANCP/SLX4. Molecular cell 54, 460-471.

Knipscheer, P., Raschle, M., Smogorzewska, A., Enoiu, M., Ho, T.V., Scharer, O.D., Elledge, S.J., and Walter, J.C. (2009). The Fanconi anemia pathway promotes replication-dependent DNA interstrand cross-link repair. Science 326, 1698-1701.

Ko, J., Ou, S., and Patterson, P.H. (2001). New anti-huntingtin monoclonal antibodies: implications for huntingtin conformation and its binding proteins. Brain research bulletin 56, 319-329.

Kocaturk, N.M., and Gozuacik, D. (2018). Crosstalk Between Mammalian Autophagy and the Ubiquitin-Proteasome System. Frontiers in cell and developmental biology 6, 128.

Korsmeyer, S.J. (1999). BCL-2 gene family and the regulation of programmed cell death. Cancer research 59, 1693s-1700s.

Kotaja, N., Karvonen, U., Janne, O.A., and Palvimo, J.J. (2002). PIAS proteins modulate transcription factors by functioning as SUMO-1 ligases. Molecular and cellular biology 22, 5222-5234.

Kovalenko, M., Dragileva, E., St Claire, J., Gillis, T., Guide, J.R., New, J., Dong, H., Kucherlapati, R., Kucherlapati, M.H., Ehrlich, M.E.*, et al.* (2012). Msh2 acts in medium-spiny striatal neurons as an enhancer of CAG instability and mutant huntingtin phenotypes in Huntington's disease knock-in mice. PloS one 7, e44273.

Kovtun, I.V., Liu, Y., Bjoras, M., Klungland, A., Wilson, S.H., and McMurray, C.T. (2007). OGG1 initiates age-dependent CAG trinucleotide expansion in somatic cells. Nature 447, 447-452.

Koyuncu, S., Fatima, A., Gutierrez-Garcia, R., and Vilchez, D. (2017). Proteostasis of Huntingtin in Health and Disease. International journal of molecular sciences 18.

Krokan, H.E., and Bjoras, M. (2013). Base excision repair. Cold Spring Harbor perspectives in biology 5, a012583.

Krumova, P., Meulmeester, E., Garrido, M., Tirard, M., Hsiao, H.H., Bossis, G., Urlaub, H., Zweckstetter, M., Kugler, S., Melchior, F.*, et al.* (2011). Sumoylation inhibits alpha-synuclein aggregation and toxicity. The Journal of cell biology 194, 49-60.

Kumar, A., Vaish, M., and Ratan, R.R. (2014). Transcriptional dysregulation in Huntington's disease: a failure of adaptive transcriptional homeostasis. Drug discovery today 19, 956-962.

Kumar, R., Gonzalez-Prieto, R., Xiao, Z., Verlaan-de Vries, M., and Vertegaal, A.C.O. (2017). The STUbL RNF4 regulates protein group SUMOylation by targeting the SUMO conjugation machinery. Nature communications 8, 1809.

Kunkel, T.A., and Erie, D.A. (2005). DNA mismatch repair. Annual review of biochemistry 74, 681-710.

Kunz, K., Piller, T., and Muller, S. (2018). SUMO-specific proteases and isopeptidases of the SENP family at a glance. Journal of cell science 131.

Kuroiwa, M., Snyder, G.L., Shuto, T., Fukuda, A., Yanagawa, Y., Benavides, D.R., Nairn, A.C., Bibb, J.A., Greengard, P., and Nishi, A. (2012). Phosphodiesterase 4 inhibition enhances the dopamine D1 receptor/PKA/DARPP-32 signaling cascade in frontal cortex. Psychopharmacology 219, 1065-1079.

Kurtishi, A., Rosen, B., Patil, K.S., Alves, G.W., and Moller, S.G. (2019). Cellular Proteostasis in Neurodegeneration. Molecular neurobiology 56, 3676-3689.

Labadorf, A., Hoss, A.G., Lagomarsino, V., Latourelle, J.C., Hadzi, T.C., Bregu, J., MacDonald, M.E., Gusella, J.F., Chen, J.F., Akbarian, S.*, et al.* (2015). RNA Sequence Analysis of Human Huntington Disease Brain Reveals an Extensive Increase in Inflammatory and Developmental Gene Expression. PloS one 10, e0143563.

Laine, J.P., and Egly, J.M. (2006). Initiation of DNA repair mediated by a stalled RNA polymerase IIO. The EMBO journal 25, 387-397.

Langbehn, D.R., Brinkman, R.R., Falush, D., Paulsen, J.S., and Hayden, M.R. (2004). A new model for prediction of the age of onset and penetrance for Huntington's disease based on CAG length. Clinical genetics 65, 267-277.

Langfelder, P., Cantle, J.P., Chatzopoulou, D., Wang, N., Gao, F., Al-Ramahi, I., Lu, X.H., Ramos, E.M., El-Zein, K., Zhao, Y.*, et al.* (2016). Integrated genomics and proteomics define huntingtin CAG length-dependent networks in mice. Nature neuroscience 19, 623-633.

Leavitt, B.R., Guttman, J.A., Hodgson, J.G., Kimel, G.H., Singaraja, R., Vogl, A.W., and Hayden, M.R. (2001). Wild-type huntingtin reduces the cellular toxicity of mutant huntingtin in vivo. American journal of human genetics 68, 313-324.

Lecona, E., Rodriguez-Acebes, S., Specks, J., Lopez-Contreras, A.J., Ruppen, I., Murga, M., Munoz, J., Mendez, J., and Fernandez-Capetillo, O. (2016). USP7 is a SUMO deubiquitinase essential for DNA replication. Nature structural & molecular biology 23, 270-277.

Lee, J.M., Chao, M.J., Harold, D., Abu Elneel, K., Gillis, T., Holmans, P., Jones, L., Orth, M., Myers, R.H., Kwak, S.*, et al.* (2017). A modifier of Huntington's disease onset at the MLH1 locus. Human molecular genetics 26, 3859-3867.

Lee, J.M., Kang, H.J., Lee, H.R., Choi, C.Y., Jang, W.J., and Ahn, J.H. (2003). PIAS1 enhances SUMO-1 modification and the transactivation activity of the major immediate-early IE2 protein of human cytomegalovirus. FEBS letters 555, 322-328.

Lee, J.M., Pinto, R.M., Gillis, T., St Claire, J.C., and Wheeler, V.C. (2011). Quantification of age-dependent somatic CAG repeat instability in Hdh CAG knock-in mice reveals different expansion dynamics in striatum and liver. PloS one 6, e23647.

Lee, J.M., Zhang, J., Su, A.I., Walker, J.R., Wiltshire, T., Kang, K., Dragileva, E., Gillis, T., Lopez, E.T., Boily, M.J.*, et al.* (2010). A novel approach to investigate tissue-specific trinucleotide repeat instability. BMC systems biology 4, 29.

Legleiter, J., Lotz, G.P., Miller, J., Ko, J., Ng, C., Williams, G.L., Finkbeiner, S., Patterson, P.H., and Muchowski, P.J. (2009). Monoclonal antibodies recognize distinct conformational epitopes formed by polyglutamine in a mutant huntingtin fragment. The Journal of biological chemistry 284, 21647-21658.

Legleiter, J., Mitchell, E., Lotz, G.P., Sapp, E., Ng, C., DiFiglia, M., Thompson, L.M., and Muchowski, P.J. (2010). Mutant huntingtin fragments form oligomers in a polyglutamine length-dependent manner in vitro and in vivo. The Journal of biological chemistry 285, 14777-14790.

Li, J.Y., Popovic, N., and Brundin, P. (2005). The use of the R6 transgenic mouse models of Huntington's disease in attempts to develop novel therapeutic strategies. NeuroRx : the journal of the American Society for Experimental NeuroTherapeutics 2, 447-464.

Liberti, S.E., Larrea, A.A., and Kunkel, T.A. (2013). Exonuclease 1 preferentially repairs mismatches generated by DNA polymerase alpha. DNA repair 12, 92-96.

Liebelt, F., and Vertegaal, A.C. (2016). Ubiquitin-dependent and independent roles of SUMO in proteostasis. American journal of physiology Cell physiology 311, C284-296.

Lione, L.A., Carter, R.J., Hunt, M.J., Bates, G.P., Morton, A.J., and Dunnett, S.B. (1999). Selective discrimination learning impairments in mice expressing the human Huntington's disease mutation. The Journal of neuroscience : the official journal of the Society for Neuroscience 19, 10428-10437.

Liu, B., Liao, J., Rao, X., Kushner, S.A., Chung, C.D., Chang, D.D., and Shuai, K. (1998). Inhibition of Stat1-mediated gene activation by PIAS1. Proceedings of the National Academy of Sciences of the United States of America 95, 10626-10631.

Liu, B., and Shuai, K. (2008). Targeting the PIAS1 SUMO ligase pathway to control inflammation. Trends in pharmacological sciences 29, 505-509.

Liu, B., Yang, R., Wong, K.A., Getman, C., Stein, N., Teitell, M.A., Cheng, G., Wu, H., and Shuai, K. (2005). Negative regulation of NF-kappaB signaling by PIAS1. Molecular and cellular biology 25, 1113-1123.

Liu, J.P., and Zeitlin, S.O. (2017). Is Huntingtin Dispensable in the Adult Brain? Journal of Huntington's disease 6, 1-17.

Lomash, R.M., Gu, X., Youle, R.J., Lu, W., and Roche, K.W. (2015). Neurolastin, a Dynamin Family GTPase, Regulates Excitatory Synapses and Spine Density. Cell reports 12, 743-751.

Long, D.T., Raschle, M., Joukov, V., and Walter, J.C. (2011). Mechanism of RAD51-dependent DNA interstrand cross-link repair. Science 333, 84-87.

Longley, M.J., Pierce, A.J., and Modrich, P. (1997). DNA polymerase delta is required for human mismatch repair in vitro. The Journal of biological chemistry 272, 10917-10921.

Lou, Z., Minter-Dykhouse, K., Franco, S., Gostissa, M., Rivera, M.A., Celeste, A., Manis, J.P., van Deursen, J., Nussenzweig, A., Paull, T.T., *et al.* (2006). MDC1 maintains genomic stability by participating in the amplification of ATM-dependent DNA damage signals. Molecular cell 21, 187-200.

Love, M.I., Huber, W., and Anders, S. (2014). Moderated estimation of fold change and dispersion for RNA-seq data with DESeq2. Genome biology 15, 550.

Luo, H.B., Xia, Y.Y., Shu, X.J., Liu, Z.C., Feng, Y., Liu, X.H., Yu, G., Yin, G., Xiong, Y.S., Zeng, K.*, et al.* (2014). SUMOylation at K340 inhibits tau degradation through deregulating its phosphorylation and ubiquitination. Proceedings of the National Academy of Sciences of the United States of America 111, 16586-16591.

Luo, K., Zhang, H., Wang, L., Yuan, J., and Lou, Z. (2012). Sumoylation of MDC1 is important for proper DNA damage response. The EMBO journal 31, 3008-3019.

Luthi-Carter, R., Strand, A., Peters, N.L., Solano, S.M., Hollingsworth, Z.R., Menon, A.S., Frey, A.S., Spektor, B.S., Penney, E.B., Schilling, G.*, et al.* (2000). Decreased expression of striatal signaling genes in a mouse model of Huntington's disease. Human molecular genetics 9, 1259-1271.

Lynch, G., Kramar, E.A., Rex, C.S., Jia, Y., Chappas, D., Gall, C.M., and Simmons, D.A. (2007). Brain-derived neurotrophic factor restores synaptic plasticity in a knock-in mouse model of Huntington's disease. The Journal of neuroscience : the official journal of the Society for Neuroscience 27, 4424-4434.

Ma, L., Herren, A.W., Espinal, G., Randol, J., McLaughlin, B., Martinez-Cerdeno, V., Pessah, I.N., Hagerman, R.J., and Hagerman, P.J. (2019). Composition of the Intranuclear Inclusions of Fragile X-associated Tremor/Ataxia Syndrome. Acta neuropathologica communications 7, 143.

Ma, Y., Pannicke, U., Schwarz, K., and Lieber, M.R. (2002). Hairpin opening and overhang processing by an Artemis/DNA-dependent protein kinase complex in nonhomologous end joining and V(D)J recombination. Cell 108, 781-794.

Madabhushi, R., Gao, F., Pfenning, A.R., Pan, L., Yamakawa, S., Seo, J., Rueda, R., Phan, T.X., Yamakawa, H., Pao, P.C.*, et al.* (2015). Activity-Induced DNA Breaks Govern the Expression of Neuronal Early-Response Genes. Cell 161, 1592-1605.

Madabhushi, R., Pan, L., and Tsai, L.H. (2014). DNA damage and its links to neurodegeneration. Neuron 83, 266-282.

Maiuri, T., Mocle, A.J., Hung, C.L., Xia, J., van Roon-Mom, W.M., and Truant, R. (2017). Huntingtin is a scaffolding protein in the ATM oxidative DNA damage response complex. Human molecular genetics 26, 395-406.

Maiuri, T., Suart, C.E., Hung, C.L.K., Graham, K.J., Barba Bazan, C.A., and Truant, R. (2019). DNA Damage Repair in Huntington's Disease and Other Neurodegenerative Diseases. Neurotherapeutics : the journal of the American Society for Experimental NeuroTherapeutics.

Mallette, F.A., and Ferbeyre, G. (2007). The DNA damage signaling pathway connects oncogenic stress to cellular senescence. Cell Cycle 6, 1831-1836.

Mangiarini, L., Sathasivam, K., Seller, M., Cozens, B., Harper, A., Hetherington, C., Lawton, M., Trottier, Y., Lehrach, H., Davies, S.W., and Bates, G.P. (1996). Exon 1 of the HD gene with an expanded CAG repeat is sufficient to cause a progressive neurological phenotype in transgenic mice. Cell 87, 493-506.

Marcellin, D., Abramowski, D., Young, D., Richter, J., Weiss, A., Marcel, A., Maassen, J., Kauffmann, M., Bibel, M., Shimshek, D.R.*, et al.* (2012). Fragments of HdhQ150 mutant huntingtin form a soluble oligomer pool that declines with aggregate deposition upon aging. PloS one 7, e44457.

Marechal, A., and Zou, L. (2013). DNA damage sensing by the ATM and ATR kinases. Cold Spring Harbor perspectives in biology 5.

Marteijn, J.A., Lans, H., Vermeulen, W., and Hoeijmakers, J.H. (2014). Understanding nucleotide excision repair and its roles in cancer and ageing. Nature reviews Molecular cell biology 15, 465-481.

Martin, L.J., and Liu, Z. (2002). Injury-induced spinal motor neuron apoptosis is preceded by DNA single-strand breaks and is p53- and Bax-dependent. Journal of neurobiology 50, 181-197.

Martin, S., Nishimune, A., Mellor, J.R., and Henley, J.M. (2007). SUMOylation regulates kainate-receptor-mediated synaptic transmission. Nature 447, 321-325.

Mascle, X.H., Lussier-Price, M., Cappadocia, L., Estephan, P., Raiola, L., Omichinski, J.G., and Aubry, M. (2013). Identification of a non-covalent ternary complex formed by PIAS1, SUMO1, and UBC9 proteins involved in transcriptional regulation. The Journal of biological chemistry 288, 36312-36327.

Mason, A.G., Tome, S., Simard, J.P., Libby, R.T., Bammler, T.K., Beyer, R.P., Morton, A.J., Pearson, C.E., and La Spada, A.R. (2014). Expression levels of DNA replication and repair genes predict regional somatic repeat instability in the brain but are not altered by polyglutamine disease protein expression or age. Human molecular genetics 23, 1606-1618.

Massey, T.H., and Jones, L. (2018). The central role of DNA damage and repair in CAG repeat diseases. Disease models & mechanisms 11.

Mathkar, P.P., Suresh, D., Dunn, J., Tom, C.M., and Mattis, V.B. (2019). Characterization of Neurodevelopmental Abnormalities in iPSC-Derived Striatal Cultures from Patients with Huntington's Disease. Journal of Huntington's disease 8, 257-269.

Matsuzaki, S., Lee, L., Knock, E., Srikumar, T., Sakurai, M., Hazrati, L.N., Katayama, T., Staniszewski, A., Raught, B., Arancio, O., and Fraser, P.E. (2015). SUMO1 Affects Synaptic Function, Spine Density and Memory. Scientific reports 5, 10730.

Mattis, V.B., Tom, C., Akimov, S., Saeedian, J., Ostergaard, M.E., Southwell, A.L., Doty, C.N., Ornelas, L., Sahabian, A., Lenaeus, L.*, et al.* (2015). HD iPSC-derived neural progenitors accumulate in culture and are susceptible to BDNF withdrawal due to glutamate toxicity. Human molecular genetics 24, 3257-3271.

Mattson, M.P., Duan, W., Wan, R., and Guo, Z. (2004). Prophylactic activation of neuroprotective stress response pathways by dietary and behavioral manipulations. NeuroRx : the journal of the American Society for Experimental NeuroTherapeutics 1, 111-116.

McKinnon, P.J. (2009). DNA repair deficiency and neurological disease. Nature reviews Neuroscience 10, 100-112.

McKinnon, P.J. (2016). Topoisomerases and the regulation of neural function. Nature reviews Neuroscience 17, 673-679.

McKinnon, P.J. (2017). Genome integrity and disease prevention in the nervous system. Genes & development 31, 1180-1194.

McKinstry, S.U., Karadeniz, Y.B., Worthington, A.K., Hayrapetyan, V.Y., Ozlu, M.I., Serafin-Molina, K., Risher, W.C., Ustunkaya, T., Dragatsis, I., Zeitlin, S.*, et al.* (2014). Huntingtin is required for normal excitatory synapse development in cortical and striatal circuits. The Journal of neuroscience : the official journal of the Society for Neuroscience 34, 9455-9472.

Menalled, L., and Brunner, D. (2014). Animal models of Huntington's disease for translation to the clinic: best practices. Movement disorders : official journal of the Movement Disorder Society 29, 1375-1390.

Menalled, L.B., Kudwa, A.E., Miller, S., Fitzpatrick, J., Watson-Johnson, J., Keating, N., Ruiz, M., Mushlin, R., Alosio, W., McConnell, K.*, et al.* (2012). Comprehensive behavioral and molecular characterization of a new knock-in mouse model of Huntington's disease: zQ175. PloS one 7, e49838.

Menoni, H., Wienholz, F., Theil, A.F., Janssens, R.C., Lans, H., Campalans, A., Radicella, J.P., Marteijn, J.A., and Vermeulen, W. (2018). The transcription-coupled DNA repair-initiating protein CSB promotes XRCC1 recruitment to oxidative DNA damage. Nucleic acids research 46, 7747-7756.

Meredith, L.J., Wang, C.M., Nascimento, L., Liu, R., Wang, L., and Yang, W.H. (2016). The Key Regulator for Language and Speech Development, FOXP2, is a Novel Substrate for SUMOylation. Journal of cellular biochemistry 117, 426-438.

Miles, J.A., Frost, M.G., Carroll, E., Rowe, M.L., Howard, M.J., Sidhu, A., Chaugule, V.K., Alpi, A.F., and Walden, H. (2015). The Fanconi Anemia DNA Repair Pathway Is Regulated by an Interaction between Ubiquitin and the E2-like Fold Domain of FANCL. The Journal of biological chemistry 290, 20995-21006.

Miller, J., Arrasate, M., Brooks, E., Libeu, C.P., Legleiter, J., Hatters, D., Curtis, J., Cheung, K., Krishnan, P., Mitra, S.*, et al.* (2011). Identifying polyglutamine protein species in situ that best predict neurodegeneration. Nature chemical biology 7, 925-934.

Mischo, H.E., Hemmerich, P., Grosse, F., and Zhang, S. (2005). Actinomycin D induces histone gamma-H2AX foci and complex formation of gamma-H2AX with Ku70 and nuclear DNA helicase II. The Journal of biological chemistry 280, 9586-9594.

Mollersen, L., Rowe, A.D., Illuzzi, J.L., Hildrestrand, G.A., Gerhold, K.J., Tveteras, L., Bjolgerud, A., Wilson, D.M., 3rd, Bjoras, M., and Klungland, A. (2012). Neil1 is a genetic modifier of somatic and germline CAG trinucleotide repeat instability in R6/1 mice. Human molecular genetics 21, 4939-4947.

Moreira, M.C., Barbot, C., Tachi, N., Kozuka, N., Uchida, E., Gibson, T., Mendonca, P., Costa, M., Barros, J., Yanagisawa, T.*, et al.* (2001). The gene mutated in ataxia-ocular apraxia 1 encodes the new HIT/Zn-finger protein aprataxin. Nature genetics 29, 189-193.

Morozko, E.L., Ochaba, J., Hernandez, S.J., Lau, A., Sanchez, I., Orellana, I., Kopan, L., Crapser, J., Duong, J.H., Overman, J.*, et al.* (2018). Longitudinal Biochemical Assay Analysis of Mutant Huntingtin Exon 1 Protein in R6/2 Mice. Journal of Huntington's disease 7, 321-335.

Morris, J.R., Boutell, C., Keppler, M., Densham, R., Weekes, D., Alamshah, A., Butler, L., Galanty, Y., Pangon, L., Kiuchi, T.*, et al.* (2009). The SUMO modification pathway is involved in the BRCA1 response to genotoxic stress. Nature 462, 886-890.

Moss, D.J.H., Pardinas, A.F., Langbehn, D., Lo, K., Leavitt, B.R., Roos, R., Durr, A., Mead, S., Holmans, P., Jones, L., and Tabrizi, S.J. (2017). Identification of genetic variants associated with Huntington's disease progression: a genome-wide association study. The Lancet Neurology 16, 701-711.

Moumne, L., Betuing, S., and Caboche, J. (2013). Multiple Aspects of Gene Dysregulation in Huntington's Disease. Frontiers in neurology 4, 127.

Mukherjee, S., Thomas, M., Dadgar, N., Lieberman, A.P., and Iniguez-Lluhi, J.A. (2009). Small ubiquitin-like modifier (SUMO) modification of the androgen receptor attenuates polyglutamine-mediated aggregation. The Journal of biological chemistry 284, 21296-21306.

Muller, S., Berger, M., Lehembre, F., Seeler, J.S., Haupt, Y., and Dejean, A. (2000). c-Jun and p53 activity is modulated by SUMO-1 modification. The Journal of biological chemistry 275, 13321-13329.

Nance, M.A., and Myers, R.H. (2001). Juvenile onset Huntington's disease--clinical and research perspectives. Mental retardation and developmental disabilities research reviews 7, 153-157.

Nasir, J., Floresco, S.B., O'Kusky, J.R., Diewert, V.M., Richman, J.M., Zeisler, J., Borowski, A., Marth, J.D., Phillips, A.G., and Hayden, M.R. (1995). Targeted disruption of the Huntington's disease gene results in embryonic lethality and behavioral and morphological changes in heterozygotes. Cell 81, 811-823.

Neueder, A., Landles, C., Ghosh, R., Howland, D., Myers, R.H., Faull, R.L.M., Tabrizi, S.J., and Bates, G.P. (2017). The pathogenic exon 1 HTT protein is produced by incomplete splicing in Huntington's disease patients. Scientific reports 7, 1307.

Neyret-Kahn, H., Benhamed, M., Ye, T., Le Gras, S., Cossec, J.C., Lapaquette, P., Bischof, O., Ouspenskaia, M., Dasso, M., Seeler, J.*, et al.* (2013). Sumoylation at chromatin governs coordinated repression of a transcriptional program essential for cell growth and proliferation. Genome research 23, 1563-1579.

Niikura, T., Kita, Y., and Abe, Y. (2014). SUMO3 modification accelerates the aggregation of ALS-linked SOD1 mutants. PloS one 9, e101080.

Nikolaev, A., McLaughlin, T., O'Leary, D.D., and Tessier-Lavigne, M. (2009). APP binds DR6 to trigger axon pruning and neuron death via distinct caspases. Nature 457, 981-989.

Nithianantharajah, J., and Hannan, A.J. (2013). Dysregulation of synaptic proteins, dendritic spine abnormalities and pathological plasticity of synapses as experience-dependent mediators of cognitive and psychiatric symptoms in Huntington's disease. Neuroscience 251, 66-74.

Norremolle, A., Sorensen, S.A., Fenger, K., and Hasholt, L. (1995). Correlation between magnitude of CAG repeat length alterations and length of the paternal repeat in paternally inherited Huntington's disease. Clinical genetics 47, 113-117.

O'Driscoll, M., Ruiz-Perez, V.L., Woods, C.G., Jeggo, P.A., and Goodship, J.A. (2003). A splicing mutation affecting expression of ataxia-telangiectasia and Rad3-related protein (ATR) results in Seckel syndrome. Nature genetics 33, 497-501.

O'Rourke, J.G., Gareau, J.R., Ochaba, J., Song, W., Rasko, T., Reverter, D., Lee, J., Monteys, A.M., Pallos, J., Mee, L.*, et al.* (2013). SUMO-2 and PIAS1 modulate insoluble mutant huntingtin protein accumulation. Cell reports 4, 362-375.

Ochaba, J., Lukacsovich, T., Csikos, G., Zheng, S., Margulis, J., Salazar, L., Mao, K., Lau, A.L., Yeung, S.Y., Humbert, S.*, et al.* (2014). Potential function for the Huntingtin protein as a scaffold for selective autophagy. Proceedings of the National Academy of Sciences of the United States of America 111, 16889-16894.

Ochaba, J., Monteys, A.M., O'Rourke, J.G., Reidling, J.C., Steffan, J.S., Davidson, B.L., and Thompson, L.M. (2016). PIAS1 Regulates Mutant Huntingtin Accumulation and Huntington's Disease-Associated Phenotypes In Vivo. Neuron 90, 507-520.

Ochaba, J., Morozko, E.L., O'Rourke, J.G., and Thompson, L.M. (2018). Fractionation for Resolution of Soluble and Insoluble Huntingtin Species. Journal of visualized experiments : JoVE.

Okamoto, Y., Hejna, J., and Takata, M. (2019). Regulation of R-loops and genome instability in Fanconi anemia. Journal of biochemistry 165, 465-470.

Oltvai, Z.N., Milliman, C.L., and Korsmeyer, S.J. (1993). Bcl-2 heterodimerizes in vivo with a conserved homolog, Bax, that accelerates programmed cell death. Cell 74, 609-619.

Pani, B., and Nudler, E. (2017). Mechanistic insights into transcription coupled DNA repair. DNA repair 56, 42-50.

Parsons, J.L., Khoronenkova, S.V., Dianova, II, Ternette, N., Kessler, B.M., Datta, P.K., and Dianov, G.L. (2012). Phosphorylation of PNKP by ATM prevents its proteasomal degradation and enhances resistance to oxidative stress. Nucleic acids research 40, 11404-11415.

Pascucci, B., Fragale, A., Marabitti, V., Leuzzi, G., Calcagnile, A.S., Parlanti, E., Franchitto, A., Dogliotti, E., and D'Errico, M. (2018). CSA and CSB play a role in the response to DNA breaks. Oncotarget 9, 11581-11591.

Passos, J.F., Nelson, G., Wang, C., Richter, T., Simillion, C., Proctor, C.J., Miwa, S., Olijslagers, S., Hallinan, J., Wipat, A.*, et al.* (2010). Feedback between p21 and reactive oxygen production is necessary for cell senescence. Molecular systems biology 6, 347.

Pearson, C.E., Eichler, E.E., Lorenzetti, D., Kramer, S.F., Zoghbi, H.Y., Nelson, D.L., and Sinden, R.R. (1998). Interruptions in the triplet repeats of SCA1 and FRAXA reduce the propensity and complexity of slipped strand DNA (S-DNA) formation. Biochemistry 37, 2701-2708.

Pearson, C.E., Ewel, A., Acharya, S., Fishel, R.A., and Sinden, R.R. (1997). Human MSH2 binds to trinucleotide repeat DNA structures associated with neurodegenerative diseases. Human molecular genetics 6, 1117-1123.

Pearson, C.E., Nichol Edamura, K., and Cleary, J.D. (2005). Repeat instability: mechanisms of dynamic mutations. Nature reviews Genetics 6, 729-742.

Pearson, C.E., Tam, M., Wang, Y.H., Montgomery, S.E., Dar, A.C., Cleary, J.D., and Nichol, K. (2002). Slipped-strand DNAs formed by long (CAG)*(CTG) repeats: slipped-out repeats and slip-out junctions. Nucleic acids research 30, 4534-4547.

Pelegri, C., Duran-Vilaregut, J., del Valle, J., Crespo-Biel, N., Ferrer, I., Pallas, M., Camins, A., and Vilaplana, J. (2008). Cell cycle activation in striatal neurons from Huntington's disease patients and rats treated with 3-nitropropionic acid. International journal of developmental neuroscience : the official journal of the International Society for Developmental Neuroscience 26, 665-671.

Peng, Q., Wu, B., Jiang, M., Jin, J., Hou, Z., Zheng, J., Zhang, J., and Duan, W. (2016). Characterization of Behavioral, Neuropathological, Brain Metabolic and Key Molecular Changes in zQ175 Knock-In Mouse Model of Huntington's Disease. PloS one 11, e0148839.

Peters, M., Wielsch, B., and Boltze, J. (2017). The role of SUMOylation in cerebral hypoxia and ischemia. Neurochemistry international 107, 66-77.

Petrini, J.H., and Stracker, T.H. (2003). The cellular response to DNA double-strand breaks: defining the sensors and mediators. Trends in cell biology 13, 458-462.

Pinto, R.M., Dragileva, E., Kirby, A., Lloret, A., Lopez, E., St Claire, J., Panigrahi, G.B., Hou, C., Holloway, K., Gillis, T.*, et al.* (2013). Mismatch repair genes Mlh1 and Mlh3 modify CAG instability in Huntington's disease mice: genome-wide and candidate approaches. PLoS genetics 9, e1003930.

Plant, L.D., Dowdell, E.J., Dementieva, I.S., Marks, J.D., and Goldstein, S.A. (2011). SUMO modification of cell surface Kv2.1 potassium channels regulates the activity of rat hippocampal neurons. The Journal of general physiology 137, 441-454.

Plant, L.D., Marks, J.D., and Goldstein, S.A. (2016). SUMOylation of NaV1.2 channels mediates the early response to acute hypoxia in central neurons. eLife 5.

Poirier, M.A., Li, H., Macosko, J., Cai, S., Amzel, M., and Ross, C.A. (2002). Huntingtin spheroids and protofibrils as precursors in polyglutamine fibrilization. The Journal of biological chemistry 277, 41032-41037.

Pommier, Y., Sun, Y., Huang, S.N., and Nitiss, J.L. (2016). Roles of eukaryotic topoisomerases in transcription, replication and genomic stability. Nature reviews Molecular cell biology 17, 703-721.

Prakash, R., Zhang, Y., Feng, W., and Jasin, M. (2015). Homologous recombination and human health: the roles of BRCA1, BRCA2, and associated proteins. Cold Spring Harbor perspectives in biology 7, a016600.

Princz, A., and Tavernarakis, N. (2019). SUMOylation in Neurodegenerative Diseases. Gerontology, 1-9.

Qi, Y., Wang, J., Bomben, V.C., Li, D.P., Chen, S.R., Sun, H., Xi, Y., Reed, J.G., Cheng, J., Pan, H.L.*, et al.* (2014). Hyper-SUMOylation of the Kv7 potassium channel diminishes the M-current leading to seizures and sudden death. Neuron 83, 1159-1171.

Rajan, S., Plant, L.D., Rabin, M.L., Butler, M.H., and Goldstein, S.A. (2005). Sumoylation silences the plasma membrane leak K+ channel K2P1. Cell 121, 37-47.

Rattray, I., Smith, E., Gale, R., Matsumoto, K., Bates, G.P., and Modo, M. (2013). Correlations of behavioral deficits with brain pathology assessed through longitudinal MRI and histopathology in the R6/2 mouse model of HD. PloS one 8, e60012.

Ravikumar, B., Vacher, C., Berger, Z., Davies, J.E., Luo, S., Oroz, L.G., Scaravilli, F., Easton, D.F., Duden, R., O'Kane, C.J., and Rubinsztein, D.C. (2004). Inhibition of mTOR induces autophagy and reduces toxicity of polyglutamine expansions in fly and mouse models of Huntington disease. Nature genetics 36, 585-595.

Reddy, K., Tam, M., Bowater, R.P., Barber, M., Tomlinson, M., Nichol Edamura, K., Wang, Y.H., and Pearson, C.E. (2011). Determinants of R-loop formation at convergent bidirectionally transcribed trinucleotide repeats. Nucleic acids research 39, 1749-1762.

Reverter, D., and Lima, C.D. (2004). A basis for SUMO protease specificity provided by analysis of human Senp2 and a Senp2-SUMO complex. Structure 12, 1519-1531.

Riquelme, C., Barthel, K.K., and Liu, X. (2006). SUMO-1 modification of MEF2A regulates its transcriptional activity. Journal of cellular and molecular medicine 10, 132-144.

Rodier, F., Coppe, J.P., Patil, C.K., Hoeijmakers, W.A., Munoz, D.P., Raza, S.R., Freund, A., Campeau, E., Davalos, A.R., and Campisi, J. (2009). Persistent DNA damage signalling triggers senescence-associated inflammatory cytokine secretion. Nature cell biology 11, 973-979.

Rogakou, E.P., Pilch, D.R., Orr, A.H., Ivanova, V.S., and Bonner, W.M. (1998). DNA double-stranded breaks induce histone H2AX phosphorylation on serine 139. The Journal of biological chemistry 273, 5858-5868.

Rosonina, E., Akhter, A., Dou, Y., Babu, J., and Sri Theivakadadcham, V.S. (2017). Regulation of transcription factors by sumoylation. Transcription 8, 220-231.

Ross, C.A., Kronenbuerger, M., Duan, W., and Margolis, R.L. (2017). Mechanisms underlying neurodegeneration in Huntington disease: applications to novel disease-modifying therapies. Handbook of clinical neurology 144, 15-28.

Ross, C.A., and Poirier, M.A. (2004). Protein aggregation and neurodegenerative disease. Nature medicine 10 Suppl, S10-17.

Ross, C.A., and Tabrizi, S.J. (2011). Huntington's disease: from molecular pathogenesis to clinical treatment. The Lancet Neurology 10, 83-98.

Rub, U., Seidel, K., Heinsen, H., Vonsattel, J.P., den Dunnen, W.F., and Korf, H.W. (2016). Huntington's disease (HD): the neuropathology of a multisystem neurodegenerative disorder of the human brain. Brain Pathol 26, 726-740.

Rui, Y.N., Xu, Z., Patel, B., Chen, Z., Chen, D., Tito, A., David, G., Sun, Y., Stimming, E.F., Bellen, H.J.*, et al.* (2015). Huntingtin functions as a scaffold for selective macroautophagy. Nature cell biology 17, 262-275.

Rytinki, M.M., Kaikkonen, S., Pehkonen, P., Jaaskelainen, T., and Palvimo, J.J. (2009). PIAS proteins: pleiotropic interactors associated with SUMO. Cellular and molecular life sciences : CMLS 66, 3029-3041.

Ryu, J., Cho, S., Park, B.C., and Lee, D.H. (2010). Oxidative stress-enhanced SUMOylation and aggregation of ataxin-1: Implication of JNK pathway. Biochemical and biophysical research communications 393, 280-285.

Saito, K., Kagawa, W., Suzuki, T., Suzuki, H., Yokoyama, S., Saitoh, H., Tashiro, S., Dohmae, N., and Kurumizaka, H. (2010). The putative nuclear localization signal of the human RAD52 protein is a potential sumoylation site. Journal of biochemistry 147, 833-842.

Sambataro, F., and Pennuto, M. (2017). Post-translational Modifications and Protein Quality Control in Motor Neuron and Polyglutamine Diseases. Frontiers in molecular neuroscience 10, 82.

Sassone, J., Maraschi, A., Sassone, F., Silani, V., and Ciammola, A. (2013). Defining the role of the Bcl-2 family proteins in Huntington's disease. Cell death & disease 4, e772.

Sathasivam, K., Neueder, A., Gipson, T.A., Landles, C., Benjamin, A.C., Bondulich, M.K., Smith, D.L., Faull, R.L., Roos, R.A., Howland, D.*, et al.* (2013). Aberrant splicing of HTT generates the pathogenic exon 1 protein in Huntington disease. Proceedings of the National Academy of Sciences of the United States of America 110, 2366-2370.

Scherzinger, E., Lurz, R., Turmaine, M., Mangiarini, L., Hollenbach, B., Hasenbank, R., Bates, G.P., Davies, S.W., Lehrach, H., and Wanker, E.E. (1997). Huntingtin-encoded polyglutamine expansions form amyloid-like protein aggregates in vitro and in vivo. Cell 90, 549-558.

Schmidt, M.H.M., and Pearson, C.E. (2016). Disease-associated repeat instability and mismatch repair. DNA repair 38, 117-126.

Schorova, L., and Martin, S. (2016). Sumoylation in Synaptic Function and Dysfunction. Frontiers in synaptic neuroscience 8, 9.

Schwab, R.A., Nieminuszczy, J., Shah, F., Langton, J., Lopez Martinez, D., Liang, C.C., Cohn, M.A., Gibbons, R.J., Deans, A.J., and Niedzwiedz, W. (2015). The Fanconi Anemia Pathway Maintains Genome Stability by Coordinating Replication and Transcription. Molecular cell 60, 351-361.

Schwertman, P., Bekker-Jensen, S., and Mailand, N. (2016). Regulation of DNA double-strand break repair by ubiquitin and ubiquitin-like modifiers. Nature reviews Molecular cell biology 17, 379-394.

Sedghi, M., Salari, M., Moslemi, A.R., Kariminejad, A., Davis, M., Goullee, H., Olsson, B., Laing, N., and Tajsharghi, H. (2018). Ataxia-telangiectasia-like disorder in a family deficient for MRE11A, caused by a MRE11 variant. Neurology Genetics 4, e295.

Segal-Raz, H., Mass, G., Baranes-Bachar, K., Lerenthal, Y., Wang, S.Y., Chung, Y.M., Ziv-Lehrman, S., Strom, C.E., Helleday, T., Hu, M.C., *et al.* (2011). ATM-mediated phosphorylation of polynucleotide kinase/phosphatase is required for effective DNA double-strand break repair. EMBO reports 12, 713-719.

Semaka, A., Creighton, S., Warby, S., and Hayden, M.R. (2006). Predictive testing for Huntington disease: interpretation and significance of intermediate alleles. Clinical genetics 70, 283-294.

Shahpasandzadeh, H., Popova, B., Kleinknecht, A., Fraser, P.E., Outeiro, T.F., and Braus, G.H. (2014). Interplay between sumoylation and phosphorylation for protection against alpha-synuclein inclusions. The Journal of biological chemistry 289, 31224-31240.

Shalizi, A., Bilimoria, P.M., Stegmuller, J., Gaudilliere, B., Yang, Y., Shuai, K., and Bonni, A. (2007). PIASx is a MEF2 SUMO E3 ligase that promotes postsynaptic dendritic morphogenesis. The Journal of neuroscience : the official journal of the Society for Neuroscience 27, 10037-10046.

Shalizi, A., Gaudilliere, B., Yuan, Z., Stegmuller, J., Shirogane, T., Ge, Q., Tan, Y., Schulman, B., Harper, J.W., and Bonni, A. (2006). A calcium-regulated MEF2 sumoylation switch controls postsynaptic differentiation. Science 311, 1012-1017.

Shelbourne, P.F., Keller-McGandy, C., Bi, W.L., Yoon, S.R., Dubeau, L., Veitch, N.J., Vonsattel, J.P., Wexler, N.S., Arnheim, N., and Augood, S.J. (2007). Triplet repeat mutation length gains correlate with cell-type specific vulnerability in Huntington disease brain. Human molecular genetics 16, 1133-1142.

Shen, J., Gilmore, E.C., Marshall, C.A., Haddadin, M., Reynolds, J.J., Eyaid, W., Bodell, A., Barry, B., Gleason, D., Allen, K., *et al.* (2010). Mutations in PNKP cause microcephaly, seizures and defects in DNA repair. Nature genetics 42, 245-249.

Sherwin, E., Dinan, T.G., and Cryan, J.F. (2018). Recent developments in understanding the role of the gut microbiota in brain health and disease. Annals of the New York Academy of Sciences 1420, 5-25.

Shinbo, Y., Niki, T., Taira, T., Ooe, H., Takahashi-Niki, K., Maita, C., Seino, C., Iguchi-Ariga, S.M., and Ariga, H. (2006). Proper SUMO-1 conjugation is essential to DJ-1 to exert its full activities. Cell death and differentiation 13, 96-108.

Shuai, K., and Liu, B. (2005). Regulation of gene-activation pathways by PIAS proteins in the immune system. Nature reviews Immunology 5, 593-605.

Simon, D.J., Pitts, J., Hertz, N.T., Yang, J., Yamagishi, Y., Olsen, O., Tesic Mark, M., Molina, H., and Tessier-Lavigne, M. (2016). Axon Degeneration Gated by Retrograde Activation of Somatic Pro-apoptotic Signaling. Cell 164, 1031-1045.

Sin, Y., Tanaka, K., and Saijo, M. (2016). The C-terminal Region and SUMOylation of Cockayne Syndrome Group B Protein Play Critical Roles in Transcription-coupled Nucleotide Excision Repair. The Journal of biological chemistry 291, 1387-1397.

Singh, V.K., Kumar, N., Kalsan, M., Saini, A., and Chandra, R. (2015). Mechanism of Induction: Induced Pluripotent Stem Cells (iPSCs). Journal of stem cells 10, 43-62.

Slean, M.M., Reddy, K., Wu, B., Nichol Edamura, K., Kekis, M., Nelissen, F.H., Aspers, R.L., Tessari, M., Scharer, O.D., Wijmenga, S.S., and Pearson, C.E. (2013). Interconverting conformations of slipped-DNA junctions formed by trinucleotide repeats affect repair outcome. Biochemistry 52, 773-785.

Sohn, S.Y., and Hearing, P. (2012). Adenovirus regulates sumoylation of Mre11-Rad50-Nbs1 components through a paralog-specific mechanism. Journal of virology 86, 9656-9665.

Sollier, J., Stork, C.T., Garcia-Rubio, M.L., Paulsen, R.D., Aguilera, A., and Cimprich, K.A. (2014). Transcription-coupled nucleotide excision repair factors promote R-loop-induced genome instability. Molecular cell 56, 777-785.

Song, J., Durrin, L.K., Wilkinson, T.A., Krontiris, T.G., and Chen, Y. (2004). Identification of a SUMO-binding motif that recognizes SUMO-modified proteins. Proceedings of the National Academy of Sciences of the United States of America 101, 14373-14378.

Sontag, E.M., Lotz, G.P., Yang, G., Sontag, C.J., Cummings, B.J., Glabe, C.G., Muchowski, P.J., and Thompson, L.M. (2012). Detection of Mutant Huntingtin Aggregation Conformers and Modulation of SDS-Soluble Fibrillar Oligomers by Small Molecules. Journal of Huntington's disease 1, 119-132.

Soria-Bretones, I., Cepeda-Garcia, C., Checa-Rodriguez, C., Heyer, V., Reina-San-Martin, B., Soutoglou, E., and Huertas, P. (2017). DNA end resection requires constitutive sumoylation of CtIP by CBX4. Nature communications 8, 113.

Southwell, A.L., Smith-Dijak, A., Kay, C., Sepers, M., Villanueva, E.B., Parsons, M.P., Xie, Y., Anderson, L., Felczak, B., Waltl, S.*, et al.* (2016). An enhanced Q175 knock-in mouse model of Huntington disease with higher mutant huntingtin levels and accelerated disease phenotypes. Human molecular genetics 25, 3654-3675.

Spivak, G., and Ganesan, A.K. (2014). The complex choreography of transcription-coupled repair. DNA repair 19, 64-70.

Steffan, J.S., Agrawal, N., Pallos, J., Rockabrand, E., Trotman, L.C., Slepko, N., Illes, K., Lukacsovich, T., Zhu, Y.Z., Cattaneo, E.*, et al.* (2004). SUMO modification of Huntingtin and Huntington's disease pathology. Science 304, 100-104.

Steffan, J.S., Bodai, L., Pallos, J., Poelman, M., McCampbell, A., Apostol, B.L., Kazantsev, A., Schmidt, E., Zhu, Y.Z., Greenwald, M.*, et al.* (2001). Histone deacetylase inhibitors arrest polyglutamine-dependent neurodegeneration in Drosophila. Nature 413, 739-743.

Steffan, J.S., Kazantsev, A., Spasic-Boskovic, O., Greenwald, M., Zhu, Y.Z., Gohler, H., Wanker, E.E., Bates, G.P., Housman, D.E., and Thompson, L.M. (2000). The Huntington's disease protein interacts with p53 and CREB-binding protein and represses transcription. Proceedings of the National Academy of Sciences of the United States of America 97, 6763-6768.

Stehmeier, P., and Muller, S. (2009). Phospho-regulated SUMO interaction modules connect the SUMO system to CK2 signaling. Molecular cell 33, 400-409.

Su, H.L., and Li, S.S. (2002). Molecular features of human ubiquitin-like SUMO genes and their encoded proteins. Gene 296, 65-73.
Su, S., Zhang, Y., and Liu, P. (2019). Roles of Ubiquitination and SUMOylation in DNA Damage Response. Current issues in molecular biology 35, 59-84.
Sun, H., Leverson, J.D., and Hunter, T. (2007). Conserved function of RNF4 family proteins in eukaryotes: targeting a ubiquitin ligase to SUMOylated proteins. The EMBO journal 26, 4102-4112.
Svilar, D., Goellner, E.M., Almeida, K.H., and Sobol, R.W. (2011). Base excision repair and lesion-dependent subpathways for repair of oxidative DNA damage. Antioxidants & redox signaling 14, 2491-2507.
Swami, M., Hendricks, A.E., Gillis, T., Massood, T., Mysore, J., Myers, R.H., and Wheeler, V.C. (2009). Somatic expansion of the Huntington's disease CAG repeat in the brain is associated with an earlier age of disease onset. Human molecular genetics 18, 3039-3047.
Tai, D.J., Liu, Y.C., Hsu, W.L., Ma, Y.L., Cheng, S.J., Liu, S.Y., and Lee, E.H. (2016). MeCP2 SUMOylation rescues Mecp2-mutant-induced behavioural deficits in a mouse model of Rett syndrome. Nature communications 7, 10552.
Takahashi, K., Ishida, M., Komano, H., and Takahashi, H. (2008). SUMO-1 immunoreactivity co-localizes with phospho-Tau in APP transgenic mice but not in mutant Tau transgenic mice. Neuroscience letters 441, 90-93.
Takashima, H., Boerkoel, C.F., John, J., Saifi, G.M., Salih, M.A., Armstrong, D., Mao, Y., Quiocho, F.A., Roa, B.B., Nakagawa, M.*, et al.* (2002). Mutation of TDP1, encoding a topoisomerase I-dependent DNA damage repair enzyme, in spinocerebellar ataxia with axonal neuropathy. Nature genetics 32, 267-272.
Tang, L.T., Craig, T.J., and Henley, J.M. (2015). SUMOylation of synapsin Ia maintains synaptic vesicle availability and is reduced in an autism mutation. Nature communications 6, 7728.
Tang, Z., El Far, O., Betz, H., and Scheschonka, A. (2005). Pias1 interaction and sumoylation of metabotropic glutamate receptor 8. The Journal of biological chemistry 280, 38153-38159.
Tatham, M.H., Geoffroy, M.C., Shen, L., Plechanovova, A., Hattersley, N., Jaffray, E.G., Palvimo, J.J., and Hay, R.T. (2008). RNF4 is a poly-SUMO-specific E3 ubiquitin ligase required for arsenic-induced PML degradation. Nature cell biology 10, 538-546.
Telenius, H., Kremer, B., Goldberg, Y.P., Theilmann, J., Andrew, S.E., Zeisler, J., Adam, S., Greenberg, C., Ives, E.J., Clarke, L.A., and et al. (1994). Somatic and gonadal mosaicism of the Huntington disease gene CAG repeat in brain and sperm. Nature genetics 6, 409-414.
Telezhkin, V., Schnell, C., Yarova, P., Yung, S., Cope, E., Hughes, A., Thompson, B.A., Sanders, P., Geater, C., Hancock, J.M.*, et al.* (2016). Forced cell cycle exit and modulation of GABAA, CREB, and GSK3beta signaling promote functional maturation of induced pluripotent stem cell-derived neurons. American journal of physiology Cell physiology 310, C520-541.
Terashima, T., Kawai, H., Fujitani, M., Maeda, K., and Yasuda, H. (2002). SUMO-1 co-localized with mutant atrophin-1 with expanded polyglutamines accelerates intranuclear aggregation and cell death. Neuroreport 13, 2359-2364.

Thompson, L.M., Aiken, C.T., Kaltenbach, L.S., Agrawal, N., Illes, K., Khoshnan, A., Martinez-Vincente, M., Arrasate, M., O'Rourke, J.G., Khashwji, H., *et al.* (2009). IKK phosphorylates Huntingtin and targets it for degradation by the proteasome and lysosome. The Journal of cell biology 187, 1083-1099.

Tishkoff, D.X., Amin, N.S., Viars, C.S., Arden, K.C., and Kolodner, R.D. (1998). Identification of a human gene encoding a homologue of Saccharomyces cerevisiae EXO1, an exonuclease implicated in mismatch repair and recombination. Cancer research 58, 5027-5031.

Tome, S., Manley, K., Simard, J.P., Clark, G.W., Slean, M.M., Swami, M., Shelbourne, P.F., Tillier, E.R., Monckton, D.G., Messer, A., and Pearson, C.E. (2013). MSH3 polymorphisms and protein levels affect CAG repeat instability in Huntington's disease mice. PLoS genetics 9, e1003280.

Trottier, Y., Devys, D., Imbert, G., Saudou, F., An, I., Lutz, Y., Weber, C., Agid, Y., Hirsch, E.C., and Mandel, J.L. (1995). Cellular localization of the Huntington's disease protein and discrimination of the normal and mutated form. Nature genetics 10, 104-110.

Usui, N., Co, M., Harper, M., Rieger, M.A., Dougherty, J.D., and Konopka, G. (2017). Sumoylation of FOXP2 Regulates Motor Function and Vocal Communication Through Purkinje Cell Development. Biological psychiatry 81, 220-230.

Uzoma, I., Hu, J., Cox, E., Xia, S., Zhou, J., Rho, H.S., Guzzo, C., Paul, C., Ajala, O., Goodwin, C.R., *et al.* (2018). Global Identification of Small Ubiquitin-related Modifier (SUMO) Substrates Reveals Crosstalk between SUMOylation and Phosphorylation Promotes Cell Migration. Molecular & cellular proteomics : MCP 17, 871-888.

van der Horst, G.T., van Steeg, H., Berg, R.J., van Gool, A.J., de Wit, J., Weeda, G., Morreau, H., Beems, R.B., van Kreijl, C.F., de Gruijl, F.R., *et al.* (1997). Defective transcription-coupled repair in Cockayne syndrome B mice is associated with skin cancer predisposition. Cell 89, 425-435.

van Deursen, J.M. (2014). The role of senescent cells in ageing. Nature 509, 439-446.

van Eyk, C.L., and Richards, R.I. (2012). Dynamic mutations: where are they now? Advances in experimental medicine and biology 769, 55-77.

van Niekerk, E.A., Willis, D.E., Chang, J.H., Reumann, K., Heise, T., and Twiss, J.L. (2007). Sumoylation in axons triggers retrograde transport of the RNA-binding protein La. Proceedings of the National Academy of Sciences of the United States of America 104, 12913-12918.

Vanni, S., Colini Baldeschi, A., Zattoni, M., and Legname, G. (2019). Brain aging: A Janus-faced player between health and neurodegeneration. Journal of neuroscience research.

Vashishtha, M., Ng, C.W., Yildirim, F., Gipson, T.A., Kratter, I.H., Bodai, L., Song, W., Lau, A., Labadorf, A., Vogel-Ciernia, A., *et al.* (2013). Targeting H3K4 trimethylation in Huntington disease. Proceedings of the National Academy of Sciences of the United States of America 110, E3027-3036.

Vijayakumaran, S., and Pountney, D.L. (2018). SUMOylation, aging and autophagy in neurodegeneration. Neurotoxicology 66, 53-57.

Vos, S.M., Tretter, E.M., Schmidt, B.H., and Berger, J.M. (2011). All tangled up: how cells direct, manage and exploit topoisomerase function. Nature reviews Molecular cell biology 12, 827-841.

Waelter, S., Boeddrich, A., Lurz, R., Scherzinger, E., Lueder, G., Lehrach, H., and Wanker, E.E. (2001). Accumulation of mutant huntingtin fragments in aggresome-like inclusion bodies as a result of insufficient protein degradation. Molecular biology of the cell 12, 1393-1407.

Wang, Q.E., Zhu, Q., Wani, G., El-Mahdy, M.A., Li, J., and Wani, A.A. (2005). DNA repair factor XPC is modified by SUMO-1 and ubiquitin following UV irradiation. Nucleic acids research 33, 4023-4034.

Wang, T., Xu, W., Qin, M., Yang, Y., Bao, P., Shen, F., Zhang, Z., and Xu, J. (2016). Pathogenic Mutations in the Valosin-containing Protein/p97(VCP) N-domain Inhibit the SUMOylation of VCP and Lead to Impaired Stress Response. The Journal of biological chemistry 291, 14373-14384.

Wang, X.J., Cao, Q., Zhang, Y., and Su, X.D. (2015). Activation and regulation of caspase-6 and its role in neurodegenerative diseases. Annual review of pharmacology and toxicology 55, 553-572.

Wanker, E.E., Scherzinger, E., Heiser, V., Sittler, A., Eickhoff, H., and Lehrach, H. (1999). Membrane filter assay for detection of amyloid-like polyglutamine-containing protein aggregates. Methods in enzymology 309, 375-386.

Watson, M.B., Richter, F., Lee, S.K., Gabby, L., Wu, J., Masliah, E., Effros, R.B., and Chesselet, M.F. (2012). Regionally-specific microglial activation in young mice over-expressing human wildtype alpha-synuclein. Experimental neurology 237, 318-334.

Wei, H., Chadman, K.K., McCloskey, D.P., Sheikh, A.M., Malik, M., Brown, W.T., and Li, X. (2012). Brain IL-6 elevation causes neuronal circuitry imbalances and mediates autism-like behaviors. Biochimica et biophysica acta 1822, 831-842.

Wei, L., Nakajima, S., Bohm, S., Bernstein, K.A., Shen, Z., Tsang, M., Levine, A.S., and Lan, L. (2015). DNA damage during the G0/G1 phase triggers RNA-templated, Cockayne syndrome B-dependent homologous recombination. Proceedings of the National Academy of Sciences of the United States of America 112, E3495-3504.

Wei, M.C., Zong, W.X., Cheng, E.H., Lindsten, T., Panoutsakopoulou, V., Ross, A.J., Roth, K.A., MacGregor, G.R., Thompson, C.B., and Korsmeyer, S.J. (2001). Proapoptotic BAX and BAK: a requisite gateway to mitochondrial dysfunction and death. Science 292, 727-730.

Weidenheim, K.M., Dickson, D.W., and Rapin, I. (2009). Neuropathology of Cockayne syndrome: Evidence for impaired development, premature aging, and neurodegeneration. Mechanisms of ageing and development 130, 619-636.

Weiss, A., Klein, C., Woodman, B., Sathasivam, K., Bibel, M., Regulier, E., Bates, G.P., and Paganetti, P. (2008). Sensitive biochemical aggregate detection reveals aggregation onset before symptom development in cellular and murine models of Huntington's disease. Journal of neurochemistry 104, 846-858.

Wexler, N.S., Lorimer, J., Porter, J., Gomez, F., Moskowitz, C., Shackell, E., Marder, K., Penchaszadeh, G., Roberts, S.A., Gayan, J., *et al.* (2004). Venezuelan kindreds reveal that genetic and environmental factors modulate Huntington's disease age of onset. Proceedings of the National Academy of Sciences of the United States of America 101, 3498-3503.

Wheeler, V.C., Auerbach, W., White, J.K., Srinidhi, J., Auerbach, A., Ryan, A., Duyao, M.P., Vrbanac, V., Weaver, M., Gusella, J.F*., et al.* (1999). Length-dependent gametic CAG repeat instability in the Huntington's disease knock-in mouse. Human molecular genetics 8, 115-122.

Wheeler, V.C., Lebel, L.A., Vrbanac, V., Teed, A., te Riele, H., and MacDonald, M.E. (2003). Mismatch repair gene Msh2 modifies the timing of early disease in Hdh(Q111) striatum. Human molecular genetics 12, 273-281.

Wilkinson, K.A., and Henley, J.M. (2011). Analysis of metabotropic glutamate receptor 7 as a potential substrate for SUMOylation. Neuroscience letters 491, 181-186.

Wilkinson, K.A., Nishimune, A., and Henley, J.M. (2008). Analysis of SUMO-1 modification of neuronal proteins containing consensus SUMOylation motifs. Neuroscience letters 436, 239-244.

Williams, S.A., Wilson, J.B., Clark, A.P., Mitson-Salazar, A., Tomashevski, A., Ananth, S., Glazer, P.M., Semmes, O.J., Bale, A.E., Jones, N.J., and Kupfer, G.M. (2011). Functional and physical interaction between the mismatch repair and FA-BRCA pathways. Human molecular genetics 20, 4395-4410.

Woods, Y.L., Xirodimas, D.P., Prescott, A.R., Sparks, A., Lane, D.P., and Saville, M.K. (2004). p14 Arf promotes small ubiquitin-like modifier conjugation of Werners helicase. The Journal of biological chemistry 279, 50157-50166.

Xiang, C., Zhang, S., Dong, X., Ma, S., and Cong, S. (2018). Transcriptional Dysregulation and Post-translational Modifications in Polyglutamine Diseases: From Pathogenesis to Potential Therapeutic Strategies. Frontiers in molecular neuroscience 11, 153.

Xiao, Y., and Weaver, D.T. (1997). Conditional gene targeted deletion by Cre recombinase demonstrates the requirement for the double-strand break repair Mre11 protein in murine embryonic stem cells. Nucleic acids research 25, 2985-2991.

Yamada, T., Yang, Y., Huang, J., Coppola, G., Geschwind, D.H., and Bonni, A. (2013). Sumoylated MEF2A coordinately eliminates orphan presynaptic sites and promotes maturation of presynaptic boutons. The Journal of neuroscience : the official journal of the Society for Neuroscience 33, 4726-4740.

Yang, J., Liu, X., Bhalla, K., Kim, C.N., Ibrado, A.M., Cai, J., Peng, T.I., Jones, D.P., and Wang, X. (1997). Prevention of apoptosis by Bcl-2: release of cytochrome c from mitochondria blocked. Science 275, 1129-1132.

Youle, R.J., and Strasser, A. (2008). The BCL-2 protein family: opposing activities that mediate cell death. Nature reviews Molecular cell biology 9, 47-59.

Yun, S.M., Cho, S.J., Song, J.C., Song, S.Y., Jo, S.A., Jo, C., Yoon, K., Tanzi, R.E., Choi, E.J., and Koh, Y.H. (2013). SUMO1 modulates Abeta generation via BACE1 accumulation. Neurobiology of aging 34, 650-662.

Yunus, A.A., and Lima, C.D. (2009). Structure of the Siz/PIAS SUMO E3 ligase Siz1 and determinants required for SUMO modification of PCNA. Molecular cell 35, 669-682.

Yurchenko, V., Xue, Z., Gama, V., Matsuyama, S., and Sadofsky, M.J. (2008). Ku70 is stabilized by increased cellular SUMO. Biochemical and biophysical research communications 366, 263-268.

Yurchenko, V., Xue, Z., and Sadofsky, M.J. (2006). SUMO modification of human XRCC4 regulates its localization and function in DNA double-strand break repair. Molecular and cellular biology 26, 1786-1794.

Yurov, Y.B., Vorsanova, S.G., and Iourov, I.Y. (2011). The DNA replication stress hypothesis of Alzheimer's disease. TheScientificWorldJournal 11, 2602-2612.
Zhao, Q., Xue, X., Longerich, S., Sung, P., and Xiong, Y. (2014). Structural insights into 5' flap DNA unwinding and incision by the human FAN1 dimer. Nature communications 5, 5726.
Zhao, X.N., and Usdin, K. (2018). FAN1 protects against repeat expansions in a Fragile X mouse model. DNA repair 69, 1-5.
Zhou, Y.F., Liao, S.S., Luo, Y.Y., Tang, J.G., Wang, J.L., Lei, L.F., Chi, J.W., Du, J., Jiang, H., Xia, K., *et al.* (2013). SUMO-1 modification on K166 of polyQ-expanded ataxin-3 strengthens its stability and increases its cytotoxicity. PloS one 8, e54214.
Zolner, A.E., Abdou, I., Ye, R., Mani, R.S., Fanta, M., Yu, Y., Douglas, P., Tahbaz, N., Fang, S., Dobbs, T., *et al.* (2011). Phosphorylation of polynucleotide kinase/ phosphatase by DNA-dependent protein kinase and ataxia-telangiectasia mutated regulates its association with sites of DNA damage. Nucleic acids research 39, 9224-9237.
Zuccato, C., and Cattaneo, E. (2009). Brain-derived neurotrophic factor in neurodegenerative diseases. Nature reviews Neurology 5, 311-322.
Zuccato, C., Valenza, M., and Cattaneo, E. (2010). Molecular mechanisms and potential therapeutical targets in Huntington's disease. Physiological reviews 90, 905-981.